Dissertations

Graduate College

4-2007

Late Pleistocene Climate Variability and Chemical Weathering in the Goriganga, Higher Central Himalaya, North India

Steven Paul Beukema
Western Michigan University

LATE PLEISTOCENE CLIMATE VARIABILITY AND CHEMICAL
WEATHERING IN THE GORIGANGA, HIGHER CENTRAL
HIMALAYA, NORTH INDIA

by

Steven Paul Beukema

A Dissertation
Submitted to the
Faculty of The Graduate College
in partial fulfillment of the
requirements for the
Degree of Doctor of Philosophy
Department of Geosciences
Dr. R.V. Krishnamurthy, Advisor

Western Michigan University
Kalamazoo, Michigan
April 2007

LATE PLEISTOCENE CLIMATE VARIABILITY AND CHEMICAL WEATHERING IN THE GORIGANGA, HIGHER CENTRAL HIMALAYA, NORTH INDIA

Steven Paul Beukema, Ph.D.

Western Michigan University, 2007

Relict lacustrine deposits in the Higher Central Himalaya, India, provide a rich repository of paleoclimate information for the period 16 ka to 11 ka. Stable isotope analysis of deposits near the village of Burfu shows the hydrologic balance between glacial meltwater and monsoon precipitation as source waters for the lake. During the period from 15.5 ka to 14 ka the Burfu lake was largely fed by melting glaciers. A warming event correlated to glacial Meltwater Pulse 1a indicates a sudden increase in carbonate weathering in the region accompanied by a gradual decrease in the ratio of glacial meltwater/monsoon precipitation feeding the lake. The Bølling-Allerød is characterized by large amplitude variability in oxygen and carbon isotopes. A short-lived, abrupt cooling event, comprising a ~300 year intense cool period followed by a ~600 year interval of moderate climate is seen. This is possibly correlated to the Younger Dryas cooling event. Isotope values sharply increase at the onset of the Holocene, likely due to an increase in temperature which results in a strengthening of the monsoon and an increase in chemical weathering.

UMI Number: 3258641

INFORMATION TO USERS

The quality of this reproduction is dependent upon the quality of the copy submitted. Broken or indistinct print, colored or poor quality illustrations and photographs, print bleed-through, substandard margins, and improper alignment can adversely affect reproduction.

In the unlikely event that the author did not send a complete manuscript and there are missing pages, these will be noted. Also, if unauthorized copyright material had to be removed, a note will indicate the deletion.

UMI®

UMI Microform 3258641

Copyright by
Steven Paul Beukema
2007

ACKNOWLEDGMENTS

This dissertation would not have been possible without the support and encouragement from many people. I'd like to thank the Michigan Space Grant Consortium for two years of funding. Frank Severance and Bonnie Bryant were very helpful in facilitating all of the funding issues.

In six years as a graduate student in the Department of Geosciences at Western Michigan University there are too many times to count the help and support of Beth Steele and Kathy Wright in the office, and I am grateful for all of their assistance over the years and for the warm and friendly atmosphere they give our department.

I have grown tremendously through many faculty members, through interactions in courses, through informal discussions, and in many other ways. I owe a deep dept of gratitude to Al Kehew for taking me under his wing when I arrived here as a masters student and for all of his guidance over the years, both on campus and in other parts of the world.

Being cooped up in a lab with no windows was made more enjoyable by the company of Tsigabu Gebrehiwet and Nathaniel Barnes. My initial isotope lab training came from Ahmed Murad. Indeed, I have learned much from these guys. I would also like to thank Rennie Kaunda for giving me much to ponder and for many stimulating conversations. I would also like to thank Rennie for putting up with me and my piano for a year as my roommate. Others, including Lisa Anderson, Soumya Das, Haile Mengistu, Andy Kozlowski, Nathan Brandner, and Jenny McCrary have made graduate student life enjoyable and interesting and have provided much needed

ii

Acknowledgments—continued

companionship and encouragement as we all work together toward this seemingly endless goal.

My committee members, Elen Cutrim, Mike Grammer, and Mohamed Sultan, deserve thanks and appreciation for their time in meetings, their time reviewing the dissertation, and their helpful comments and questions. Many, many thanks go to my main advisor, R.V. Krishnamurthy. I had no idea what I was getting myself into when I signed up for the stable isotope course during my masters program, but R.V. showed me the fascinating world of stable isotopes and their many applications. R.V. was a constant guiding force behind this project, from its conception through completion, continually offering support, guidance, and wisdom. I have learned much from R.V., much about Indian culture, the WorldCup, science and how to think scientifically, and many, many other things.

I have received incredible support from people at the Portage First United Methodist Church, from the Chancel Choir, the Handbell Choir, the Praise Choir, the staff, and from many other people.

And lastly, I would like to thank my family. My parents have been incredibly supportive throughout my academic career as has the rest of my family.

Steven Paul Beukema

iii

TABLE OF CONTENTS

iv

Table of Contents—continued

Table of Contents—continued

LIST OF TABLES

LIST OF FIGURES

CHAPTER I

INTRODUCTION

Statement of research objectives

During the Late Pleistocene there was a major transition from a glacial to an interglacial climate. This dissertation is a study of climate changes that took place in the Goriganga valley, Higher Central Himalaya, in North India during this important climatic transition. The Goriganga valley in the Higher Central Himalaya is relatively inaccessible, and thus very little is known about climate changes during the Late Pleistocene in this region.

As the Higher Central Himalaya is a mountainous region dotted with glaciers and ice sheets, this study uses lacustrine sediments from a relict proglacial lake as a method of tracking glacial changes during a time of deglaciation. Stable isotopes of oxygen are used as a proxy of the relative amount of glacial meltwater versus precipitation that feeds the lake. This ratio is expected to change as glaciers retreat from the direct vicinity of the lake basin and as the monsoon strengthens due to an increase in temperature. Stable isotopes of carbon from the inorganic fraction of the lacustrine sediments are used in conjunction with ^{14}C ages of sediments to track changes in chemical weathering of carbonate bedrock in the catchment area as related to changes in climate. Stable isotopes of carbon from the organic fraction, along with

1

the C/N ratio are used to determine changes in C_3/C_4 vegetation types and the source of organic carbon in the lake.

There are several well-documented global climate events during the Late Pleistocene, including Meltwater Pulse 1a at 14,500 years before present (Fairbanks, 1989), the Bølling-Allerød warm phase from approximately 14,500 to 12,500 years before present (Alley et al., 1993), the Younger Dryas at approximately 12,000 years before present (Mangarud et al., 1974), and the onset of the Holocene, marked by Meltwater Pulse 1b (Fairbanks, 1989). An important goal of this study is to determine the nature of these global events in a proglacial lacustrine environment in the Higher Central Himalaya, including whether or not there is evidence that these events were experienced in the Higher Central Himalaya, and if so, the effect these events may have had on the hydrology of the lake, chemical weathering of carbonates, and changes in vegetation.

Global climate change

Human beings have, for at least thousands of years, altered their environment in some manner in order to make their own existence more comfortable. Primitive activities, including building fires and making tools out of rocks, had little effect other than the purpose for which they were used. Since the industrial revolution, however, the side effects of altering the natural environment may have serious consequences. One particular area of concern is climate. The 20th century has seen substantial increases in atmospheric CO_2 concentrations as well as average global temperatures.

Atmospheric CO_2 concentrations have increased by over 30% since 1750 (Prentice et al., 2001) to approximately 380 ppm in 2001. There is evidence that atmospheric CO_2 concentrations were much higher during the geologic past and had begun to decline by 60 million years before present (Ma), falling below 300 ppm by 20 Ma (Pagani et al., 1999a; Pearson and Palmer, 1999, 2000). Very low levels of atmospheric CO_2 between 7 and 5 Ma may have contributed to the evolution of plants that use the C_4 photosynthetic pathway, which is more efficient in its use of CO_2 (Cerling et al., 1993, 1997; Pagani et al., 1999b). It is very likely that the current concentration of atmospheric CO_2 has not been exceeded in 20 million years (Prentice et al., 2001). Models forecast that atmospheric CO_2 concentrations in the year 2100 could reach anywhere from 540 – 970 ppm (Prentice et al., 2001).

Temperature has also increased since the Industrial Revolution. Global average surface temperatures have increased by 0.6°C during the 20th Century (Folland et al., 2001), with the 1990s being the warmest decade on record. Satellite images indicate a decrease of approximately 10% in the annual snow cover extent in the Northern Hemisphere since 1966 (Robinson, 1997, 1999). Global temperature increases seem to coincide with global increases in atmospheric CO_2. While it is beyond doubt that there is an anthropogenic signature to global climate change, it is essential to have detailed understanding of Earth's climatic history as well as natural climate variability in order to successfully model future climate changes.

Overview of Cenozoic climate

Earth's climate has experienced continual fluctuations between cold and warm periods throughout geologic time. There is evidence that extensive glaciations occurred as early as the Precambrian Era (Hoffman et al., 1998). Besides at least one Precambrian glaciation, at least two major cold intervals occurred before the most recent Pleistocene glaciation (Frakes et al., 1992). These two earlier glacial periods occurred during the Ordovician (~440 Ma) and during the Carboniferous to Permian (~300 to 250 Ma) (Figure 1). Clays produced by chemical weathering in warm,
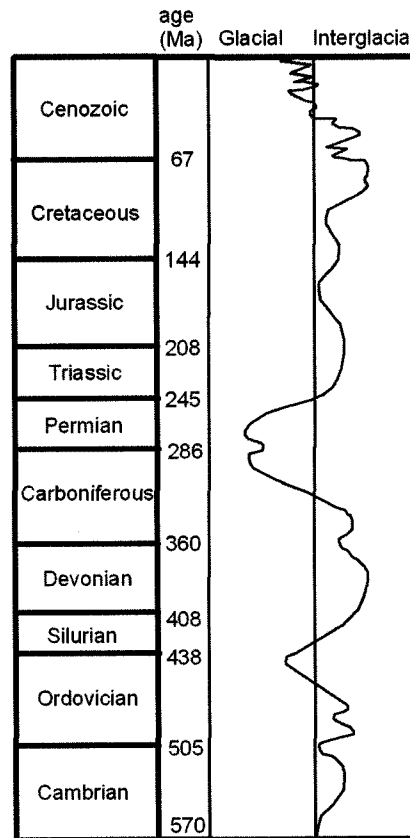
Figure 1. Generalized temperature curve from Cambrian to present (modified from Frakes et al., 1992).

humid environments have been documented in Antarctica that date to the early Cenozoic (Robert and Kennett, 1994). This testifies to a worldwide warm climate at this time.

Global climate began cooling at around 35 Ma; it is uncertain whether this cooling occurred abruptly or gradually. Temperatures of deep ocean waters have been inferred from oxygen isotope values of benthic foraminifera collected from the bottom of the Atlantic Ocean. These isotope ratios suggest a drastic decrease in the temperature of deep Atlantic water since 70 Ma, when the inferred temperature was ~15 – 20°C, to the present deep water temperature of ~2°C (Figure 2). Significant tectonic changes played an important role in the cooling climate. It was at this point when South America and Australia split from Antarctica (Figure 3). This opened a
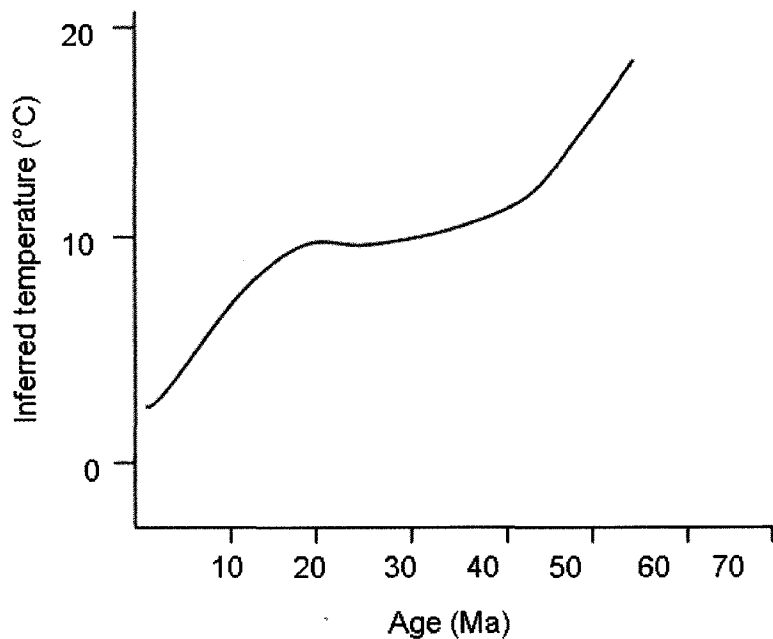
Figure 2. High latitude deep water temperature during the Cenozoic reconstructed from $\delta^{18}O$ values of benthic and pelagic foraminifera (modified after Kennett, 1982).
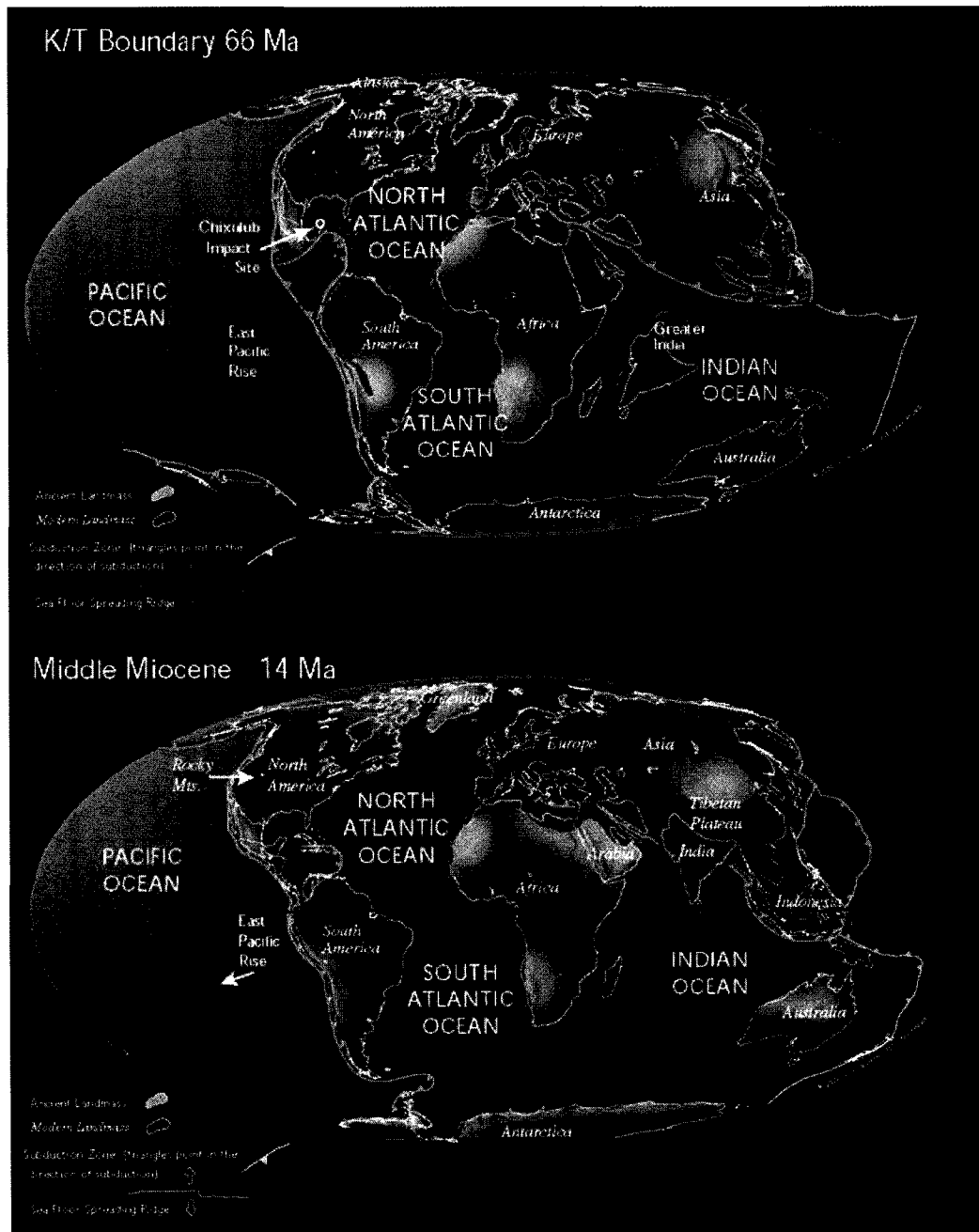
Figure 3. Orientation of continents 66 Ma and 14 Ma (Scotese, 2001).

wide body of water around the polar continent, followed by the development of the Antarctic Circumpolar Current as well as the southern hemisphere circumpolar deep flow (Kennett, 1982, p.714). There is evidence that some glaciation began in Antarctica ~27 Ma. Exposed lavas known to have erupted under ice have been dated to 27 Ma, confirming the presence of ice in Antarctica at this time (LeMasurier, 1990, p.15). The expansive East Antarctic Ice Sheet is believed to have begun growth by 15 Ma (Flower and Kennett, 1994). Besides smaller glaciers in high elevation mountains, the ice sheets in Antarctica were the only significant ice accumulations until about 3 Ma, when northern hemisphere ice began to form.

Important oceanic circulation changes occurred in conjunction with the tectonic opening of the Bering Strait and the closing of the Isthmus of Panama around 3 Ma. It was after this that the North Atlantic Deep Water (NADW) formed (Broecker, 1998). The NADW is a body of water that forms in the North Atlantic and flows southward to the circum-Antarctic region, at which point it flows eastward into the Indian and Pacific Oceans. It was also at this time when ice sheets began to form in Greenland and in North America. The overall global climate from ~2.7 Ma to 1.2 Ma was that of a warm climate, ice sheets in North America began to form and occupied only a small geographic extent. This is evident from oxygen isotope values of benthic foraminifera from the North Atlantic, which show an overall cooling trend and an increase in the volume of ice from 3.2 Ma to present (Figure 4). When temperature is colder, greater fractionation of isotopes occurs during the evaporation of water from oceans. This results in isotopically depleted water preferentially

evaporating, leaving ocean water enriched in ^{18}O. Figure 4 shows δ^{18}O values of benthic foraminifera from the North Atlantic, with more positive δ^{18}O values indicative of a greater volume of ice and colder temperatures, and with less positive δ^{18}O values indicative of a smaller ice volume and warmer temperatures. Small-scale oscillations between glacial and interglacial climates show a smaller difference in oxygen isotope values from 2.8 Ma to 1.6 Ma than from 1.2 Ma to present. These data suggest that since the initiation of North American glaciation ~3 Ma, icehouse climates were more severe during the past one million years than previously. Also evident in this figure is a dominating 90,000 year periodicity in the glacial – interglacial cycle.
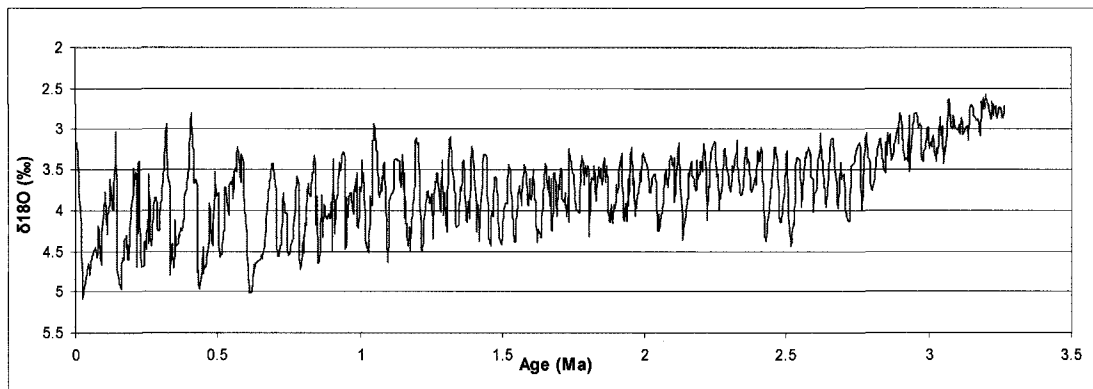
Figure 4. Benthic δ^{18}O record from DSDP site 607 in the North Atlantic (data from Raymo and Ruddiman, 2004; Raymo, 1992; Raymo et al., 1989; Ruddiman et al., 1989).

Although ice sheets began to form in North America up to ~3 Ma, fluctuations between extreme glacial and interglacial periods persisted from about 1.6 Ma to the

present. This period of time is known as the Pleistocene Epoch. The Pleistocene lasted from 1.6 Ma to 10,000 years before present (10 ka), at which point the Holocene, or the current geologic epoch, began. The major characterizing feature of the Pleistocene is the constant oscillation of glacial and interglacial climates. These fluctuations are the result of several complicated interactions of ocean circulation, atmospheric circulation, tectonic configuration, changes in insolation due to changes in Earth's orbital parameters, changes in volcanism, and chemical weathering rates.

The most detailed paleoclimate information available is from the most recent geologic past. Thus, of the major ice ages that have occurred during the Pleistocene, the greatest detail is known about the most recent ice age, known in North America as the Wisconsin glaciation (Chamberlin, 1895); less is known about the penultimate glaciation, the Illinoian glaciation (Chamberlin, 1896), and much less is known about older glaciations.

The Illinoian glaciation lasted from approximately 0.5 Ma to about 140 ka. Several advances and retreats of ice sheets and glaciers in North America, Northern Europe, the Alps, the Himalayas, and other high mountain areas occurred during this extensive time period. This glaciation was named "Illinoian" in North America because of the large amount of glacial deposits in the state of Illinois from this glaciation. An ice sheet developed in Northern Canada and progressed to the south, extending as far south as the state of Illinois, where some traces of moraines are buried under more recent (Wisconsin) glacial deposits. Most of the deposits to the

north of the Illinoian glaciation were removed by erosion when more recent ice sheets advanced over the original deposits. Thus, little is known about this period.

A rapid change in oxygen isotopic ratios occurred at about 140 ka. As indicated from various sources (e.g. Greenland ice cores, North Atlantic marine sediments). Jouzel et al. (1993) calculated a rapid temperature increase of 6°C from isotopic data from the Vostok, Antarctica core. This suggests that the Illinoian glaciation ended abruptly and that there was a drastic change to a warm, interglacial climate. This warm period, known as the Sangamon, lasted approximately 12,000 years from roughly 130 ka to 120 ka. (Mangerud, 1991, p.46). During this warm period sea level was approximately 5 – 6 meters higher than the current level. Corals grew in the tropics in the photic zone, which was at a higher elevation than modern sea level. These coral are evident as terraces above modern sea level and can be dated with uranium-thorium to ~125 ka. (Szabo et al., 1994). Global temperatures were likely slightly warmer than modern temperatures as testified in ice cores by heavier (i.e. less negative) isotope values of δD and $\delta^{18}O$ during the Sangamon interglacial than during the Holocene (Figure 5). CO_2 concentrations from air bubbles trapped in the Vostok, Antarctica core reveal a drastic increase in CO_2 concentrations from 200 ppm during the Illinoian glaciation to approximately 300 ppm during the Sangamon interglacial. Resolution of the data, however, is not high enough to determine if the interglacial period was the result of increasing CO_2 concentrations, or if the CO_2 concentrations rose because of higher global temperature. Following this brief respite
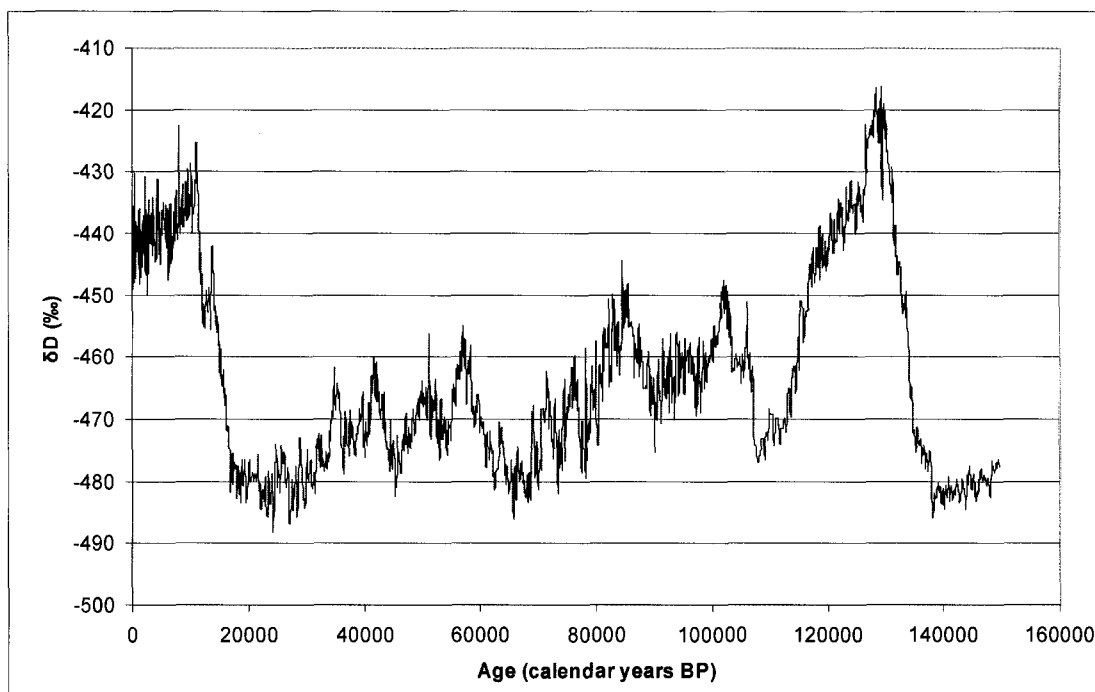
Figure 5. δD values from Vostok, Antarctica, ice core records (data from Jouzel et al., 1987; Jouzel et al., 1993; Jouzel et al., 1996; Petit et al., 1999).

from glacial conditions, a rapid cooling event occurred which began the most recent, Wisconsin, glaciation.

High-resolution data from ice cores and other sources enable a detailed picture of climate during the Wisconsin glaciation. The Wisconsin glaciation extended from 120 ka to about 15 ka. Isotopic data (Figure 5) reveal several fluctuations during this period, alternating between warmer and colder periods. These alternations, however, were not large enough to be classified as glacial – interglacial fluctuations; rather, they are termed stadial and interstadial. Stadials are relatively colder periods when

ice advances, whereas interstadial are relatively warmer periods when ice retreats but does not completely melt. Evidence suggests summer stadial temperatures in the European Alps were 7 − 8°C and winter stadial temperatures were −7 to −12°C, with the coldest winter temperatures around −20°C (Vanderberghe, 1992, p.72). Dansgaard et al. (1982, 1993), Dansgaard and Oeschger (1989), and Oeschger et al. (1985) identified 23 interstadial events between 115 ka and 10 ka. These are known as Dansgaard-Oeschger (D/O) cycles and consist of 2,000 − 3,000-year warm periods that began gradually and ended abruptly. Temperatures in Greenland fluctuated on the order of 5°C during a D/O event.

Short-term events that produced large volumes of ice-rafted debris in the North Atlantic are called Heinrich events (Broecker et al., 1992; Bond et al., 1992). Heinrich events occurred at the end of cooling cycles during which a gradual drop in sea surface temperature (SST) was immediately followed by a rapid warming event, producing a large discharge of icebergs in the North Atlantic. These icebergs transported coarse debris into the North Atlantic from eastern Canada to the coast of Spain and Portugal; the average thickness of ice-rafted dropstones in the North Atlantic is 10 cm (Heinrich, 1988). Six distinct Heinrich events have been identified, spaced approximately 5,000 − 10,000 years apart, at the following times: 65-60 ka, 44.0 ka, 33.2-35.1 ka, 26.0 ka, 22.0 ka, and 15-13 ka (Broecker, 1994). Both Dansgaard-Oeschger events and Heinrich events are thought to be related to fluctuations between ice-ocean-atmosphere interactions.

The Laurentide Ice Sheet of North America reached its greatest southern extent at approximately 20 – 22 ka, a time known as the last glacial maximum (LGM). This is the point during the entire Wisconsin glaciation when the temperatures were the coldest, the ice sheets were the largest, atmospheric CO_2 was at its lowest concentration, and sea level was the lowest (Figure 6) (Petit et al., 1999). The Laurentide Ice Sheet of North America reached as far south as 39°N. The LGM did not persist for a great length of time. Shortly after the ice reached its maximum extent, a rapid warming took place (Figure 5). The retreat of the Laurentide Ice Sheet in North America was interrupted by several small-scale readvances that deposited a complex stratigraphy of glacial sediments (e.g. Beukema, 2003). As it retreated and readvanced, the Laurentide Ice Sheet assumed a lobate nature, and advances of several lobes displayed the characteristics of fast-flowing ice streams (Kehew et al., 2005; Patterson, 1997). Temperatures at the South Pole rose approximately 8°C and within less than 10,000 years sea level rose by 120 meters (Figure 6).

As temperatures rapidly rose and ice persistently melted, temperature once again abruptly decreased, and at around 12.5 ka the North Atlantic region, and probably a large portion of the rest of the Earth, experienced near-glacial conditions. Ice sheets in North America and Europe that had been retreating began to advance once again. The Scandinavian ice sheet advanced 50 km during this time (Donner, 1995). Sea surface temperatures off the coast of Portugal dropped 7°C during this time (Bard et al., 1987). Vegetation in Europe had changed from steppe grasslands immediately following the retreat of the northern ice sheets, gradually changing to
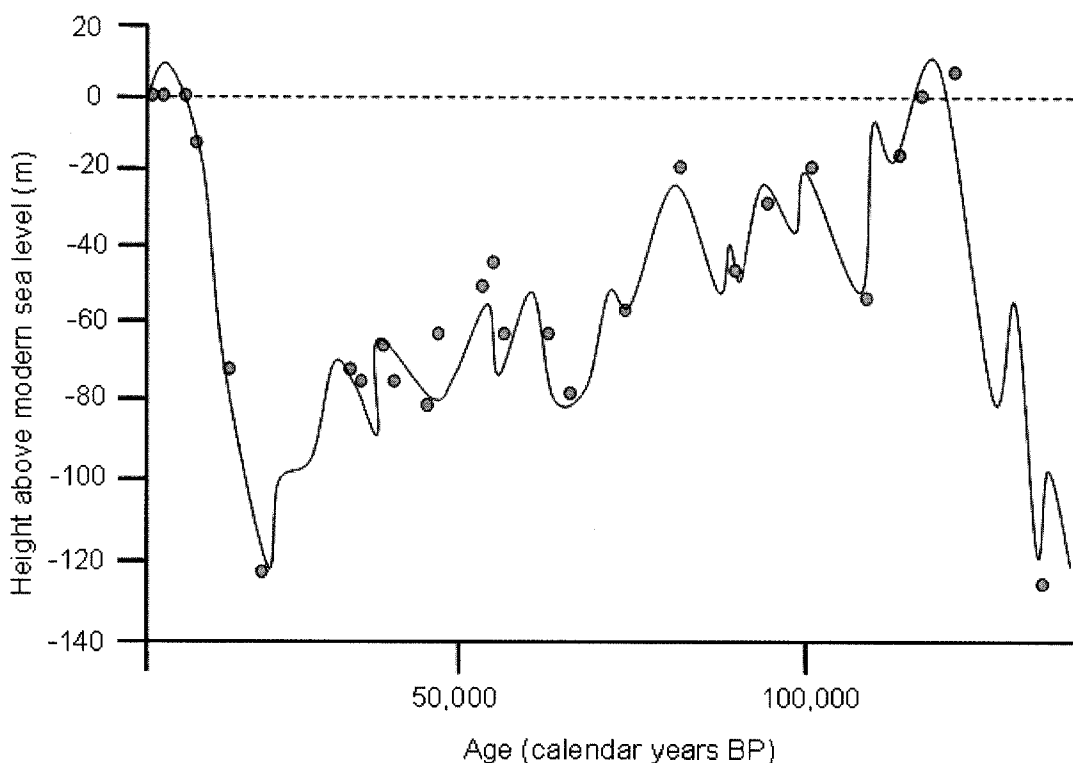
Figure 6. Late Quaternary sea-level history derived from coral-reef terrace heights and ages in Papua New Guinea (circles) and deep sea oxygen-isotope ratios (line) (modified from Chappell et al., 1996).

birch forests. The sudden cooling of climate, however, killed the birch forests that were replaced by *Dryas octopetala* tundra (Lundqvist, 1986). This brief cold period, lasting from about 12.1 – 12.9 ka to 11.4 – 11.5 ka (Cronin, 1999), is known as the Younger Dryas (Mangerud et al., 1974). The origin of this abrupt cooling is thought to have been due to the sudden flood of glacial meltwater from the St. Lawrence River into the North Atlantic, disrupting the flow of the North Atlantic Deep Water (Broecker, 1982). Within a time period of 10 – 20 years the cold temperatures of the Younger Dryas had changed once again to the overall warming trend (Alley et al.,

1993). After the Younger Dryas the ice remaining in Northern Europe remained as segregated masses of stagnant ice, which took approximately 1400 years to melt (Donner, 1995). In North America, following a readvance of the Laurentide Ice Sheet during the Younger Dryas, the ice retreated to a position north of the Great Lakes by about 11 ka. (Teller and Kehew, 1994), after which further retreating occurred until the last remnants of the great ice sheet vanished approximately 6.5 ka.

Slight changes in global climate have occurred since the Younger Dryas. Around 6000 – 3000 years before present most of the world was slightly warmer than modern temperatures (Webb et al., 1987, p.46). Average temperatures of Europe around 5000 years before present are estimated to have been 2°C warmer than today. A minor cooling event took place from about 1500 – 1750 A.D., known as the Little Ice Age (Grove, 1988). Historical documents, including the famous painting of George Washington crossing the Delaware River, record very severe winters in Europe and North America. In the painting, the river is depicted as being cluttered with chunks of ice through which the military crew rafted their boat. The Delaware River, however, is not known to have ever frozen that extensively during the 20th century. Mountain glaciers in the Himalaya, Alps, and North America experienced significant advances during this time. Since the Little Ice Age, temperatures have been steadily increasing, and since the Industrial Revolution, the atmospheric concentrations of greenhouse gases have increased from 280 ppm to ~380 ppm (Prentice et al., 2001).

CHAPTER II

STUDY AREA

Geographic setting

This research is the result of an investigation of late Pleistocene paleoclimate of Northern India that was conducted jointly by researchers at the Department of Geosciences at Western Michigan University (Kalamazoo, Michigan, USA) and the Planetary Sciences Division at the Physical Research Laboratory (Ahmadebad, India). Samples were collected from a relict lake deposit near the village of Burfu in the Goriganga basin of the Central Himalaya in Northern India (elevation of 3200 meters above sea level) during the summer of 2003 (Figure 7). The geographic coordinates of this location are 30°21'40.3N" and 80°10'57.3"E. The relict lake deposits are exposed along the flank of the Kharkhan Khotla tributary that originates from the cirque glacier to the south (Figure 7). These lacustrine deposits rest atop a ground moraine that has been associated with an advance of the last glacial maximum (Pant et al., 2006) (Figure 8). Presently, the glacier has receded to an elevation of 4500 m above sea level and is located on Kalchu and Mapa Dhura (Dhura = ridge) where it appears as a cirque glacier (Figure 7). In the Higher Central Himalaya, numerous lakes developed in proglacial environments following the recession of valley glaciers (Juyal et al., 2004). There is evidence in the Goriganga valley of an older, more extensive glacial advance corresponding to Marine Isotope Stage 4 at ~63 ka.

16
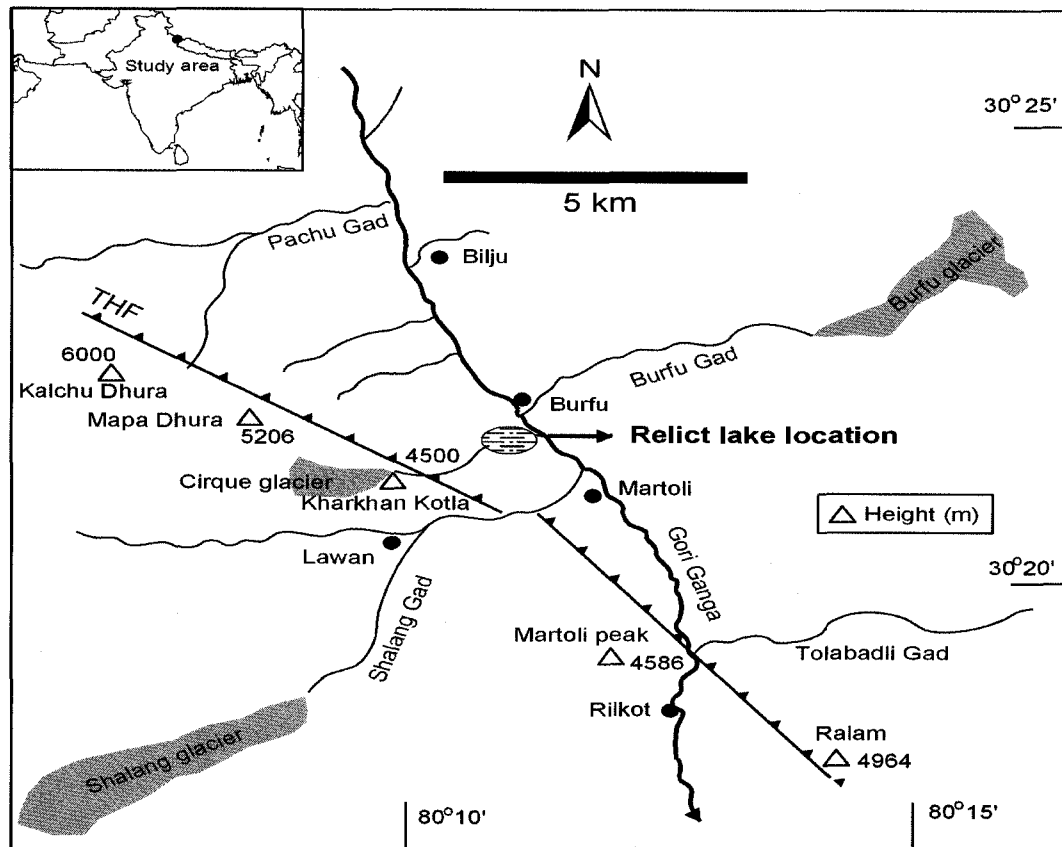
Figure 7. Geographic location of relict lake deposits near the village of Burfu, North India.

(Sharma and Owen, 1996; Pant et al., 2006). Thus, the maximum extent of glacial advances in the Himalaya does not correspond to the global last glacial maximum of continental ice sheets (Gillespie and Molnar, 1995). A NW-SE trending Trans Himadari Fault (THF) runs parallel to the Goriganga until Martoli (NW-SE) and then takes a westerly turn and continues parallel to the Kalchu and Mapa Dhura. The cirque glacier that feeds the Kharkhan Khotla stream lies on this ridge. The THF
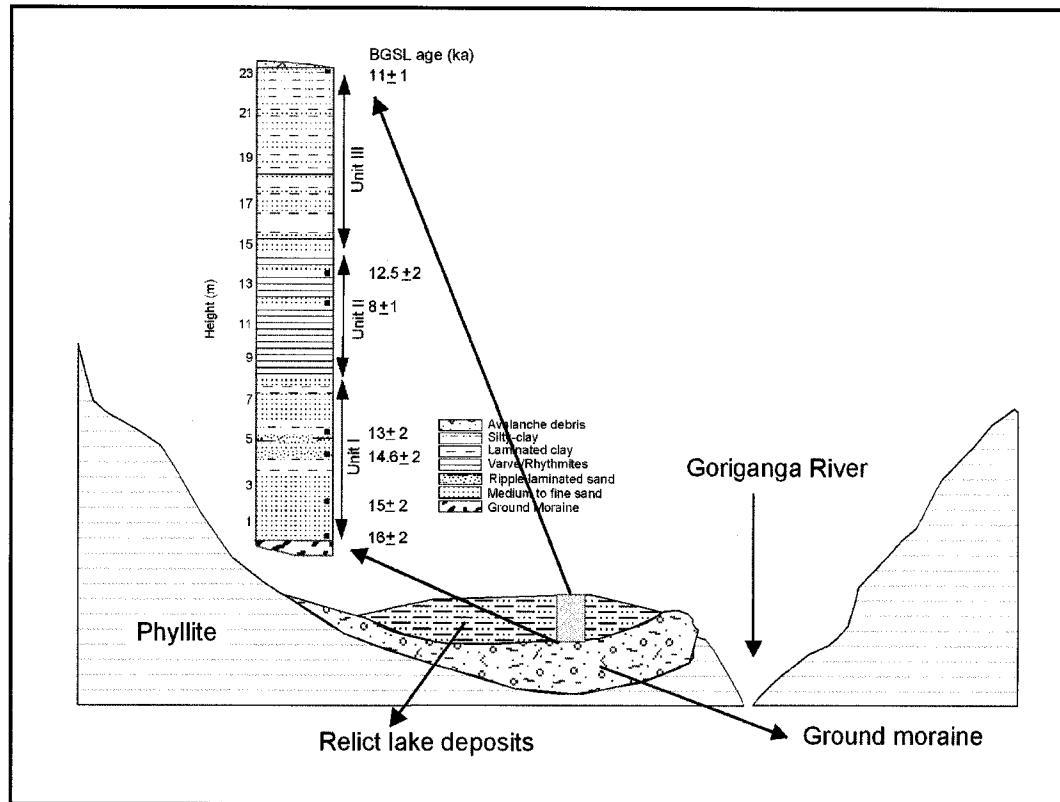
Figure 8. Generalized cross section of study area showing location of the relict lake deposits with respect to valley morphology.

defines the tectonic boundary between the southern Central crystalline rocks (quartzite, quartz schist, calcsilicate, gneisses and migmatite) and the Martoli formation Tethyan sedimentary (bedded black shale, slate and phyllites) (Pant et al., 2006). Relict lake deposits are located on the Martoli group of rocks (Figure 9).
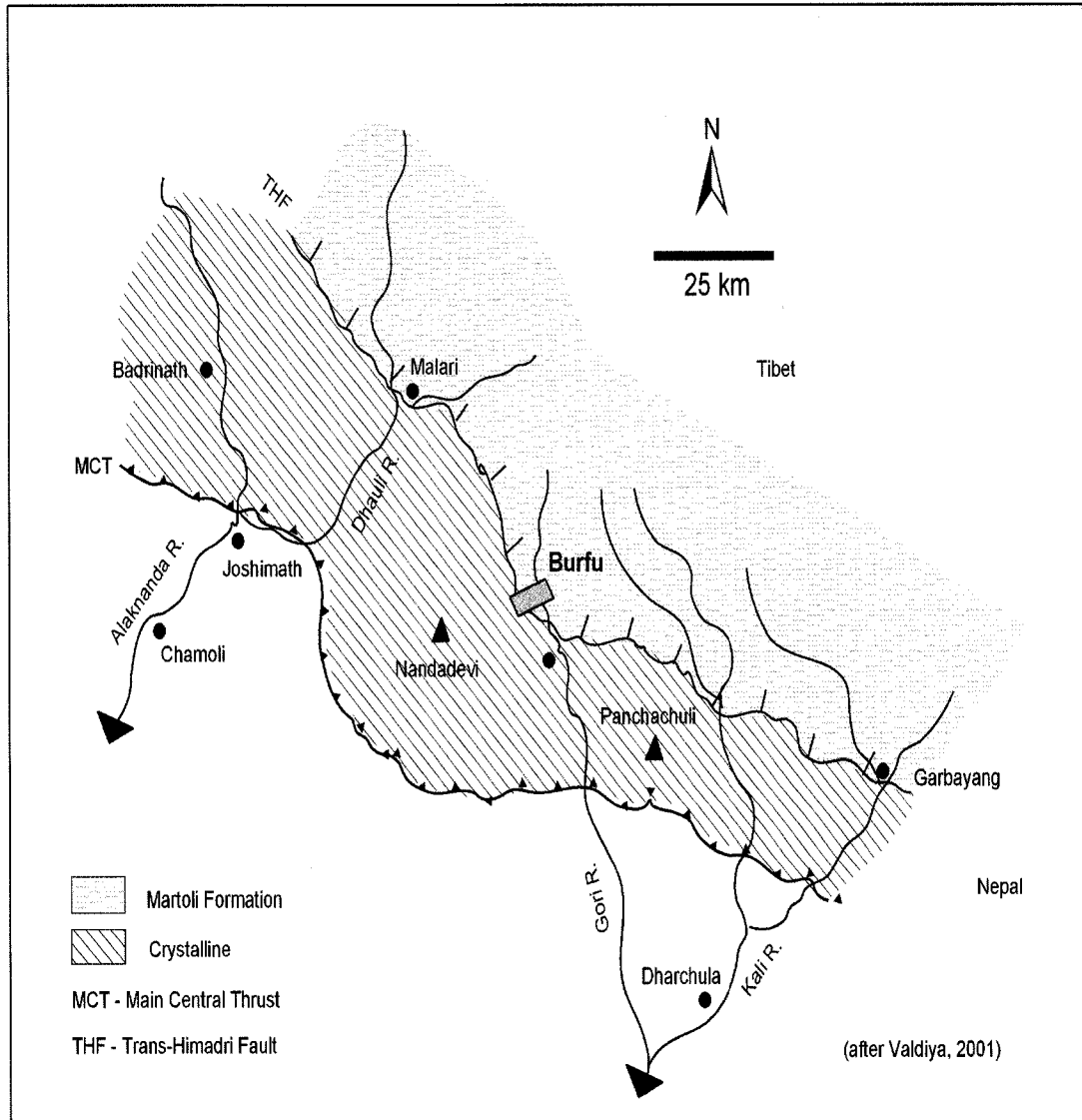
Figure 9. Regional geology. Arrows indicate direction of river flow.

Regional climate

Modern climate data from the nearest weather station, Shimla, India (31.10°N 77.09°E, 2205 meters above sea level), indicate that the area experiences a mild climate with relatively warm winters and cool summers that receives most of its precipitation during the summer monsoon season from June through September (Table 1).

Table 1. Average climate data for Shimla, India (from Global Historic Climatology Network, Version 1).

Average Precipitation for Shimla, India

	Jan	Feb	Mar	Apr	May	Jun	Jul	Aug	Sep	Oct	Nov	Dec	Year
mm	72.9	69.1	64.1	48.5	72.0	166.3	435.5	430.5	172.4	35.4	10.3	28.9	1606.6
inches	2.9	2.7	2.5	1.9	2.8	6.5	17.1	16.9	6.8	1.4	0.4	1.1	63.3

Source: SHIMLA data derived from GHCN 1. 1176 months between 1863 and 1960

Average Temperature for Shimla, India

	Jan	Feb	Mar	Apr	May	Jun	Jul	Aug	Sep	Oct	Nov	Dec	Year
°C	5.3	6.0	10.3	15.0	18.7	19.9	18.2	17.3	16.5	14.0	10.6	7.6	13.3
°F	41.5	42.8	50.5	59.0	65.7	67.8	64.8	63.1	61.7	57.2	51.1	45.7	55.9

Source: SHIMLA data derived from GHCN 1. 1003 months between 1876 and 1960

Average Station-level Pressure, Shimla, India

	Jan	Feb	Mar	Apr	May	Jun	Jul	Aug	Sep	Oct	Nov	Dec	Year
millibars	781.5	780.5	781.1	781.3	780.2	777.8	776.8	778.0	780.7	783.6	783.8	782.9	780.7

Source: SHIMLA data derived from GHCN 1. 960 months between 1881 and 1960

Several meteorological phenomena and processes shape the climate of North India. A series of permanent subtropical high pressure centers exists at approximately 30°N globally (Figure 10), creating an area of dry, subsiding air at the north end of the Hadley circulation cell. The location of this subtropical anticyclone region occurs to the north of North India in Siberia. This region of high pressure becomes well-
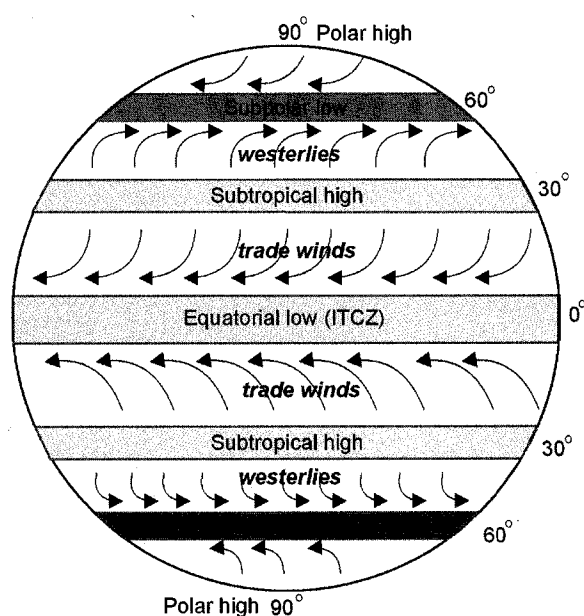
Figure 10. Generalized diagram of pressure zones on Earth (modified after Lutgens and Tarbuck, 1998).

developed during the winter months, bringing cold continental air to the south. As cold air moves to the south it converges with the Pacific northeasterlies. These two winds gradually merge between 15° and 20°N to form the winter monsoon of Southeast Asia. The weather during winter months on the Indian subcontinent is

dominated by winds and small amounts of precipitation that come from the north/northeast. The study area in North India, however, is not affected by the winter monsoon. The entire area of North India as well as a portion of Central India is sheltered from these winds by the Himalayas. The predominating surface winds in these locations during the winter come from the west.

Since India lies between approximately 5° and 30°N latitude it lies in the belt of trade winds, which is a belt of surface winds that blows from the northeast to the southwest and converges near the equator in the intertropical convergence zone (ITCZ). The ITCZ is an equatorial zone where the trade winds from the northern and southern hemispheres converge and rise. Trade winds in the northern hemisphere move from northeast to southwest, whereas southern hemisphere trade winds move from southeast to northwest. At around 5°N is the ITCZ, where Hadley circulation cells from the north and south hemisphere come together. The equatorial side of the Hadley cell consists of tropical maritime air, whereas the poleward side consists of dry, subsiding air. Due primarily to differential heating and cooling of the land relative to ocean, the ITCZ does not always occupy the same region throughout the year. Southeast Asia, with an extensive continental area directly to the north, is the area that exhibits the greatest migration of the ITCZ. The ITCZ in South Asia lies around 8°S in January, while in July it usually lies around 30°N (Figure 11). East Africa also experiences a wide migration of the ITCZ, with it located at approximately 12°N in July and 18°S in January. The migration of the ITCZ to the north is a factor that causes the change of predominant wind directions in the Indian

subcontinent from the northeast during the winter to the southwest during the summer. The southern hemisphere trade winds approach the ITCZ, which is to the
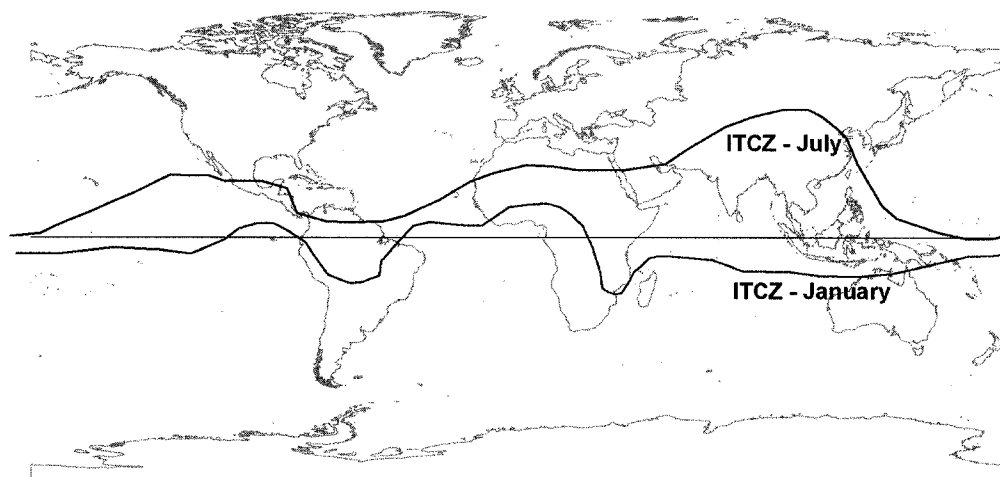
Figure 11. Average position of the intertropical convergence zone (ITCZ) for January and July (modified from Lutgens and Tarbuck, 1998).

north of India during the summer. These winds begin from the southeast blowing toward the northwest and change direction as they cross the equator due to the Coriolis Effect. These winds travel to the northeast over India, bringing with them moist tropical air and the summer monsoons, during which time India receives 80% of its annual precipitation.

The summer monsoon, which begins in June and lasts until September, is the dominating climatic feature of India. The onset and the intensity of the summer monsoon is related to the Mascarene high, which is an area of semi-permanent high pressure in the Indian Ocean, located at 30°S, 50°E (Pant and Kumar, 1997). This high pressure zone fluctuates throughout the year. The intensity of the Mascarene

high strengthens the East African low-level jet (Figure 12). The East African low-level jet is a strong cross- equatorial air current in the lower troposphere (altitude of ~1.5 km). This migrates throughout the year and hits India usually in June-July.
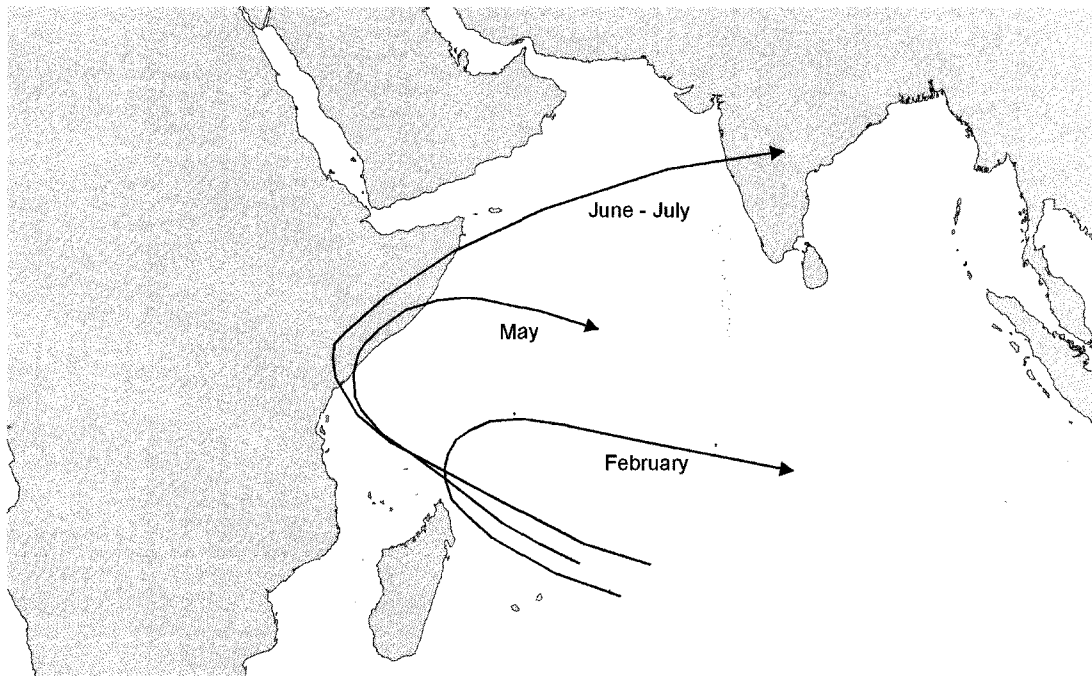
Figure 12. Average monthly position of the low-level jet stream over the
Indian Ocean (modified after Pant and Kumar, 1997).

As previously mentioned, the predominant surface winds in India change from being northeasterlies in the winter to being southwesterlies in the summer. In the upper atmosphere the climate is influenced by the subtropical westerly jet and the tropical easterly jet. The subtropical westerly jet is centered at about 12 km in altitude and 25 – 30°N latitude and is well-developed during the northern hemisphere winter.

This jet contains average wind speeds of 60 meters/second and it first appears over India after the withdrawal of the summer monsoon. The Himalaya range is directly in the path of the subtropical westerly jet, which causes it to split into two jet streams as it flows over India, one to the north and one to the south of the Himalaya range (Figure 13).

The two jets merge on the east side of the Himalaya, forming once again a single westerly jet. This jet stream shifts in latitude throughout the year due to regional climate changes associated with the migration of the ITCZ. The subtropical westerly jet shifts southward during the fall and winter until about February or March, at which point it begins to migrate north until it gradually dissipates. The subtropical westerly jet becomes reestablished again after the withdrawal of the summer monsoon.

Another significant feature of the upper atmosphere is the tropical easterly jet stream (Figure 13). This is a band of easterly winds that becomes well-developed during the summer monsoon season and is situated at approximately 9 – 14°N latitude and is centered at about 14 km in altitude. Wind speeds in this jet average around 40 meters/second. This jet stream becomes strong near Southeast Asia and flows across Africa and as far west as the Atlantic Ocean. The tropical easterly jet stream develops due to excessive heat buildup over the Asian subtropical continental area. It usually persists until September, when it dissipates. Therefore, the seasonal fluctuation of winds in India exists on two disparate levels: at the surface level winds are northeasterly during the winter and change to southwesterly during the summer; in the
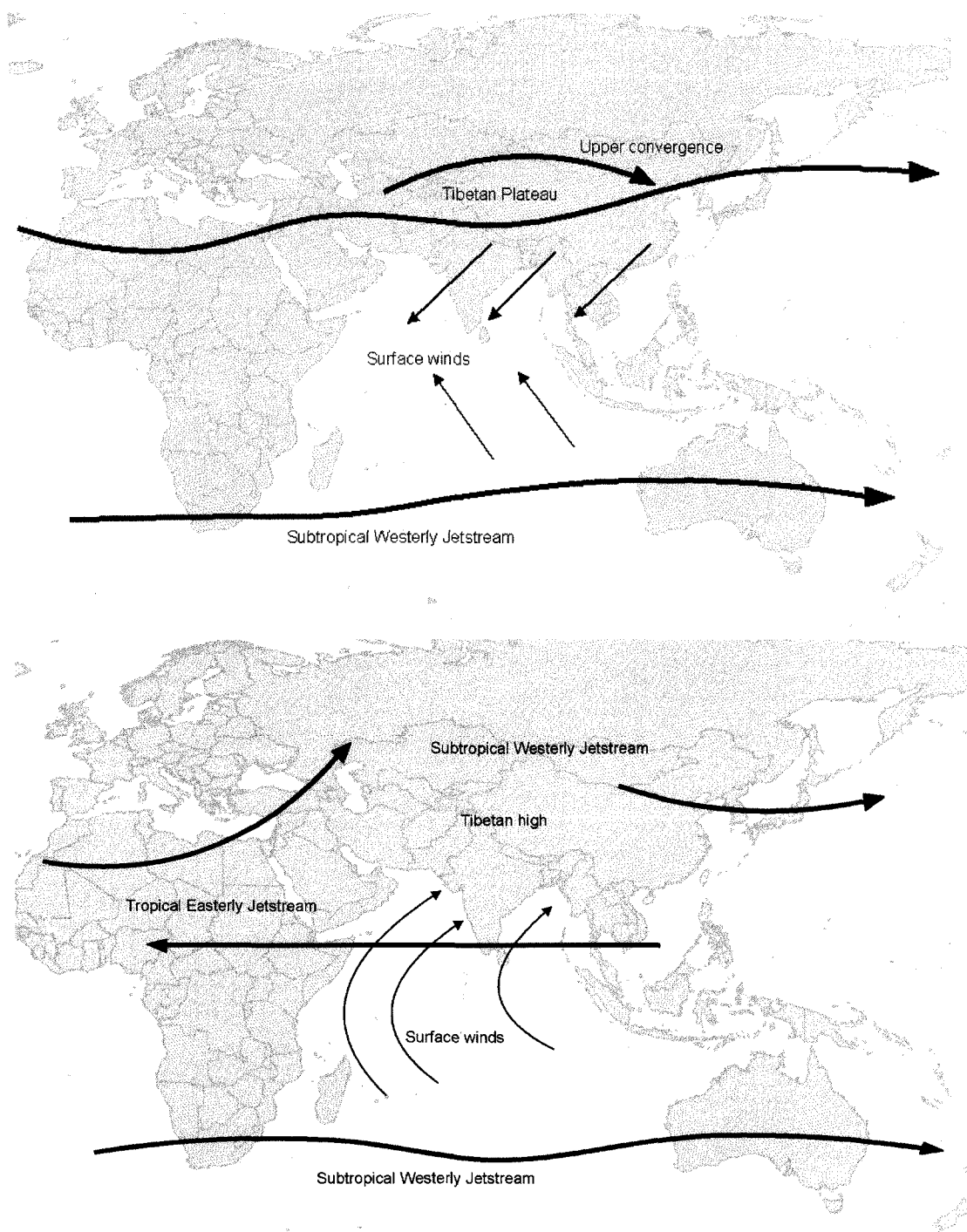
Figure 13. Average position of surface and upper atmosphere wind patterns in winter (top panel) and summer (bottom panel) (modified from Pant and Kumar, 1997).

upper atmosphere the subtropical westerlies dominate during the winter and the tropical easterlies dominate the region during the summer monsoon season.

Late Pleistocene paleoclimate of Southeast Asia

Because Southeast Asia is a climatically-sensitive region due to the balance between the summer and winter monsoon, the migrations of the ITCZ, and the high albedo caused by the abundance of many high-alpine glaciers and ice sheets, and because a large percentage of the world's population lives in this region, the climate in this region is important to understand. Data from proxy records in this region are difficult to interpret. In addition to major temperature variations that occur throughout geologic time, there are also significant variations in monsoon intensity that are related to changes in insolation, with a possible lag of several thousand years between insolation changes and the monsoon response (Clemens et al., 1991). A proxy such as the stable isotope signature can be affected by changes in the temperature of precipitation as well as by changes in amount of precipitation (Dansgaard, 1964). The study of proxy records from sediments of inland lakes involves additional challenges (Leng and Marshall, 2004). Of critical importance in interpreting a stable isotope record from lacustrine sediments is to understand the local hydrologic budget. Sources of water for a given lake can come from monsoonal rain which feeds regional rivers, from snowfall, or from melting of glacial ice. Ghosh and Bhattacharya (2003) examined the $\delta^{18}O$ values from snow, river, and glacial

meltwater in the Garhwal Himalaya and found isotopic signatures of -13.5‰, -13.0‰, and -20.3‰, respectively. Clearly, an understanding of local hydrologic conditions is essential to making sound interpretations regarding paleoclimate. Although changes in climate manifest themselves in a variety of ways, a majority of researchers have interpreted proxies as variations in monsoon strength or variations in temperature.

Records of monsoon variations

Fang et al. (1999) examined loess deposits in the Chinese Loess Plateau of Western China. The sediments record climate variability from 60 ka to present. One of the major proxies these researchers used was magnetic susceptibility of mineral grains, which can be used as a proxy for the wetness of a climate. During wetter periods the chemical weathering of soil minerals will produce a larger amount of fine-grained magnetic minerals. A higher magnetic susceptibility, therefore, is an indication of a wetter climate. Their study showed great variability in the wetness of climate during the past 60,000 years based on magnetic susceptibility (Figure 14). The authors identified 17 warm peaks during the last 60,000 years, each separated by around 1,000 – 2,000 years (Fang et al., 1999). These were interpreted as times of enhanced summer monsoons, and presumably also as times of warmer temperatures. A correlation of their data with data from the GRIP Greenland ice core shows that many of the wetter episodes correspond to Heinrich events recorded in the Greenland core. Thus, the authors interpret these data as indicating a correlation between increased summer monsoon strength in Southeast Asia with increased temperatures in

the North Atlantic. These data show no major change at the last glacial maximum

(LGM), but they do show a sharp decrease during the Younger Dryas cold period

(~12.0 ka) immediately followed by a large increase in magnetic susceptibility at
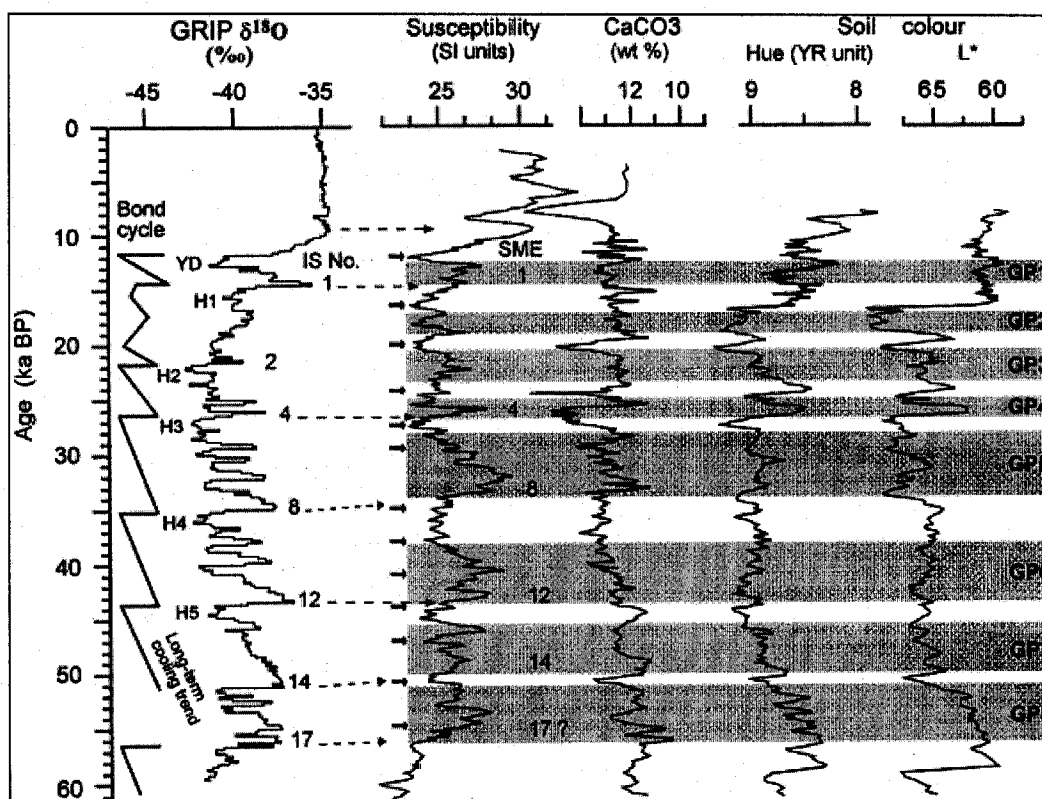
Figure 14. Comparison of magnetic susceptibility (and other) data to the GRIP
isotope record (from Fang et al., 1999). Reprinted with permission from
Elsevier.

around 11.0 ka. The authors interpret this as drier conditions during the Younger

Dryas cold period followed by very warm and wet conditions in the beginning of the

Holocene (10.0 ka). The conditions in the early Holocene appear to be warmer and

wetter than at present. The dry climate during the Younger Dryas is supported by

Hong et al. (2003), who examined peat deposits in a location in Tibet at 3400 meters above sea level (32°N, 102°E). This study also concluded a very weak monsoon during the Younger Dryas followed by a strengthening of the monsoon at 11.2 ka. Another important observation in this dataset is the large variability in monsoon strength during the Holocene in contrast to the relative stability of Holocene climate as is recorded in the Greenland ice core (Figure 14).

Kudrass et al. (2001) examined a similar time interval (~80 ka to present) recorded in a core taken from the Bay of Bengal, directly east of India. These authors also observed variations in monsoon strength with a frequency of 1,000 – 2,000 years and interpreted the variations as being synchronous with Dansgaard-Oeschger cycles in the North Atlantic. Summer monsoons were interpreted as being the most intense during the warmest part of the interstadials. With greater snow accumulation in the Himalaya, the summer monsoon would not develop to a high strength, and also the influence of the monsoon would not extend as far north as during warmer periods (Kudrass et al., 2001).

Lake sediments deposited from 42 ka to 28 ka at Goting, North India, which is close in proximity to the village of Burfu (see Figure 9), were analyzed by Ghosh and Bhattacharya (2003). The variations in stable isotopes of the lake sediments were also interpreted as variations in monsoon strength in North India. The authors identified 6 periods of enhanced southwest summer monsoon: 40.2 ka; 38.2 ka; 36.2 ka; 34.2 ka; 32.8 ka; and 29.4 ka. Three periods of more positive $\delta^{18}O$ values, signifying weakened summer monsoon, were also identified: 40.7 ka; 37.2 ka; and

35.2 ka. The times of enhanced summer monsoon, which signifies increasing precipitation, occur more frequently as the time approaches the LGM. Indeed, the last period of weakened summer monsoon occurred at 35.2 ka. The authors, in agreement with Kudrass et al. (2001), suggest a synchronous relationship between monsoon strengthening and Dansgaard-Oeschger warming cycles recorded in North Atlantic climate proxies.

Huang et al. (1997) examined a core from the northern South China Sea and also a lake core from central Taiwan that were deposited from 25 ka to present. The authors interpreted isotopic changes as reflecting changes in monsoon intensity during this time interval. Three basic climatic periods were interpreted from their results (Figure 15). The first period extends from 25.0 ka – 12.0 ka and is a period of strong winter monsoons during the last glaciation. This period is characterized by relatively high values (i.e. less negative) of $\delta^{18}O$, which the authors interpret as decreases in sea surface temperature (SST) in the South China Sea and increased productivity (i.e. increase in total organic carbon (TOC). The authors identify a period of moderate to weak monsoons from 12.0 ka – 10.0 ka. They interpret this period as a time of deglaciation. A final stage is interpreted from their data. This stage extends from 10.0 ka to the present and is characterized by enhanced summer monsoons, which is interpreted from the depleted $\delta^{18}O$ composition as well as the higher abundance of the thermophyte *Castanopsis*, which increases in abundance with an increase in moisture (Figure 16).
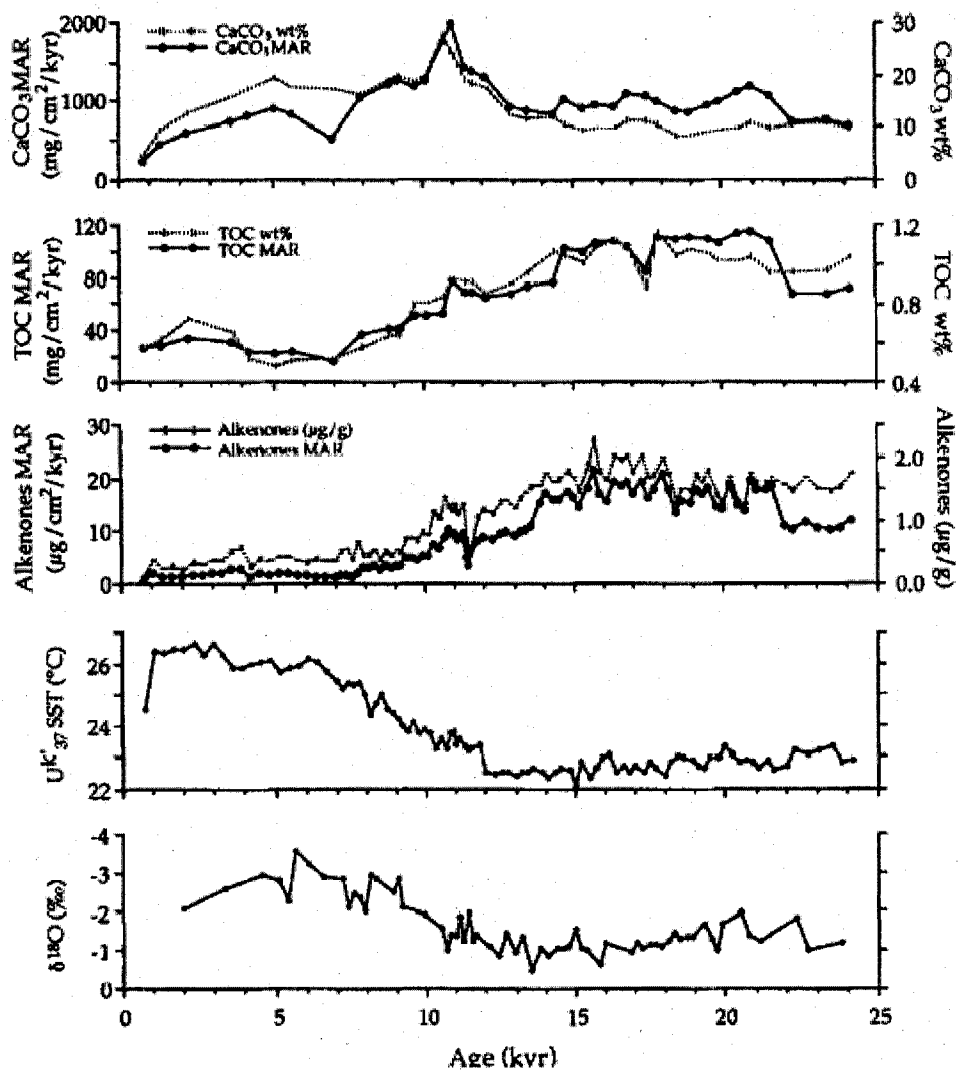
Figure 15. Paleoceanographic proxies of the South China Sea SO50-31 KL during the last 25,000 years (from Huang et al., 1997). Reprinted with permission from Elsevier.

A paleomonsoon record was also interpreted from a speleothem deposit in a cave in Eastern China (32°N, 119°E) (Zhao et al., 2003). This study was a high resolution examination of paleoclimate from 16.8 ka – 10.5 ka using $\delta^{13}C$ and $\delta^{18}O$ of
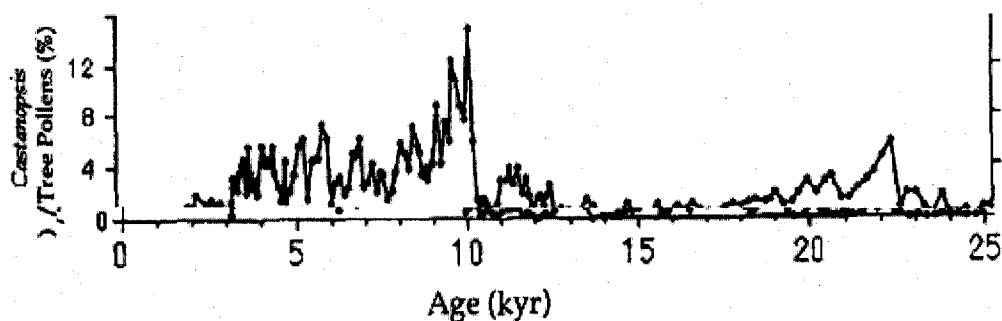
Figure 16. Abundance of *Castanopsis* in Toushe Lake core, central Taiwan (from Huang et al., 1997). Reprinted with permission from Elsevier.

speleothem calcite. In addition, the Tangshan speleothem was also correlated with two Greenland ice cores (GRIP and GISP2) (Figure 17). These data suggest an abrupt warming during 14.75 ka – 14.45 ka as is shown in the sudden ~2.8‰ decrease in $\delta^{18}O$ at that time. This occurs after the LGM when worldwide climate was in a state of warming. Differences between these paleoclimate records suggest that warming was not uniform across the world. However, the agreement in timing of the ~14.5 ka warming event suggests that this rapid warming event had a global extent. After an initial rapid warming, climate remained relatively warm and wet until about 12.5 ka – 11.5 ka, during which time isotopic values became less negative, indicating a drier climate. This was interpreted as the Younger Dryas cold period that is recorded in the Greenland ice cores. The transition to the Younger Dryas occurred as a gradual decrease in temperature beginning at 12.9 ka followed by a sharp jump at 12.5 ka (Zhao et al., 2003).
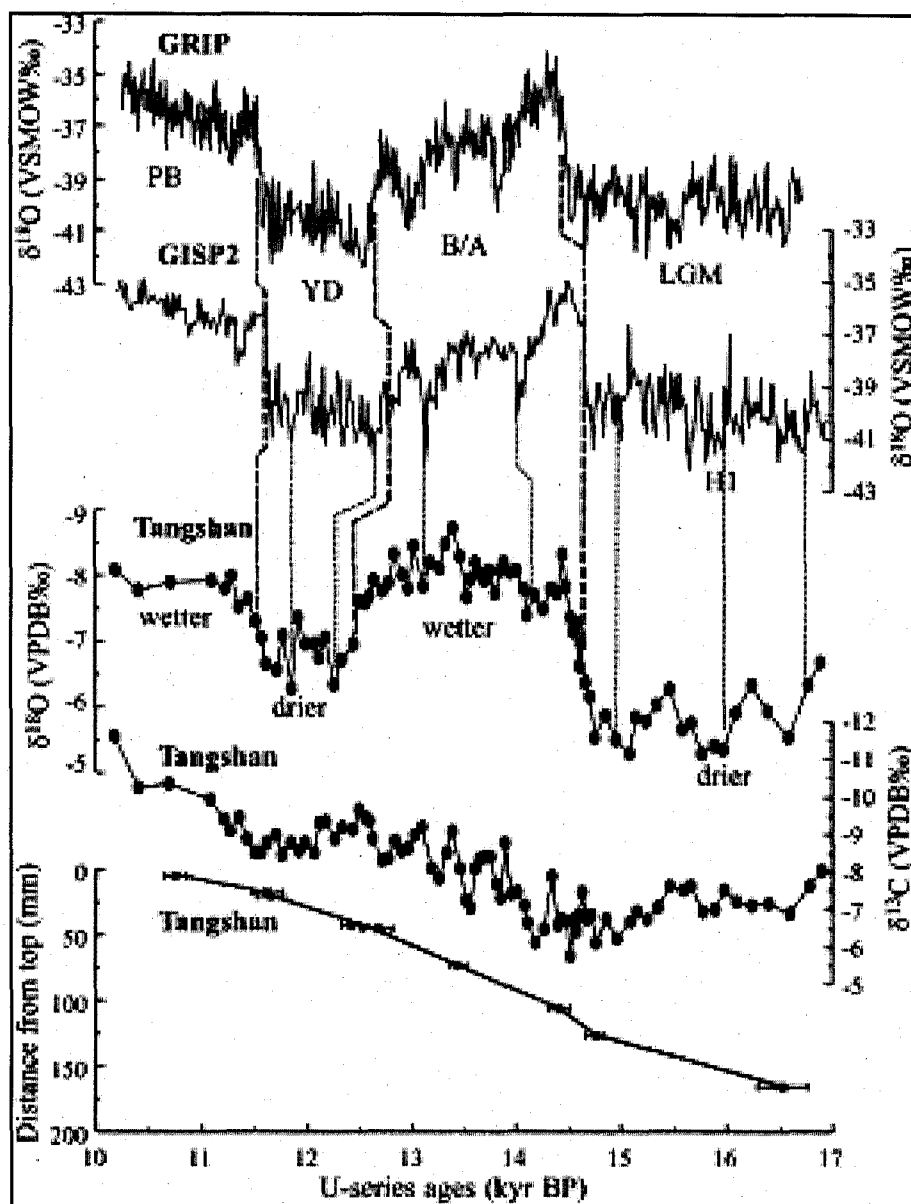
Figure 17. Comparison of isotopic data from stalagmite 996182 from Tangshan Cave and GRIP (from Zhao et al., 2003). Reprinted with permission from Elsevier.

Although isotopic values can be interpreted as proxies of temperature or of precipitation, among other things, the authors in this study interpret changes in isotopic compositions as recording changes in monsoon strength. The reason for this is that the isotopic composition of the calcite in the speleothem is a function of several parameters, one of which is temperature of the cave air. Cave air temperature is relatively constant year-round, depending on geographic location, and is not likely to change with changes in surface temperature. Therefore, a change in the isotopic composition of speleothems is most likely an indication of a change in the amount of precipitation (Zhao et al., 2003). Like other researchers, Zhao et al. (2003) indicate a weakened monsoon during the Younger Dryas. From their high-resolution data, however, they were able to interpret a stronger monsoon during the Younger Dryas than during the LGM. A conclusion drawn from their study is that rapid changes in monsoons parallel rapid temperature changes in the North Atlantic and are closely related to deglaciation (Zhao et al., 2003).

Late Pleistocene climate records have been obtained from speleothems in China and India. Sinha et al. (2005) examined a speleothem from Timta Cave, India (29°50'17"N, 80°02'01"E; 1900 m a.s.l.), a cave which is in relatively close proximity to the village of Burfu, India. The Timta Cave paleoclimate record spans the time interval from 15.5 ka to 11.5 ka and displays $\delta^{18}O$ values that are interpreted as changes in the strength of the Indian summer monsoon during the Bølling-Ållerød. The record shows a sharp decrease in oxygen isotope values at ~14.5 ka which is interpreted as strengthening of the monsoon. The monsoon remains strong from 14.5

ka to 12.7 ka, after which there is a sharp increase in oxygen isotope values, interpreted as a sharp decrease in the strength of the monsoon (Sinha et al., 2005). This is correlated with the onset of the Younger Dryas in the GISP2 core. The authors correlate the Timta climate record with a record from Hulu Cave, China (Wang et al., 2001) as well as with the GISP2 record (Stuiver and Grootes, 2000; Alley et al., 1993; Björck et al., 1998). The Hulu Cave record shows a great similarity, including evidence of a sharp decrease in oxygen isotope ratios at the onset of the Bølling-Allerød, and a sharp decrease in ratios at ~12.8 ka which is interpreted as the Younger Dryas. Wang et al. (2001) interpret oxygen isotope values as a proxy for the ratio of monsoon to non-monsoon precipitation in eastern China.

A study of sediments from the Arabian Sea also support a connection between climate changes observed in SE Asia and those observed in polar ice cores (Sirocko et al., 1993). Abrupt changes in values of $\delta^{18}O$ of *Globigerinoides ruber* indicate that the monsoon responded to gradual insolation changes in several abrupt events, occurring at 14,300, 13,500, and 13,060 ^{14}C years before present (yr BP). The authors suggest that these abrupt increases in monsoon intensity are the result of feedback mechanisms, including changes in albedo in the greater Tibetan Plateau area (Sirocko et al., 1993).

Records of temperature variations

Two significant studies in China and Tibet document temperature changes during the past ~35,000 ^{14}C years. Rhodes et al. (1996) examined lacustrine

sediments from China and interpreted past changes in temperature and moisture for Southeast Asia. From their data the authors identified a humid episode from 37,000 – 32,000 ^{14}C yr BP following an arid, colder period in the oldest section of the core. This time interval is characterized by a high percentage of carbonate minerals and a high percentage of LOM (lignocellulosic debris). A high LOM content suggests high amounts of surface runoff and soil erosion, which is consistent with warm temperatures and wetter conditions. Although their lacustrine core is continuous, the radiocarbon dates obtained within their core suggest a period of nondeposition at some point after 32,000 ^{14}C yr BP. The interval between 32,000 and 12,000 ^{14}C yr BP suggests colder, arid conditions associated with the LGM. The carbonate content of the core is minimal, and the sediments are primarily detrital. These factors suggest a period of nondeposition or erosion that could have resulted in the lake being reduced to a playa deposit during this interval. Following 12,000 ^{14}C yr BP laminated carbonate deposits begin to be present, suggesting that the lake was once again being fed. Warmer and wetter conditions are interpreted during this interval. At 10,000 ^{14}C yr BP there is an abrupt reduction of sedimentation, followed immediately by marl production in the lake. This observation, along with more positive $\delta^{18}O$ values, suggests that at this time the lake was well-established and that the early to mid-Holocene (~10,000 ^{14}C yr BP) was warmer and wetter than today, which agrees with Fang et al. (1999).

Wang et al. (2002) examined lake deposits from Tibet that were deposited from 30,000 ^{14}C yr BP to present. This study complements the work of Rhodes et al.

(1996) since the two cores cover similar areas in geography and time, and where

Rhodes et al. (1996)'s work lacks detail in the chronology between 32,000 and 12,000

^{14}C yr BP, this study contains detailed information during that time that can fill in this

gap. A positive correlation exists between δ^{18}O, δ^{13}C, and TIC and TOC (total

inorganic carbon, total organic carbon); this relationship was used to identify

paleoclimate variability (Figure 18). The authors identified the period prior to 29,000

^{14}C yr BP as a relatively warm episode of glacial melting and the birth of the lake.
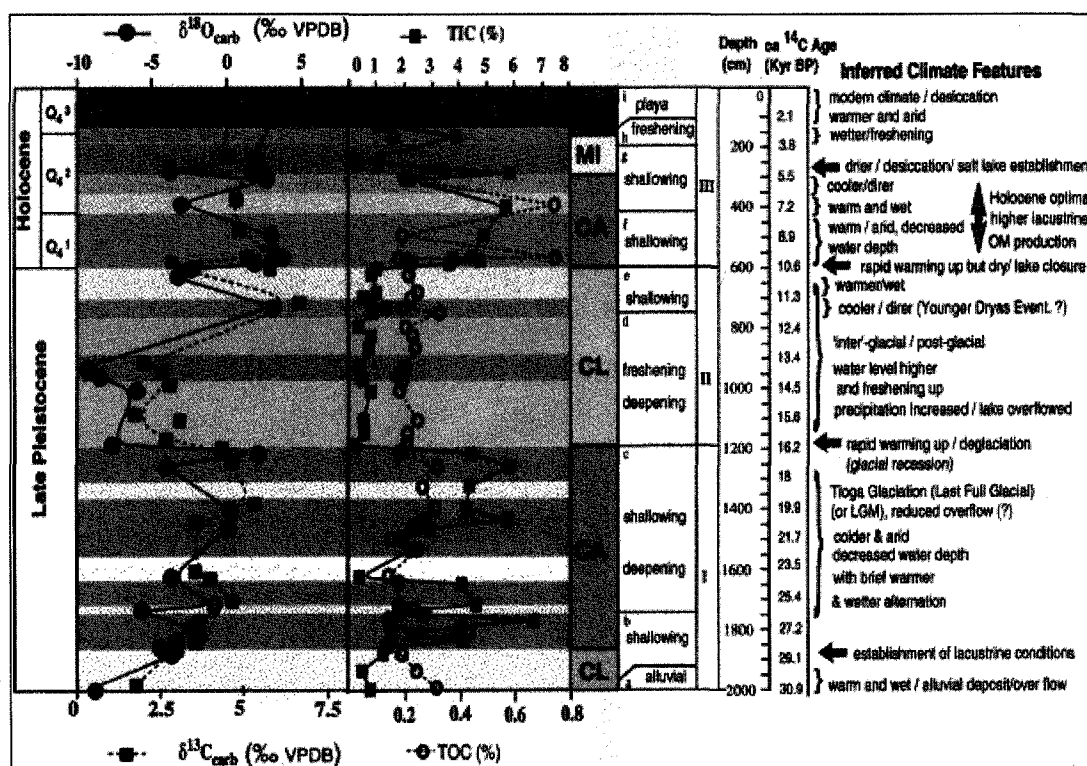
Figure 18. Carbon and oxygen isotope data and TIC and TOC data from core ZK2
from Zabuye lake sediments over the last 30,000 years (from Wang et al.,
2002). Reprinted with permission from Elsevier.

The interval spanning 29,000 to 16,000 ^{14}C yr BP is characterized by more positive $\delta^{18}O$ ratios as well as relatively high percentages of TIC and TOC. This is interpreted as being a cold and arid glacial period during the LGM, with low humidity and long residence time of lake water resulting in heavy isotopes due to evaporation. An abrupt change occurs at 16,000 ^{14}C yr BP. This signifies a warmer, wetter period that extends until 10,600 ^{14}C yr BP. This warm period began suddenly and was briefly interrupted by a sudden cooling from 12,000 – 10,500 ^{14}C yr BP, which correlates to the Younger Dryas cold interval. Rapid changes occur after this, including a sudden warming event at 10,600 ^{14}C yr BP.

These studies suggest that climate is extremely variable and high magnitude climate changes can occur very rapidly. The studies also suggest a strong connection between temperature changes worldwide and the strength of the monsoon in Southeast Asia. Small scale warming and cooling cycles, including Heinrich events and Dansgaard-Oeschger cycles, might be evident in Southeast Asia climate records, but additional studies are needed to confirm this.

Lacustrine sediments spanning the interval from 20 ka to 11 ka in the vicinity of Burfu near the village of Garbayang, India, were studied by Juyal et al. (2004). The authors interpret small-scale oscillations in magnetic susceptibility as indicating a cold and unstable climate from 20 ka to 13 ka. A short, warm event occurs at 13 ka, followed by larger climate changes, including a cold interval with high amounts of glacial meltwater, occurring from 13 ka to 11 ka. The cooling event is interpreted based on a drop in magnetic susceptibility values and lower concentrations of

aluminum, iron, and titanium oxides, which the authors use as proxies for physical weathering of glacial materials. Also, a gravel layer in the relict lacustrine sediments near Goting dates to 11 ± 1 ka. The authors argue that this cold event is the first documented evidence of the Younger Dryas in the Indian Subcontinent (Juyal et al., 2004).

A seminal record of paleoclimate over the Tibetan plateau is derived from a 300 meter ice core taken from the Guliya Ice Cap at 6710 meters above sea level (Thompson et al., 1997). The climate record extends from the Holocene to as old as ~500 ka. The record suggests that subtropical climate is tied closely to solar forcing, with a strong influence by precession (23,000 year cycle), and a weaker influence by obliquity (41,000 year cycle). Oxygen isotope values are a proxy for temperature, with the lowest values occurring at the LGM and other stadials (Thompson et al., 1997). There is an increase of 5.4‰ in $\delta^{18}O$ values from the LGM to the Holocene. The deglaciation sequence (from 15 ka to the Holocene) in the Guliya record shows a closer resemblance to an ice core taken from Huascarán (Peru) (Thompson et al., 1995) than to polar cores, suggesting a similar climatic response between these regions than between Tibet and the poles.

Relatively few studies have been done on Late Pleistocene – Holocene paleoclimate on the Indian subcontinent. Many of the above referenced works were done north or east of the Himalaya. Studies in India are significant because the influence of the Indian monsoon does not extend to the north of the Himalaya. The Himalaya range acts as an effective barrier between climates and wind patterns in

China and those in India. This study on the Burfu lake deposits provides high-resolution paleoclimate data from ~16 – 11 ka in this particular region. It clearly shows how the monsoon changes in strength going from a time of deglaciation (after the LGM) into the beginning of the Holocene.

CHAPTER III

METHODS

Acquisition of samples

During the summer of 2003 researchers led by Dr. Navin Juyal from the Planetary and Geosciences Division of the Physical Research Laboratory, Ahmedabad, India, conducted field work in North India near the borders of Tibet and Nepal to collect samples from relict lake deposits near the village of Burfu. Similar expeditions have been made by this team of scientists to relict lake deposits in this region near Garbayang (Juyal et al., 2004) and Goting (Ghosh and Bhattacharya, 2003). Approximately 250 samples were collected from a ~20 meter thick exposure for the purpose of stable isotope analysis. In addition to this, seven samples were also collected for luminescence dating. The samples collected for stable isotope analysis were transported to the Stable Isotope Geochemistry lab at Western Michigan University.

Laboratory analysis

Preparation of the organic fraction

A portion (~10 grams) of each sample was placed in a 15 ml plastic centrifuge tube and washed with ~10 ml of 0.5N HCl for the removal of carbonates. This was allowed to react for 1 – 2 hours, after which the samples were centrifuged to separate

42

the sample from the acid. The acid was decanted, and additional acid was added. Each sample received three acid washings. After decanting the acid from the third acid washing, DI water was added to the centrifuge tube. Washing of samples was repeated until a neutral pH was attained. The centrifuge tubes were covered with aluminum foil with several small holes poked into the top. These tubes were placed in an oven at approximately 100°F until the organic residue samples were dry.

Approximately 80 mg of carbonate-free residue was weighed and placed in a 9 mm diameter quartz tube along with CuO shavings. The quartz tubes with samples were heated and stretched near the top of the tube to produce a smaller diameter for easier sealing while on the vacuum extraction line. Sample tubes were then placed on a vacuum extraction line for the purpose of evacuation of the air in the tubes. Tubes were sealed with a blowtorch once a vacuum was attained. These tubes were placed in a furnace where they were heated to 900°C for three hours in order to combust the organic carbon to CO_2 gas.

After combustion, each sample tube was placed within a larger diameter tube that was connected to a vacuum extraction line. After air in the larger tube was evacuated, the sample tube was opened by moving a metal ball (within the larger tube) with a magnet (outside the tube) against the tip of the sample tube until the sample tube broke open. This released the gases that were products of the combustion reaction into the vacuum extraction line. The gases (CO_2 and H_2O) were frozen in a liquid nitrogen trap, and any noncondensable gas (i.e. N_2) was collected by means of a Toepler pump. The yield of N_2 gas was measured and recorded and the

gas was pumped away. The liquid nitrogen trap was converted to a 'slush' trap, consisting of of dry ice dissolved in alcohol; the slush was prepared to a temperature of -70°C. The liquid nitrogen was placed on a volume-calibrated tube (coldfinger). This change of traps allowed the H_2O to remain frozen while the CO_2 expanded and was trapped in an area where it could be isolated and where its volume could be measured. After measuring the yield of CO_2, the sample was collected in a sample-collection tube for isotopic analysis.

Preparation for carbonate analysis

Samples for carbonate analysis were prepared according to the method of Krishnamurthy et al. (1997). A small amount of each sample (~10 mg) was weighed and placed in the bottom of a septum tube. A boat made from 6 mm Pyrex tubing was glued to the inside of each septum tube. 100% phosphoric acid was placed in the boat, after which the septum tube was evacuated on a vacuum extraction line. Evacuated septum tubes were placed in a constant temperature bath at 25°C until the sample and acid reached this temperature. The septum tubes were then tipped for the acid to spill out of the boat and react with the sample at the bottom of the tube. Septum tubes were placed back in the constant temperature bath immediately after the reaction began, and they were allowed to react at a constant temperature for 24 hours.

After the reaction, each septum tube was connected to a vacuum extraction line by means of an extraction needle. The needle was inserted into the septum without passing through it in order to evacuate the space within the needle. The

needle was then pushed all the way through the septum in order to introduce the sample gases to the extraction line. CO_2 and H_2O were frozen in a liquid nitrogen trap, after which the H_2O was retained by a dry ice slush while the CO_2 was allowed to expand and was trapped via liquid nitrogen in the volume-calibrated coldfinger. The CO_2 was allowed to expand in the coldfinger, the pressure was recorded, and the CO_2 sample was collected in a sample collection tube.

Stable isotope ratio determination

All samples were converted to CO_2 in the process described above, after which the samples were introduced into a Micromass-Optima isotope ratio mass spectrometer. Samples were analyzed with respect to an internal lab standard and the results were given with respect to the Peedee Belemnite formation (VVPDB) in standard per mil (‰) notation as follows:

$$\delta\text{‰} = [(R_{sample}/R_{standard}) - 1]\, 10^3$$

where R is the ratio of the heavy to the light isotope ($^{18}O/^{16}O$, $^{13}C/^{12}C$). Analytical precision for $\delta^{13}C$ is 0.1‰ and for $\delta^{18}O$ is 0.2‰. Data were recorded and analyzed in Microsoft Excel®. Included in the data were organic residue sample weight, carbonate sample weight, yield of N_2 from organic sample, yield of CO_2 from organic sample, yield of CO_2 from carbonate sample, $\delta^{13}C$ from organic CO_2, $\delta^{13}C$ from carbonate CO_2, and $\delta^{18}O$ from carbonate CO_2. Percent nitrogen, percent organic

carbon, and percent carbonate were calculated from the yields of the respective compounds. C/N ratios were calculated by dividing the yield of CO_2 by two-times the yield of N_2. In order to eliminate random variations due to the coarseness of sampling (1 sample per approximately 20 years) all data were smoothed with a 5-point running average.

CHAPTER IV

CHRONOLOGY

Optically-stimulated luminescence

Seven samples for luminescence dating were collected from freshly exposed trenches using specially designed aluminum pipes (Chandel et al., 2006). Basic principles of luminescence dating are discussed in Singhvi et al. (2001). Samples were treated with 10% HCl and 30% H_2O_2 to remove the carbonate and organic carbon, respectively. This was followed by dry sieving and a narrow grain size (210 - 150 μm to 150 - 105 μm) was obtained and quartz and feldspar minerals were separated using Na-polytungstate (ρ= 2.58 g/cm^3). Quartz samples were further etched for 80 minutes in 40% HF and then treated with 12N HCl for 30 minutes. The etched grains were mounted as a monolayer on stainless steel discs using Silkospray™ and the purity of these grains was checked by infrared stimulated luminescence. All the samples were stimulated using blue-green light stimulation source provided with a Riso TA-DA-15 reader. The detection optics comprised 2×U-340 and BG-39 filters. Beta irradiation was made using a 25 mCi ^{90}Sr / ^{90}Y source. The dose-rate estimates relied on thick source ZnS(Ag) alpha counting for elemental concentrations of uranium and thorium, whereas the potassium concentration was estimated using gamma ray spectrometry (hyper-pure germanium detector). A constant cosmic ray dose of 190μGy/yr was used.

47

The samples were analyzed using the single aliquot regeneration (SAR) protocol of Murray and Wintle (2000). In the SAR method, estimation of the paleodose is made on single aliquots by recording its natural luminescence and then reconstructing a regenerated luminescence versus dose growth curve corrected for the sensitivity changes using a fixed test dose. Optically Stimulated Luminescence (OSL) photon count for fixed test dose was used to monitor and correct for the sensitivity changes during irradiation, preheat and read out cycles (Murray and Roberts, 1998). The aliquots were preheated to 240°C for 10 seconds and the cut heat was 200°C for 0 seconds. The sensitivity corrected luminescence intensity from a virgin sample is then read on this growth curve to estimate the paleodose. Typically about 50 – 60 discs were measured and of these around 20 – 40 satisfied the criterion of a recycling ratio of 0.90 – 1.10.

The paleodose for age calculations was based on a weighted mean of values in the region defined by the minimum value and the minimum value + (2 × error). Typically, about 5 – 10 paleodoses belonged to this realm. Table 2 provides the details of radioactivity assays, dose rate and SAR ages (both minimum and mean). Stratigraphic locations of OSL ages are shown in Figure 21.

<center>Radiocarbon</center>

In addition to the OSL ages, AMS ^{14}C ages from six bulk organic carbon samples and from five authigenic carbonate samples were obtained. Sediment

samples were converted to CO_2 gas in the Stable Isotope Geochemistry Lab at WMU

and sent

Table 2. OSL ages of the Burfu lake succession.

Sample No.	U (ppm)	Th (ppm)	^{40}K (%)	Dose Rate (Gy/ka)	De (Gy)	Age (ka)
BLTL-13	3.82±0.06	19.3±0.3	2.6±0.03	3.9±0.5	44±1	11±1
BLTL-10	3.14±0.05	16.1±0.3	1.81±0.02	3.1±0.4	38±1	12±2
BLTL-9	3.24±0.05	16.6±0.3	2.11±0.02	3.4±0.4	28±1	8±1
BLTL-6	3.01±0.04	17.0±0.2	1.41±0.01	2.8±0.4	37±1	13±2
BLTL-5	3.28±0.05	18.5±0.3	2.47±0.02	3.7±0.5	54±2	14.5±2
BLTL-2	3.15±0.05	20.5±0.3	1.64±0.01	3.2±0.4	48±2	15±2
BLTL-1	3.4±0.05	21.1±0.3	1.66±0.02	3.3±0.4	53±1	16±2

Cosmic ray dose assumed 190±40 µGy/a; Water content assumed 20%

to the University of Arizona AMS laboratory for dating. Results are shown in Table 3. Two samples, Ind-E-org, and Ind-B-carb, were lost. In addition, three samples, Ind-66-W, Ind-161-W, and Ind-202-W, were of wood fragments found in the sediment.

Samples from organic carbon give ages ranging from 16,840 to 13,170 ^{14}C yr BP, and samples from the carbonate fraction give ages ranging from 27,300 to 16,524 ^{14}C yr BP. The ages, however, do not coincide with the classic geologic principles of superposition; samples with older ^{14}C ages are at higher stratigraphic positions than samples with younger ^{14}C ages.

In order to explain these stratigraphic anomalies, an understanding of carbon cycling and ^{14}C dating is required. The upper atmosphere is the source of ^{14}C, where it is generated from the reaction of N_2 with cosmic-ray neutrons. Vegetation takes in

$^{14}CO_2$ during photosynthesis and an equilibrium is reached between the ^{14}C concentration within living vegetation and the ^{14}C concentration of the atmosphere

Table 3. Radiocarbon ages of the Burfu lake succession.

Univ. of Arizona sample ID	WMU Sample ID	Elevation from bottom (m)	Suite Material	$\delta^{13}C$	F ^{14}C	^{14}C age BP
AA64512	Ind-A-org	3.6	CO_2	-23.4	0.1940+0.0029	13,170+120
AA64513	Ind-B-org	6.6	CO_2	-23.7	0.1940+0.0018	13,173+72
AA64514	Ind-C-org	11.2	CO_2	-23.8	0.1744+0.0033	14,030+150
AA64515	Ind-D-org	13.9	CO_2	-24.2	0.1515+0.0025	15,160+130
AA64516	Ind-E-org	15.4	CO_2	M		
AA64517	Ind-F-org	18.3	CO_2	-23.9	0.1920+0.0018	13,257+75
AA64518	Ind-G-org	19.1	CO_2	-24.9	0.1229+0.0015	16,840+100
AA64519	Ind-A-carb	3.6	CO_2	-3.1	0.1278+0.0014	16,524+87
AA64520	Ind-B-carb	6.6	CO_2	M		
AA64521	Ind-C-carb	11.2	CO_2	-1.8	0.0334+0.0012	27,300+280
AA64522	Ind-D-carb	13.9	CO_2	-1	0.0558+0.0014	23,180+200
AA64523	Ind-E-carb	15.4	CO_2	-1.8	0.0359+0.0012	26,720+260
AA64524	Ind-G-carb	19.1	CO_2	-0.9	0.0694+0.0013	21,440+150
AA64525	Ind-66-W	8.0	CO_2	-24.1	1.1121+0.0049	post-bomb
AA64526	Ind-161-W	12.7	CO_2	-24.1	1.1229+0.0063	post-bomb
AA64527	Ind-202-W	15.9	CO_2	-23	1.2765+0.0054	post-bomb

where it is generated. Since ^{14}C is constantly being generated in the atmosphere, terrestrial vegetation that takes in CO_2 from the atmosphere contains ^{14}C concentration in equilibrium with the atmosphere. When this vegetation dies, it no longer exchanges ^{14}C with the atmosphere, and its ^{14}C concentration will begin to decrease. A radiocarbon age of this material would represent the time at which the

vegetation died. [14]C ages are determined by measuring the concentration of ^{14}C in the sample in units of disintegrations per minute per gram of carbon (dpm/g C), denoted by A, and comparing this value to an oxalic acid standard, denoted by A_o. Wood that was alive between 1840 and 1860 contains 95% of the ^{14}C concentration of the oxalic acid standard (Faure, 1977). Thus, the age given by a ^{14}C date is the age of death of a sample, i.e. the age when it no longer took in ^{14}C from the atmosphere. This age is given in ^{14}C years before present, where present is 1950. Carbon ages are calculated by the following equation:

$$A = A_o e^{-\lambda t}$$

The unknowns A and A_o are defined above, and λ is a constant based on the half-life of ^{14}C, which is 5730 years (Godwin, 1962), and t is years before present, with present being 1950.

In terrestrial organic material, such as vegetation, carbon is primarily attained from CO_2 in the atmosphere. The determination of the ^{14}C age of the sample is relatively straightforward.

However, dating lacustrine samples by means of ^{14}C can be problematic. If the dissolved inorganic carbon (DIC) is in equilibrium with atmospheric CO_2, the ^{14}C concentration of the vegetation will not be contaminated by older carbon sources, and hence the ^{14}C age will be reliable. However, this is rarely the case. Often DIC is comprised of carbon from sources other than the atmosphere. One of the sources for

DIC is dissolved marine carbonate rocks. Marine carbonate rocks can have a wide range of ages, most, if not all, of which are on the order of millions of years old. Radiocarbon ages can extend to ~50,000 ^{14}C yr BP, beyond this time the ^{14}C concentration in the sample is negligible, and an accurate date cannot be attained. Such samples are said to contain "dead" carbon, as they are beyond the dating capabilities of modern analytical techniques.

Therefore, when aquatic vegetation take in carbon, a portion may be derived from atmospheric CO_2, the ^{14}C of which is being constantly replenished, and a portion may also come from DIC, which may be derived from dissolved marine carbonate that contain "dead" carbon. This is particularly the case in lacustrine environments near carbonate bedrock. When this occurs, the concentration of ^{14}C within the aquatic vegetation is always less than the concentration of ^{14}C in the atmosphere, as only a portion of the carbon is derived from the atmosphere. The remaining portion of carbon is derived from DIC, which may be completely depleted of [14]C. This phenomenon is known as the "hardwater effect", and the resulting ^{14}C ages are anomalously old.

Erroneous ^{14}C ages were anticipated in this study due to the abundance of carbonate bedrock in the catchment area and due to prior documentation of the hardwater effect in this region (e.g. Juyal et al., 2004). The carbon dates were therefore rejected because of probable contamination due to the hardwater effect. The anomalous carbon ages, however, can provide important insight into the geochemical cycling within the lacustrine environment. This is discussed in Chapter VI. Despite

large errors on the OSL ages, OSL ages were used for this study and as a best-case scenario a constant accumulation rate was used. This may not be true *sensu stricto* but a glance at Figure 19 indicates that due to a limited range of ages (~11 to 16 ka) there can not be much variability between any sedimentation model that can be applied to these ages compared to the constant sedimentation rate. It is unlikely that the interpretations in this study would change appreciably with a variable sedimentation rate. The age model for the Burfu lacustrine section was calculated by performing a weighted linear least squares regression on six OSL ages (Figure 19).
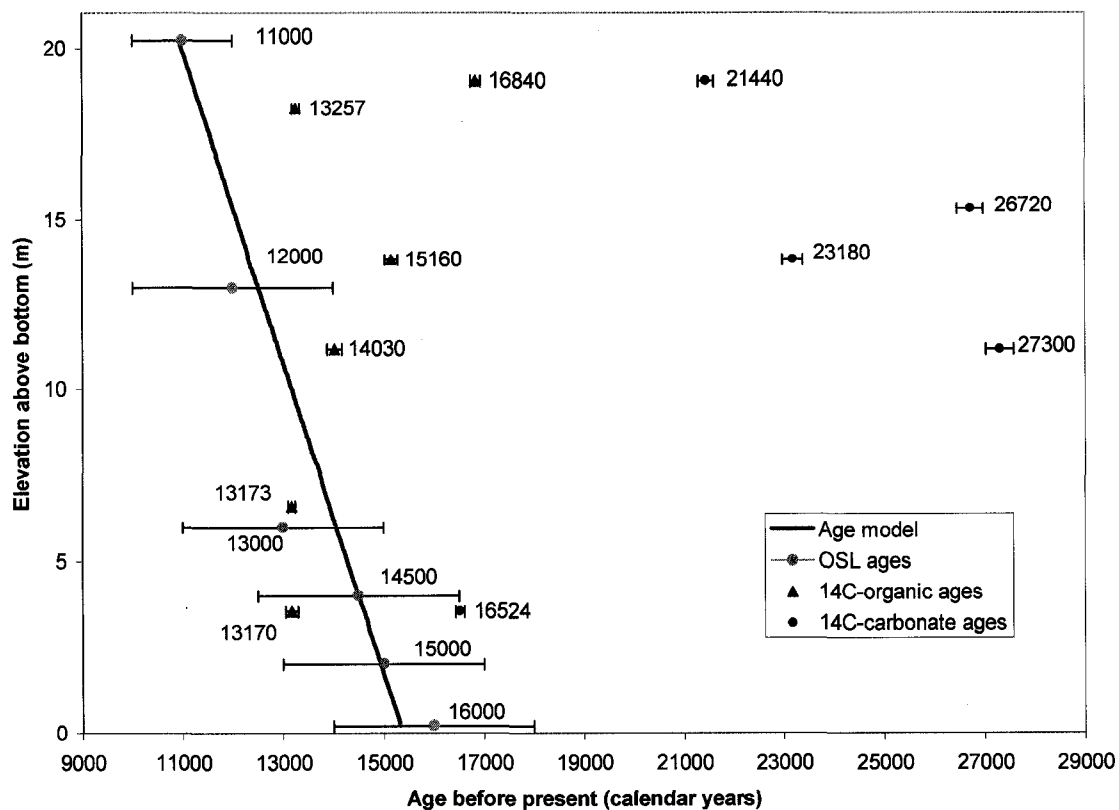
Figure 19. Age model of the Burfu section. Purple squares are OSL ages (in calendar years); orange triangles are ^{14}C ages from bulk organic material; brown circles are ^{14}C ages from carbonates; age model is shown as a blue solid line. ^{14}C ages are expressed in uncalibrated radiocarbon years BP, however, the y-axis is in calendar years. This figure is not intended as a quantitative analysis of all dates, rather as a model of OSL ages and a relative comparison of hardwater effect in ^{14}C ages.

CHAPTER V

RESULTS

Sedimentology and stratigraphy

Broadly three sedimentary units can be discerned (Fig. 20). The lowermost
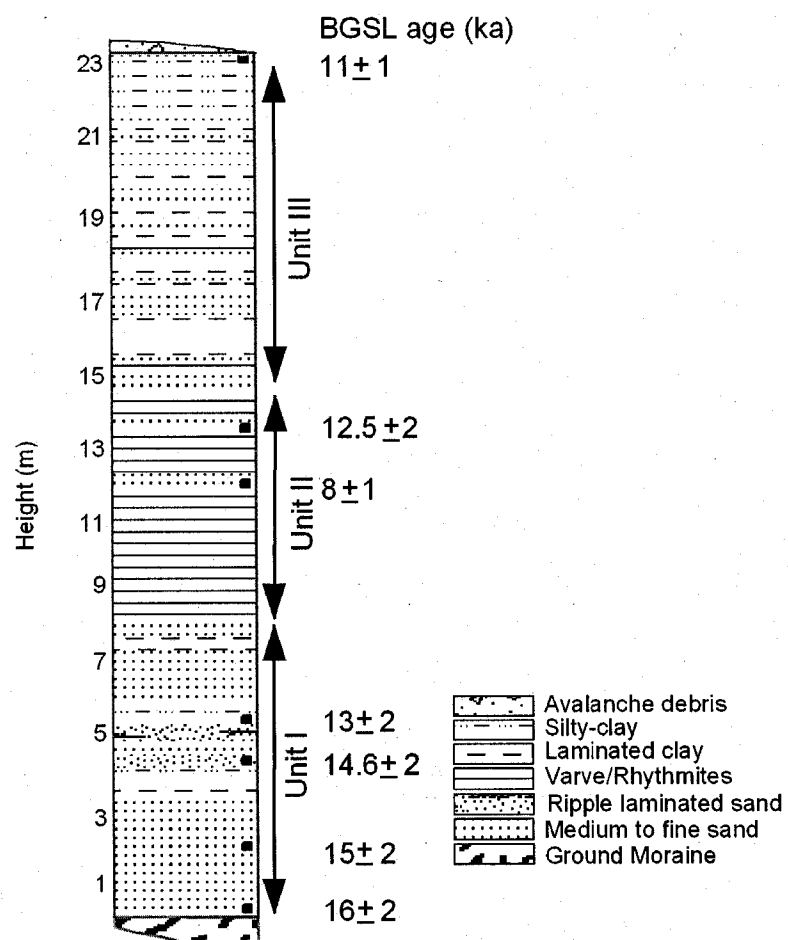
Figure 20. Sedimentology of the Burfu relict lake deposits.

55

Unit-I (7.2 m) that overlies the ground moraine is dominantly well-sorted medium to fine sand with occasional clay laminae. This is overlain by intermediate Unit-II (6.2 m), comprising clay rich varve/rhythmites with mm- to cm-thick sand intercalations. At places drop stones were observed embedded in the varve layers. The uppermost Unit-III (10 m) is comprised of thicker internally laminated clay horizons (maximum 120 cm). The clay horizons are generally separated by medium to fine sand layers (maximum 30 cm). The succession terminates with the deposition of ~2 m thick debris-flow deposits.

Geochemical results

Organic carbon

The percent organic carbon varies from 0.04 to 0.25% (Figure 21). The amount of organic carbon at 15.5 ka is 0.1% and rises to nearly 0.15% at 14.9 ka. This is followed by a decline in percent organic carbon from 0.15% to 0.06% during the time interval from 14.9 to 14.2 ka. This is followed by another rise in percent organic carbon from 0.06% to 0.17% at 13.8 ka. The time interval from 13.8 ka to 12.3 ka is characterized by an overall declining trend in percent organic carbon that includes two major abrupt spikes in percent organic carbon. One of these spikes is at 13.5 ka, when percent organic carbon went from 0.07% to 0.24%. The second major spike is at 13.2 ka, when organic carbon went from 0.12% to 0.20%, and shortly thereafter to 0.05%. The percent organic carbon reaches its lowest value of 0.04% at

12.0 ka. After this values rise and remain relatively steady from 0.8% to 0.13% during the time interval from 11.9 ka to 11.0 ka.
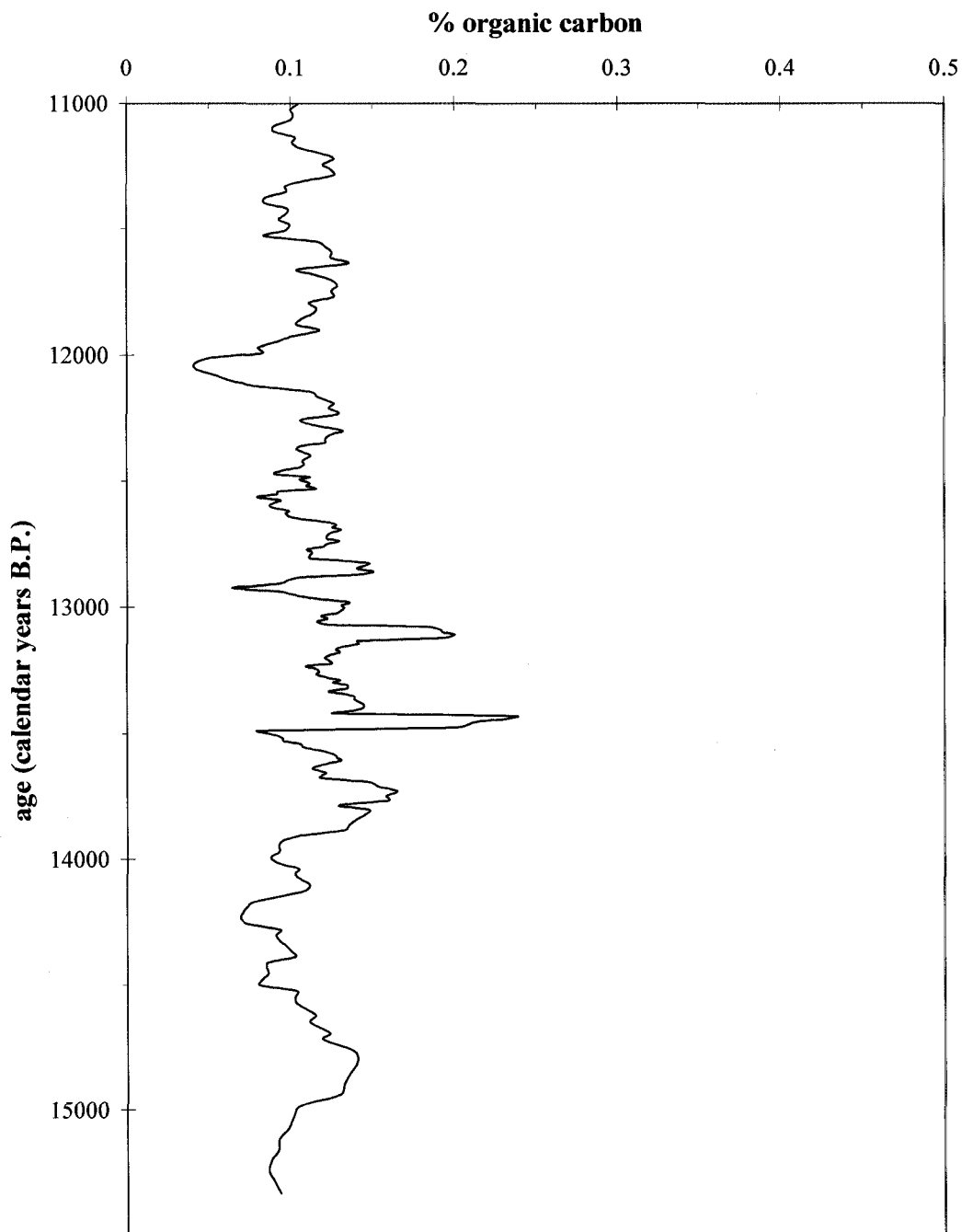
Figure 21. Percent organic carbon of Burfu samples.

C/N ratios display a narrow range from 3 to 8 for most of the sediments

(Figure 22). The beginning of the lake core consists of C/N ratios of 9, followed by a
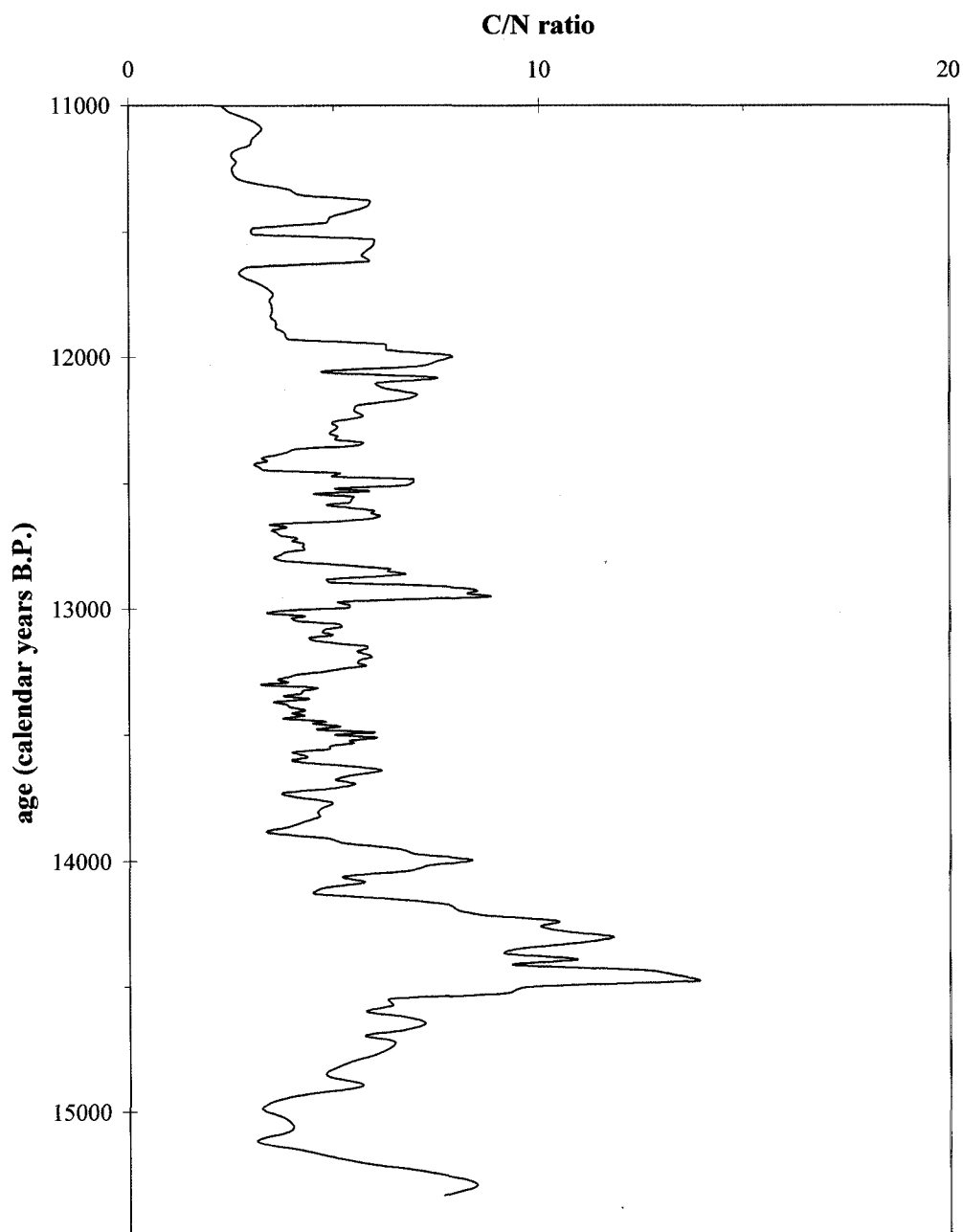
C/N ratio

Figure 22. C/N ratio of Burfu samples.

negative shift to 3 at 15.1 ka. Ratios steadily increase from 3 to 6 from 15.1 ka to 15.5 ka, after which there is a sharp spike to C/N ratios near 14, the highest values attained in the core. C/N ratios remain greater than 10 from 15.5 ka to 15.2 ka, after which they decline to values near 5. During the time interval from 14.5 ka to 11.3 ka C/N ratios remain fairly constant near 5. This interval is also punctuated with minor spikes with values around 9. These spikes occur at 14.0 ka, 13.0 ka, and 12.0 ka. Immediately following the last spike, C/N ratios drop to values near 3 at 12.0 ka where they remain until 11.6 ka, after which they oscillate between 6 and 3 from 11.6 to 11.3 ka. From 11.3 ka to 11.0 ka C/N ratios are around 3 to 4.

Values of $\delta^{13}C_{organic}$ are displayed in Figure 23. Isotope values of carbon display a narrow range from -27‰ to -23‰ (VVPDB), with values averaging approximately -24‰. Low values occur at 14.9 ka, 14.5 ka, 13.8 ka, 13.4 ka, 12.5 ka, and 11.3 ka, with the lowest value of -27% occurring at 12.5 ka.
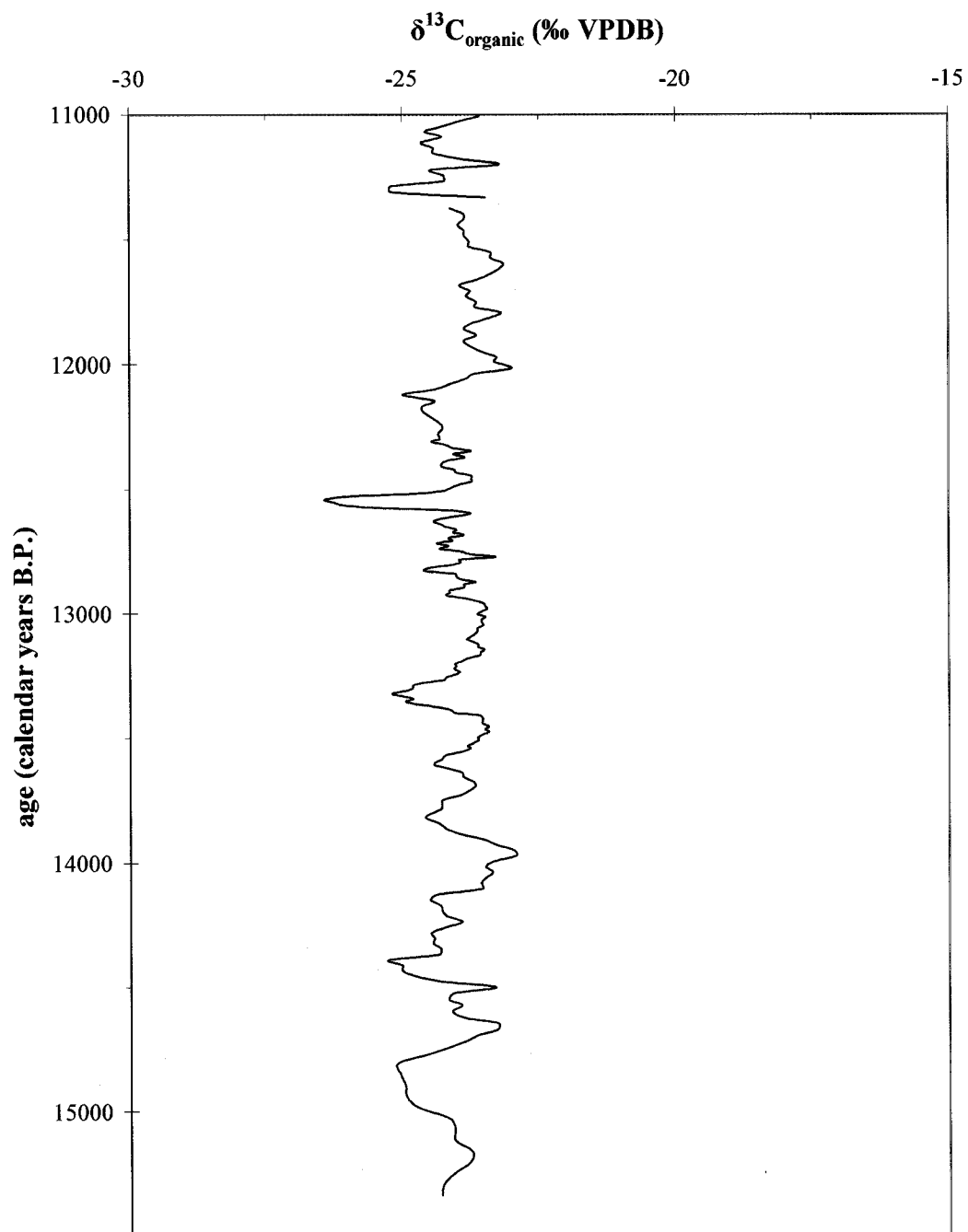
Figure 23. $\delta^{13}C_{organic}$ of Burfu samples.

Carbonate

Percent carbonate is displayed in Figure 24. The percentage of carbonate at
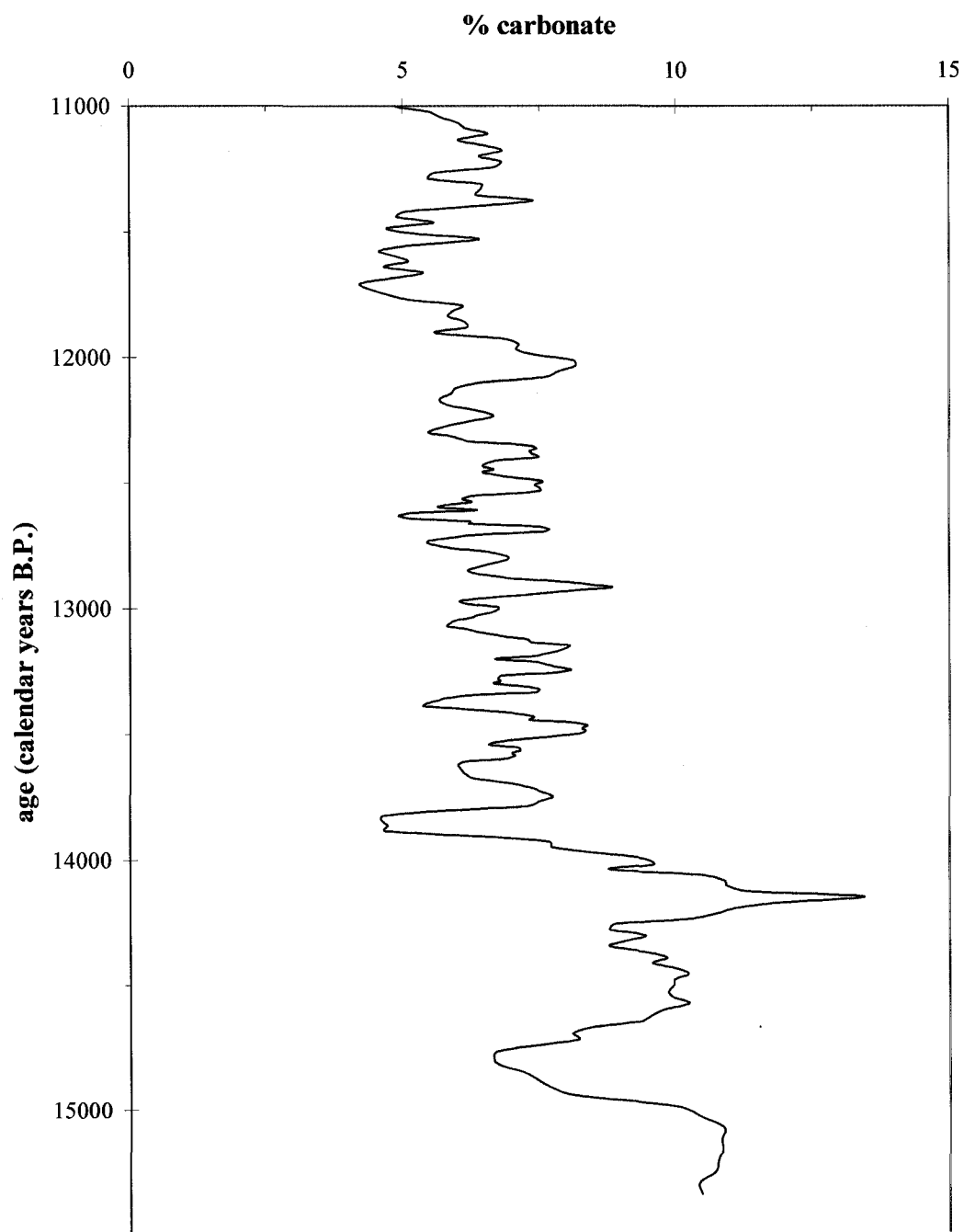
Figure 24. Percent carbonate of Burfu samples.

15.5 ka is approximately 11% and remains constant until 15.0 ka, when it falls sharply to 7% at 14.9 ka. Following this, percent carbonate climbs to approximately 10% at 14.6 ka and remains relatively constant until 14.4 ka. From 14.4 ka to 14.2 ka percent carbonate climbs sharply from 10% to 13%, the highest values attained in this core. Percent carbonate falls sharply during the time interval from 14.2 ka to 14.0 ka from 13% to slightly less than 5%. Between the time interval from 13.9 ka to 12.1 ka percent carbonate values remain fairly constant, ranging from 5% to 8%. Percent carbonate values fall from 8% at 12.1 ka to approximately 4% at 11.8 ka, which is the lowest percentage of carbonate in the core. From 11.8 ka to 11.0 ka there is a slight increase in values to approximately 7%, followed by a minor decline to 5%.

Stable isotope ratios of oxygen are presented in Figure 25. Oxygen isotope values show great variability and show an overall enriching trend from -15‰ to -10‰ (VVPDB). An increase of 2‰ from 14.5‰ to 12.5‰ at 14.6 ka is followed by a decrease in 2‰ in $\delta^{18}O$ values to -14‰, after which there is a steady enrichment in oxygen isotope values during the time interval from 14 ka to 13.2 ka. From 13.2 ka to 11 ka oxygen isotope values average around -12‰ to -13‰, punctuated by a series of rapid high-amplitude changes in $\delta^{18}O$ values, including a spike in the positive direction to -10.0‰ and -10.5‰ at 13.0 ka and 12.3 ka, respectively, both of which are followed by sharp spikes in the negative direction of 2 − 3‰. A final sharp shift to the positive occurs at 11.3 ka with values shifting from -12.0‰ to -10.5‰.
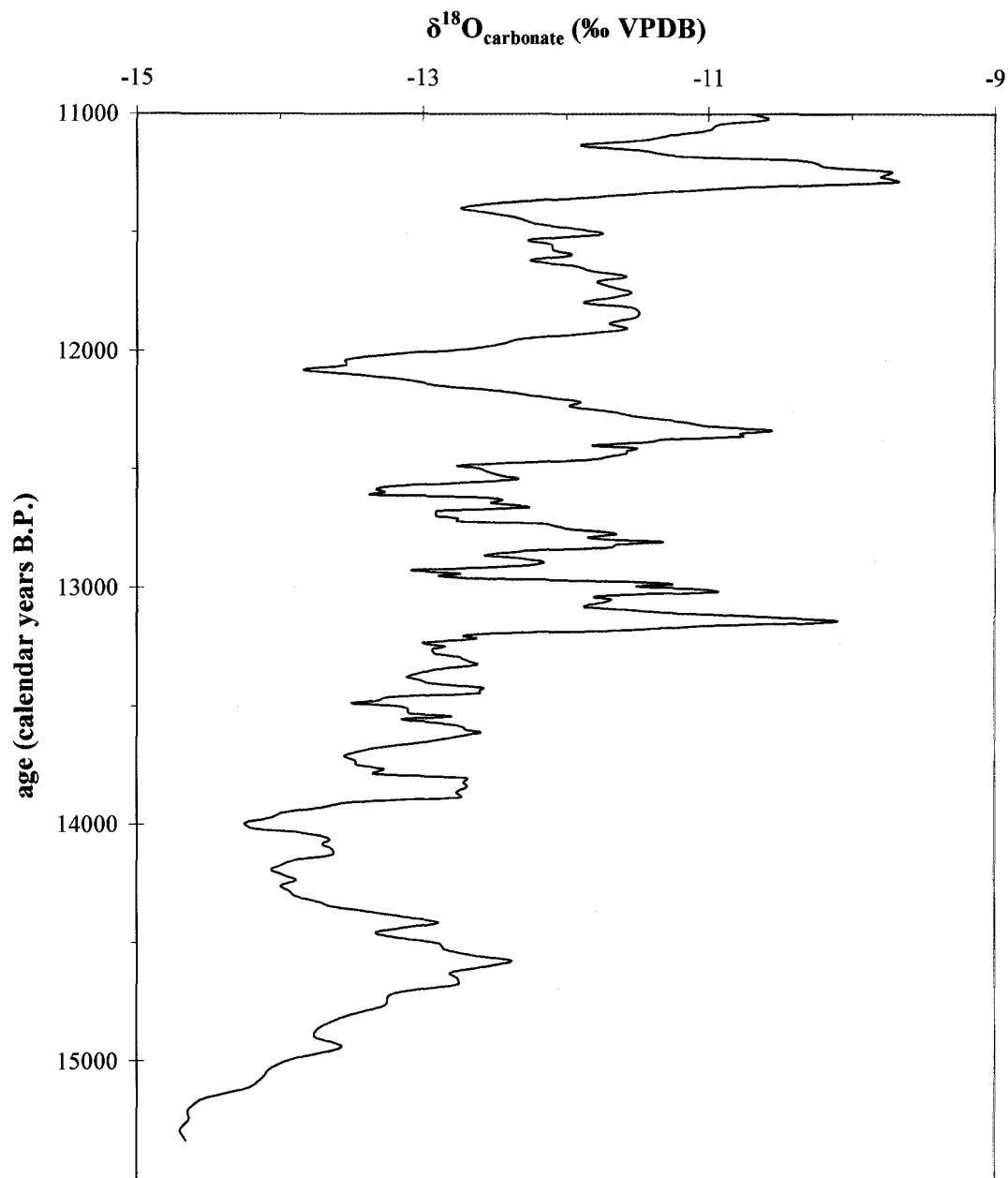
Figure 25. $\delta^{18}O$ of Burfu samples.

$\delta^{13}C_{carbonate}$ values, displayed in Figure 26, also show an overall enrichment
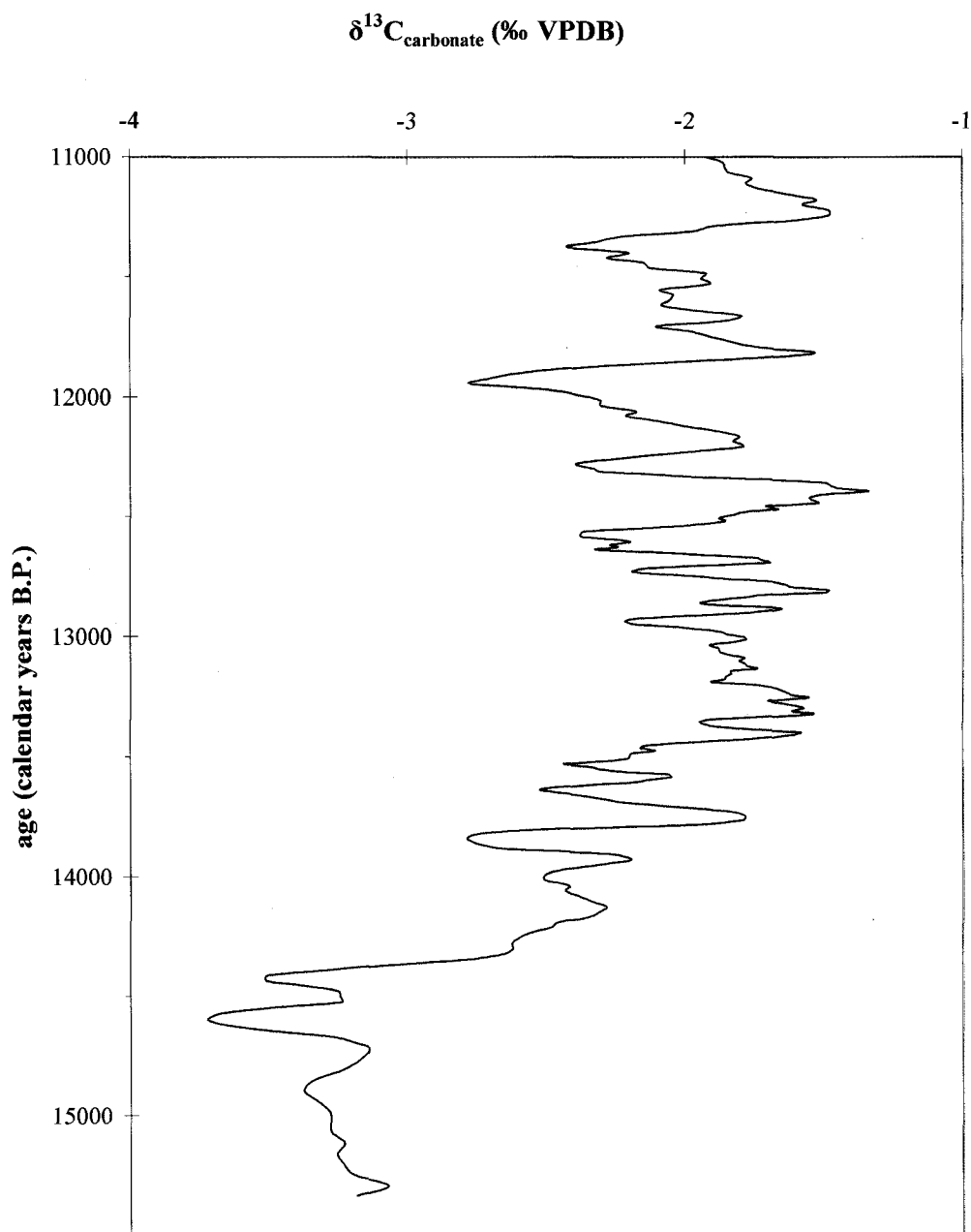
$$\delta^{13}C_{carbonate} \text{ (‰ VPDB)}$$

Figure 26. $\delta^{13}C_{carbonate}$ of Burfu samples.

trend from -3.5‰ to -1‰. Values in the early stages of the lake are depleted, approximately -3.5‰ from 15.5 ka to 14.4 ka. The largest shift in carbon isotope values occurs at 14.4 ka, where isotope values shift from -3.5‰ to -2.5‰. This is followed by a gradual shift from -2.5‰ to approximately -1.5‰ from 14.4 ka to 13.5 ka. From 13.5 to 12.3 ka average carbon isotope values are relatively constant between -2‰ and -1.5‰, although during this time interval there are several high-amplitude changes. At 12.3 there is a large shift to negative values from -1.8‰ to -2.9‰, followed by a large sudden shift in the positive direction to -1.5‰. Carbon isotope values steadily decline from 11.8 ka to 11.3 ka from -1.5‰ to -2.5‰, after which a final shift in the positive direction of 1‰ occurs at 11.3 ka.

CHAPTER VI

DISCUSSION

Interpretation of stable isotope data

The interpretation of stable isotopes from lacustrine sediments is a complicated task (Leng and Marshall, 2004). The $\delta^{18}O$ of carbonate precipitated in the lake is a reflection of the $\delta^{18}O$ signature of the lake water from which the carbonate precipitated. This, in turn, is controlled by the temperature of the lake water, the $\delta^{18}O$ signature of the water feeding the lake, and changes in hydrology, such as evaporation (Dansgaard, 1964). Studies in Southeast Asia link oxygen isotope values to the strength of the monsoon (e.g. Morrill et al., 2006; Sinha et al, 2005), which is directly linked to changes in global temperature; studies also link oxygen isotope values to temperature (e.g. Thompson et al., 1997). It is impossible to link the oxygen isotope values as a proxy for any one climatic variable as all of the variables are intricately connected (Leng and Marshall, 2004), and changes in one (e.g. temperature) are likely to result in concomitant changes in other variables (e.g. monsoon strength, amount of glacial meltwater, evaporation, hydrologic changes).

Oxygen isotope values of the Burfu lacustrine sediments range from approximately -15‰ at 16 ka to -10‰ at 11 ka. These values are a reflection of the oxygen isotope signature of the water from which the carbonates precipitated. Oxygen isotopes are fractionated during the precipitation of calcite, with a greater

66

amount of fractionation occurring at lower temperatures. The fractionation factor, α, is a function of temperature at which fractionation occurs (i.e. water temperature). This value can be calculated by the following equation, using the temperature of water in Kelvin (T) (Friedmann and O'Neil, 1977):

$$1000 \ln \alpha = (2{,}780{,}000 \,/\, T^2) - 2.89$$

Since oxygen isotope fractionation is temperature dependent, one possible interpretation for the 5‰ change in oxygen isotope values from the oldest to the youngest sediments in the Burfu lacustrine section could be due to a change in water temperature of the lake. It is not possible to calculate an exact temperature of water based only on a given oxygen isotope value for calcite precipitated from the lake. However, it is possible to determine the $\delta^{18}O$ value of the water from which the calcite precipitated, assuming a given temperature, using the above equation in conjunction with the following equation:

$$10^3 \ln \alpha = (1000 + \delta^{18}O_{calcite})/(1000 + \delta^{18}O_{water})$$

Because oxygen isotope values for calcite are reported with respect to VPDB, and oxygen isotope values for water are reported with respect to a different international standard, VSMOW, a conversion between the two standards is necessary:

$$\delta^{18}O\text{-calcite(VSMOW)} = 1.03086 * [\delta^{18}O\text{-calcite(VPDB)}] + 30.86$$

Using these equations, $\delta^{18}O$ values of water were calculated for each $\delta^{18}O$ value of calcite (from -15 to -10‰) for temperatures ranging from 2 to 15 degrees Celsius. Results of these calculations are given in Appendix H. Figure 27 displays $\delta^{18}O$ (VSMOW) values of water versus $\delta^{18}O$ (VPDB) values of calcite for temperatures ranging from 2 to 12 degrees Celsius. These calculations also show an approximate range of oxygen isotope values for water during the time of calcite precipitation. As the Burfu lake was a proglacial lake nestled at 3200 meters above sea level, a reasonable range of temperatures for the Burfu lake water might be from 3 to 8°C. The resulting isotope values of water that would lead to isotope values of calcite ranging from -15 to -10‰ at these temperatures are -18 to -12‰ (VSMOW). At a given temperature, for a 5‰ change in $\delta^{18}O$ of calcite, there is a corresponding ~5‰ change in $\delta^{18}O$ of water. At a given $\delta^{18}O$ value of calcite, the result of changing the water temperature by 5°C is a difference of 1‰ in $\delta^{18}O$ of water. Therefore, to account for a 5‰ total change in $\delta^{18}O$ values of calcite due only to water temperature effects, a change in water temperature of 25°C would be required.

Because temperature effects will result in only small isotopic changes, and because sources of water in this region have been shown to exhibit widely varying stable isotopic signatures, it is likely that the $\delta^{18}O$ signature of the source water plays the strongest role in determining the $\delta^{18}O$ values of the carbonates precipitated in the
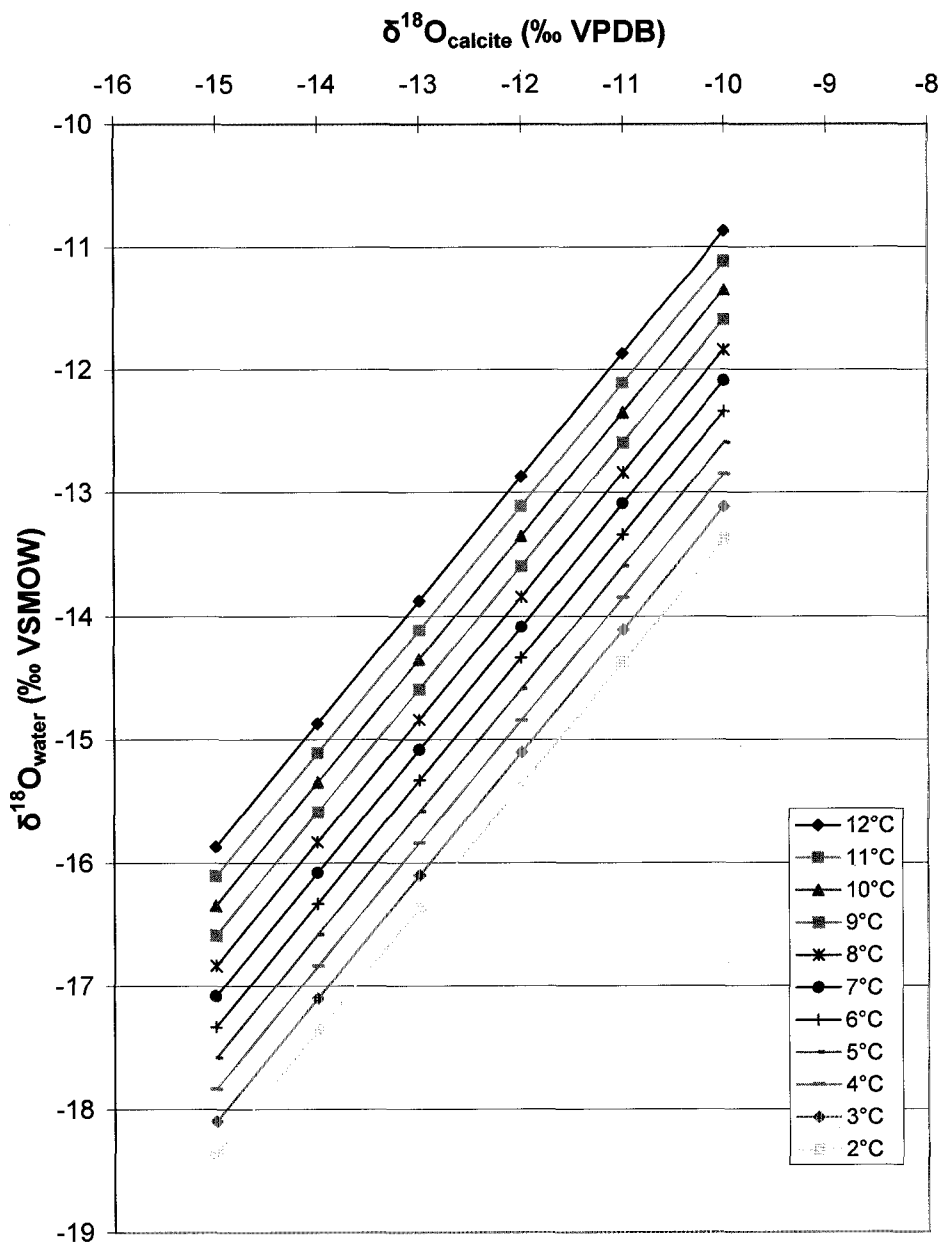
Figure 27. $\delta^{18}O$ (VSMOW) values of water versus $\delta^{18}O$ (VPDB) values of calcite
for temperatures ranging from 2 to 12 degrees Celsius.

lake. River and lacustrine environments at high elevations in the Himalaya are

dominated by glacial meltwater (Owen and Sharma, 1998). The precipitation that

feeds these glaciers is likely to be very isotopically depleted due to the preferential removal of heavy isotopes as the water vapor moves inland away from its source and also due to a greater fractionation at lower temperatures. Since equilibrium lines are commonly higher than 4500 meters above sea level (Sharma and Owen, 1996), much of the precipitation that feeds glaciers occurs at a very high altitude and would thus occur at very low temperatures. Local glacial meltwater measured by Ghosh and Bhattacharya (2003) has an average $\delta^{18}O$ value of -20.3‰, whereas river water and snowmelt in the area contain more enriched values of -13.0‰ and -13.5‰, respectively (Ghosh and Bhattacharya, 2003). Sinha et al. (2005) argue that the $\delta^{18}O$ values of carbonate in speleothems in the region are controlled by the 'amount effect', with stronger monsoons resulting in more depleted isotope values. They estimate the yearly average $\delta^{18}O$ value in precipitation at -8.0‰ (Bowen and Revenaugh, 2003), with average values of precipitation during the monsoon season at -10.0‰ (IAEA, 2003) and the $\delta^{18}O$ of precipitation during non-monsoon months at +1.0‰ (Rozanski et al., 1993). Sinha et al. (2005) argue that the isotope signature of the calcite is a reflection of the mass balance between the relative amount of monsoon versus non-monsoon precipitation, with lighter isotope values being indicative of periods of stronger monsoons, due to the 'amount effect'. It is likely that the varying strength of the monsoon played a role in the $\delta^{18}O$ values of the water of the relict Burfu lake, however, regardless of the strength of the monsoon (or whether the precipitation has a local convective origin), any direct precipitation on the lake would result in water that is relatively enriched in ^{18}O compared to water derived from nearby melting glaciers.

Thus, a likely interpretation of oxygen isotope values for the Burfu section would be a mass balance approach between relative amounts of glacial meltwater and direct precipitation.

Values of $\delta^{13}C_{carbonate}$ range from approximately -3.5 to -1.5‰. The $\delta^{13}C$ of the carbonate is a function of the $\delta^{13}C$ values of the dissolved inorganic carbon (DIC) of the lake water. This, in turn, is controlled by temperature, evaporation, productivity in the lake, and the source of DIC. With an increase in temperature a concomitant increase in the amount of productivity in the lake would be expected. This would lead to more positive values of $\delta^{13}C$ as plants preferentially take in ^{12}C. This probably accounts for a portion of the change in carbon isotope values. However, the change in source of DIC is likely to be the dominant cause of $\delta^{13}C$ changes in the Burfu section. Two major sources of DIC include oxidized organic carbon, characterized by highly depleted carbon isotope values, and dissolved marine carbonates, which are characterized by much more enriched $\delta^{13}C$ values.

It is possible to approximate isotopic compositions of calcite from a known isotopic composition of soil CO_2 derived from oxidized organic matter. Like oxygen isotope fractionation calculations, the temperature of fractionation is unknown and must be estimated. However, unlike oxygen isotope fractionation calculations, the initial organic carbon isotope value can be reasonably approximated. Isotope values of organic carbon in the Burfu region during this time interval are approximately -24‰. At 0 and 5 degrees Celsius, the magnitude of fractionation between $CO_2(g)$ and $CaCO_3(s)$ is +13.5‰ and +14.4‰, respectively. If initial $\delta^{13}C$ of organic carbon is -

24‰, carbonate that is derived from this will have a $\delta^{13}C$ value of -10.5‰ and -9.6‰ at 5 and 0 degrees Celsius, respectively.

Marine carbonate bedrock in the catchment area would have an isotope composition approximately equal to the VPDB reference, which would give it a $\delta^{13}C$ value of ≈0‰. Dissolution of this and its reprecipitation would yield a similar isotopic value, provided that there is no major change in temperature during the course of this process. The $\delta^{13}C$ values for carbonate that is derived from dissolved marine carbonates would thus be approximately 0‰. Since $\delta^{13}C_{carbonate}$ values for the Burfu samples range from -3.5 to -1.5‰, it is likely that the change in the proportion of oxidized organic carbon to dissolved marine carbonate carbon accounts for the majority of changes in $\delta^{13}C_{carbonate}$ values in the Burfu sediments.

Data from AMS ^{14}C of authigenic carbonates support this hypothesis. A sample (age of 16,524 ^{14}C yr BP) that is depleted in ^{13}C also shows very little hardwater effect on its ^{14}C age, with the ^{14}C age agreeing well with the OSL-model age (not accounting for calibration of ^{14}C years to calendar years). However, samples that are more enriched in ^{13}C also show much older ^{14}C ages, indicating a greater hardwater effect that can be attributed to a larger fraction of dissolved carbonates entering the lake environment (Figure 28). Additional properties of the samples used in $^{14}C_{carboante}$ dating support this hypothesis. There is a positive relationship between both C/N ratio and $^{14}C_{carboante}$ age as well as between % carbonate and $^{14}C_{carbonate}$ age (Figure 29). Low C/N ratios are indicative of an aquatic origin for organic carbon. C/N ratios >20 are typical of terrestrial organic matter (Meyers et al., 1984). Samples

δ¹³C$_{carbonate}$ (‰ VPDB)
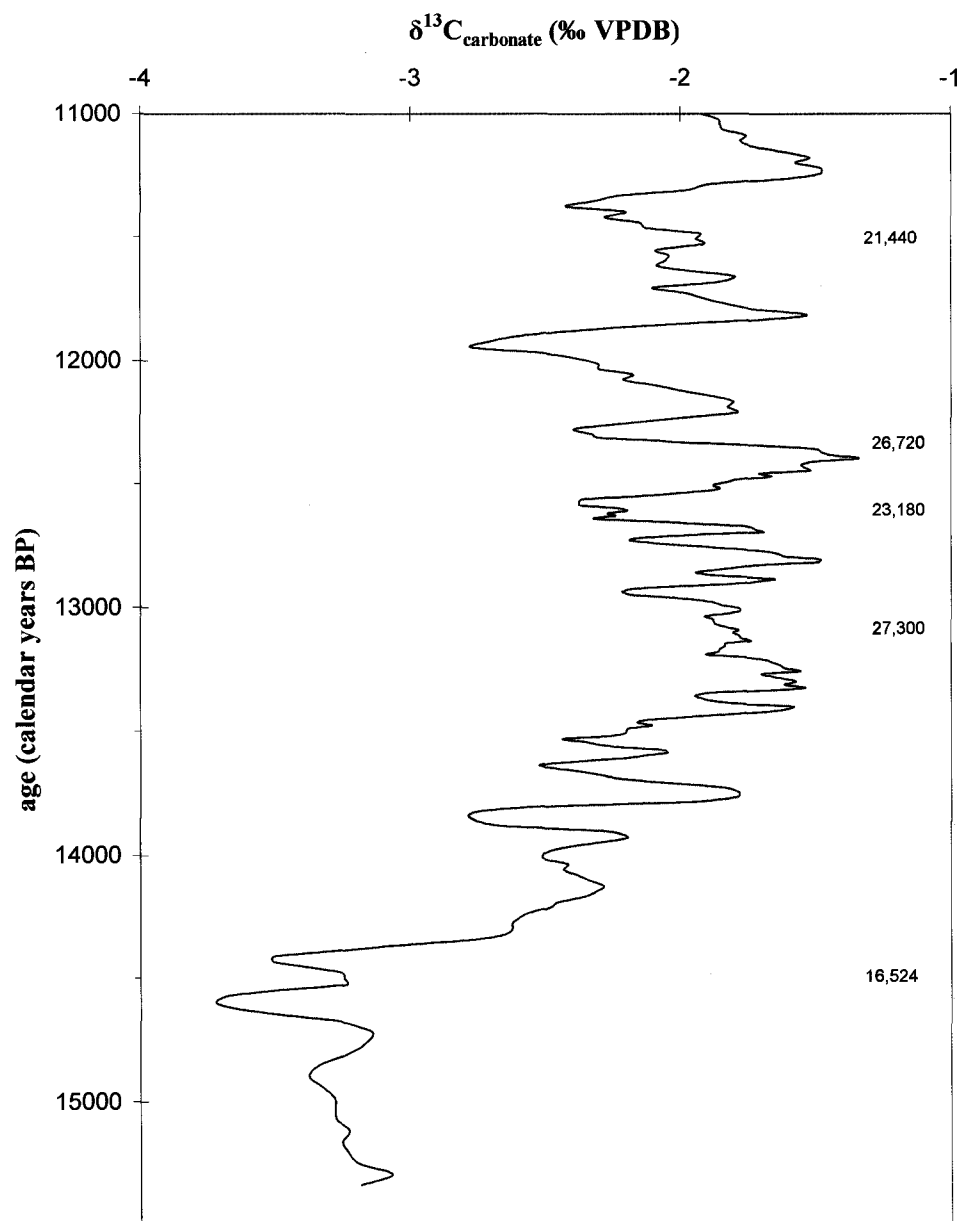
Figure 28. $\delta^{13}C_{carbonate}$ showing $^{14}C_{carbonate}$ ages. Y-axis is age in calendar years before present. $^{14}C_{carbonate}$ ages are shown at the right of figure in their relative stratigraphic positions.

with higher C/N ratios also display more of a hardwater effect. A greater amount of terrestrial input would likely flush in a greater amount of dissolved Tethyan
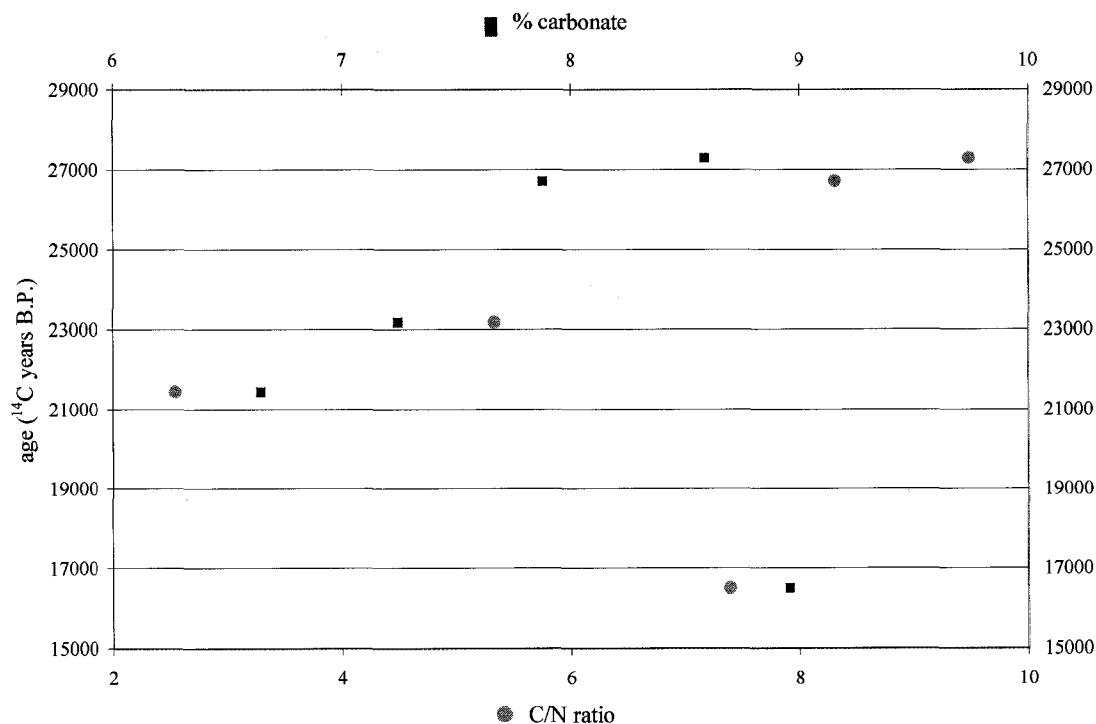
Figure 29. C/N ratio (scale on bottom axis; purple circles) versus $^{14}C_{carbonate}$ age and percent carbonate (scale on top axis; dark blue squares) versus $^{14}C_{carbonate}$ age.

carbonates, thereby skewing the ^{14}C age.

Additionally, as % carbonate increases, samples show a greater hardwater effect. This can be related to DIC in the lake if % carbonate is used as a proxy for DIC. A portion of DIC is likely derived from equilibration with atmospheric CO_2 and also from the oxidation of organic carbon. The data below suggest that another portion of DIC is derived from dissolved marine carbonates, and that the amount of this component of the DIC pool is variable. An increase in chemical weathering of catchment carbonates results in an increase in the proportion of DIC comprised of

dissolved carbonates, as is reflected in the greater hardwater effect in these samples. The sample with an age of 16,524 ^{14}C yr BP does not follow this data trend. A possible explanation for this could be that during this time interval the lacustrine system had a greatly different hydrologic balance from the following time interval. This is discussed below. Jin et al. (2005) argue that intensity of chemical weathering in the Tibetan Plateau is largely a function of temperature and monsoon intensity (both positively correlated), and thus it responds to well-known climatic events, such as the Younger Dryas and Holocene Optimum. Barnard et al. (2004a, 2004b) also show a strong connection between climate and landscape evolution in the Garhwal Himalaya. The geochemistry of streams in the Himalaya is dominated by the Ca^{2+} - Mg^{2+} -HCO_3^- facies (Jacobson et al., 2002), with chemical weathering of carbonates contributing more dissolved ions than weathering of silicates (e.g. Sarin et al., 1989; Bartarya, 1993; Harris et al., 1998; Singh and Hasnain, 1998; Singh et al., 1998a; Galy and France-Lanord, 1999; Pandey et al., 1999; Dalai et al., 2002). With a catchment dominated by Tethyan carbonates, it is reasonable to assume that changes in climate would result in changes in chemical weathering rates, and hence changes in the amount of dissolved carbonates that are delivered to the Burfu lake. The δ13C values are therefore interpreted as a mass balance between oxidized organic carbon and dissolved carbonates as sources of DIC in the lake water.

Climate variations recorded in the Burfu relict lake section

Unit-I of Burfu lake begins with oxygen isotope values that are very depleted (-15‰) (Figure 30). Since the lake formed following a retreat of a cirque glacier after the last glacial maximum (Pant et al., 2006), it is reasonable to assume that the lake received the majority of its initial water from melting glaciers. The relatively coarse grain size (medium- to fine-sand) also suggests a higher energy glacial source for the sediment. $\delta^{13}C_{carbonate}$ is very depleted (-3.5‰) at the bottom of the lake section. An AMS ^{14}C date of 16,524 ^{14}C yr BP agrees fairly well with the OSL-model age (Fig. 6), indicating little hardwater effect and thus negligible input of dissolved carbonates
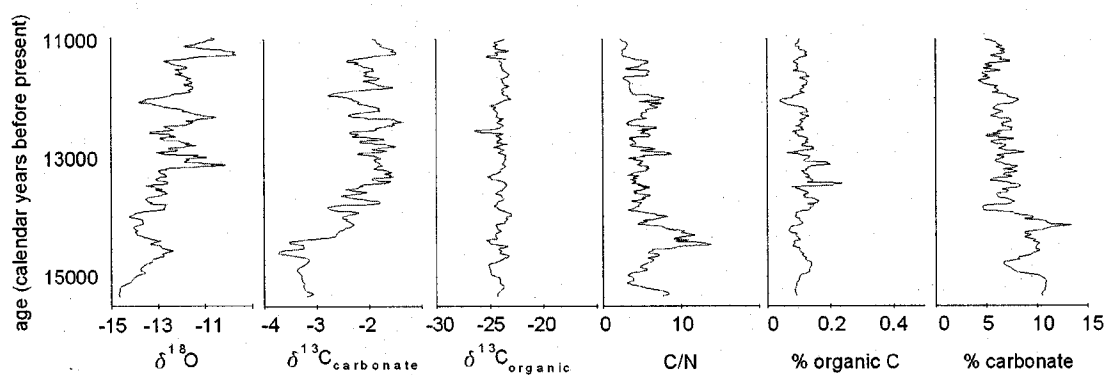
Figure 30. Geochemical data of the Burfu section.

during this phase of the lake. This suggests a relatively cool climate and weak monsoon during the ending stages of the last glaciation, with a slow rate of chemical weathering in the catchment area. Oxygen isotope values steadily increase from -15‰ to approximately -13‰ between 15.3 ka and 14.6 ka, reflecting a strengthening

monsoon and gradual increase in the direct precipitation on the lake. At 14.4 ka there is a large abrupt shift in $\delta^{13}C_{carbonate}$ values from -3.5‰ to -2.5‰. Oxygen isotope values shift steadily toward the negative direction at this point, going from -13 to nearly -15‰. This marks a sudden warming at the onset of the Bølling-Ållerød, coincident within dating error to the beginning of Meltwater Pulse 1a, that resulted in an increase in sea-level as documented by Barbados coral sediments (Fairbanks, 1989). The sudden enrichment of $\delta^{13}C_{carbonate}$ values indicates a greater contribution of dissolved carbonates to DIC in the lake, and can be interpreted as an increase in intensity of weathering of carbonates in the catchment area due to an abrupt increase in temperature and monsoon intensity. Oxygen isotope values indicate a large pulse of glacial meltwater feeding the lake during this time. Rapid melting and retreat of area glaciers would likely expose fresh Tethyan carbonate surfaces, which, along with an increase in temperature and precipitation, would lead to a greater amount of chemical weathering.

C/N ratios also increase to values near 15 during this time interval. Organic carbon deposited in the Burfu section has primarily an aquatic signature with the exception of the time interval from ~14.5 to ~14.2 ka, during which there is a significant contribution from terrestrial sources. A greater contribution from terrestrial organic carbon could be the result of an increase in glacial meltwater or an increase in runoff during this time interval, both of which could be attributed to an increase in temperature and monsoonal precipitation.

From 14.3 ka to 12.3 ka there is an overall increasing trend in both $\delta^{18}O$ and $\delta^{13}C_{carbonate}$. In addition to this, two ^{14}C dates show a significant hardwater effect, suggesting an overall warming and intensifying monsoon trend resulting in a large contribution of dissolved carbonates to the DIC of the lake water, and also resulting in a higher monsoon precipitation/glacial meltwater ratio for the source of the Burfu lake water. The time period from 13.2 to 12.3 ka is punctuated with high-amplitude changes in $\delta^{13}C$ and $\delta^{18}O$. The sediments deposited during this time interval are characterized by clay varve/rhythmite layers and are classified as sedimentologic Unit-II. This can be interpreted as a very unstable climate during the late Bølling-Ållerød, characterized by large changes in temperature, chemical weathering rates, and hydrologic inputs. Unit-III begins with a sharp decrease in $\delta^{18}O$ and $\delta^{13}C$ at 12.2 ka that can be correlated to the onset of the Younger Dryas. A sharp decrease in temperatures that lasted only a short period of time (~300 years) resulted in an abrupt decrease in the supply of dissolved carbonates to the DIC of the lake. The decrease in $\delta^{18}O$ values with a corresponding increase in C/N ratios and decrease in organic carbon content signifies an increase in glacial meltwater. A possible mechanism that could explain a large input of glacial meltwater during a cool interval is supported by the oxygen isotope record as follows. High-amplitude changes in $\delta^{18}O$ during the late Bølling-Ållerød could be caused by a two-step sequence, including 1) warming that results in greater precipitation occurring over Burfu lake, which would yield enriched values of $\delta^{18}O$ of the lake water. This increased precipitation could result in greater snowfall at higher elevations, which could lead to nearby glaciers advancing to lower

elevations, followed by 2) an increase in meltwater due to glaciers advancing to areas downvalley where the temperature is lower. Himalayan glaciers fed by monsoons are characterized by simultaneous accumulation and ablation during the summer monsoon season (Shi, 2002). This mechanism could explain the large shifts of $\delta^{18}O$ and $\delta^{13}C$ values during the late Bølling-Allerød in which a warming period would be characterized by an enrichment of isotope values followed by a sharp decrease in values as advancing glaciers melt. Thus, the low oxygen isotope values during the beginning of the Younger Dryas is the result of a decrease in the strength of the monsoon, which would cause a large proportion of the origin of the lake water to be glacial meltwater.

Following a brief cold interval, there is an increase of $\delta^{13}C$ and $\delta^{18}O$ values to Bølling-Allerød levels, after which isotope values gradually decrease during the time interval from 11.9 to 11.3 ka. These data suggest that climate in North India during the Younger Dryas consisted of a brief intensely cool interval followed by a longer (~600 years) period of moderate climate. The oxygen isotope record from a speleothem at Timta cave in North India also shows a shift in oxygen isotope values mid-way through the Younger Dryas (Sinha et al., 2005). Jin et al. (2005) also show evidence for a shorter Younger Dryas interval in Tibet than in the North Atlantic region. Evidence similar to this was obtained from the relict lake succession at Garbayang located in the adjoining Kali river basin. A sudden drop in magnetic susceptibility and elemental concentration corresponding to the period between 11 – 12 ka was attributed to the cooling associated with the Younger Dryas (Juyal et al.,

2004). A warming at 11.3 ka in the Burfu section marks the beginning of the Holocene as is indicated by a sharp increase in both carbon and oxygen isotope values, suggesting an abrupt warming and intensification of the monsoon, resulting in an increase in the contribution of dissolved carbonates to the DIC. A ^{14}C age of 21,440 ^{14}C yr BP in these sediments indicates an amplified hardwater effect, and thus supports a warming phase.

Values of δ^{13}C from the organic fraction of lacustrine sediments can provide useful information in paleoclimate studies (Krishnamurthy et al., 1986). Most plants use either the C_3 or C_4 photosynthetic pathway, each of which is characterized by a distinctive range of isotope values: C_3 plants average -26 to -28‰, and C_4 plants average -11 to -13‰ (Smith and Epstein, 1971). There is some debate about the conditions that are favorable for C_3 versus C_4 plants. C_3 plants can thrive in moist soil conditions, whereas C_4 plants can withstand drier conditions (Tiezen et al., 1979). C_4 plants use CO_2 more efficiently and thus are better adapted to lower concentrations of atmospheric pCO_2. This may have led to the evolution of the C_4 photosynthetic pathway during a period of very low atmospheric CO_2 concentrations during the Miocene (Cerling et al., 1993, 1997). However, temperature and aridity may be more important factors in vegetation type than CO_2 concentration (Gu et al., 2003). Strong evidence from the Chinese loess plateau indicates a positive correlation between amount of C_4 vegetation and higher temperatures and precipitation (Liu et al., 2005). Values of δ^{13}C from the organic fraction are relatively constant throughout the Burfu lake section, with an average value of ~ -24‰, indicating the dominance of C_3

vegetation. Three pieces of wood recovered from the area dated as modern and also have similar $\delta^{13}C$ values (Table 3). Thus, climatic and environmental variations have changed hydrologic conditions and weathering rates in this regions, but have not caused major changes in vegetation from the late glacial to modern.

Liu et al. (2005) examined $\delta^{13}C$ values of total organic carbon (TOC) from loess deposits in China and found a strong correlation between $\delta^{13}C$ values and magnetic susceptibility over the past 140,000 years, both of which decrease during glacial and stadial periods and both of which increase during interglacial and interstadials. Values of $\delta^{13}C$ increase from -23‰ to -18‰ during deglaciation from the LGM to the beginning of the Holocene (Liu et al., 2005), which the authors interpret as an increase in the ratio of C_4 to C_3 vegetation in the greater loess plateau area. Several individual loess records across a climatic gradient from the same study showed mixed results, with three records exhibiting a ~2‰ increase in $\delta^{13}C_{organic}$ values during deglaciation (15 ka to 10 ka), and two records displaying no variation in carbon isotope values during this time interval. The authors attribute the change in the ratio of C_4 to C_3 vegetation to changes in the East Asian summer monsoon, with colder and drier conditions suppressing the extent of C_4 vegetation (Liu et al., 2005). The TOC analyzed in the loess plateau is likely wind-blown, and hence, it is representative of a wide geographic area. This contrasts from the organic material in the Burfu lacustrine deposits, which is largely aquatic, as is shown by low C/N ratios. Thus, changes in the abundance of C_4/C_3 vegetation have occurred during the transition from glacial to interglacial conditions, however, these changes are not

expected to have occurred within a small lake basin, and they are not likely to be recorded in a proglacial lacustrine setting.

Comparison of oxygen isotopes between Burfu and Timta

A useful comparison can be made between this study (Burfu, 30°21'40.3N" and 80°10'57.3"E, 3200 meters a.s.l.) and the Timta Cave (29°50'17"N, 80°02'01"E; 1900 meters a.s.l.). A speleothem from the Timta Cave was the subject of a paleoclimate study of Sinha et al. (2005). The age model for the speleothem was developed from 22 ^{230}Th dates, as well as from tying major inflection points in the oxygen isotope record to inflection points in a speleothem from the Hulu Cave in China (Wang et al., 2001). Since the Burfu village is in relative close proximity to the Timta Cave, the two isotopic records should show similarities. Major differences in these two paleoclimate records can be attributed to differences in climatic responses in the two locations based on their vastly different elevations (Burfu at 3200 m.a.s.l., and Timta at 1900 m.a.s.l.). In addition to that, other differences in the isotopic record could result from differences in isotopic fractionation processes, the one data set reflective of lacustrine processes, whereas the other data set reflective of groundwater and vadose zone processes.

The Timta Cave study interprets a depletion in oxygen isotope values as a warming/wet climate and an enrichment in oxygen isotope values as a cooling/dry climate (Sinha et al., 2005). Although the oxygen isotope trends were given an opposite interpretation in the Timta study compared to the Burfu study, both studies

use similar reasoning to support their respective interpretations. The Sinha et al. (2005) study assumes that a warming in climate leads to an intensified monsoon. A stronger monsoon yields precipitation that is depleted in oxygen isotope values, a phenomenon called the 'amount effect'. Oxygen isotope values of calcite precipitated in the Timta speleothem display a range from -5.1 to -8.4‰. Thus, oxygen isotope values from calcite that precipitated during the most depleted rainfall yield values of ~ -8‰. This same assumption is made for the Burfu lacustrine sediments. However, since Burfu is situated at a much higher elevation and is in close proximity to several glaciers (indeed, its genesis is as a proglacial lake), glacial meltwater is an important hydrologic input for the Burfu sediments that is not present near the Timta Cave. Hence, although the monsoon would bring isotopically depleted precipitation, water that results from melting glaciers would likely be much more depleted, as this was originally precipitated as snow at much higher elevations. The range of oxygen isotope values of the Burfu sediments is from -9.8 to -14.7‰. Thus, an increase in oxygen isotope values to less negative values in the Burfu section would signify a greater contribution of monsoon precipitation to the hydrology of the Burfu lake, and this would be reflected in a decrease in oxygen isotope values in the Timta Cave. Figure 31 displays oxygen isotope data from these two sites (oxygen isotope scales are opposite for the two cores in order to make trends more visible). Both data sets are characterized by an initial warming/intensification of the monsoon, followed by a cooling/drying interval, followed by a gradual warming/wetting trend. The time interval in the middle section of each data set is characterized by high-amplitude

climatic variations, immediately followed by a sharp cooling/drying trend. Both data sets show a slight-to-significant rebound toward warmer/wetter conditions shortly after the coolest/driest interval. The Timta Cave dataset ends in the cool/dry climatic conditions, whereas the Burfu dataset continues and contains a major shift to warm/wet conditions. Variations in timing of climatic events could be related to either dating errors or differences in local climate, or both. Since there is considerable error associated with the OSL dates used to develop the age model for
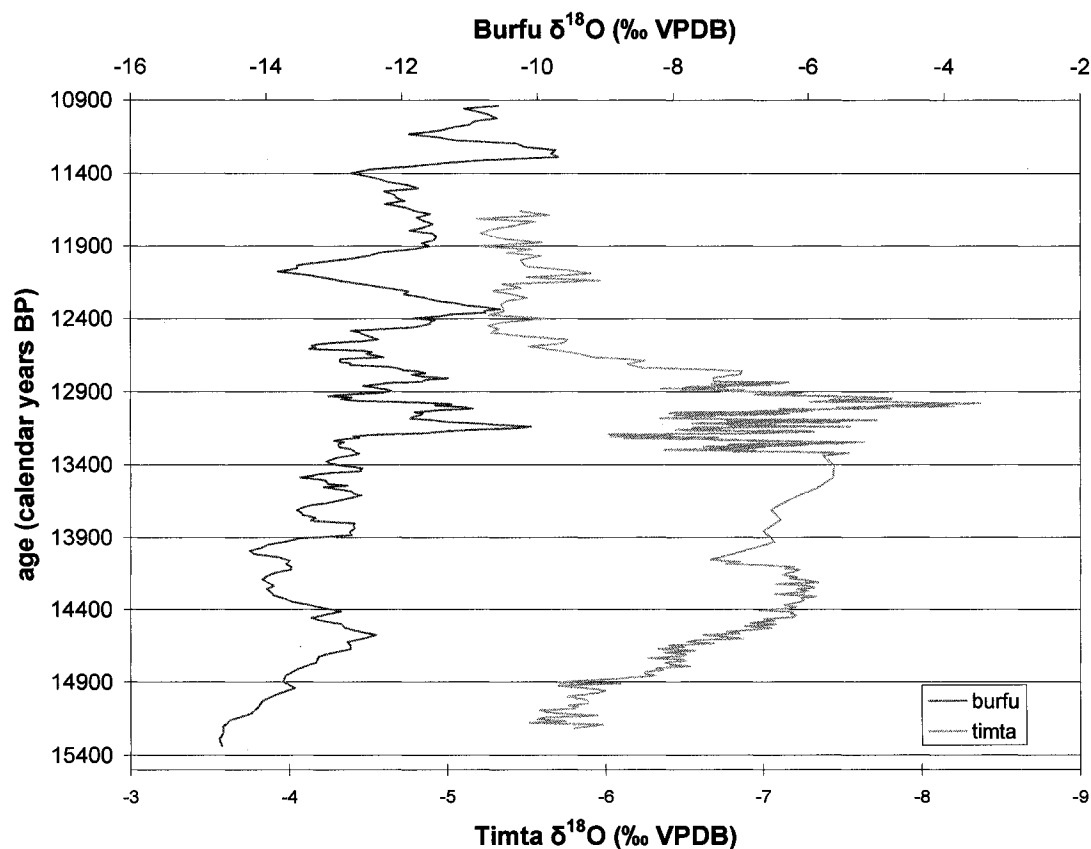
Figure 31. Burfu oxygen isotope record (on left; top x-axis scale) and Timta oxygen isotope record (on right; bottom x-axis scale).

the Burfu dataset, and since there are a greater number of dates exhibiting smaller error ranges associated with the Timta dataset, it is useful to compare timing of major climatic events between the two datasets.

The Burfu dataset shows a warming/wetting trend from 15.3 to 14.6 ka. A similar trend appears in the Timta record, culminating 300 years later, at 14.3 ka. Following this is a trend in the opposite direction, toward cooler and drier conditions. This climatic event was much more pronounced in the Burfu record than in the Timta record, with oxygen isotope values decreasing during the time interval from 14.6 to 14.0 ka to nearly their original values in the Burfu record. The Timta record shows a slight cooling/drying event from 14.2 to 14.0 ka. Interestingly, both records indicate an inflection point at approximately 14.0 ka.

After 14.0 ka, both records indicate a warming/wetting trend from 14.0 to 12.3 ka in the Burfu record, and from 14.0 to 13.1 ka in the Timta record. There are at least three possible explanations for the discrepancy of timing. One possibility is dating error between the two datasets. The warm/wet peak at 12.3 in the Burfu dataset could be misdated and could actually have occurred earlier, and could thus be correlated with the 13.1 ka peak in the Timta dataset. Another possible explanation would be dating errors associated with both datasets, which could put this warm/wet peak at a date at some point between 12.3 and 13.1 ka. A third possibility could be that the warm/wet peak at 13.2 in the Burfu dataset correlates to the 13.1 peak in the Timta dataset, and that following this is a major cooling event in both datasets. The

12.3 ka event in the Burfu dataset could be a local climatic response, or it could correlate with the warming/wetting event at 12.1 ka in the Timta dataset.

Sinha et al. (2005) interpret the 12.5 ka cooling/drying event in the Timta dataset as the Younger Dryas. The greatest decrease in oxygen isotope values in the Burfu dataset occurs at ~ 12.1 ka; this is interpreted as the manifestation of the Younger Dryas in the Burfu region. Cronin summarizes several studies that document and attempt to date the Younger Dryas, based on tree ring, lake, varve, and ice core records (Cronin, 1999). Dates for the onset of the Younger Dryas range from 11.9 ka to 12.9 ka (Hajdas et al., 1995; Alley et al., 1993), and dates for the end of the Younger Dryas range from 11.5 ka to 11.0 ka (Johnsen et al., 1992; Hajdas et al., 1993). Again, errors in dating between the Burfu and Timta dataset could account for this discrepancy in the onset of the Younger Dryas. However, the Burfu oxygen isotope data could show either the complexities of the response in a high altitude, glacial environment, or it could indicate that the response in the Himalaya to the Younger Dryas lagged behind the response at lower elevations in North India. Regardless, the interpreted dates for the onset of the Younger Dryas in the Timta and the Burfu record both fall within the range of reported dates worldwide from several different proxies.

The record of the Younger Dryas in the Timta and the Burfu datasets show similarities. According to the Burfu record, conditions during the Younger Dryas were initially very severe (cold/dry) for a short time interval (100 – 300 years), followed by a longer interval (11.9 to 11.4 ka) of warmer/wetter conditions. In the

Burfu record, this second time interval exhibited conditions that were similar to those of the Bølling-Allerød (~ 14.0 to 12.4 ka). The Timta record also shows a cool/dry beginning to the Younger Dryas (from ~ 12.5 to 12.2 ka), followed by a slight warming/wetting at 12.1 ka. Both records show a slight cooling/drying of conditions after this and immediately preceding the onset of the Holocene, which occurs at ~ 11.4 ka in the Burfu dataset, and which is not recorded in the Timta dataset.

CHAPTER VII

CONCLUSIONS

Stable isotopes of carbon and oxygen from sediments from relict lake deposits in North India near the village of Burfu reveal climate variability and changes in chemical weathering of carbonates during the time interval from 16 ka to 11 ka.

The time interval from 16 ka to ~14.5 ka is characterized by cool, dry conditions with the source water for the lake dominated by glacial meltwater. As temperature and precipitation were relatively low, and as much of the local bedrock was likely covered in ice, chemical weathering of carbonates was low. This is evident by low values of $\delta^{13}C_{carbonate}$.

A major change in hydrology occurred at ~14 ka, as is evident by a sudden decrease in $\delta^{18}O$, a sharp increase in $\delta^{13}C_{carbonate}$, and a large increase in the C/N ratio. This time, within dating error, is coincident with Meltwater Pulse 1a, an abrupt warming event. Changes in isotope values suggest a sudden pulse in glacial meltwater, possibly caused by sudden warming and retreating of area glaciers. $\delta^{13}C_{carbonate}$ values sharply increase at this point, suggesting an increase in the amount of chemical weathering of carbonates in catchment area rocks. The increase in C/N ratio suggests a strong terrestrial input from ~14.5 ka to 13.5 ka.

The time interval from ~14 ka to ~12 ka is characterized by warmer conditions, resulting in a stronger monsoon and a relatively high degree of chemical

88

weathering of carbonates. Not only are $\delta^{13}C_{carbonate}$ values relatively positive during this time interval, but also ^{14}C ages from this time interval show a large amount of hardwater effect, which also suggests enhanced chemical weathering that brings in "dead" carbon into the lake. Oxygen isotope values are relatively enriched, but also are characterized by several abrupt spikes in both the positive and negative direction. This attests to instability in climate during this time interval.

At ~12 ka both $\delta^{18}O$ and $\delta^{13}C_{carbonate}$ as well as % organic carbon abruptly decrease. This marks a sudden decrease in temperature and moisture, resulting in a decrease in chemical weathering of carbonates, and a decrease in the ratio of monsoon precipitation to glacial meltwater. This event likely correlates with the Younger Dryas. Severe conditions persisted for only a brief period of time (~100 – 300 years), followed by a longer period (~600 years) characterized by warmer and wetter conditions.

At 11 ka there is an abrupt increase in both carbon and oxygen isotope values, coincident with the onset of the Holocene.

Values of $\delta^{13}C_{organic}$ remain nearly constant at ~ -24‰ throughout the entire time interval of this study, which suggests no major changes in vegetation patterns in the vicinity of Burfu.

Appendix A

Burfu lab data: Organic fraction

Sample	wt mg	height (m)	wt least sq age	N2 yield	CO2 yield	% C	%org C5pt	% N2	C/N	C/N 5 pt	$\delta^{13}C_{org}$	13C-org 5pt
1	96.2	0.2	15336	1.73	8.5193	0.106	0.093452956	0.0504	2.462	7.653658	-22.502	-24.308
2	80.3	0.4	15292	0.11	7.2672	0.109	0.090052652	0.0038	7.25	8.460415	-22.995	-24.2852
3	89.3	0.6	15248	0.22	6.1469	0.083	0.086405933	0.0069	13.97	7.461653	-27.164	-24.09
4	93.8	0.8	15204	0.53	6.4764	0.083	0.087943455	0.0158	6.11	5.608437	-21.7	-23.793
5	71.2	1	15160	0.16	5.1584	0.087	0.092390742	0.0063	8.476	4.41767	-25.083	-23.7548
6	72	1.2	15116	0.47	5.3561	0.089	0.092518824	0.0183	6.496	3.108464	-22.368	-24.0686
7	75.5	1.4	15072	1.26	5.6856	0.09	0.098452612	0.0468	2.256	3.943637	-24.342	-24.065
8	85.2	1.6	15028	0.05	6.4105	0.09	0.101590983	0.0016	4.704	3.833354	-25.966	-24.1804
9	73.2	1.8	14984	20.55	6.4105	0.105	0.105670215	0.7866	0.156	3.229086	-23.214	-24.7536
10	77	2	14940	1.45	5.6197	0.088	0.129380319	0.0528	1.93	3.87388	-24.168	-24.9604
11	81.3	2.2	14896	0.05	8.058	0.119	0.132402752	0.0017	10.67	5.66788	-22.934	-24.9736
12	94.9	2.4	14852	2.46	8.3875	0.106	0.136074862	0.0726	1.705	4.78894	-22.297	-25.0674
13	69.5	2.6	14808	0.02	6.4105	0.111	0.140314162	0.0008	1.683	5.232588	-22.767	-25.1108
14	186.8	2.8	14764	5.15	34.8134	0.224	0.137926033	0.0773	3.38	6.076852	-26.948	-24.4666
15	80.3	3	14720	0.11	6.8718	0.103	0.119739763	0.0038	10.9	6.451844	-23.471	-23.8824
16	68.7	3.2	14695.55552	0.16	7.8603	0.137	0.123645048	0.0065	6.277	5.731844	-22.535	-23.6472
17	73.5	3.3	14671.11108	0.36	7.7944	0.127	0.117636065	0.0137	3.923	6.696409	-23.721	-23.2844
18	73.9	3.4	14646.66664	6.27	6.081	0.099	0.111316211	0.2377	5.904	7.191806	-23.833	-23.2748
19	67.5	3.5	14622.2222	0.5	7.4649	0.133	0.114859976	0.0208	5.255	6.72199	NA	-23.8822
20	72	3.6	14597.77776	0.5	7.3331	0.122	0.10944816	0.0195	7.3	5.772586	NA	-24.1126
21	67.3	3.7	14573.33332	6.83	6.0151	0.107	0.10319554	0.2844	11.1	6.420168	-24.121	-23.9384
22	95.3	3.8	14548.88888	0.19	7.5967	0.096	0.102378024	0.0056	6.4	6.313674	-23.622	-24.1804
23	74.2	3.9	14524.44444	1.73	7.2013	0.116	0.103624524	0.0653	3.555	9.159763	NA	-24.0888
24	78.8	4	14500	6.83	6.9377	0.106	0.080855165	0.2429	0.508	9.72027	-24.194	-23.3142
25	186.3	4.1	14478	0.67	14.1208	0.091	0.082599345	0.0101	10.54	13.85058	-23.569	-24.278
26	69.2	4.2	14456	0.81	5.9492	0.103	0.086047117	0.0328	10.57	13.34299	-24.08	-24.782
27	75.5	4.3	14434	0.14	6.4105	0.102	0.085299958	0.0052	20.63	12.49749	-23.245	-25.0238
28	200.7	4.4	14412	0.976	0.15	0.003	0.08585155	0.0136	6.358	9.349029	-23.141	-25.0314
29	72.1	4.5	14390	0.11	6.8718	0.114	0.102506543	0.0043	21.16	10.91563	-22.633	-25.2692
30	71.1	4.6	14368	0.08	6.4105	0.108	0.100188461	0.0032	8	9.161493	-23.595	-24.3646
31	71.8	4.7	14346	0.19	5.9492	0.099	0.0971965	0.0074	6.34	9.519413	-22	-24.314
32	78.8	4.8	14324	0.25	6.8718	0.105	0.092866937	0.0089	4.888	10.85141	-23.447	-24.4564
33	86.8	4.9	14302	0.11	6.2128	0.086	0.089921996	0.0036	14.19	11.78553	-23.933	-24.4298
34	81	5	14280	0.28	6.9377	0.103	0.09212223	0.0097	12.39	10.72933	-23.568	-24.4898
35	63	5.1	14258	0.25	4.8948	0.093	0.091272569	0.0111	9.79	10.02332	-24.855	-24.2332
36	105	5.2	14236	79.39	6.8059	0.078	0.068521618	2.1186	13	10.42484	-22.978	-23.9258

Sample	wt mg	height (m)	wt least sq age	N2 yield	CO2 yield	% C	%org C5pt	% N2	C/N	C/N 5 pt	$\delta^{13}C_{org}$	13C-org 5pt
37	94.6	5.3	14214	0.39	7.4649	0.095	0.067020202	0.0116	9.559	8.696886	-22.416	-24.2244
38	78.2	5.4	14192	0.22	6.4764	0.099	0.07070106	0.0079	8.91	8.01225	-23.164	-24.296
39	210.3	5.5	14170	0.92	0.15	0.002	0.073125733	0.0123	8.859	7.776548	-23.342	-24.3232
40	185.4	5.6	14148	0.47	11.0894	0.072	0.076882485	0.0071	11.8	6.321229	-23.412	-24.5114
41	88.2	5.7	14126	0.72	6.2787	0.085	0.093815157	0.0229	4.36	4.524902	-23.795	-24.3836
42	77.2	5.8	14104	0.56	6.8718	0.107	0.108654532	0.0203	6.136	4.771194	-24.677	-23.562
43	73.8	5.9	14082	0.47	7.2672	0.118	0.111599485	0.0178	7.731	5.729332	-23.579	-23.5842
44	104	6	14060	2.38	7.5308	0.087	0.106659374	0.0641	1.582	5.21512	-22.74	-23.48775
45	177.3	6.1	14038	3.83	21.5675	0.146	0.102336952	0.0605	2.816	6.770922	-24.562	-23.371
46	100.5	6.2	14016	0.75	8.3875	0.1	0.104353866	0.0209	5.592	7.274216	-23.33	-23.491
47	194.8	6.3	13994	0.61	13.33	0.082	0.092638071	0.0088	10.93	8.336858	-23.587	-23.341
48	89.5	6.4	13972	185.66	7.2013	0.097	0.08763822	5.8125	5.16	7.04951	-22.151	-22.953
49	83.4	6.5	13950	0.36	6.74	0.097	0.09260026	0.0121	9.361	6.517117	-22.926	-22.9735
50	102.5	6.6	13928	0.7	7.4649	0.087	0.092629143	0.0191	5.332	5.260256	-23	-23.2935
51	119.2	6.7	13906	0.19	7.4649	0.075	0.094490914	0.0045	10.9	4.806853	-26.721	-23.5282
52	78.6	6.8	13884	0.78	7.0036	0.107	0.104909009	0.0278	4.489	3.362368	-24.375	-23.9772
53	173.6	6.9	13862	2.8	13.989	0.097	0.132995184	0.0452	2.498	3.89155	-23.705	-24.2186
54	88	7	13840	0.92	7.7944	0.106	0.135628323	0.0293	3.077	4.290606	NA	-24.3556
55	88.6	7.1	13821.66663	1.68	10.2986	0.139	0.140758876	0.0531	3.065	4.626117	-25.178	-24.586
56	75.3	7.2	13803.3333	1.54	13.5277	0.216	0.145251732	0.0573	3.682	4.586212	NA	-24.5162
57	71.3	7.3	13784.99997	0.5	7.1354	0.12	0.147856605	0.0196	7.135	4.729943	-24.993	-24.3058
58	75.8	7.4	13766.66664	0.86	7.7285	0.122	0.129383141	0.0318	4.493	4.946388	-23.708	-24.29
59	96.6	7.5	13748.33331	1.09	10.3645	0.129	0.159771309	0.0316	4.754	4.225945	-24.041	-24.287
60	71.7	7.6	13729.99998	1.59	9.1124	0.153	0.158151664	0.0621	2.866	3.733427	-24.598	-23.9764
61	100.3	7.7	13711.66665	1.17	10.2986	0.123	0.164822357	0.0327	4.401	4.832725	-24.004	-23.793
62	87	7.8	13693.33332	1.2	19.7223	0.272	0.153550692	0.0386	8.218	5.498715	-25.357	-23.6764
63	96.4	7.85	13674.99999	5.15	9.1783	0.114	0.147824769	0.1497	0.891	5.023447	-23.59	-23.717
64	77.7	7.9	13656.66666	2.29	10.4963	0.162	0.118074298	0.0826	2.292	5.532495	-24.812	-23.9046
65	98.1	7.95	13638.33333	0.47	7.8603	0.096	0.12123422	0.0134	8.362	6.148542	-23.238	-23.9228
66	92.2	8	13620	0.47	7.2672	0.095	0.113108694	0.0143	7.731	5.198801	-23.395	-24.2452
67	88.7	8.05	13609	0.78	9.1124	0.123	0.122216721	0.0246	5.841	4.299118	-23.722	-24.4222
68	78	8.1	13598	1.23	8.4534	0.13	0.130427299	0.0442	3.436	3.965199	-25.164	-24.4114
69	79.6	8.15	13587	0.75	8.058	0.121	0.128606016	0.0264	5.372	4.34218	-23.797	-24.2908
70	75.5	8.2	13576	17.75	8.9147	0.142	0.128246943	0.6587	3.613	4.148614	-24.622	-24.2576
71	84.7	8.25	13565	342.8	9.5737	0.136	0.128365395	11.34	3.233	4.002712	-24.068	-24.1384
72	83.3	8.3	13554	0.95	7.9262	0.114	0.117228304	0.032	4.172	4.881618	-23.742	-23.8928

Sample	wt mg	height (m)	wt least sq age	N2 yield	CO2 yield	% C	%org C5pt	% N2	C/N	C/N 5 pt	$\delta^{13}C_{org}$	13C-org 5pt
73	75.4	8.35	13543	0.72	7.6626	0.122	0.110673674	0.0268	5.321	4.901419	-24.059	-23.7686
74	91.4	8.4	13532	0.84	7.399	0.097	0.106148932	0.0258	4.404	5.468769	-23.602	-23.818
75	79.7	8.45	13521	1.26	7.2672	0.109	0.10595892	0.0443	2.884	5.375935	-23.24	-23.712
76	74.3	8.5	13510	0.39	5.9492	0.096	0.095620738	0.0147	7.627	6.046004	-24.081	-23.62
77	106.2	8.55	13499	1.09	9.3101	0.105	0.095258558	0.0288	4.271	5.018164	-23.723	-23.638
78	83.6	8.6	13488	0.3	4.8948	0.07	0.092300527	0.0101	8.158	5.986784	-25.201	-23.545
79	86.5	8.65	13477	70.52	6.8718	0.095	0.085160043	2.2844	3.94	4.593769	-24.357	-23.4262
80	83.8	8.7	13466	0.53	6.6082	0.095	0.079643108	0.0177	6.234	5.146157	-23.989	-23.4972
81	86.8	8.75	13455	0.08	4.3676	0.06	0.201537752	0.0026	2.488	4.480998	-26.694	-23.4356
82	93	8.8	13444	0.33	6.0151	0.078	0.208949913	0.0099	9.114	4.775719	-30.11	-23.5436
83	76.7	8.85	13433	18.21	43.4463	0.68	0.213915162	0.6652	1.193	3.763856	-26.989	-23.5462
84	81.4	8.9	13422	0.67	8.9806	0.132	0.231018798	0.0231	6.702	4.283303	-23.62	-23.5446
85	78.3	8.95	13411	1.34	7.7944	0.119	0.237906141	0.048	2.908	3.972383	-23.026	-23.6202
86	78.2	9	13400	1.2	9.5078	0.146	0.126301862	0.043	3.962	4.292861	-23.679	-24.055
87	99	9.05	13389	1.14	9.2442	0.112	0.136664584	0.0323	4.054	3.942324	-23.861	-24.128
88	71	9.1	13378	0.95	7.2013	0.122	0.143852554	0.0375	3.79	3.836982	-24.66	-24.3782
89	73.1	9.15	13367	1.09	11.2212	0.184	0.144662449	0.0418	5.147	3.554204	-24.626	-24.6934
90	83.6	9.2	13356	1.2	10.8258	0.155	0.141439594	0.0402	4.511	4.391314	-24.54	-24.9532
91	89.8	9.25	13345	2.54	11.2212	0.15	0.138889961	0.0793	2.209	3.777231	-24.499	-24.8126
92	90.9	9.3	13334	1.03	7.2672	0.096	0.138712034	0.0317	3.528	4.192749	-23.19	-24.992
93	194.7	9.35	13323	3.72	17.6794	0.109	0.132120852	0.0535	2.376	4.250753	-24.261	-25.1974
94	78.2	9.4	13312	0.64	11.9461	0.183	0.123233719	0.0229	9.333	4.5636	-23.636	-24.947
95	75.1	9.45	13301	2.66	7.6626	0.122	0.134532364	0.0992	1.44	3.237813	-24.798	-24.824
96	81.9	9.5	13290	0.84	7.2013	0.106	0.13470105	0.0287	4.286	3.867324	-23.511	-24.812
97	217	9.55	13279	3.61	27.5644	0.152	0.126069147	0.0466	3.818	3.638173	-24.596	-24.5874
98	89.5	9.6	13268	19.61	8.1898	0.11	0.130318839	0.6139	3.941	3.918872	-23.957	-24.261
99	190.3	9.65	13257	4.11	22.2265	0.14	0.121839993	0.0605	2.704	4.161476	-25.061	-24.2038
100	72.8	9.7	13246	0.95	8.717	0.144	0.115818765	0.0366	4.588	4.835672	-23.692	-24.0424
101	177	9.75	13235	1.14	9.3101	0.063	0.117393368	0.018	3.141	5.303896	NA	-23.967
102	88.1	9.8	13224	0.86	8.9806	0.122	0.115584783	0.0274	5.221	5.77625	-23.092	-24.0582
103	103	9.85	13213	0.98	10.1009	0.118	0.10938982	0.0267	5.154	5.581804	-23.178	-24.0216
104	83.4	9.9	13202	0.75	9.1124	0.131	0.125173229	0.0252	6.075	5.639538	-23.269	-24.0472
105	90	9.95	13191	0.61	8.4534	0.113	0.123301862	0.019	6.929	5.920442	-26.321	-23.9132
106	78.1	10	13180	0.84	9.2442	0.142	0.121169995	0.0301	5.503	5.819918	-23.87	-23.7944
107	166.1	10.05	13169	1.84	15.6365	0.113	0.118684076	0.031	4.249	5.567418	-24.481	-23.5962
108	167.2	10.1	13158	1.37	14.9116	0.107	0.127854711	0.023	5.442	5.807841	-24.551	-23.5804

Sample	wt mg	height (m)	wt least sq age	N2 yield	CO2 yield	% C	%org C5pt	% N2	C/N	C/N 5 pt	$\delta^{13}C_{org}$	13C-org 5pt
109	76.9	10.15	13147	0.64	9.5737	0.149	0.127441251	0.0233	7.479	5.811848	-23.668	-23.51275
110	82.4	10.2	13136	0.75	9.6396	0.14	0.131726764	0.0255	6.426	5.070696	-24.059	-23.616
111	96.2	10.25	13125	1.23	10.4304	0.13	0.140219621	0.0358	4.24	4.525416	-23.83	-23.6266667
112	79.8	10.3	13114	0.86	9.376	0.141	0.141630787	0.0302	5.451	4.408075	-23.609	-23.722
113	72.1	10.35	13103	0.81	8.8488	0.147	0.14050854	0.0315	5.462	4.969676	-23.191	-23.8256667
114	183.3	10.4	13092	2.91	21.9629	0.144	0.193733546	0.0445	3.774	4.726374	-24.691	-23.748
115	87.4	10.45	13081	0.84	29.6073	0.407	0.200250545	0.0269	3.7	4.804527	-24.071	-23.6686
116	189.7	10.5	13070	3.52	25.7192	0.163	0.193128606	0.052	3.653	5.181378	-25.131	-23.631
117	79	10.55	13059	0.42	6.9377	0.105	0.190994775	0.0149	8.259	5.108155	-23.611	-23.6298
118	73.1	10.6	13048	0.98	8.3216	0.137	0.183183717	0.0376	4.246	4.143736	-23.513	-23.53
119	87.8	10.65	13037	0.92	7.6626	0.105	0.123126434	0.0294	4.164	3.962553	-23.118	-23.5578
120	102.2	10.7	13026	0.81	9.0465	0.106	0.116023333	0.0222	5.584	4.27092	-23.15	-23.5586
121	189.2	10.75	13015	3.05	20.0518	0.127	0.122188433	0.0452	3.287	3.367727	-24.265	-23.4922
122	79.7	10.8	13004	21.95	9.0465	0.136	0.118850065	0.7717	3.437	3.979932	-23.401	-23.6294
123	102.4	10.85	12993	2.94	10.2327	0.12	0.127684434	0.0804	3.34	5.367994	-23.355	-23.565
124	74.5	10.9	12982	0.81	9.2442	0.149	0.130715441	0.0305	5.706	5.363322	-23.654	-23.4578
125	94	10.95	12971	4.45	9.5078	0.121	0.132693456	0.1326	1.068	5.108763	-23.472	-23.4894
126	86.7	11	12960	0.78	9.9032	0.137	0.131279948	0.0252	6.348	7.282309	-23.579	-23.5314
127	81	11.05	12949	0.42	8.717	0.129	0.135204292	0.0145	10.38	8.793971	-23.733	-23.7046
128	84.6	11.1	12938	17.75	9.8373	0.14	0.118121693	0.5879	3.316	8.250687	-23.351	-23.8888
129	83.8	11.15	12927	0.5	4.4335	0.063	0.106315343	0.0167	4.434	8.4874	-23.515	-24.2034
130	179.2	11.2	12916	0.39	9.3101	0.062	0.100350443	0.0061	11.94	8.219778	-23.971	-24.139
131	102.7	11.25	12905	0.33	9.1783	0.107	0.092158132	0.009	13.91	7.097823	-23.585	-24.1386
132	98	11.3	12894	0.47	7.2013	0.088	0.064658599	0.0134	7.661	4.920389	-23.921	-23.8784
133	88.3	11.35	12883	16.81	0.15	0.002	0.078019562	0.5334	4.5	4.815358	-23.251	-23.876
134	186.5	11.4	12872	5.71	20.2495	0.13	0.094470678	0.0858	3.095	5.727645	NA	-23.6714
135	88.2	11.45	12861	0.84	10.6281	0.145	0.098580433	0.0267	6.326	6.72101	-23.66	-23.9434
136	99.8	11.5	12850	1.76	10.6281	0.128	0.106899995	0.0494	3.019	6.30972	-23.299	-24.027
137	73.9	11.55	12839	0.56	7.9921	0.13	0.139791964	0.0212	7.136	6.363392	-23.889	-24.037
138	72.8	11.6	12828	0.05	10.1009	0.166	0.150589463	0.0019	9.061	5.529355	-23.203	-24.6025
139	73.5	11.65	12817	0.7	11.2871	0.184	0.140897877	0.0267	8.062	4.569793	-23.851	-24.50275
140	134.3	11.7	12806	1.26	10.7599	0.096	0.143755532	0.0263	4.27	3.777693	-23.739	-24.1595
141	181.6	11.75	12795	3.27	21.5016	0.142	0.147591115	0.0505	3.288	3.534369	-24.29	-23.946
142	155.7	11.8	12784	61.64	19.3269	0.149	0.130806899	1.1093	2.966	3.702924	-24.483	-23.965
143	148.7	11.85	12773	1.2	10.2327	0.083	0.111586072	0.0226	4.264	3.831269	-23.873	-23.30775
144	156.3	11.9	12762	1.4	11.4848	0.088	0.115447072	0.0251	4.102	4.273312	-23.723	-23.75575

Sample	wt mg	height (m)	wt least sq age	N2 yield	CO2 yield	% C	%org C5pt	% N2	C/N	C/N 5 pt	δ13C$_{org}$	13C-org 5pt
145	139.3	11.95	12751	1.87	11.4189	0.098	0.104518839	0.0376	3.053	4.239114	-23.922	-23.9505
146	147	12	12740	2.18	18.0089	0.147	0.104032968	0.0416	4.13	4.263629	-23.834	-24.3265
147	150.7	12.05	12729	2.35	16.9545	0.135	0.117140144	0.0437	3.607	3.989707	-24.86	-24.1634
148	160	12.1	12718	1.34	17.3499	0.13	0.127627444	0.0235	6.474	4.091213	-24.68	-24.3846
149	158.6	12.15	12707	1.704	13.3959	0.101	0.122373179	0.0301	3.931	3.708289	-24.009	-24.0996
150	164.5	12.2	12696	2.908	18.4702	0.135	0.129646958	0.0495	3.176	3.607414	-25.554	-24.1604
151	168.8	12.25	12685	2.796	15.4388	0.11	0.122195572	0.0464	2.761	3.487016	-24.957	-23.8792
152	138.1	12.3	12674	1.9	15.6365	0.136	0.1223686	0.0386	4.115	3.841293	-24.92	-24.0768
153	138.9	12.35	12663	1.816	16.5591	0.143	0.124955585	0.0366	4.559	3.469536	-25.295	-24.0252
154	165.9	12.4	12652	2.628	18.0089	0.13	0.13073702	0.0444	3.426	4.849691	-25.261	-24.2232
155	148.6	12.45	12641	2.628	13.5277	0.109	0.125637853	0.0496	2.574	5.824511	-24.527	-24.303
156	138.4	12.5	12630	1.536	13.9231	0.121	0.127831057	0.0311	4.532	6.126112	-24.06	-24.4372
157	150.1	12.55	12619	2.852	12.8687	0.103	0.121233038	0.0532	2.256	5.905661	-25.623	-24.2732
158	229	12.6	12608	0.696	15.966	0.084	0.109354127	0.0085	11.46	5.976277	-23.996	-23.9704
159	160.4	12.65	12597	0.668	11.0894	0.083	0.099894088	0.0117	8.3	5.364277	-23.685	-23.7692
160	158.9	12.7	12586	1.536	12.5392	0.095	0.096984856	0.0271	4.082	4.82438	-23.276	-24.235
161	161.3	12.75	12575	0.136	17.4158	0.13	0.098753908	0.0024	3.43	5.378577	-23.695	-25.4848
162	226.6	12.8	12564	0.136	12.4074	0.066	0.091318818	0.0017	2.609	5.424384	-23.449	-26.0878
163	206.8	12.85	12553	0.164	10.8917	0.063	0.087226163	0.0022	8.4	5.477254	-23.618	-26.2804
164	167.9	12.9	12542	0.36	14.0549	0.1	0.090723931	0.006	5.601	4.501665	-23.693	-26.4278
165	161.2	12.95	12531	1.088	14.9116	0.111	0.093985819	0.0189	6.853	5.860515	-23.263	-26.0702
166	168.8	13	12520	0.08	8.058	0.057	0.079529535	0.0013	3.659	5.042134	-23.155	-24.7928
167	151.7	13.05	12507.77774	2.824	16.2296	0.128	0.092064785	0.0522	2.874	6.731716	-23.757	-24.2702
168	153.6	13.1	12495.55552	1.172	8.2557	0.064	0.092324045	0.0214	3.522	6.932699	-23.263	-24.1204
169	151	13.15	12483.3333	0.36	26.9713	0.214	0.115101949	0.0067	12.4	6.940272	-24.287	-23.9694
170	160.5	13.2	12471.11108	2.068	11.4189	0.085	0.109976047	0.0361	2.761	4.963164	-23.728	-23.741
171	158.7	13.25	12458.88886	0.36	8.717	0.066	0.111701783	0.0064	12.11	5.149761	-23.065	-23.7448
172	159.7	13.3	12446.66664	1.676	13.0005	0.098	0.105562805	0.0294	3.878	3.31394	-24.217	-23.7422
173	171.9	13.35	12434.44442	1.9	13.5277	0.094	0.111550115	0.031	3.56	3.199972	-23.793	-24.0186
174	191.4	13.4	12422.2222	3.496	17.5476	0.11	0.090685083	0.0512	2.51	3.072025	-24.04	-24.0576
175	164	13.45	12409.99998	1.956	14.4503	0.106	0.094756873	0.0334	3.694	3.389596	-24.349	-24.2786
176	189.6	13.5	12397.77776	3.188	18.6679	0.118	0.105204518	0.0471	2.928	3.252033	-24.293	-24.2746
177	148.8	13.55	12385.55554	2.124	14.0549	0.113	0.108336329	0.04	3.309	3.628081	-24.813	-24.14
178	221.3	13.6	12373.33332	2.824	16.4932	0.089	0.107336374	0.0358	2.92	3.896498	-23.959	-23.8632
179	154.6	13.65	12361.1111	1.9	15.5706	0.121	0.109504808	0.0344	4.098	4.065359	-24.643	-24.0662
180	202.8	13.7	12348.88888	3.412	20.5131	0.121	0.112633886	0.0471	3.006	5.583551	-24.403	-23.7514

Sample	wt mg	height (m)	wt least sq age	N2 yield	CO2 yield	% C	%org C5pt	% N2	C/N	C/N 5 pt	$\delta^{13}C_{org}$	13C-org 5pt
181	153.9	13.75	12336.66666	1.256	12.0779	0.094	0.111254541	0.0229	4.808	5.724149	-23.408	-24.0784
182	149.3	13.85	12324.44444	1.256	11.6825	0.094	0.106461714	0.0236	4.651	5.050201	-23.201	-24.2002
183	157.8	13.95	12312.22222	1.788	13.4618	0.102	0.107577653	0.0317	3.764	5.101553	-23.868	-24.4722
184	196.2	14.05	12300	1.368	31.9797	0.196	0.102955811	0.0195	11.69	4.908656	-23.705	-24.318
185	200.6	14.15	12278	2.712	20.1177	0.12	0.121509612	0.0379	3.709	5.101912	-24.2	-24.3416
186	156.4	14.25	12256	4.588	13.1982	0.101	0.121276723	0.0822	1.438	4.975211	-23.991	-24.2688
187	168.3	14.35	12234	1.62	15.9001	0.113	0.122694783	0.027	4.907	5.704806	-24.118	-24.335
188	154.3	14.45	12212	39.695	16.5591	0.129	0.126589084	0.7208	2.8	5.508224	-25.421	-24.48
189	192.8	14.55	12190	0.164	16.6909	0.104	0.131871079	0.0024	12.65	5.583075	-23.72	-24.6263333
190	149.7	14.65	12168	1.76	10.8258	0.087	0.113529234	0.0329	3.076	6.711868	-24.279	-24.6253333
191	201.5	14.75	12146	3.5	35.6042	0.212	0.106816193	0.0487	5.086	7.037461	-25.043	-24.4193333
192	161.3	14.85	12124	1.48	11.6166	0.086	0.128970188	0.0257	3.925	6.244937	-24.467	-24.99475
193	196.4	14.95	12102	3.636	23.0832	0.141	0.123580712	0.0519	3.174	6.041676	-24.269	-24.45025
194	172.3	15.05	12080	0.024	8.2557	0.057	0.126032074	0.0004	18.3	7.500986	-23.035	-24.1454
195	158.4	15.15	12058	0.304	8.3875	0.064	0.116754544	0.0054	4.703	4.691297	-23.072	-23.8346
196	173	15.25	12036	0.024	7.6626	0.053	0.112106885	0.0004	1.124	7.036587	-22.798	-23.677
197	266.7	15.35	12014	3.356	19.52	0.088	0.080330094	0.0353	2.908	7.564746	-23.368	-22.9988
198	188.5	15.45	11992	0.36	15.2411	0.097	0.080611435	0.0054	10.47	7.8427	-22.989	-23.3112
199	323	15.55	11970	3.468	29.48	0.11	0.071808972	0.0301	4.25	6.283901	-23.405	-23.274
200	169.9	15.65	11948	0.08	7.8603	0.056	0.082214092	0.0013	16.43	6.252092	-24.236	-23.5596
201	164.9	15.75	11926	1.788	13.4618	0.098	0.080609184	0.0304	3.764	3.902202	-23.248	-23.7776
202	189.1	15.85	11904	2.992	25.7192	0.163	0.089571662	0.0443	4.298	3.816497	-23.011	-23.8706
203	160.1	15.95	11882	2.096	11.2212	0.084	0.104647889	0.0367	2.677	3.59322	-23.456	-23.6406
204	180	16.05	11860	0.416	8.8488	0.059	0.102064061	0.0065	4.091	3.604316	-23.97	-23.86575
205	156.3	16.15	11838	1.424	13.33	0.102	0.091957817	0.0255	4.68	3.472923	-24.125	-23.762
206	152.9	16.25	11816	3.44	22.9514	0.18	0.101322722	0.063	3.336	3.503345	-27.356	-23.457
207	160.1	16.35	11794	2.012	12.8028	0.096	0.11775579	0.0352	3.182	3.495608	-23.65	-23.1846667
208	178.1	16.45	11772	2.572	14.0549	0.095	0.104305964	0.0405	2.732	3.445588	-22.515	-23.6656667
209	156	16.55	11750	1.816	12.4733	0.096	0.106424464	0.0326	3.434	3.526718	-23.834	-23.64125
210	156.5	16.65	11728	1.536	14.8457	0.114	0.113815756	0.0275	4.833	3.416536	-23.767	-23.8335
211	200.7	16.75	11706	4	26.3782	0.158	0.116113995	0.0558	3.297	3.184487	-25.863	-23.7562
212	178.9	16.85	11684	4.308	25.2579	0.169	0.11163169	0.0675	2.932	2.860774	-25.187	-23.95075
213	171.4	16.95	11662	2.04	12.8028	0.09	0.126323756	0.0333	3.138	2.69832	-23.798	-23.63575
214	219	17.05	11640	3.58	20.6449	0.113	0.125310877	0.0458	2.883	2.915706	-23.534	-23.402
215	163.2	17.15	11618	1.788	13.1323	0.097	0.128745733	0.0307	3.672	5.857105	-23.9	-23.225
216	192.5	17.25	11596	5.148	17.284	0.108	0.12529137	0.0749	1.679	5.683763	-25.151	-23.1576667

Sample	wt mg	height (m)	wt least sq age	N2 yield	CO2 yield	% C	%org C5pt	% N2	C/N	C/N 5 pt	$\delta^{13}C_{org}$	13C-org 5pt
217	188	17.35	11574	4.28	18.1407	0.116	0.115296815	0.0638	2.119	5.794378	-25.44	-23.38825
218	191.4	17.45	11552	4.588	38.7674	0.243	0.101765681	0.0672	4.225	5.966141	-28.321	-23.38175
219	199.6	17.55	11530	0.22	10.4304	0.063	0.108304972	0.0031	17.59	5.976135	-22.345	-23.772
220	176.9	17.65	11508	131.86	14.4503	0.098	0.140788237	2.0886	2.806	3.046733	-23.862	-23.772
221	168.8	17.75	11486	2.824	12.6051	0.09	0.132324933	0.0469	2.232	3.028223	-23.942	-23.86625
222	193.2	17.85	11464	2.404	14.3185	0.089	0.129894708	0.0349	2.978	4.813867	-22.92	-23.8765
223	192.5	17.95	11442	1.536	13.1323	0.082	0.12183771	0.0224	4.275	4.920411	-23.502	-23.979
224	177.2	18.05	11420	3.16	18.602	0.126	0.116466326	0.05	2.943	5.416485	-26.218	-23.8715
225	178.3	18.15	11398	3.076	16.6909	0.112	0.084227904	0.0483	2.713	5.842486	-24.32	-23.8715
226	221.3	18.25	11376	0.416	10.4304	0.057	0.096880923	0.0053	11.16	5.871265	-22.732	-24.121
227	163.9	18.35	11354	2.18	15.307	0.112	0.099742939	0.0373	3.511	4.234828	-23.791	
228	226	18.45	11332	1.172	15.8342	0.084	0.093132771	0.0145	6.755	3.908739	-22.35	-23.471
229	201.5	18.55	11310	0.976	9.9032	0.059	0.09775997	0.0136	5.073	3.17634	-23.181	-25.2095
230	197	18.65	11288	3.244	18.5361	0.113	0.098202312	0.0461	2.857	2.674237	-24.368	-25.2095
231	171.6	18.75	11266	2.88	17.1522	0.12	0.084803104	0.047	2.978	2.555311	-24.546	-24.2386667
232	156.5	18.85	11244	3.86	14.5162	0.111	0.084918436	0.0691	1.88	2.548511	-24.967	-24.2386667
233	169	18.95	11222	3.188	19.7223	0.14	0.097595751	0.0529	3.093	2.647128	-25.271	-24.471
234	200	19.05	11200	4.812	24.6648	0.148	0.097442861	0.0674	2.563	2.520006	-26.402	-23.2263333
235	156.5	19.15	11178	3.048	13.7913	0.106	0.108635782	0.0546	2.262	2.60473	-24.151	-23.91125
236	177.1	19.25	11156	2.376	13.989	0.095	0.126438167	0.0376	2.944	2.964324	-24.077	-24.4225
237	166.6	19.35	11134	4.252	20.1836	0.145	0.125005714	0.0715	2.373	3.014653	-24.901	-24.4225
238	160.5	19.45	11112	2.712	13.33	0.1	0.119974048	0.0473	2.458	3.147341	-24.237	-24.65125
239	208.3	19.55	11090	2.32	13.8572	0.08	0.126788797	0.0312	2.986	3.259535	-23.536	-24.27275
240	171.6	19.65	11068	1.536	12.4733	0.087	0.118713507	0.0251	4.06	3.120533	-23.574	-24.57225
241	173.2	19.75	11046	2.292	14.648	0.101	0.105081796	0.0371	3.195	2.803446	-24.095	-24.2355
242	173	19.85	11024	1.956	11.8802	0.082	0.101377374	0.0317	3.037	2.441928	-23.332	-23.8888
243	160.4	19.95	11002	2.208	13.33	0.1	0.102717408	0.0386	3.019	2.293195	-24.428	-23.59025
244	191	20.05	10980	4.476	20.5131	0.129	0.090122596	0.0657	2.291	2.051404	-25.021	-24.2203333
245	210.2	20.15	10958	3.412	16.8886	0.096	0.090135023	0.0455	2.475	1.931378	-24.55	-22.7485
246	151.5	20.25	10936	4.28	11.8802	0.094	0.099944597	0.0792	1.388	1.387874	-24.209	-22.502

Appendix B

Burfu lab data: Carbonate fraction

Sample	wt mg	height (m)	wt least sq age	CO2 yield	%carbonate	%carb 5pt	$\delta^{13}C_{carb}$	13C-carb 5pt	$\delta^{18}O$	18O 5pt
1	101.7	0.2	15336	112.64	11.07571288	10.46767822	-3.63	-3.1838	-14.63	-14.656
2	105.9	0.4	15292	101.97	9.628895184	10.42336898	-2.798	-3.0708	-14.69	-14.692
3	100.5	0.6	15248	108.89	10.83482587	10.71818197	-3.029	-3.1962	-14.56	-14.633
4	101.1	0.8	15204	105.85	10.46983185	10.77132677	-3.333	-3.232	-14.75	-14.633
5	110.9	1	15160	114.55	10.32912534	10.83988531	-3.129	-3.254	-14.64	-14.533
6	182.4	1.2	15116	197.98	10.85416667	10.82143634	-3.065	-3.2282	-14.81	-14.226
7	155.4	1.4	15072	172.54	11.1029601	10.86602251	-3.425	-3.2746	-14.4	-14.12
8	127.3	1.6	15028	141.31	11.10054988	10.46133007	-3.208	-3.28	-14.57	-14.053
9	150.5	1.8	14984	162.73	10.81262458	9.992709455	-3.443	-3.283	-14.25	-13.859
10	137.2	2	14940	140.45	10.23688047	8.099617311	-3	-3.3264	-13.1	-13.568
11	44.1	2.2	14896	48.85	11.07709751	7.572865521	-3.297	-3.3754	-14.29	-13.749
12	23.9	2.4	14852	21.7	9.079497908	7.244638138	-3.452	-3.3406	-14.06	-13.707
13	23.5	2.6	14808	20.58	8.757446809	6.672290353	-3.223	-3.2372	-13.6	-13.526
14	190.4	2.8	14764	25.65	1.347163866	6.714464358	-3.66	-3.1726	-12.8	-13.267
15	89.7	3	14720	68.2	7.603121516	8.195756223	-3.245	-3.1406	-14	-13.227
16	40.6	3.2	14695.55552	38.31	9.435960591	8.088488686	-3.123	-3.1926	-14.08	-13.036
17	47.3	3.3	14671.11108	29.41	6.217758985	8.408439424	-2.935	-3.2746	-13.16	-12.753
18	50.5	3.4	14646.66664	45.29	8.968316832	9.311859804	-2.9	-3.4836	-12.3	-12.759
19	34.5	3.5	14622.2222	30.2	8.753623188	9.532181112	-3.5	-3.6464	-12.6	-12.803
20	113.8	3.6	14597.77776	80.42	7.066783831	9.770508544	-3.505	-3.7218	-13.04	-12.565
21	19.6	3.7	14573.33332	21.63	11.03571429	10.23306166	-3.533	-3.686	-12.67	-12.38
22	61.1	3.8	14548.88888	65.59	10.73486088	9.926680704	-3.98	-3.5072	-13.18	-12.655
23	104.4	3.9	14524.44444	105.13	10.06992337	9.849333774	-3.714	-3.2384	-12.52	-12.847
24	74.9	4	14500	74.49	9.945260347	9.952857517	-3.877	-3.246	-11.41	-12.891
25	57.7	4.1	14478	54.12	9.379549393	9.973234019	-3.326	-3.2536	-12.12	-13.16
26	105	4.2	14456	99.79	9.503809524	10.2199547	-2.639	-3.3702	-14.04	-13.33
27	101.4	4.3	14434	104.93	10.34812623	10.02329464	-2.636	-3.5092	-14.15	-13.128
28	59.4	4.4	14412	62.89	10.58754209	9.561411324	-3.752	-3.508	-12.74	-12.891
29	70	4.5	14390	70.33	10.04714286	9.823288078	-3.915	-3.291	-12.76	-13.131
30	103.4	4.6	14368	109.74	10.6131528	9.399235851	-3.909	-3.0618	-12.96	-13.35
31	141.4	4.7	14346	120.48	8.520509194	8.769725928	-3.334	-2.7794	-13.03	-13.625
32	46.5	4.8	14324	37.38	8.038709677	9.086804645	-2.63	-2.652	-12.96	-13.729
33	55.3	4.9	14302	65.79	11.89692586	9.420967471	-2.667	-2.6236	-13.95	-13.889
34	46.5	5	14280	36.86	7.92688172	8.782227461	-2.769	-2.6244	-13.85	-13.928
35	100.3	5.1	14258	74.88	7.46560319	8.872685563	-2.497	-2.601	-14.34	-13.988
36	57.6	5.2	14236	58.21	10.10590278	10.20917122	-2.697	-2.5616	-13.56	-13.884

Sample	wt mg	height (m)	wt least sq age	CO2 yield	%carbonate	%carb 5pt	$\delta^{13}C_{carb}$	13C-carb 5pt	$\delta^{18}O$	18O 5pt
37	63	5.3	14214	61.17	9.70952381	10.75435757	-2.488	-2.4856	-13.76	-13.963
38	93	5.4	14192	80.94	8.703225806	11.12599816	-2.671	-2.4554	-14.14	-14.052
39	74.9	5.5	14170	62.76	8.37917223	11.91430037	-2.652	-2.3538	-14.15	-13.981
40	63.5	5.6	14148	89.84	14.1480315	13.4317117	-2.3	-2.3136	-13.82	-13.878
41	111.2	5.7	14126	142.69	12.83183453	11.32304828	-2.317	-2.2854	-13.95	-13.634
42	84.9	5.8	14104	98.21	11.56772674	10.93258499	-2.337	-2.3398	-14.21	-13.632
43	76	5.9	14082	96.1	12.64473684	10.88327041	-2.163	-2.3826	-13.78	-13.7
44	53.3	6	14060	85.1	15.96622889	10.44945818	-2.451	-2.4332	-13.64	-13.653
45	110.3	6.1	14038	39.76	3.604714415	8.767389749	-2.159	-2.4192	-12.6	-13.812
46	83	6.2	14016	90.3	10.87951807	9.572037822	-2.589	-2.5068	-13.94	-14.18
47	52	6.3	13994	58.87	11.32115385	9.397501729	-2.551	-2.5056	-14.55	-14.242
48	55.5	6.4	13972	58.14	10.47567568	8.54726587	-2.416	-2.4388	-13.54	-14.068
49	67.1	6.5	13950	50.7	7.555886736	7.72587253	-2.381	-2.3028	-14.44	-13.978
50	97.3	6.6	13928	74.22	7.627954779	7.670287652	-2.597	-2.1956	-14.44	-13.706
51	58.5	6.7	13906	58.54	10.00683761	6.49745449	-2.583	-2.2728	-14.25	-13.504
52	78.6	6.8	13884	55.57	7.069974555	4.663544101	-2.217	-2.6562	-13.68	-12.735
53	91.4	6.9	13862	58.21	6.368708972	4.715258919	-1.736	-2.7554	-13.09	-12.764
54	90.3	7	13840	65.72	7.277962348	4.588911064	-1.845	-2.7876	-13.08	-12.689
55	83.4	7.1	13821.66663	14.71	1.763788969	4.6245742	-2.983	-2.7372	-13.43	-12.713
56	274.1	7.2	13803.3333	22.95	0.837285662	5.721447856	-4.5	-2.4804	-10.4	-12.69
57	62.7	7.3	13784.99997	45.95	7.328548644	7.294440161	-2.713	-1.9452	-13.83	-13.339
58	82.5	7.4	13766.66664	47.33	5.736969697	7.495068287	-1.897	-1.7876	-12.72	-13.269
59	89.2	7.5	13748.33331	66.51	7.456278027	7.73945517	-1.593	-1.7842	-13.19	-13.459
60	81.4	7.6	13729.99998	59	7.248157248	7.522049443	-1.699	-1.8396	-13.32	-13.469
61	89	7.7	13711.66665	77.45	8.702247191	7.320313494	-1.824	-2.0284	-13.64	-13.546
62	81.1	7.8	13693.33332	67.57	8.331689273	6.881629706	-1.925	-2.2156	-13.47	-13.462
63	102.2	7.85	13674.99999	71.12	6.95890411	6.292502312	-1.88	-2.3142	-13.67	-13.315
64	82.6	7.9	13656.66666	52.61	6.369249395	6.126258483	-1.87	-2.4154	-13.24	-13.051
65	68.9	7.95	13638.33333	42.99	6.239477504	6.051694319	-2.643	-2.5234	-13.7	-12.862
66	62.3	8	13620	40.55	6.50882825	5.998763853	-2.76	-2.3548	-13.23	-12.682
67	80.3	8.05	13609	43.25	5.386052304	6.129474838	-2.418	-2.1978	-12.74	-12.594
68	83.8	8.1	13598	51.35	6.127684964	6.823404349	-2.386	-2.1224	-12.35	-12.697
69	84	8.15	13587	50.37	5.996428571	7.033057229	-2.41	-2.05	-12.3	-12.723
70	71.5	8.2	13576	42.72	5.974825175	6.991953333	-1.8	-2.0652	-12.8	-12.81
71	85.6	8.25	13565	61.31	7.162383178	7.138149248	-1.975	-2.221	-12.79	-12.969
72	69.3	8.3	13554	61.37	8.855699856	7.110505754	-2.041	-2.2976	-13.25	-13.147

Sample	wt mg	height (m)	wt least sq age	CO2 yield	%carbonate	%carb 5pt	$\delta^{13}C_{carb}$	13C-carb 5pt	$\delta^{18}O$	18O 5pt
73	79	8.35	13543	56.69	7.175949367	6.571939073	-2.024	-2.3528	-12.48	-12.798
74	88	8.4	13532	50.96	5.790909091	6.735445419	-2.486	-2.4366	-12.74	-13.088
75	75.8	8.45	13521	50.83	6.705804749	7.142588678	-2.579	-2.2876	-13.6	-13.105
76	86.9	8.5	13510	61.04	7.024165708	7.746192126	-2.358	-2.2098	-13.68	-13.106
77	92.1	8.55	13499	56.76	6.16286645	8.240146863	-2.317	-2.2012	-11.51	-13.201
78	76.7	8.6	13488	61.31	7.993481095	8.336210633	-2.443	-2.1932	-13.93	-13.499
79	64.6	8.65	13477	50.56	7.826625387	8.272386209	-1.741	-2.1082	-12.82	-13.314
80	76.4	8.7	13466	74.29	9.72382199	8.35987399	-2.19	-2.1618	-13.6	-13.258
81	99	8.75	13455	93.99	9.493939394	8.054235275	-2.315	-2.1354	-14.15	-12.994
82	65.3	8.8	13444	43.38	6.643185299	7.318504721	-2.277	-1.9824	-13	-12.604
83	78	8.85	13433	59.86	7.674358974	7.39787737	-2.018	-1.821	-13	-12.604
84	87.1	8.9	13422	71.98	8.264064294	7.142905492	-2.009	-1.7048	-12.54	-12.579
85	91.5	8.95	13411	74.99	8.195628415	6.759836223	-2.058	-1.6126	-12.28	-12.776
86	125.6	9	13400	73.04	5.815286624	6.107254882	-1.55	-1.5842	-12.2	-12.959
87	82.4	9.05	13389	58.01	7.040048544	5.375059627	-1.47	-1.7784	-13	-13.038
88	119.9	9.1	13378	76.73	6.399499583	5.441829113	-1.437	-1.8808	-12.88	-13.11
89	97.5	9.15	13367	61.9	6.348717949	5.608742638	-1.548	-1.9272	-13.53	-13.064
90	98.1	9.2	13356	48.39	4.932721713	5.816583678	-1.916	-1.9448	-13.2	-12.987
91	116	9.25	13345	24.99	2.154310345	6.314453951	-2.521	-1.884	-12.6	-12.909
92	101.9	9.3	13334	75.14	7.373895976	7.425636139	-1.982	-1.6464	-13.36	-12.752
93	86.3	9.35	13323	62.43	7.234067207	7.498977245	-1.669	-1.5374	-12.64	-12.621
94	109.3	9.4	13312	80.75	7.387923147	7.210116777	-1.636	-1.6136	-13.14	-12.677
95	134.1	9.45	13301	99.53	7.42207308	6.660685301	-1.612	-1.5734	-12.8	-12.713
96	94.9	9.5	13290	73.17	7.710221286	6.777436186	-1.333	-1.5988	-11.81	-12.747
97	133	9.55	13279	102.95	7.740601504	6.738780119	-1.437	-1.6582	-12.71	-12.911
98	72.3	9.6	13268	41.86	5.789764869	6.812058123	-2.05	-1.6968	-12.92	-12.927
99	88.8	9.65	13257	41.21	4.640765766	7.699273216	-1.435	-1.557	-13.32	-12.928
100	85.8	9.7	13246	68.69	8.005827506	8.074453397	-1.739	-1.61	-12.97	-12.846
101	103.3	9.75	13235	77.65	7.516940949	7.815374226	-1.63	-1.6302	-12.63	-13.001
102	94.4	9.8	13224	76.53	8.106991525	7.630361671	-1.63	-1.6546	-12.78	-12.848
103	95.2	9.85	13213	97.35	10.22584034	7.410485105	-1.351	-1.6856	-12.93	-12.627
104	96	9.9	13202	62.56	6.516666667	6.679741673	-1.7	-1.7712	-12.91	-12.707
105	111.2	9.95	13191	74.62	6.710431655	7.427845556	-1.84	-1.9016	-13.75	-12.414
106	98.5	10	13180	64.93	6.591878173	7.615686233	-1.752	-1.8602	-11.87	-11.64
107	92	10.05	13169	64.47	7.007608696	7.854020555	-1.785	-1.8506	-11.68	-11.326
108	61.7	10.1	13158	40.55	6.572123177	7.997356584	-1.779	-1.8342	-13.33	-10.948

Sample	wt mg	height (m)	wt least sq age	CO2 yield	%carbonate	%carb 5pt	$\delta^{13}C_{carb}$	13C-carb 5pt	$\delta^{18}O$	18O 5pt
109	66.1	10.15	13147	67.8	10.25718608	8.043958564	-2.352	-1.8334	-11.45	-10.286
110	95.9	10.2	13136	73.36	7.649635036	7.353696584	-1.633	-1.7396	-9.88	-10.098
111	92.4	10.25	13125	71.92	7.783549784	7.286708173	-1.704	-1.773	-10.3	-10.542
112	91.4	10.3	13114	70.6	7.72428884	6.870063363	-1.703	-1.784	-9.788	-10.919
113	105.2	10.35	13103	71.59	6.80513308	6.607814291	-1.775	-1.8034	-10.02	-11.361
114	95.3	10.4	13092	64.86	6.80587618	6.323351832	-1.883	-1.7832	-10.5	-11.568
115	91.2	10.45	13081	66.71	7.314692982	6.116313025	-1.8	-1.8298	-12.1	-11.869
116	122.8	10.5	13070	70	5.700325733	5.811487938	-1.759	-1.8694	-12.18	-11.842
117	92	10.55	13059	59	6.413043478	5.860073755	-1.8	-1.875	-12	-11.738
118	94.3	10.6	13048	50.76	5.382820785	5.962543278	-1.674	-1.8796	-11.05	-11.687
119	68.9	10.65	13037	39.76	5.770682148	6.263863737	-2.116	-1.9108	-12.01	-11.802
120	125.1	10.7	13026	72.44	5.790567546	6.375271349	-1.998	-1.8382	-11.97	-11.492
121	93.4	10.75	13015	55.51	5.943254818	6.625972429	-1.787	-1.7798	-11.66	-10.942
122	83.1	10.8	13004	57.55	6.925391095	6.741178215	-1.823	-1.7856	-11.74	-11.068
123	62.4	10.85	12993	42.99	6.889423077	6.745343024	-1.83	-1.8412	-11.63	-11.505
124	77.2	10.9	12982	48.85	6.327720207	6.202658408	-1.753	-1.8734	-10.46	-11.258
125	65.8	10.95	12971	46.35	7.044072948	6.042841239	-1.706	-1.9386	-9.216	-11.747
126	72.6	11	12960	47.33	6.519283747	6.530089642	-1.816	-2.0564	-12.3	-12.623
127	100.4	11.05	12949	69.74	6.946215139	7.088455114	-2.101	-2.1836	-13.92	-12.89
128	75	11.1	12938	31.32	4.176	7.703851262	-1.991	-2.2168	-10.39	-12.741
129	68.1	11.15	12927	37.65	5.528634361	8.338752272	-2.079	-2.1812	-12.91	-13.084
130	76.2	11.2	12916	72.24	9.480314961	8.829557192	-2.295	-2.0258	-13.6	-12.713
131	94.5	11.25	12905	87.99	9.311111111	8.367753459	-2.452	-1.8002	-13.63	-12.285
132	77.6	11.3	12894	77.78	10.02319588	7.828214943	-2.267	-1.7036	-13.18	-12.153
133	99	11.35	12883	72.77	7.350505051	6.985524017	-1.813	-1.6562	-12.11	-12.234
134	69.2	11.4	12872	55.24	7.98265896	6.71058917	-1.302	-1.855	-11.05	-12.383
135	108	11.45	12861	77.45	7.171296296	6.32856515	-1.167	-1.9426	-11.46	-12.568
136	62.6	11.5	12850	41.4	6.61341853	6.182192489	-1.969	-1.8792	-12.97	-12.383
137	65.7	11.55	12839	38.17	5.809741248	6.322162681	-2.03	-1.7898	-13.59	-12.167
138	66.2	11.6	12828	39.56	5.975830816	6.511460969	-2.807	-1.701	-12.85	-11.688
139	96.5	11.65	12817	58.6	6.07253886	6.74511325	-1.74	-1.491	-11.98	-11.644
140	77.6	11.7	12806	49.97	6.43943299	6.903719095	-0.85	-1.4816	-10.53	-11.319
141	73.1	11.75	12795	53.46	7.313269494	6.925134822	-1.522	-1.6166	-11.89	-11.689
142	72.2	11.8	12784	48.78	6.756232687	6.75462268	-1.586	-1.6348	-11.2	-11.847
143	69.4	11.85	12773	49.58	7.144092219	6.467792458	-1.757	-1.6976	-12.63	-11.648
144	115.3	11.9	12762	79.16	6.865568083	5.997266697	-1.693	-1.8462	-10.35	-11.744

Sample	wt mg	height (m)	wt least sq age	CO2 yield	%carbonate	%carb 5pt	δ13C-carb	13C-carb 5pt	δ18O	18O 5pt
145	86	11.95	12751	56.3	6.546511628	5.66776031	-1.525	-1.963	-12.38	-11.96
146	64.9	12	12740	41.93	6.460708783	5.454339802	-1.613	-2.1024	-12.68	-12.065
147	71.1	12.05	12729	37.84	5.322081575	5.478625478	-1.9	-2.1898	-10.2	-12.162
148	82	12.1	12718	39.29	4.791463415	5.869764718	-2.5	-2.1448	-13.11	-12.757
149	79.3	12.15	12707	41.34	5.213114754	6.368769333	-2.277	-1.9532	-11.43	-12.751
150	70.2	12.2	12696	38.5	5.484330484	7.579933993	-2.222	-1.694	-12.91	-12.903
151	62.7	12.25	12685	41.27	6.582137161	7.67960692	-2.05	-1.7202	-13.16	-12.907
152	70.2	12.3	12674	51.09	7.27777778	7.43172946	-1.675	-1.742	-13.17	-12.898
153	74	12.35	12663	53.92	7.286486486	6.20313251	-1.542	-1.9378	-13.08	-12.263
154	67.8	12.4	12652	76.2	11.23893805	6.243015953	-0.981	-2.09	-12.19	-12.343
155	73.8	12.45	12641	44.37	6.012195122	5.161645134	-2.353	-2.3184	-12.93	-12.52
156	64.2	12.5	12630	34.35	5.350467290	4.928389469	-2.159	-2.243	-13.12	-12.441
157	292.3	12.55	12619	35.47	1.213479302	5.238847065	-2.654	-2.2702	-10	-12.566
158	71	12.6	12608	52.54	7.4	6.355558612	-2.303	-2.1978	-13.48	-13.358
159	66.7	12.65	12597	38.9	5.832083968	5.659785741	-2.123	-2.249	-13.08	-13.262
160	64.9	12.7	12586	31.45	4.845916795	5.861537117	-1.976	-2.3718	-12.53	-13.326
161	61.7	12.75	12575	42.59	6.902755267	6.267869577	-2.295	-2.3766	-13.74	-13.25
162	67.5	12.8	12564	45.88	6.797037037	6.094714973	-2.292	-2.3644	-13.96	-12.99
163	63.4	12.85	12553	24.86	3.921135647	6.276716016	-2.559	-2.211	-13	-12.576
164	66.6	12.9	12542	45.56	6.840840841	7.171002619	-2.737	-2.0464	-13.4	-12.337
165	72.7	12.95	12531	50	6.877579092	7.525887886	-2	-1.918	-12.15	-12.425
166	67.6	13	12520	40.81	6.036982249	7.500584231	-2.234	-1.8534	-12.44	-12.494
167	71	13.05	12507.7774	54.72	7.70704254	7.28954205	-1.525	-1.8764	-11.89	-12.561
168	61.9	13.1	12495.55552	51.95	8.392568659	7.56192847	-1.736	-1.8306	-11.8	-12.614
169	65.5	13.15	12483.3333	56.43	8.615267176	7.186851727	-2.095	-1.7826	-13.84	-12.748
170	70.7	13.2	12471.1108	47.73	6.751060082	6.768920786	-1.677	-1.6634	-12.5	-12.243
171	54.8	13.25	12458.88886	31.12	5.678832117	6.465249503	-2.349	-1.7038	-12.78	-11.825
172	64.8	13.3	12446.66664	54.25	8.37191358	6.600064119	-1.296	-1.5192	-12.16	-11.693
173	61.1	13.35	12434.44442	39.82	6.517184943	6.47122016	-1.496	-1.5382	-12.47	-11.578
174	89.8	13.4	12422.2222	58.6	6.525612472	6.548469872	-1.499	-1.5488	-11.31	-11.575
175	79.5	13.45	12409.99998	41.6	5.232704403	6.800320671	-1.879	-1.4942	-10.4	-11.507
176	65.4	13.5	12397.77776	43.51	6.652905199	7.478241134	-1.426	-1.3396	-12.12	-11.816
177	52.2	13.55	12385.55554	38.77	7.427203065	7.369256339	-1.391	-1.439	-11.59	-11.433
178	73.9	13.6	12373.33332	51.02	6.903924222	7.325273585	-1.549	-1.4758	-12.46	-11.296
179	67.4	13.65	12361.1111	52.47	7.784866469	7.44448874	-1.226	-1.4906	-10.97	-10.757
180	78.9	13.7	12348.88888	68.03	8.622306717	7.138790234	-1.106	-1.6612	-11.95	-10.777

103

| Sample	wt mg	height (m)	wt least sq age	CO2 yield	%carbonate	%carb 5pt	$\delta^{13}C_{carb}$	13C-carb 5pt	$\delta^{18}O$	18O 5pt
181	63.9	13.75	12336.66666	39.03	6.107981221	6.257108182	-1.923	-1.9608	-10.21	-10.554
182	87.8	13.85	12324.44444	63.28	7.207289294	6.051107013	-1.575	-2.1186	-10.9	-10.764
183	56	13.95	12312.22222	42	7.5	5.823865633	-1.623	-2.3058	-9.76	-11.049
184	70.6	14.05	12300	44.17	6.256373938	5.47298402	-2.079	-2.3276	-11.08	-11.158
185	73.4	14.15	12278	30.93	4.213896458	5.754330822	-2.604	-2.3912	-10.83	-11.506
186	73.1	14.25	12256	37.12	5.077975376	6.196122959	-2.712	-2.212	-11.26	-11.668
187	61.9	14.35	12234	37.58	6.071082391	6.658333371	-2.511	-2.003	-12.32	-11.967
188	79.4	14.45	12212	45.62	5.74559194	6.349319204	-1.732	-1.7914	-10.31	-11.903
189	84.3	14.55	12190	64.6	7.663107948	5.824906699	-2.397	-1.8238	-12.81	-12.219
190	70	14.65	12168	44.96	6.422857143	5.675331086	-1.708	-1.804	-11.64	-12.493
191	80.2	14.75	12146	59.26	7.389027431	5.873677807	-1.667	-1.8784	-12.75	-12.881
192	69.2	14.85	12124	31.32	4.526011561	5.980803828	-1.453	-2.0022	-12	-13.109
193	68	14.95	12102	21.24	3.123529412	6.430263895	-1.894	-2.0982	-11.89	-13.417
194	69.6	15.05	12080	48.13	6.915229885	7.59258199	-2.298	-2.2118	-14.18	-13.829
195	56.2	15.15	12058	41.67	7.414590747	7.846051926	-2.08	-2.1786	-13.58	-13.538
196	58.4	15.25	12036	46.28	7.924657534	8.162525874	-2.286	-2.3036	-13.89	-13.538
197	62.2	15.35	12014	42.13	6.773311897	8.114256279	-1.933	-2.305	-13.54	-13.196
198	70.9	15.45	11992	63.35	8.935119887	7.445172346	-2.462	-2.3878	-13.95	-12.702
199	59.7	15.55	11970	48.85	8.182579564	7.089990945	-2.132	-2.5184	-12.73	-12.456
200	65.8	15.65	11948	59.2	8.996960486	7.119332917	-2.705	-2.7718	-13.58	-12.31
201	70.1	15.75	11926	53.86	7.683309558	6.811712972	-2.293	-2.7102	-12.18	-11.861
202	63.1	15.85	11904	21.63	3.427892235	5.588997006	-2.347	-2.6116	-11.08	-11.578
203	55.9	15.95	11882	40.02	7.15921288	6.173048189	-3.115	-2.4228	-12.72	-11.695
204	57.7	16.05	11860	48.06	8.329289428	6.134457147	-3.399	-2.1222	-12	-11.517
205	63.2	16.15	11838	47.14	7.458860759	5.840338392	-2.397	-1.745	-11.34	-11.486
206	92.5	16.25	11816	14.52	1.56972973	5.919348848	-1.8	-1.5298	-10.76	-11.537
207	67.5	16.35	11794	42.85	6.348148148	6.089613429	-1.403	-1.7266	-11.67	-11.875
208	65.2	16.45	11772	45.42	6.966257669	5.178917133	-1.612	-1.826	-11.82	-11.66
209	64.4	16.55	11750	44.17	6.858695652	4.701469052	-1.513	-1.906	-11.84	-11.541
210	57.5	16.65	11728	45.16	7.853913043	4.385340894	-1.321	-1.981	-11.6	-11.683
211	72.2	16.75	11706	17.48	2.421052632	4.240680734	-2.784	-2.1026	-12.45	-11.776
212	75	16.85	11684	13.46	1.794666667	4.866679998	-1.9	-1.8634	-10.59	-11.576
213	75.3	16.95	11662	34.48	4.579017264	5.377389522	-2.012	-1.7966	-11.22	-11.817
214	80.2	17.05	11640	42.33	5.278054863	4.662824234	-1.888	-1.952	-12.56	-11.939
215	73.5	17.15	11618	52.41	7.130612245	5.102305955	-1.929	-2.0828	-12.06	-12.248
216	71.5	17.25	11596	39.69	5.551048951	4.842417272	-1.588	-2.0556	-11.45	-11.959

Sample	wt mg	height (m)	wt least sq age	CO2 yield	%carbonate	%carb 5pt	$\delta^{13}C_{carb}$	13C-carb 5pt	$\delta^{18}O$	18O 5pt
217	78.4	17.35	11574	34.09	4.348214286	4.586775082	-1.566	-2.0446	-11.79	-12.084
218	274.6	17.45	11552	27.63	1.006190823	5.195583838	-2.789	-2.0864	-11.84	-12.099
219	91.7	17.55	11530	68.55	7.475463468	6.410254764	-2.542	-1.9094	-14.1	-12.254
220	77	17.65	11508	44.9	5.831168831	5.296881034	-1.793	-1.9406	-10.62	-11.759
221	82.1	17.75	11486	35.08	4.272838002	4.715773429	-1.533	-1.925	-12.08	-11.903
222	77.5	17.85	11464	57.29	7.392258065	5.572020248	-1.775	-2.1268	-11.87	-12.204
223	70.4	17.95	11442	49.84	7.079545455	4.899892746	-1.904	-2.1498	-12.61	-12.326
224	73.3	18.05	11420	13.99	1.908594816	5.063053423	-2.698	-2.2798	-11.63	-12.515
225	75.3	18.15	11398	22.03	2.92563081	6.323286966	-1.715	-2.2064	-11.34	-12.734
226	74.9	18.25	11376	64.07	8.554072096	7.389800148	-2.542	-2.4246	-13.58	-12.472
227	75.9	18.35	11354	30.6	4.031620553	6.361521305	-1.89	-2.3184	-12.48	-11.85
228	77.4	18.45	11332	61.11	7.895348837	6.436629555	-2.554	-2.2214	-13.55	-11.377
229	75.8	18.55	11310	62.23	8.209762533	6.448981356	-2.331	-1.977	-12.73	-10.762
230	73.2	18.65	11288	60.45	8.258196721	5.490579763	-2.806	-1.8908	-10.03	-9.6828
231	77.3	18.75	11266	26.38	3.412677878	5.592338477	-2.011	-1.6208	-10.47	-9.7988
232	75.4	18.85	11244	33.23	4.407161804	6.646602901	-1.405	-1.481	-10.11	-9.727
233	81.6	18.95	11222	64.93	7.957107843	6.810348876	-1.332	-1.48	-10.48	-10.185
234	76.6	19.05	11200	26.18	3.417754569	6.402713946	-1.9	-1.573	-7.33	-10.31
235	82.4	19.15	11178	72.24	8.766990291	6.829188739	-1.456	-1.5218	-10.61	-11.202
236	75	19.25	11156	65.13	8.684	6.469587207	-1.312	-1.6234	-10.11	-11.469
237	75.7	19.35	11134	39.56	5.225891678	6.023921228	-1.4	-1.7332	-12.4	-11.894
238	75.74	19.45	11112	44.83	5.918933193	6.567851803	-1.797	-1.7772	-11.1	-11.448
239	77.8	19.55	11090	43.18	5.550128535	6.178714846	-1.644	-1.7574	-11.79	-11.252
240	80.6	19.65	11068	56.17	6.96898263	6.012008977	-1.964	-1.8372	-11.94	-10.994
241	97	19.75	11046	62.62	6.455670103	5.711324696	-1.861	-1.852	-12.23	-10.922
242	80.8	19.85	11024	64.2	7.945544554	5.487907211	-1.62	-1.8592	-10.17	-10.591
243	78.5	19.95	11002	31.19	3.973248408	4.873497875	-1.698	-1.919	-10.12	-10.695
244	74.1	20.05	10980	34.95	4.71659919	5.173581031	-2.043	-1.99266667	-10.5	-10.886
245	78.4	20.15	10958	42.85	5.465561224	5.402071951	-2.038	-1.9675	-11.58	-11.079
246	76.2	20.25	10936	40.68	5.338582677	5.338582677	-1.897	-1.897	-10.57	-10.574

Appendix C

Graphs of raw data versus height: Organic fraction

106

% organic carbon raw

$\delta^{13}C_{organic}$ raw (‰ VPDB)
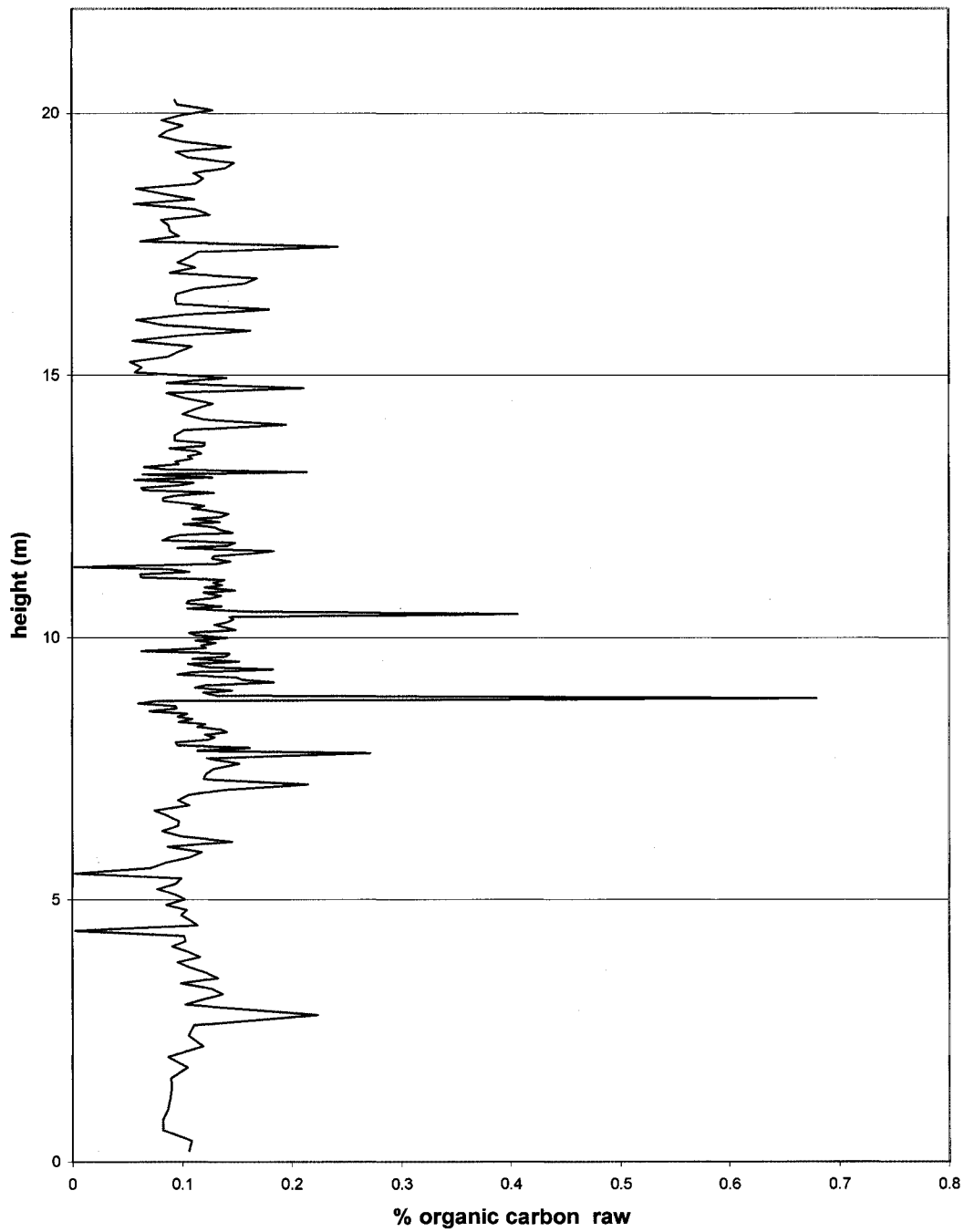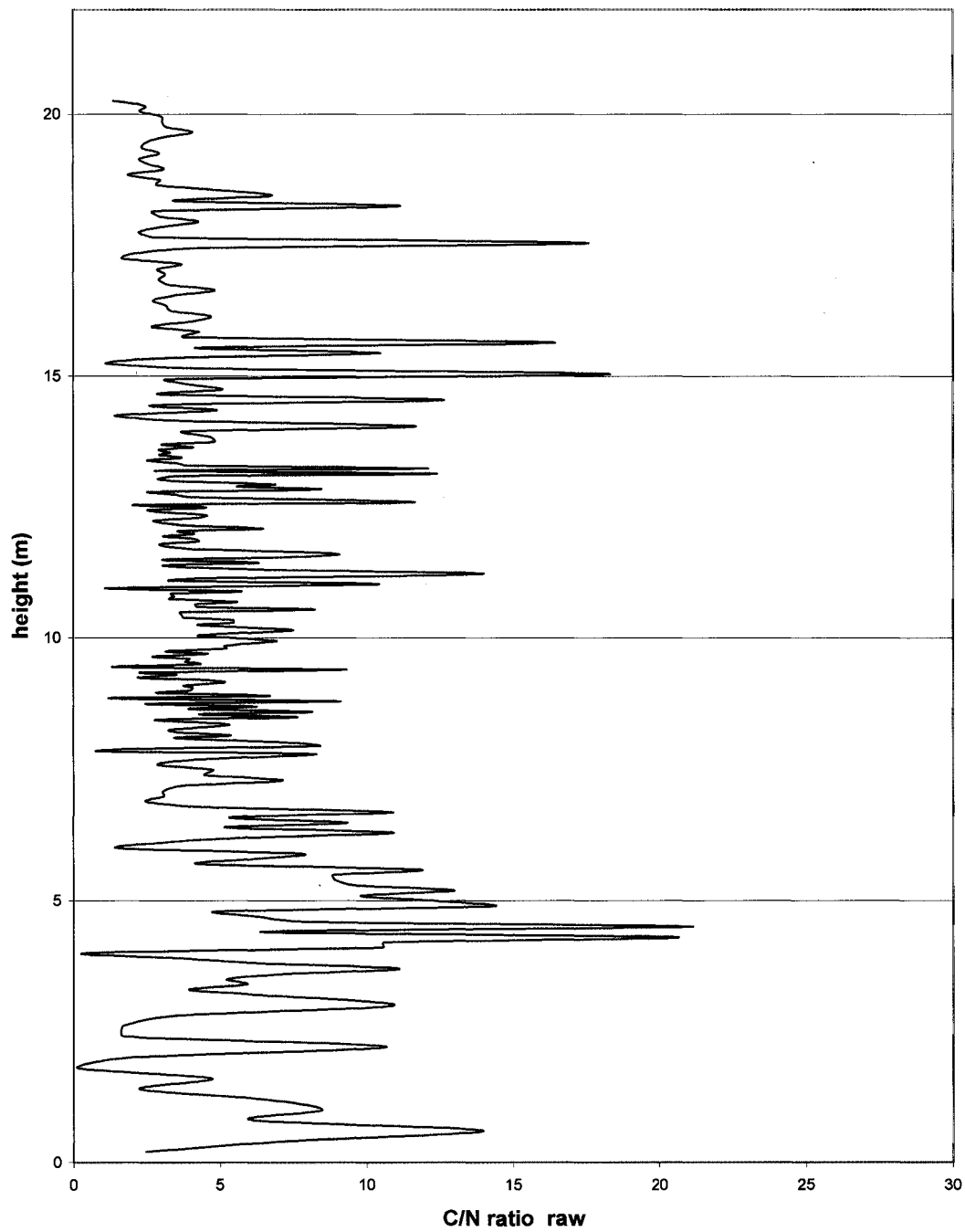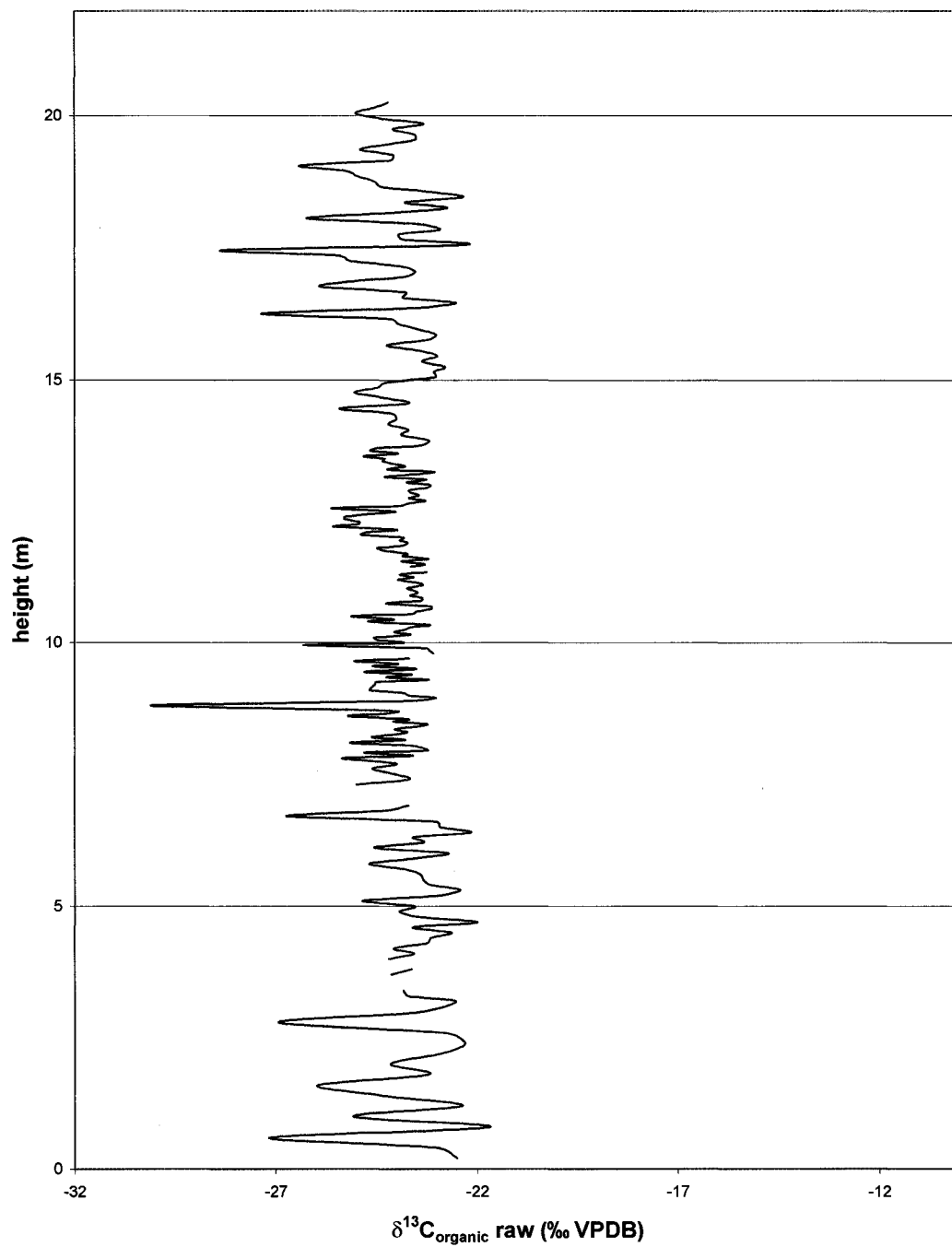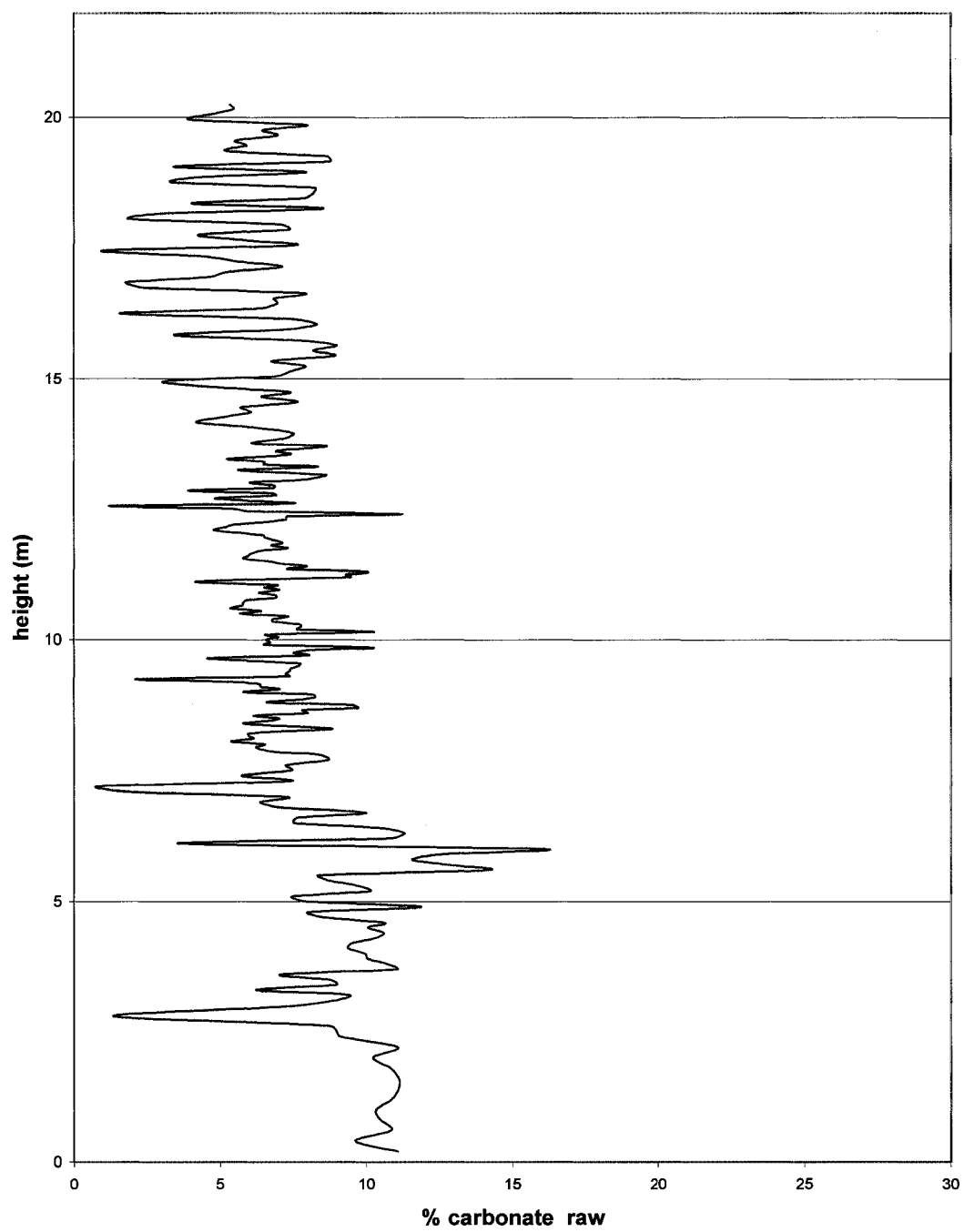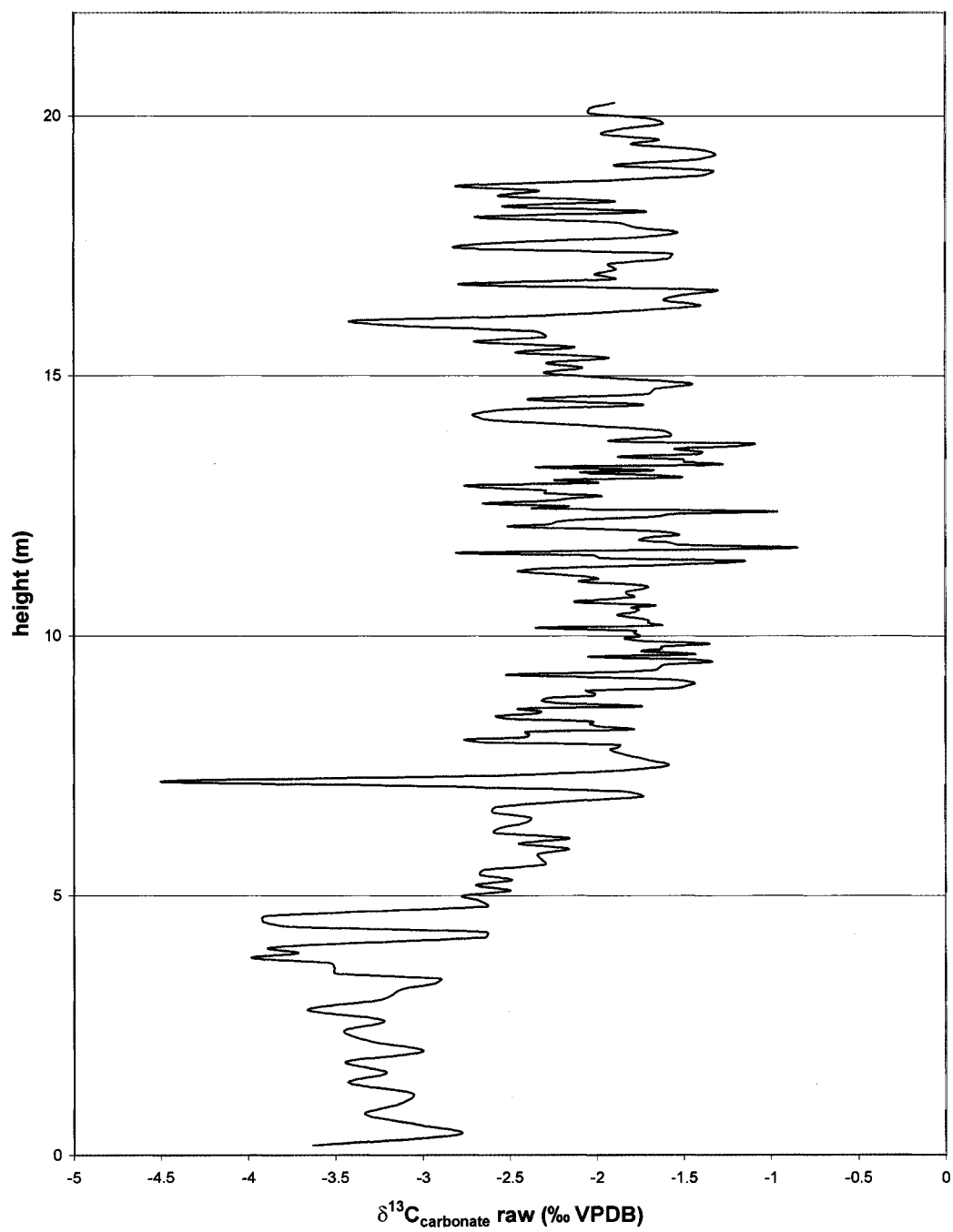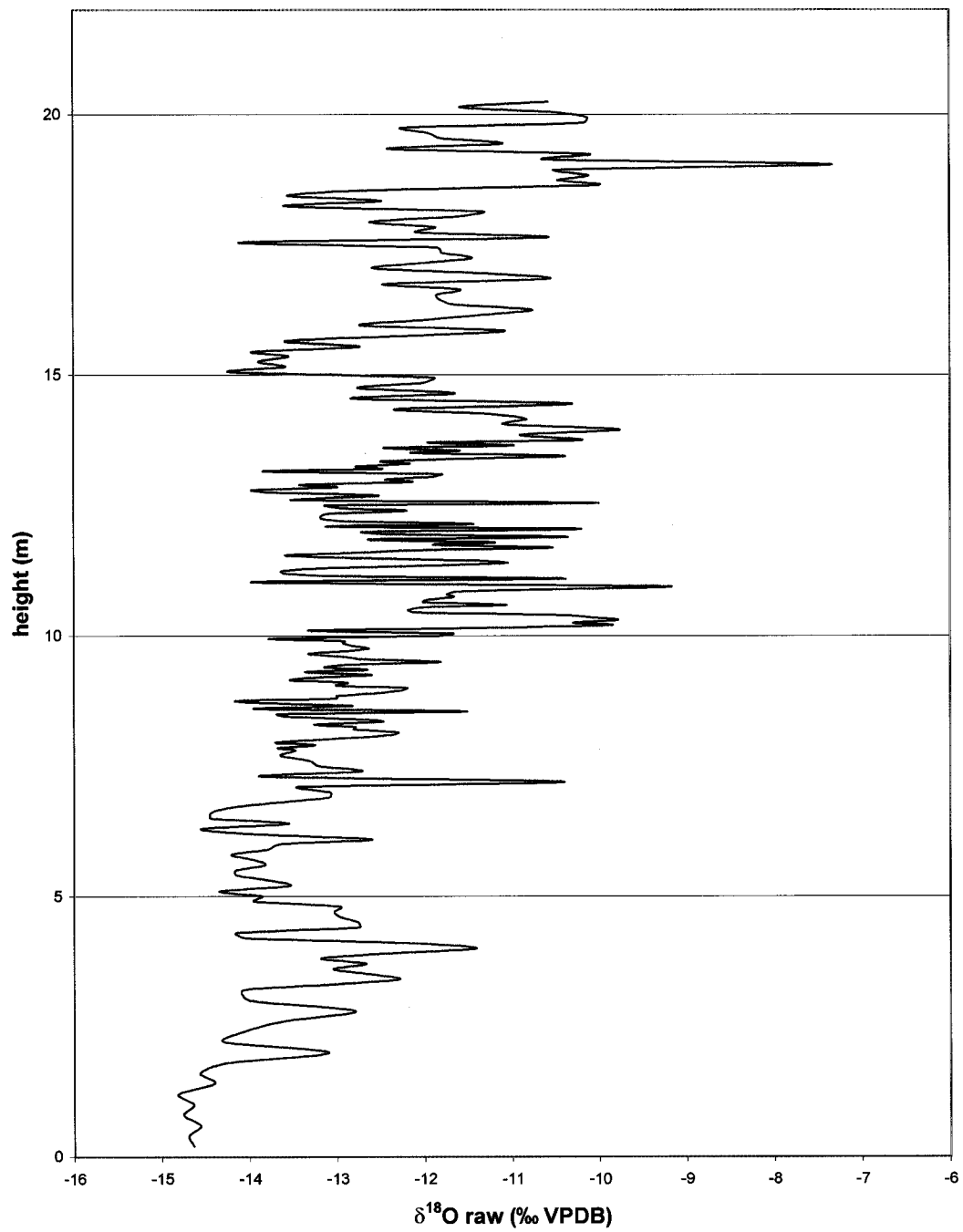
Appendix D

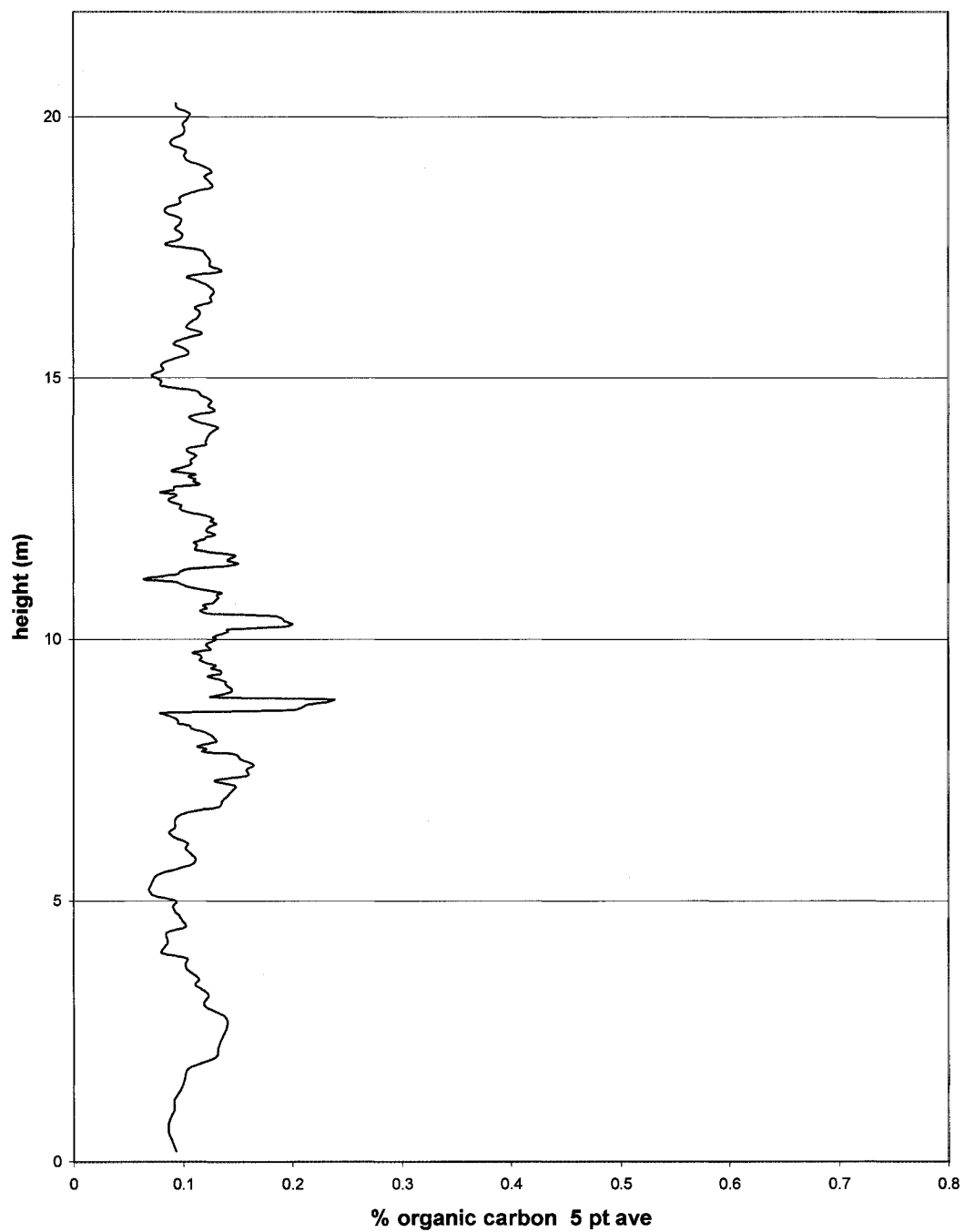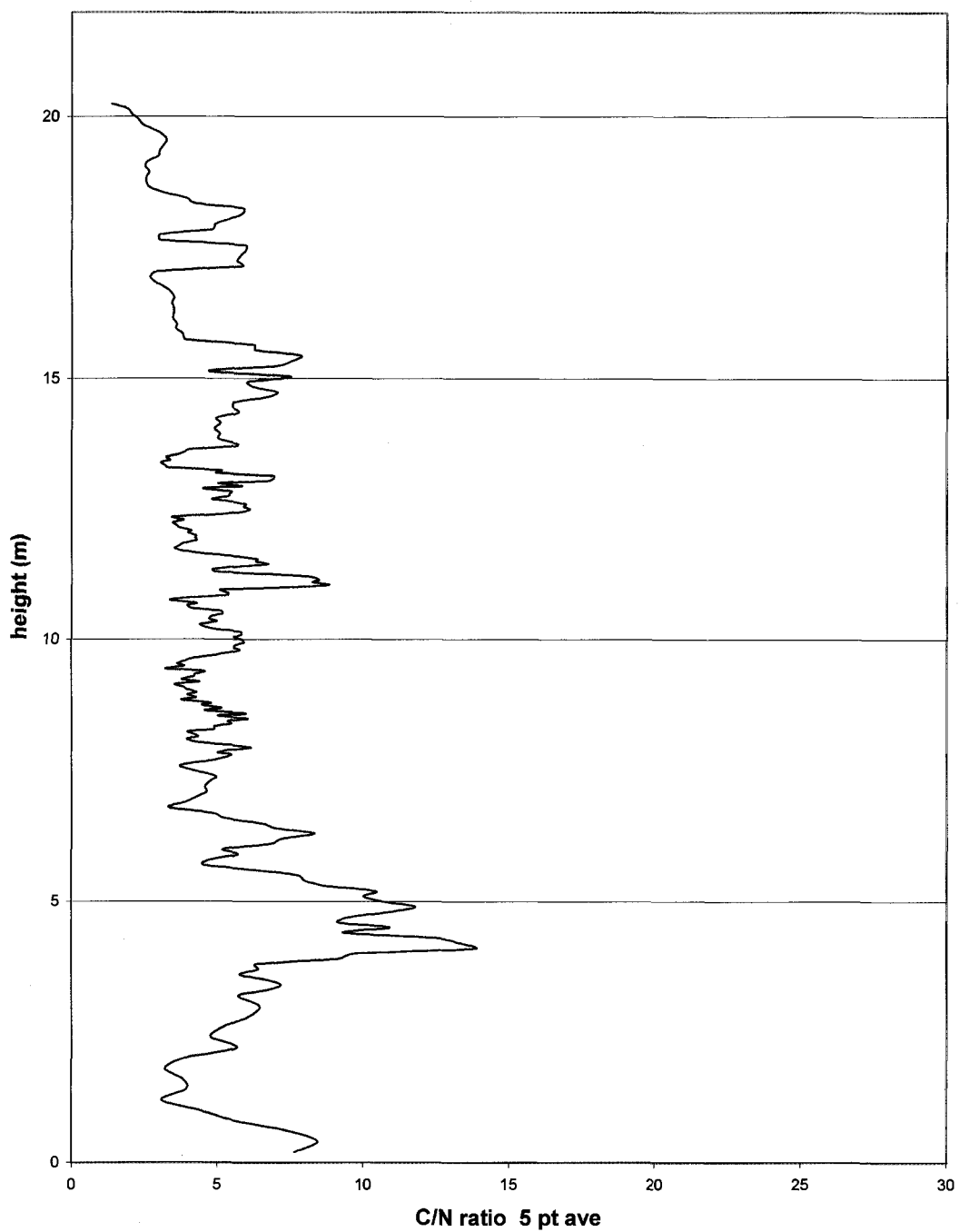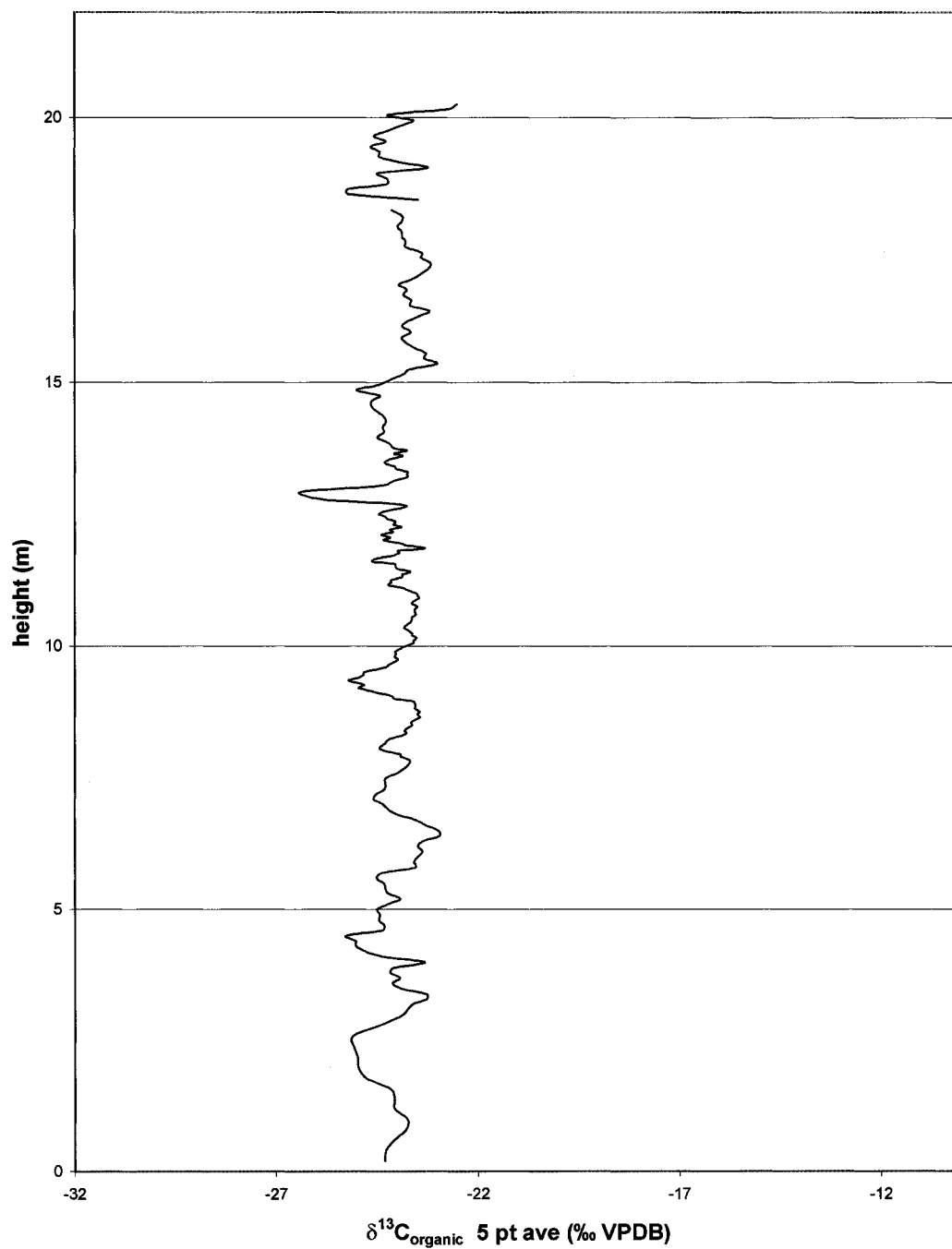Graphs of raw data versus height: Carbonate fraction

110

Appendix E

Graphs of 5-point average data versus height:
Organic fraction

114

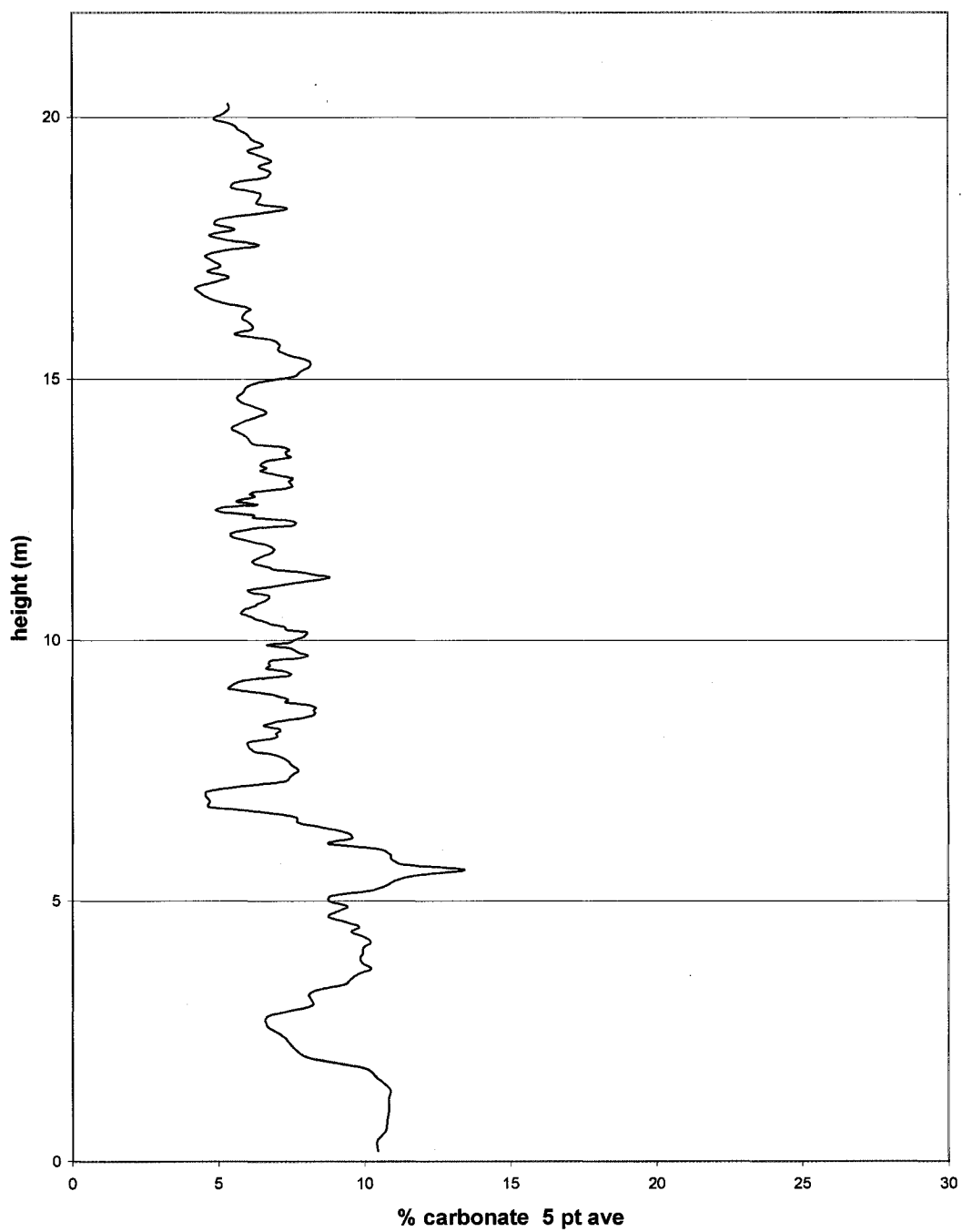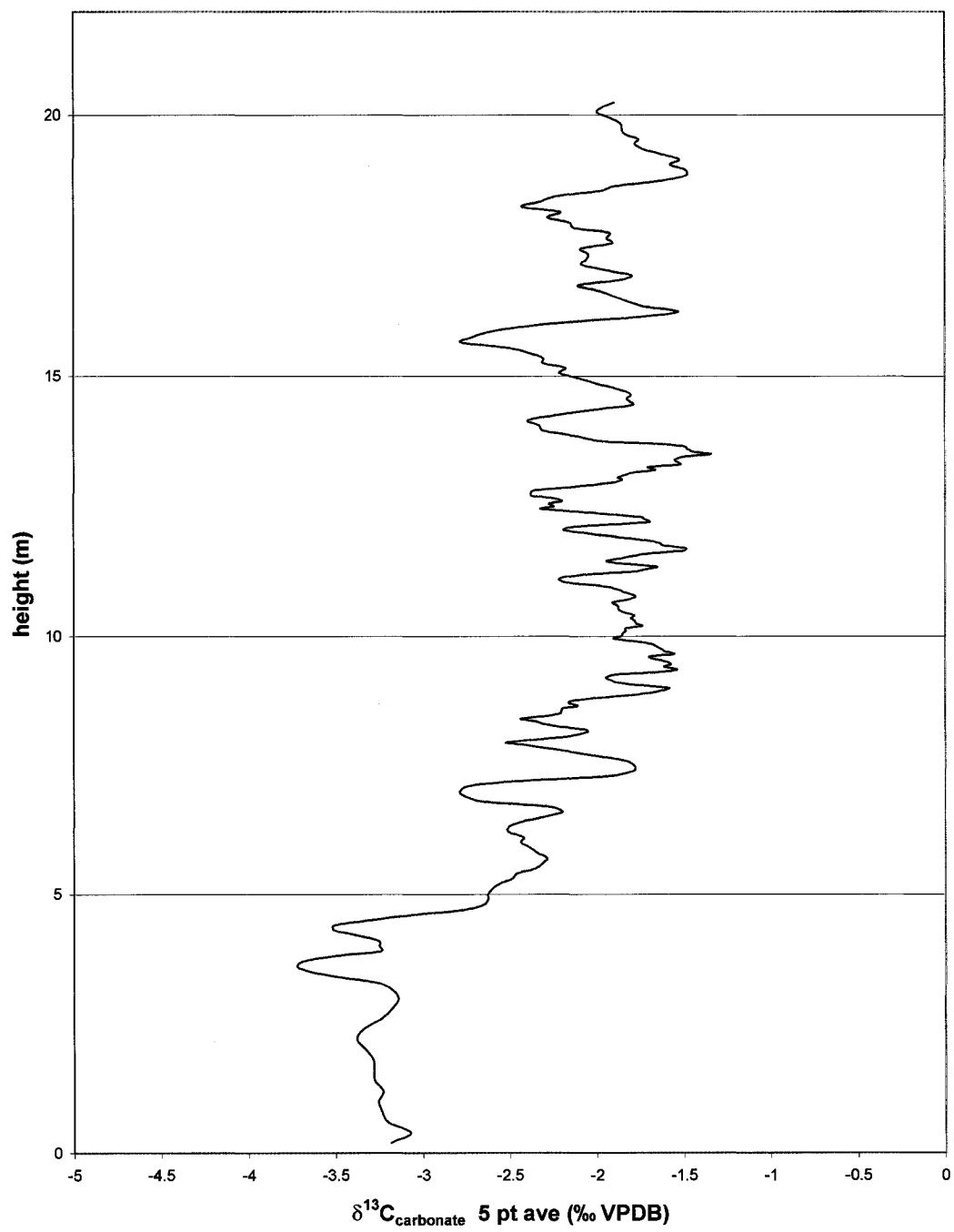**% organic carbon 5 pt ave**

height (m)

C/N ratio 5 pt ave

$\delta^{13}C_{organic}$ **5 pt ave (‰ VPDB)**

Appendix F

Graphs of 5- point average data versus height:
Carbonate fraction

% carbonate 5 pt ave

$\delta^{13}C_{carbonate}$ 5 pt ave (‰ VPDB)

δ¹⁸O 5 pt ave (‰ VPDB)
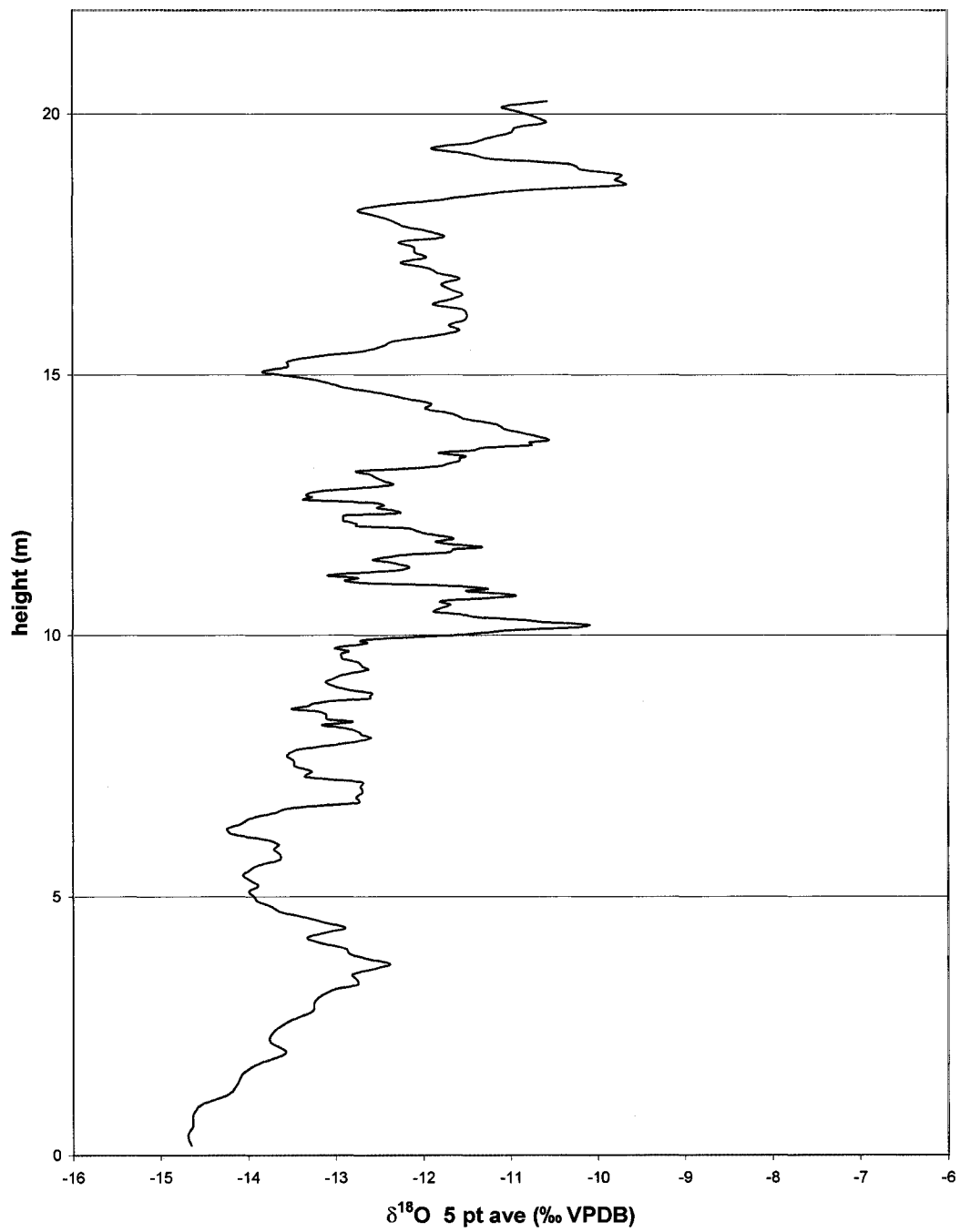
Appendix G

QA/QC: Duplicate analyses

122

sample	del 13C 1	del 13C 2	del 13C 3	del 18O 1	del 18O 2	del 18O 3
86	-1.588	-1.537	-1.459	-13.739	-12.176	-12.181
19				-12.862	-12.339	-12.657
70				-12.628	-12.997	-12.872
203	-3.115	-3.072		-12.715	-12.955	
204	-3.399	-3.391		-12.222	-11.868	
226	-2.542	-2.54		-13.582	-13.615	
234	-2.005	-1.944	-1.73			
244	-2.043	-2.109				

Appendix H

Oxygen isotope fractionation calculations

124

125

d18O-calcite (PDB)	d18O-calcite (SMOW)	water temp (C)	w(#	1000ln(alpha)	ln(alpha)	alpha	18O-calcite + 1000	d18O-water (SMOW)
-10	20.5514	2	#	33.80358464	0.033804	1.034	1020.5514	-13.37032755
-11	19.52054	2	#	33.80358464	0.033804	1.034	1019.52054	-14.36692318
-12	18.48968	2	#	33.80358464	0.033804	1.034	1018.48968	-15.36351881
-13	17.45882	2	#	33.80358464	0.033804	1.034	1017.45882	-16.36011444
-14	16.42796	2	#	33.80358464	0.033804	1.034	1016.42796	-17.35671007
-15	15.3971	2	#	33.80358464	0.033804	1.034	1015.3971	-18.3533057
-10	20.5514	3	#	33.53841056	0.033538	1.034	1020.5514	-13.10866424
-11	19.52054	3	#	33.53841056	0.033538	1.034	1019.52054	-14.10552417
-12	18.48968	3	#	33.53841056	0.033538	1.034	1018.48968	-15.10238411
-13	17.45882	3	#	33.53841056	0.033538	1.034	1017.45882	-16.09924404
-14	16.42796	3	#	33.53841056	0.033538	1.034	1016.42796	-17.09610398
-15	15.3971	3	#	33.53841056	0.033538	1.034	1015.3971	-18.09296392
-10	20.5514	4	#	33.27610062	0.033276	1.034	1020.5514	-12.84975888
-11	19.52054	4	#	33.27610062	0.033276	1.034	1019.52054	-13.84688034
-12	18.48968	4	#	33.27610062	0.033276	1.034	1018.48968	-14.84400179
-13	17.45882	4	#	33.27610062	0.033276	1.034	1017.45882	-15.84112325
-14	16.42796	4	#	33.27610062	0.033276	1.034	1016.42796	-16.83824471
-15	15.3971	4	#	33.27610062	0.033276	1.034	1015.3971	-17.83536616
-10	20.5514	5	#	33.01661374	0.033017	1.034	1020.5514	-12.59357311
-11	19.52054	5	#	33.01661374	0.033017	1.034	1019.52054	-13.59095334
-12	18.48968	5	#	33.01661374	0.033017	1.034	1018.48968	-14.58833357
-13	17.45882	5	#	33.01661374	0.033017	1.034	1017.45882	-15.5857138
-14	16.42796	5	#	33.01661374	0.033017	1.034	1016.42796	-16.58309403
-15	15.3971	5	#	33.01661374	0.033017	1.034	1015.3971	-17.58047426
-10	20.5514	6	#	32.75990955	0.03276	1.033	1020.5514	-12.34006921
-11	19.52054	6	#	32.75990955	0.03276	1.033	1019.52054	-13.3377055
-12	18.48968	6	#	32.75990955	0.03276	1.033	1018.48968	-14.33534179
-13	17.45882	6	#	32.75990955	0.03276	1.033	1017.45882	-15.33297809
-14	16.42796	6	#	32.75990955	0.03276	1.033	1016.42796	-16.33061438
-15	15.3971	6	#	32.75990955	0.03276	1.033	1015.3971	-17.32825068
-10	20.5514	7	#	32.50594841	0.032506	1.033	1020.5514	-12.0892101
-11	19.52054	7	#	32.50594841	0.032506	1.033	1019.52054	-13.08709979
-12	18.48968	7	#	32.50594841	0.032506	1.033	1018.48968	-14.08498948
-13	17.45882	7	#	32.50594841	0.032506	1.033	1017.45882	-15.08287916
-14	16.42796	7	#	32.50594841	0.032506	1.033	1016.42796	-16.08076885
-15	15.3971	7	#	32.50594841	0.032506	1.033	1015.3971	-17.07865854

d18O-calcite (PDB)	d18O-calcite (SMOW)	water temp (C)	v(l	1000ln(alpha)	ln(alpha)	alpha	18O-calcite + 1000	d18O-water (SMOW)
-10	20.5514	8	#	32.25469136	0.032255	1.033	1020.5514	-11.84095937
-11	19.52054	8	#	32.25469136	0.032255	1.033	1019.52054	-12.83909982
-12	18.48968	8	#	32.25469136	0.032255	1.033	1018.48968	-13.83724026
-13	17.45882	8	#	32.25469136	0.032255	1.033	1017.45882	-14.83538071
-14	16.42796	8	#	32.25469136	0.032255	1.033	1016.42796	-15.83352115
-15	15.3971	8	#	32.25469136	0.032255	1.033	1015.3971	-16.8316616
-10	20.5514	9	#	32.00610016	0.032006	1.033	1020.5514	-11.59528119
-11	19.52054	9	#	32.00610016	0.032006	1.033	1019.52054	-12.5936698
-12	18.48968	9	#	32.00610016	0.032006	1.033	1018.48968	-13.5920584
-13	17.45882	9	#	32.00610016	0.032006	1.033	1017.45882	-14.59044701
-14	16.42796	9	#	32.00610016	0.032006	1.033	1016.42796	-15.58883561
-15	15.3971	9	#	32.00610016	0.032006	1.033	1015.3971	-16.58722422
-10	20.5514	10	#	31.76013722	0.03176	1.032	1020.5514	-11.35214037
-11	19.52054	10	#	31.76013722	0.03176	1.032	1019.52054	-12.35077457
-12	18.48968	10	#	31.76013722	0.03176	1.032	1018.48968	-13.34940877
-13	17.45882	10	#	31.76013722	0.03176	1.032	1017.45882	-14.34804297
-14	16.42796	10	#	31.76013722	0.03176	1.032	1016.42796	-15.34667717
-15	15.3971	10	#	31.76013722	0.03176	1.032	1015.3971	-16.34531137
-10	20.5514	11	#	31.51676563	0.031517	1.032	1020.5514	-11.11150228
-11	19.52054	11	#	31.51676563	0.031517	1.032	1019.52054	-12.11037955
-12	18.48968	11	#	31.51676563	0.031517	1.032	1018.48968	-13.10925682
-13	17.45882	11	#	31.51676563	0.031517	1.032	1017.45882	-14.1081341
-14	16.42796	11	#	31.51676563	0.031517	1.032	1016.42796	-15.10701137
-15	15.3971	11	#	31.51676563	0.031517	1.032	1015.3971	-16.10588864
-10	20.5514	12	#	31.27594912	0.031276	1.032	1020.5514	-10.87333292
-11	19.52054	12	#	31.27594912	0.031276	1.032	1019.52054	-11.87245077
-12	18.48968	12	#	31.27594912	0.031276	1.032	1018.48968	-12.87156861
-13	17.45882	12	#	31.27594912	0.031276	1.032	1017.45882	-13.87068646
-14	16.42796	12	#	31.27594912	0.031276	1.032	1016.42796	-14.86980431
-15	15.3971	12	#	31.27594912	0.031276	1.032	1015.3971	-15.86892215
-10	20.5514	13	#	31.03765203	0.031038	1.032	1020.5514	-10.63759883
-11	19.52054	13	#	31.03765203	0.031038	1.032	1019.52054	-11.63695479
-12	18.48968	13	#	31.03765203	0.031038	1.032	1018.48968	-12.63631076
-13	17.45882	13	#	31.03765203	0.031038	1.032	1017.45882	-13.63566672
-14	16.42796	13	#	31.03765203	0.031038	1.032	1016.42796	-14.63502268
-15	15.3971	13	#	31.03765203	0.031038	1.032	1015.3971	-15.63437864

d18O-calcite (PDB)	d18O-calcite (SMOW)	water temp (C)	v (1 1000ln(alpha)	ln(alpha)	alpha	18O-calcite + 1000	d18O-water (SMOW)
-10	20.5514	14	#	30.80183935	0.030802	1.031	1020.5514	-10.40426712
-11	19.52054	14	#	30.80183935	0.030802	1.031	1019.52054	-11.40385877
-12	18.48968	14	#	30.80183935	0.030802	1.031	1018.48968	-12.48345042
-13	17.45882	14	#	30.80183935	0.030802	1.031	1017.45882	-13.48304207
-14	16.42796	14	#	30.80183935	0.030802	1.031	1016.42796	-14.40263372
-15	15.3971	14	#	30.80183935	0.030802	1.031	1015.3971	-15.40222537
-10	20.5514	15	#	30.56847666	0.030568	1.031	1020.5514	-10.17330546
-11	19.52054	15	#	30.56847666	0.030568	1.031	1019.52054	-11.17311304
-12	18.48968	15	#	30.56847666	0.030568	1.031	1018.48968	-12.17295535
-13	17.45882	15	#	30.56847666	0.030568	1.031	1017.45882	-13.12778029
-14	16.42796	15	#	30.56847666	0.030568	1.031	1016.42796	-14.17260523
-15	15.3971	15	#	30.56847666	0.030568	1.031	1015.3971	-15.17243018

Appendix I

Sedimentary organic hydrogen pilot experiments

128

Background and statement of research objective

The use of stable isotopes of hydrogen in sedimentary organic matter deposited in lakes has the potential of becoming a new proxy for paleoclimate research (Krishnamurthy, 1995; Lovan, 1998). Earlier paleoclimate studies using hydrogen isotopes of organic material were conducted on cellulose from wood (e.g. Yapp and Epstein, 1977). Cellulose has a well-understood chemical structure (Heuser, 1944). 70% of hydrogen in cellulose is carbon-bound (C—H) and 30% of hydrogen is hydroxyl hydrogen (O—H) (Heuser, 1944). The hydroxyl hydrogen is known to easily exchange with environmental water after the biosynthesis of the cellulose (Heuser, 1944). The result of this exchange is a change in the δD value since the time of biosynthesis. The δD value of the cellulose is a combination of its original δD value and the δD value of water with which isotopic exchange has taken place since the time of biosynthesis. The original δD value is related to the δD of the environmental water at the time of biosynthesis, which is useful in paleoclimate research.

Epstein et al. (1976) derived a procedure for eliminating the exchangeable hydrogen in cellulose by means of a nitration technique. During nitration of cellulose, oxygen-bound H are replaced with NO_2 (Heuser, 1944). Epstein et al. (1976) demonstrated that nitrating the cellulose for less than 24 hours results in a change (enrichment) of δD of the cellulose. This method of preprocessing cellulose for

paleoclimate studies using δD of cellulose in aquatic and land plants became the standard procedure (e.g. Yapp and Epstein, 1977).

A second procedure to address exchangeable hydrogen was developed by Feng et al. (1993). In this procedure, cellulose is equilibrated with water of known δD. This procedure gives reproducible δD values after equilibration with water and works well with relative comparisons of δD values between samples that have all been equilibrated at the same temperature with water of the same isotopic composition (Feng et al., 1993).

The use of hydrogen isotopes from sedimentary organic matter (HF-HCl residue, often called kerogen) has great potential for paleoclimate research. Krishnamurthy et al. (1995) used δD from sedimentary organic matter (SOM) in lacustrine sediments to derive a late glacial paleoclimate record from a Midwestern lake. Like cellulose, a similar difficulty with exchangeable hydrogen exists in SOM, although since the molecular structure of SOM is undefined, the percentage of exchangeable hydrogen in SOM is unknown and may vary between samples. Krishnamurthy et al. (1995) estimated the amount of exchangeable hydrogen in their SOM samples at ~10% and dismissed it as negligible.

An exchange method between SOM and water of known isotopic compositions is widely used in isotopic studies of δD from kerogen (e.g. Schimmelmann et al., 1999; Mastalerz and Schimmelmann, 2002). Like the water-equilibration procedure for cellulose, this method controls the isotopic exchange in the SOM but does not eliminate the O—H hydrogen.

The experiments described below explore the possibility of eliminating exchangeable hydrogen in sedimentary organic hydrogen by means of a nitration technique, similar to that used with cellulose. The hypothesis is that soaking SOM in 100% HNO_3 will result in a change of the δD value of SOM. Complete exchange of hydroxyl hydrogen with nitrate in cellulose takes less than 24 hours (Epstein et al., 1976). It is uncertain how long it will take to completely replace all of the exchangeable hydrogen in SOM with nitrate, however, it is expected that soaking the sample in nitric acid for a longer period of time will not further change the δD value. In addition to a change in δD value in the nitrated SOM, it is anticipated that the yield of nitrogen from the combusted nitrated sample will increase along with a corresponding decrease in the yield of hydrogen. It is anticipated that there will be no change in the yield of CO_2 between untreated and nitrated samples.

Initial experiments

Several SOM samples were acquired from the Stable Isotope Biogeochemistry lab at Indiana University from Grzegorz Lis and Arndt Schimmelmann. Additional samples were also acquired from the Stable Isotope Geochemistry lab at Western Michigan University. Due to small quantities of samples from these sources, initial experiments were conducted with charcoal as a surrogate sample for SOM.

Commercial charcoal samples were treated with hydrochloric acid (HCl) to remove any carbonates. After this, samples were carefully treated with hydrofluoric acid (HF) to remove any silicates. Following each treatment, samples were

centrifuged and the supernatant was decanted. Samples were then washed with DI water until a neutral pH was attained. Following this, samples were dried in a convection oven at ~100°C.

Initial pilot experiments were designed to test the hypothesis that soaking samples in nitric acid (HNO_3) would replace exchangeable hydrogen with nitrate. This would be demonstrated by an increase in N_2 yield from untreated samples to treated samples and a corresponding decrease in the yield of H_2. A change in δD was also expected. All of these values were expected to change from the raw sample to the nitrated sample and were expected to reach an asymptote after all of the exchange had taken place. Thus, the pilot experiments consisted of analyzing the charcoal sample 1) untreated, 2) nitrated for 1,2,3...18 days, and 3) treated with heavy water.

Before the pilot experiments with charcoal could begin, it was first necessary to test the equipment to be used in the experiment, particularly lab equipment that would separate nitric acid from the sample after nitration was complete. The first method to be used was centrifuging samples after nitration. However, this did not separate the sample from nitric acid, probably due to similarities in densities of the two substances. A second attempt to centrifuge involved a much higher rotation speed for the centrifuge. This resulted in the nitric acid heating up and burning holes in the bottom of the centrifuge tubes. A third attempt to separate nitric acid from charcoal involved a filtration system already available in the Stable Isotope Geochemistry lab. This, too, was unsuccessful as again the acid burned a hole through the filter. A new filtration system that was resistant to nitric acid was

ordered. This filtration system consisted of a glass assembly including a 15 ml flask. The assembly housed a 25 mm diameter membrane made of glass microfibre with a pore space of 0.7µm. This worked well with the nitric acid. However, a portion of the sample would remain on the membrane. Thus, 100% sample recovery was not possible. The 25 mm diameter limited the surface area in order to minimize sample loss.

Results of the charcoal samples were inconclusive. Untreated δD results for sample A (charcoal sample) were ~35‰ VSMOW (Figure I-1). These values decreased sharply after two days of nitration, but further nitration resulted in increasingly heavier values. Yields of nitrogen decreased in the nitrated samples (Figure I-2). This is contrary to what was expected. After 1 – 2 days of nitration there was no additional change in the yield of N_2. The sample nitrated for 10 days was an outlier. The yield of CO_2 increased by approximately 40% from the untreated yield (Figure I-3). After 1 day of nitration the CO_2 yield increased substantially from the yield of the untreated sample. Additional days of nitration showed a slight decrease in CO_2 yield. Again, this was not expected. Although the increase in CO_2 is difficult to explain, a useful piece of information in these results is that the major change in CO_2 yield occurred after approximately 1 day, similar to major changes in the δD value and in the yield of N_2. The results of the hydrogen yield were also inconclusive (Figure I-4). Yields of H_2 increased with a longer duration of nitration, however an asymptote was never reached. Further, the sample treated for 18 days had a yield of H_2 similar to the untreated sample. Charcoal samples were not treated with

heavy water due to difficulties in creating a heavy water solution at this point in the
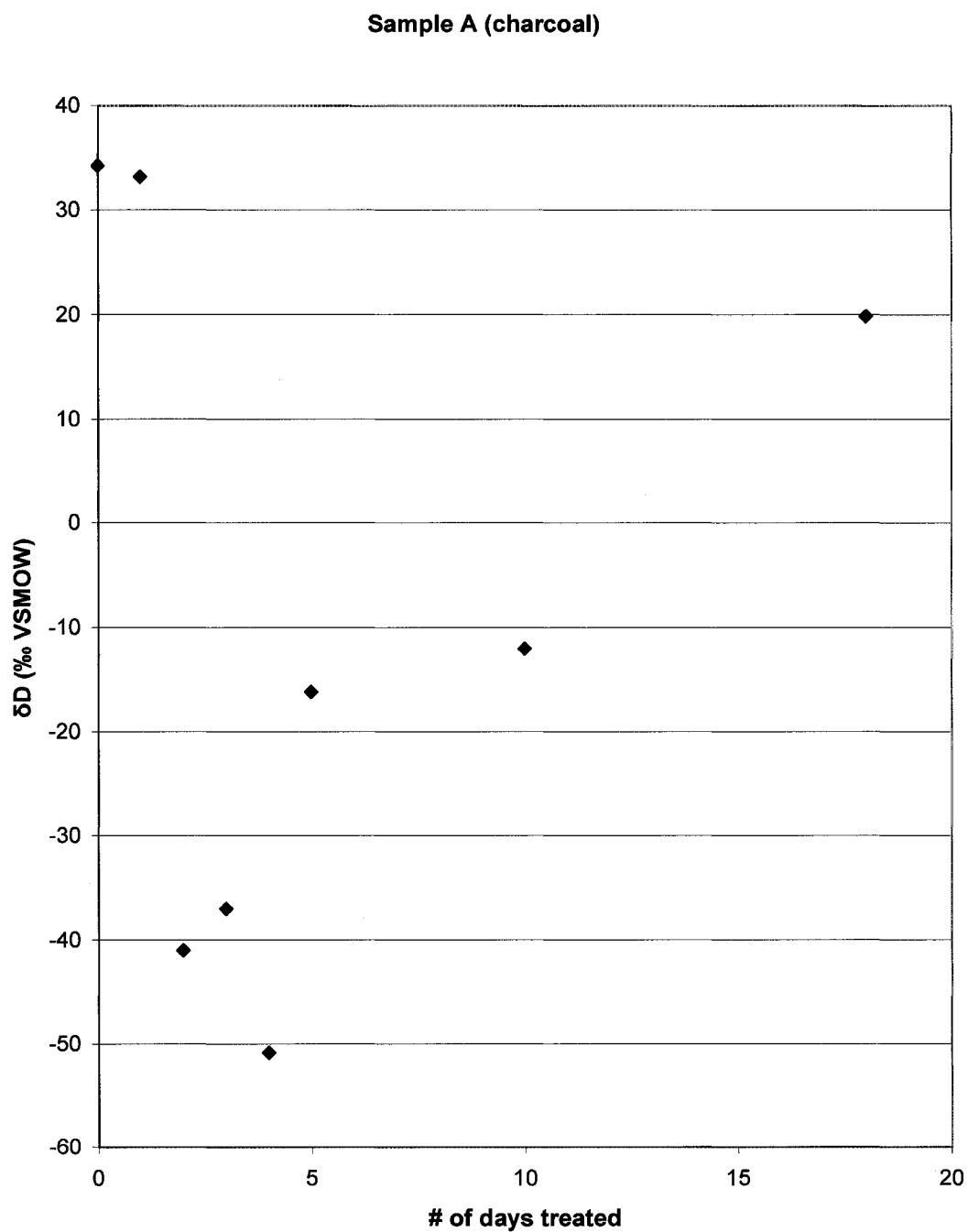
experiment.

Sample A (charcoal)

Figure I-1. δD values for sample A (charcoal) experiments.
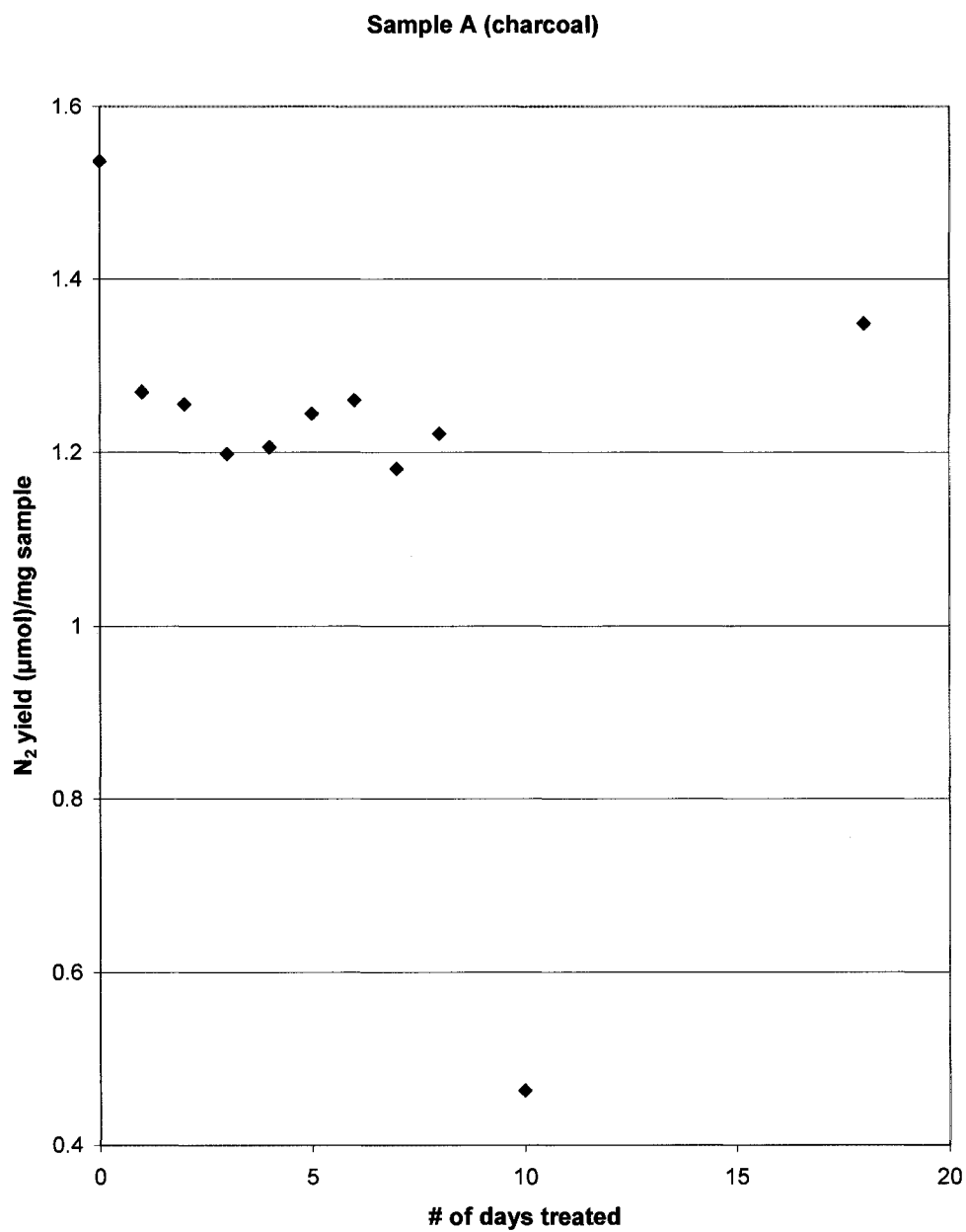
Sample A (charcoal)

Figure I-2. Nitrogen yields for sample A experiments.
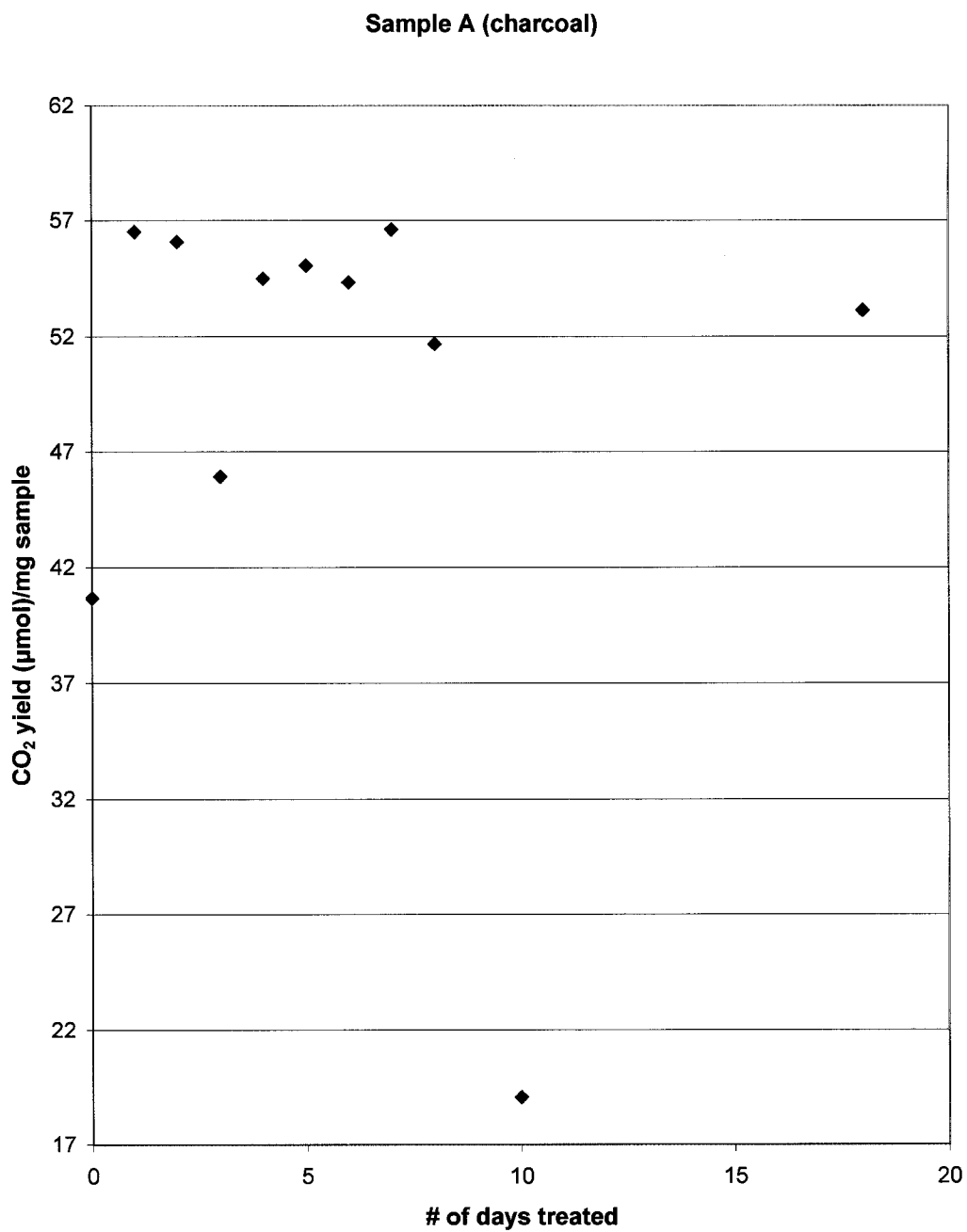
Sample A (charcoal)

Figure I-3. Yields of CO_2 for sample A experiments.
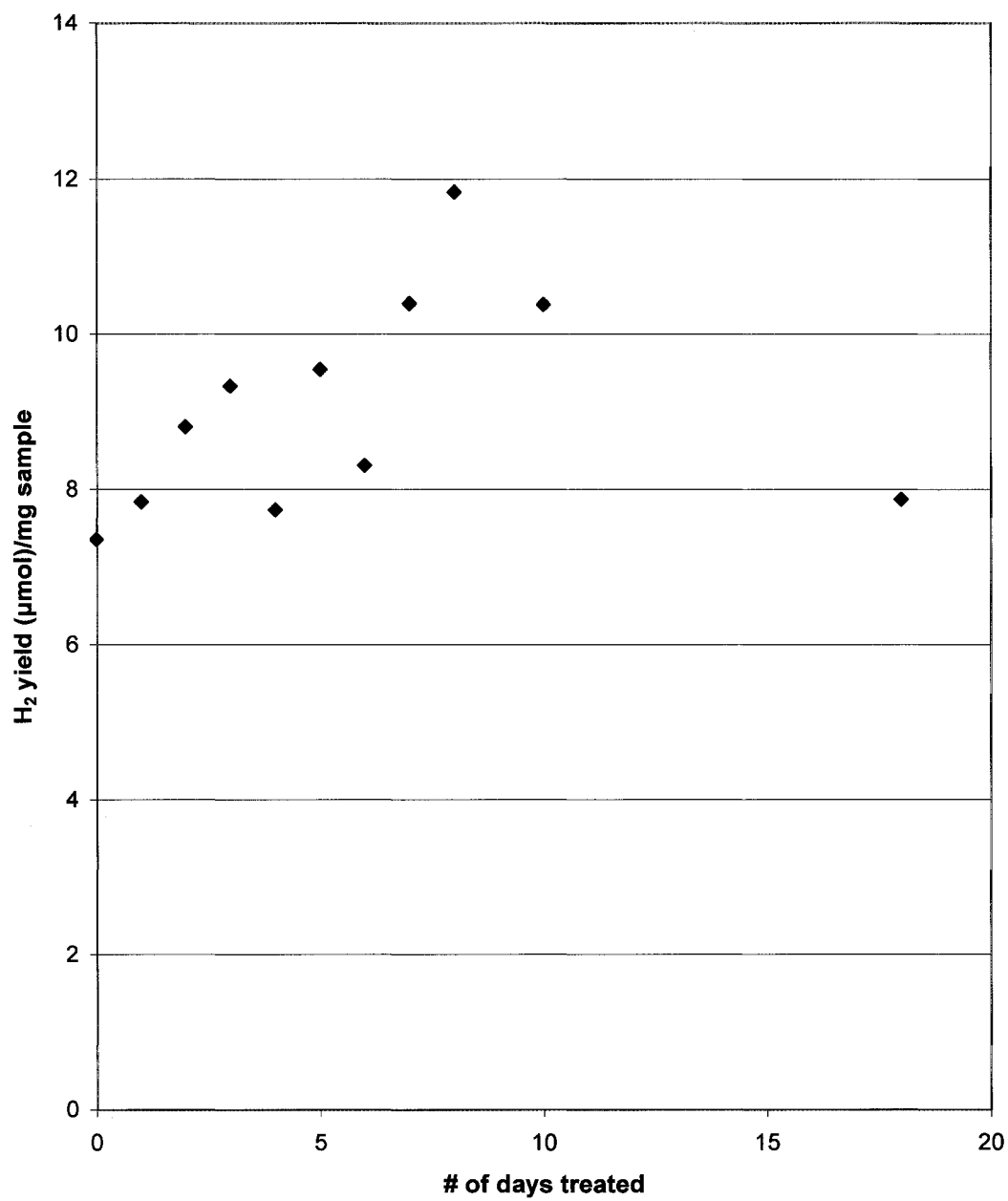
Sample A (charcoal)

Figure I-4. Yields of H_2 for sample A experiments.

The results for the initial pilot experiment with charcoal were inconclusive. The filtration of sample and nitric acid through a glass assembly with glass microfibre membrane successfully resisted reaction with nitric acid. One potential problem with this technique was a small amount of sample loss to the membrane. Although the results from this pilot experiment did not show predictable changes in δD values and yields of N_2, CO_2, and H_2, the results did suggest that the largest change occurs fairly quickly, perhaps within 24 hours. A possible explanation for the unpredicted behavior of this sample was its unknown chemical composition. Sample A was a commercial charcoal sample of unknown chemical composition. It is quite likely that nitration caused reactions in addition to the replacement of exchangeable hydrogen with nitrate.

Additional experiments – Ladd Lake

With the insight gained from the first set of experiments with charcoal, additional experiments were conducted using sedimentary organic hydrogen samples. One sample, Ladd Lake, was derived from organic-rich lacustrine deposits archived in the Stable Isotope Lab at WMU. These samples were the subject of a doctoral dissertation of Norman Lovan in 1998. Several samples of Ladd Lake were combined to create enough material to carry out the nitration experiment (Table I-1). Although δD values for these samples are not known, δD values for Ladd Lake samples from stratigraphically similar locations ranged from -115‰ to -144‰, with the majority of isotope values falling between -120‰ and -135‰ (Lovan, 1998).

139

Table I-1. Individual sample numbers for the composite Ladd Lake
sample used in this study.

Sample	Sample	Sample	Sample	Sample
LL1306	LL1386	LL1491	LL1547	LL1607
LL1314	LL1394	LL1495	LL1555	LL1611
LL1322	LL1402	LL1503	LL1559	LL1619
LL1326	LL1410	LL1507	LL1563	LL1623
LL1338	LL1418	LL1511	LL1571	LL1639
LL1346	LL1426	LL1519	LL1575	LL1643
LL1354	LL1428	LL1523	LL1579	LL1647
LL1362	LL1475	LL1535	LL1587	LL1655
LL1370	LL1479	LL1539	LL1591	LL1659
LL1378	LL1483	LL1543	LL1595	

Before all Ladd Lake samples were combined into one composite sample, the above-listed samples were combined into six Ladd Lake samples. Each sample was treated with HCl and HF as described above for the charcoal sample. After each HF digestion the samples were dried and weighed. HF digestions continued until the weight stabilized, signifying that the majority of silicates had been dissolved. After this process was finished, very little of each sample remained. Thus, the six samples

were combined into one composite Ladd Lake sample in order to carry out nitration for several different time periods. Ladd Lake samples were analyzed according to the following parameters: untreated, nitrated for 1 day, nitrated for 3 days, nitrated for 5 days, and nitrated for 10 days. A duplicate untreated sample was also analyzed. Several Ladd Lake samples were lost during analysis, mostly while sealing the tubes that held the sediment before combustion. Results were obtained from both untreated samples, and for LL-N1 (Ladd Lake nitrated for 1 day), and LL-N5. In the following graphs, only one of the untreated samples was plotted.

Isotope results of the untreated Ladd Lake sample were similar to Ladd Lake samples analyzed by Norman Lovan in 1998 (Lovan, 1998). δD values of the two untreated composite samples were -118‰ and -116‰. Nitration resulted in an enrichment of δD values (Figure I-5). However, the limited data were not enough to clearly indicate a trend. The data suggest that a large change in isotope values occurred after ~1 day of nitration.

Yields of nitrogen generally increased after nitration (Figure I-6). This trend agrees with the anticipated results, unlike the charcoal experiments. Once again, a large change occurred after 1 day of nitration. However, in this experiment, following a large increase in the yield of N_2 after 1 day of nitration, there was a large decrease in the yield of N_2 in the sample that was nitrated for 5 days. This was unexpected. With such a limited amount of data for the Ladd Lake experiment, it is difficult to surmise if LL-N1 is an outlier or if LL-N5 is an outlier. There was not enough sample to run a duplicate analysis.
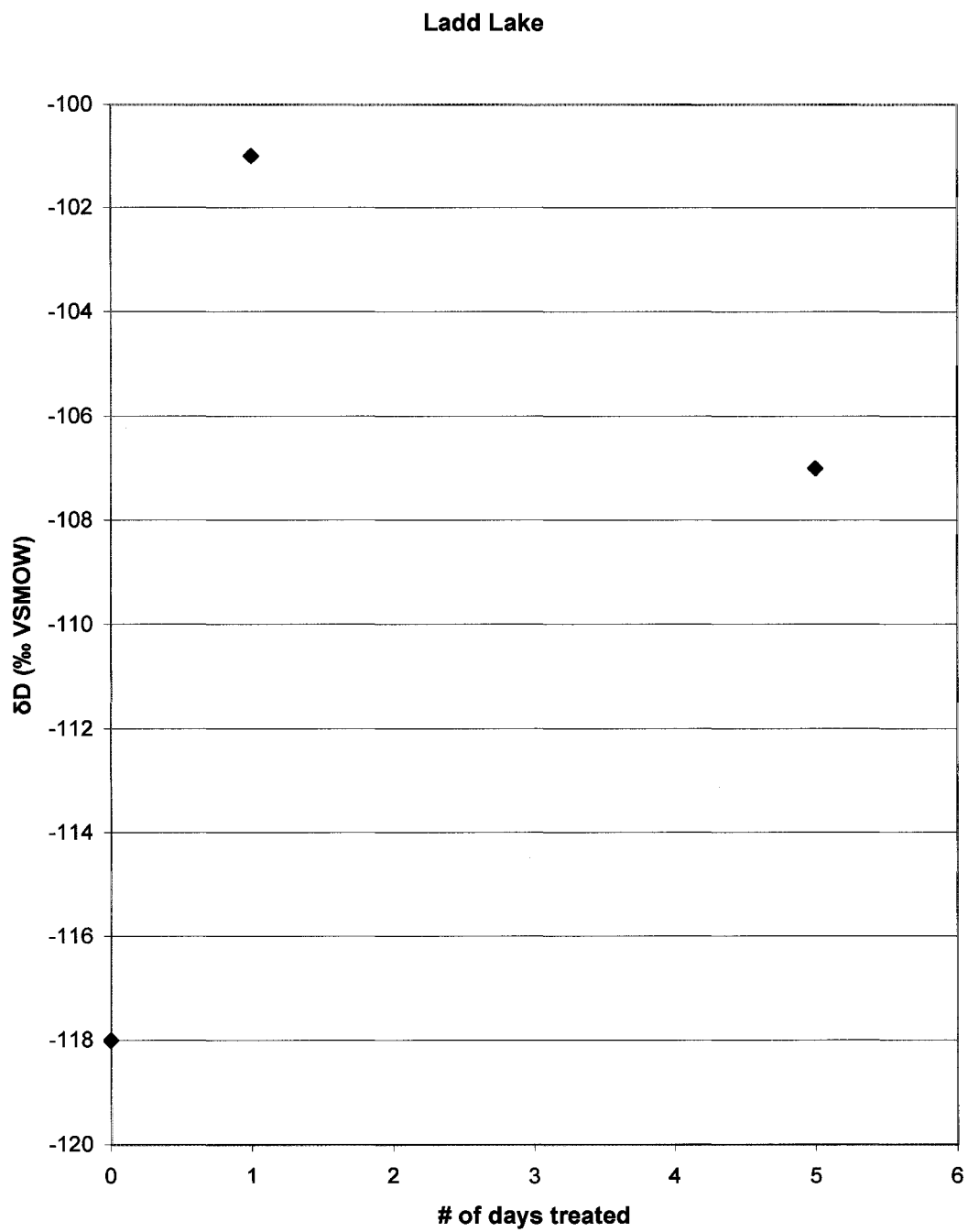
Ladd Lake

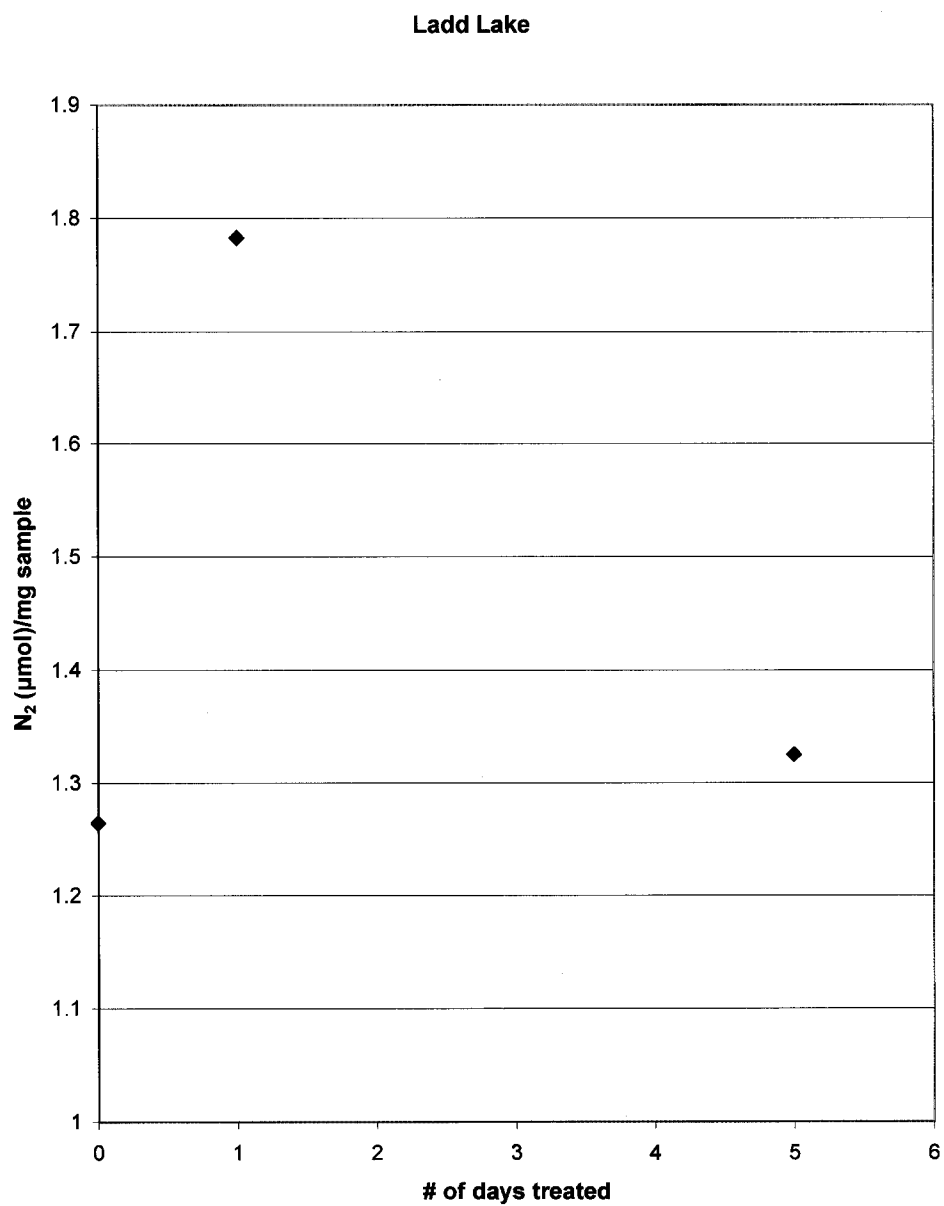Figure I-5. δD values for Ladd Lake sample experiments.

Ladd Lake

Figure I-6. Nitrogen yields for Ladd Lake sample experiments.

The yield of CO_2 significantly decreased after nitration (Figure I-7). This trend is more evident than the trend in nitrogen yields or δD values for the Ladd Lake

sample. The change in yield of CO_2 was not expected. The hypothesis of the experiment is that nitrating the sample would change the δD value and would cause
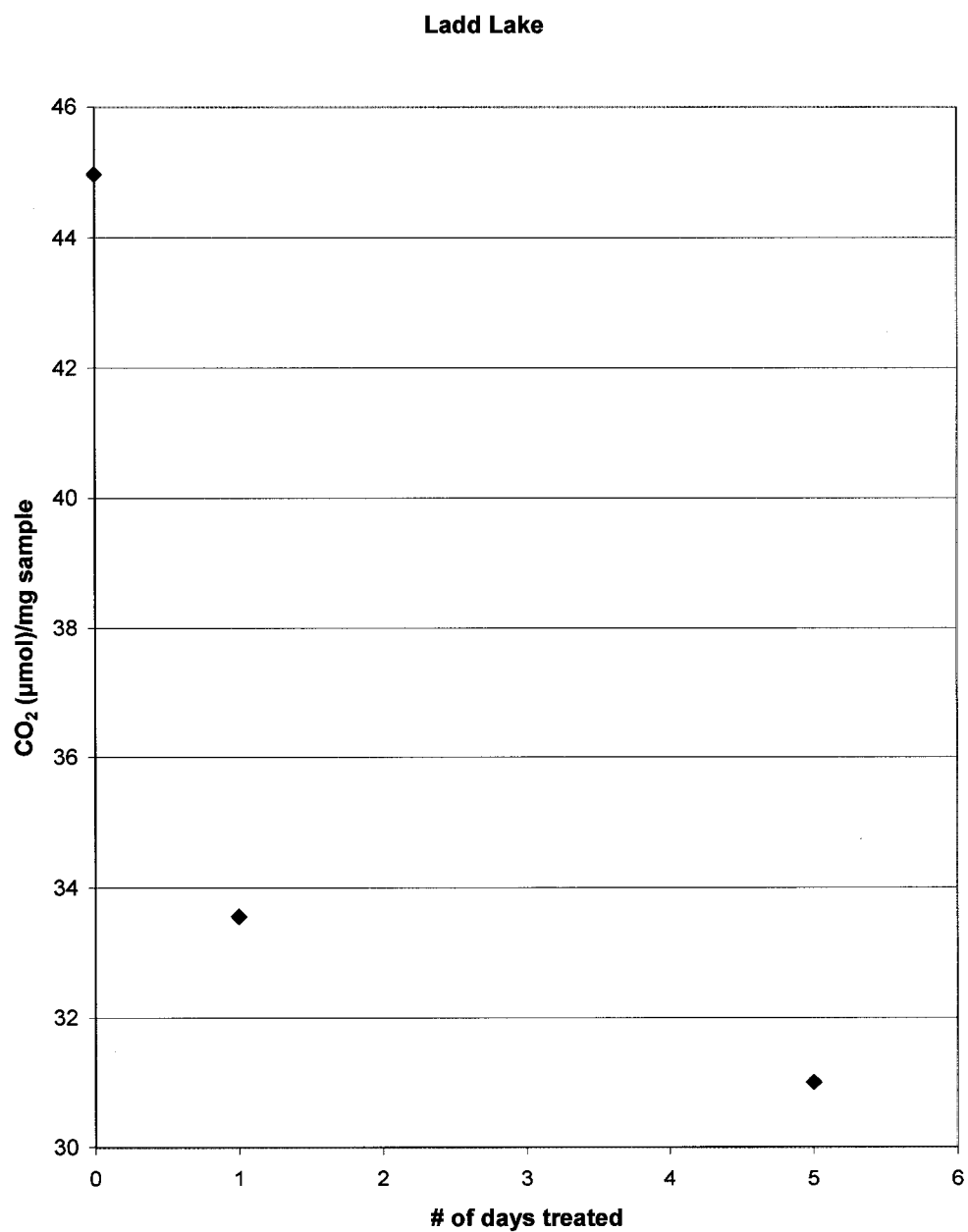
Ladd Lake

Figure I-7. Yields of CO_2 for Ladd Lake sample experiments.

an increase in nitrogen and a decrease in hydrogen. Soaking the sample in HNO_3 may cause additional chemical reactions or may break down the SOM in ways that were not predicted.

Yields of hydrogen also changed due to nitration (Figure I-8). However, again the data are limited, and no apparent trend can be discerned. A large increase in the yield of H_2 occurred after one day of nitration. However, a similarly large decrease in the yield of H_2 is evident in the sample that was treated for 5 days. It is clear that nitration has an effect on the Ladd Lake samples, however the limited data are not enough to clearly establish what effect nitration has on these samples.
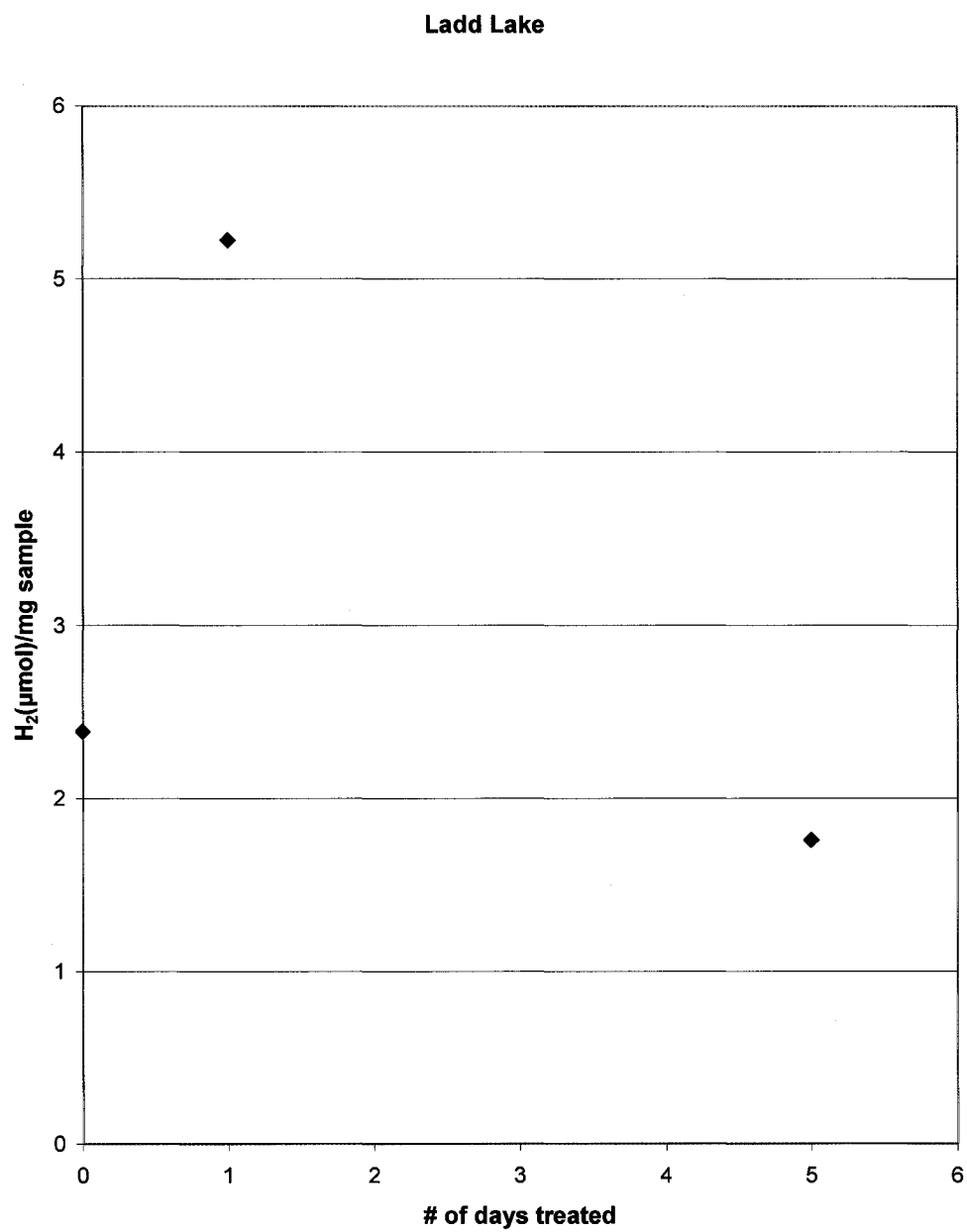
Ladd Lake

Figure I-8. Yields of H_2 for Ladd Lake sample experiments.

The third set of experiments involved a sample obtained from the Stable Isotope Biogeochemistry lab at Indiana University. This sample, 376-1RD, is SOM derived from shale. The SOM was separated from the shale at Indiana University by Grzegorz Lis using a modified $HF-BF_3$ method (Robl and Davis, 1993). This procedure involved crushing the sample, removing hydrophobic organic material coating inorganic grains by means of dichloromethane (DCM), removing carbonates with HCl, removing inorganic material with HF, the separation of acid-resistant heavy minerals using $ZnBr_2$, and a repeat washing of the sample with DCM.

A series of nitrations were carried out on sample 376-1RD. The sample was analyzed untreated, nitrated for 1 day, 3 days, 5 days, 10 days, and soaked in enriched water (δD= +133‰) for 10 days. Duplicate samples were analyzed on the untreated sample and the sample nitrated for 1 day.

Results of hydrogen isotope analyses showed the untreated sample at -104‰ and a large increase in δD values occurring after ~1 day of nitration, after which δD values stabilized at ~ -75‰ (Figure I-9). The sample soaked in heavy water also experienced a change in δD values from -104‰ to -90‰.

Results of nitration brought about a ~50% increase in the yield of nitrogen after 1 day of nitration (Figure I-10). The untreated sample contained ~0.9 μmol N_2/mg sample, whereas nitrated samples contained ~1.5 μmol N_2/mg sample. As with other experiments, the data strongly suggested that nitration was complete after ~1 day. The sample treated with heavy water had a decrease in nitrogen yield from

0.9 to 0.5 μmol N₂/mg sample. SOM equilibrated with enriched water was expected to undergo exchange of hydroxyl hydrogen. It is unclear why there would be a decrease in nitrogen yield.
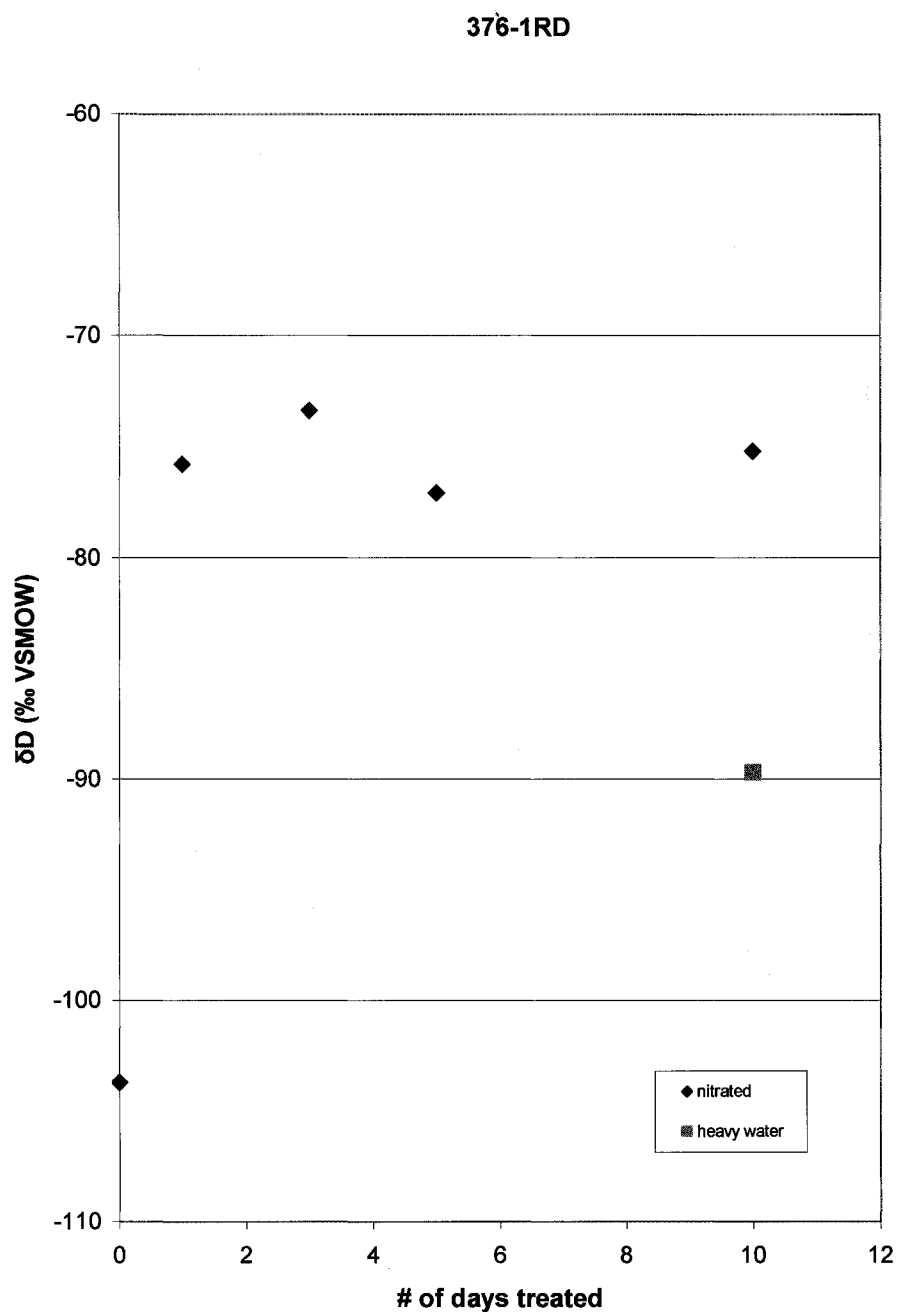
376-1RD

Figure I-9. δD values for sample 376-1RD experiments.
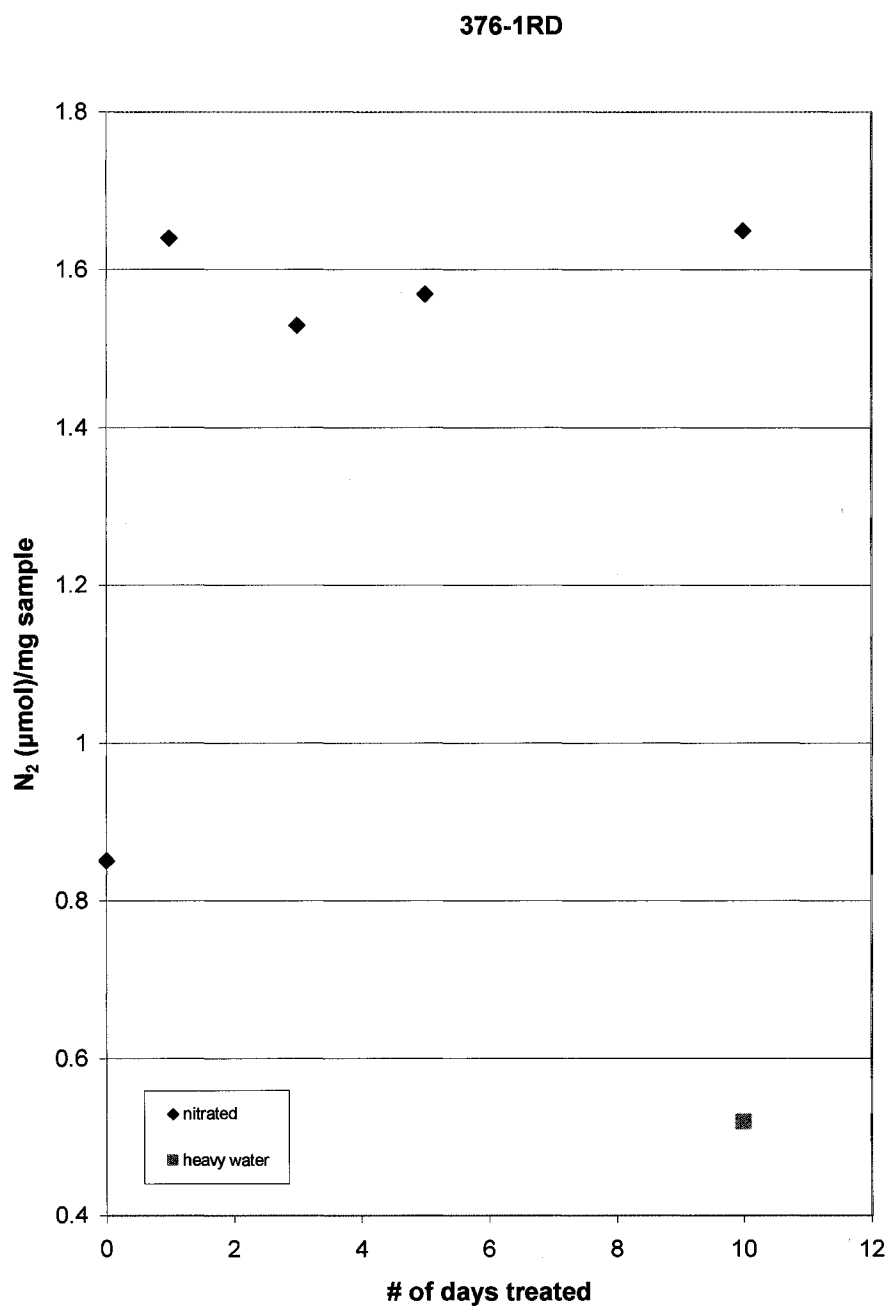
376-1RD

Figure I-10. Nitrogen yields for sample 376-1RD experiments.

Yields of CO_2 decreased by 15 – 20% after 1 day of nitration (Figure I-11).

Yields of CO_2 remained relatively constant with an increase in nitration time. Again,

the mechanism for this is unclear. The yield of CO_2 in the sample treated with heavy

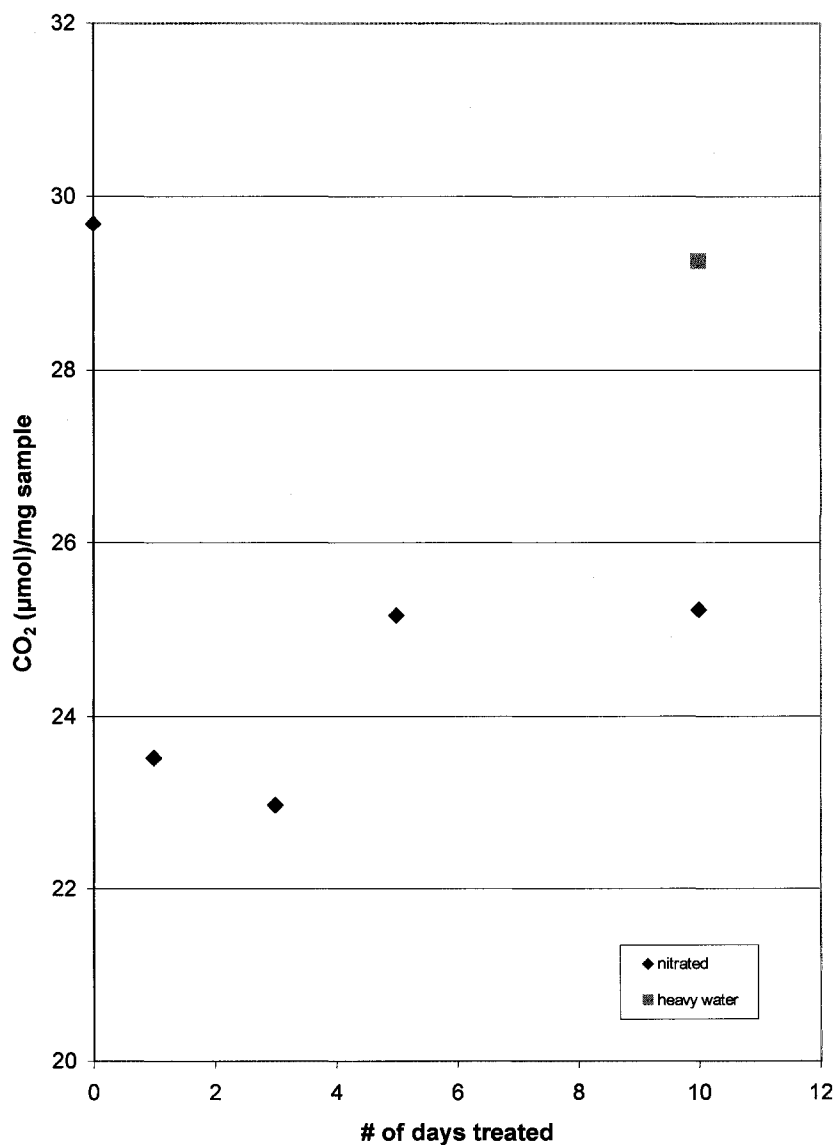water remained largely unchanged from the untreated sample.

376-1RD

Figure I-11. Yields of CO_2 for sample 376-1RD experiments.

Yields of hydrogen did not show a consistent trend (Figure I-12). There was

an initial increase in the yield of hydrogen after 1 day of nitration, however,
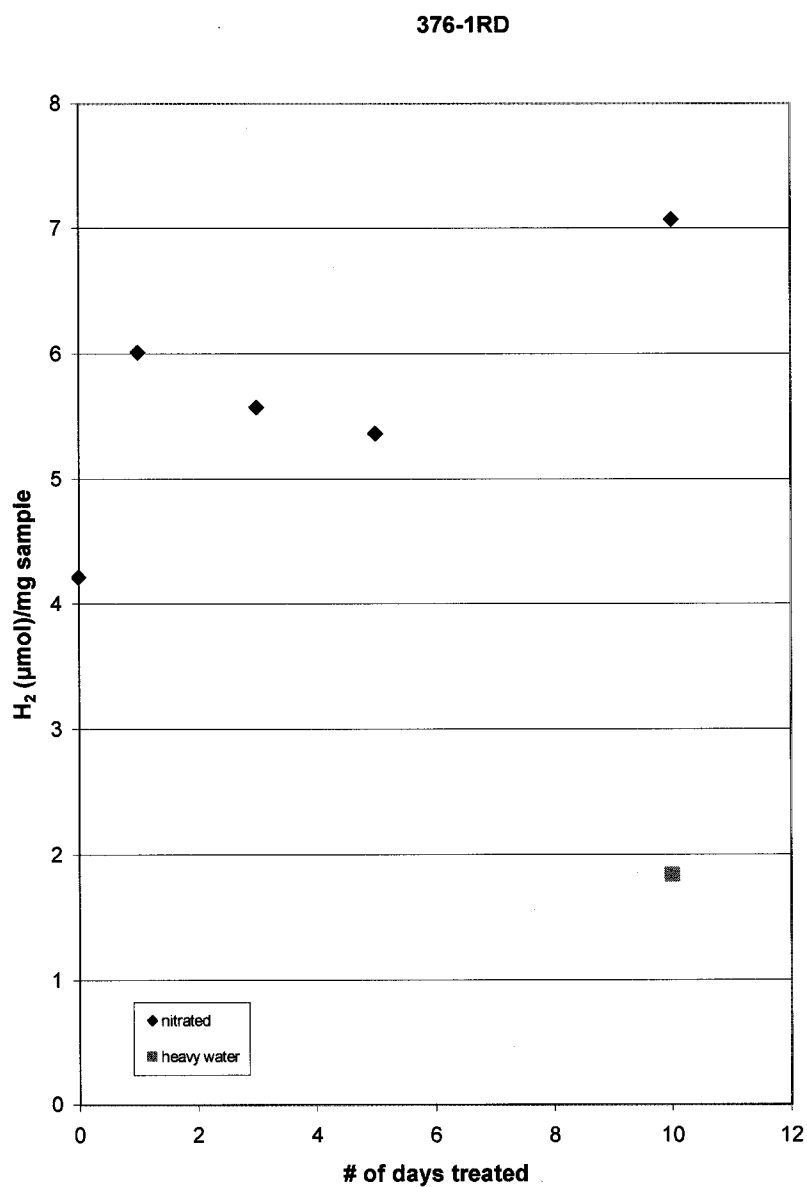
following

376-1RD

Figure I-12. Yields of H_2 for sample 376-1RD experiments.

this yields of hydrogen decreased slightly and also increased. This may have been the result of analytical error, or these data may accurately depict the change in hydrogen after nitration. The yield of hydrogen decreased during the equilibration with enriched water. Both the increase in hydrogen yields with nitration and the decrease in nitrogen yield with equilibration with enriched water were unexpected. It was expected that nitration would result in exchangeable hydrogen being replaced by nitrate, which would decrease the yield of hydrogen in the nitrated samples. Samples equilibrated with heavy water should not experience a change in hydrogen yield, according to this hypothesis.

Final experiments

Based on the above three experiments, it was assumed that nitration would change the δD value of the SOM after 1 day and that this value would not change with a longer nitration time. It was further assumed that the yield of nitrogen would increase after 1 day of nitration. Based on the Ladd Lake and the 376-1RD sample, it was expected that the yield of CO_2 would decrease with nitration, although the mechanism for this is unclear. Based on the original hypothesis, it was expected that the hydrogen yield would decrease. Previous experiments, however, indicate a possible increase in hydrogen yield. The mechanism for this is also unclear.

A final experiment was designed with the primary goal of demonstrating that 1) nitration of SOM is complete after 1 day; 2) nitration results in an enrichment of

δD values; 3) nitration of various lengths of time would result in repeatable δD values; and 4) the yield of nitrogen increases and remains constant after 1 day of nitration. This experiment was conducted with three samples provided by Grzegorz Lis and Arndt Schimmelmann of Indiana University. The samples are GSC-13531, GSC-13538, and In-Ker II, all of which are SOM derived from shale. SOM was extracted from these samples by Grzegorz Lis following the modified HF-BF$_3$ method (Robl and Davis, 1993), described above. Each sample was analyzed untreated, nitrated for 1 day, nitrated for 2 days, nitrated for 3 days, and nitrated for 5 days.

Results of the δD values are shown in Figure I-13. The δD value of GSC-13531 was -120‰ for the untreated sample. After one day of nitration the value increased to -109‰. The sample that was nitrated for 2 days was lost due to lab error. δD values for samples nitrated for 3 and 5 days were more enriched than the sample nitrated for 1 day, with isotope values of -99‰ and -103‰, respectively. There was a larger than expected difference between GSC-13531-N1 (nitrated for 1 day) and –N3 and –N5 (nitrated for 3 and 5 days). Sample GSC-13538 showed a major increase in δD values after 1 day of nitration. The untreated sample had a δD value of -128‰. Samples treated for 1, 2, and 5 days all had values of -94‰, which exhibits excellent reproducibility of δD values after nitration. GSC-13538-N3, however, had a lighter δD value of -84‰. The third sample, In-Ker II, showed the results predicted by the hypothesis. Initial δD value of the untreated sample was -91‰, and samples that were nitrated from 1 to 5 days had δD values ranging from -67‰ to -70‰.

Nitrogen yields of all samples showed the predicted pattern of an increase after one day of nitration (Figure I-14). An increase in the length of nitration resulted in no significant additional change in nitrogen yield.

Final experiments

Figure I-13. δD values for final experiments.
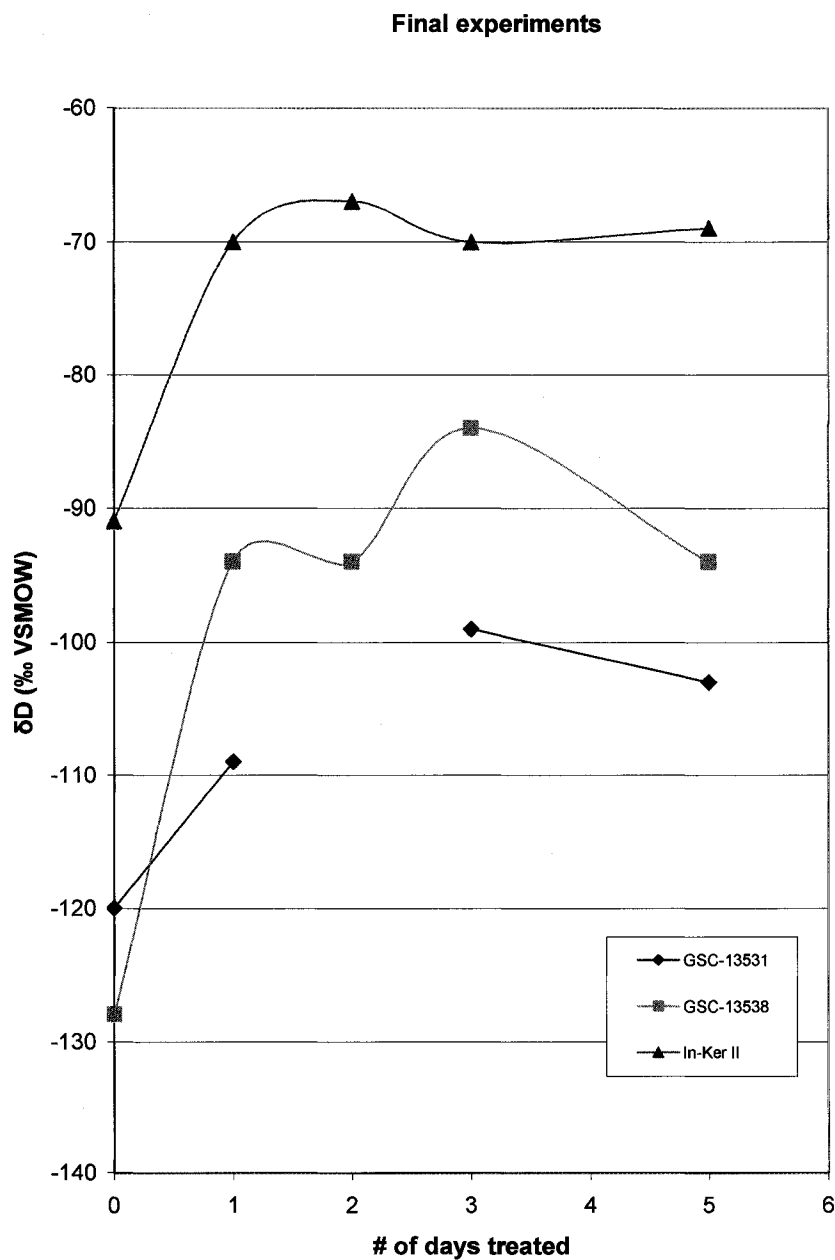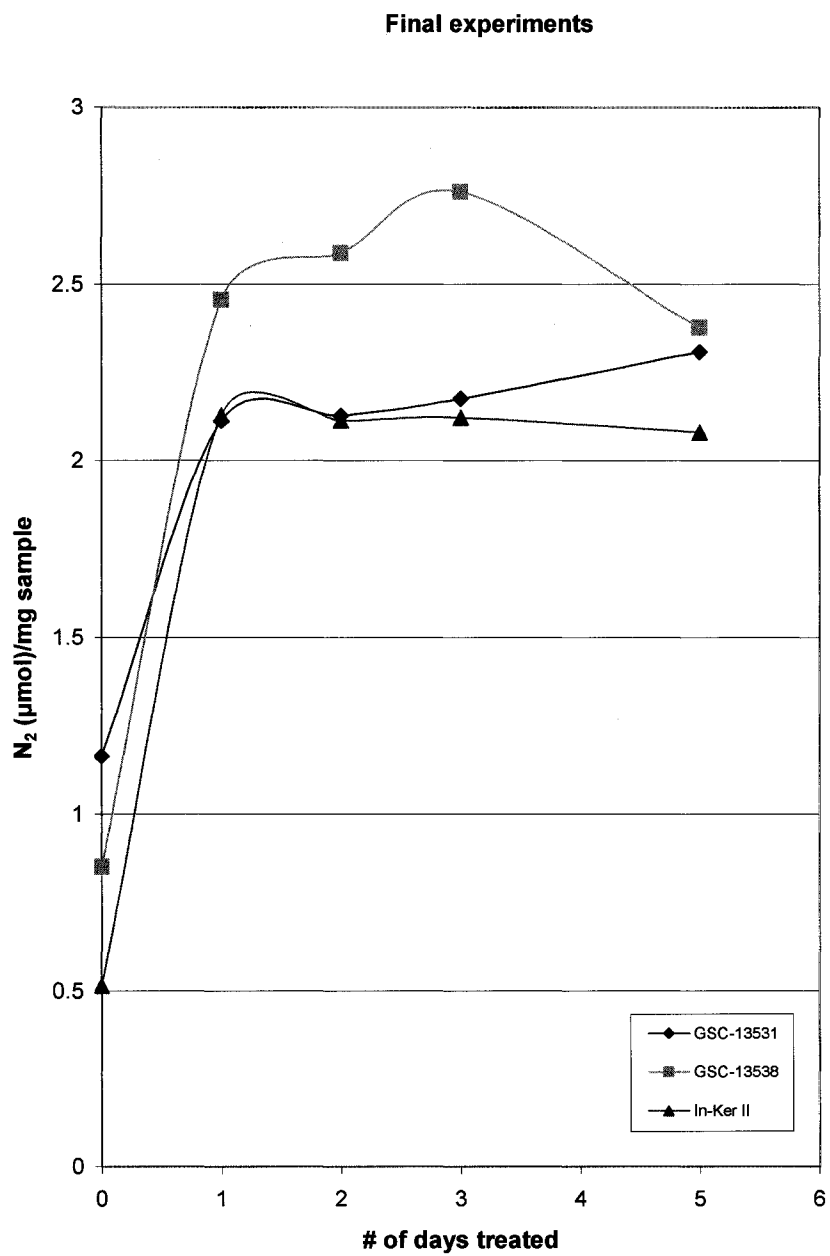
Final experiments

Figure I-14. Nitrogen yields for final experiments.

The yields of CO_2 showed less of a trend (Figure I-15). CO_2 yields of GSC-

13531 decreased significantly after 1 day of nitration and remained relatively constant
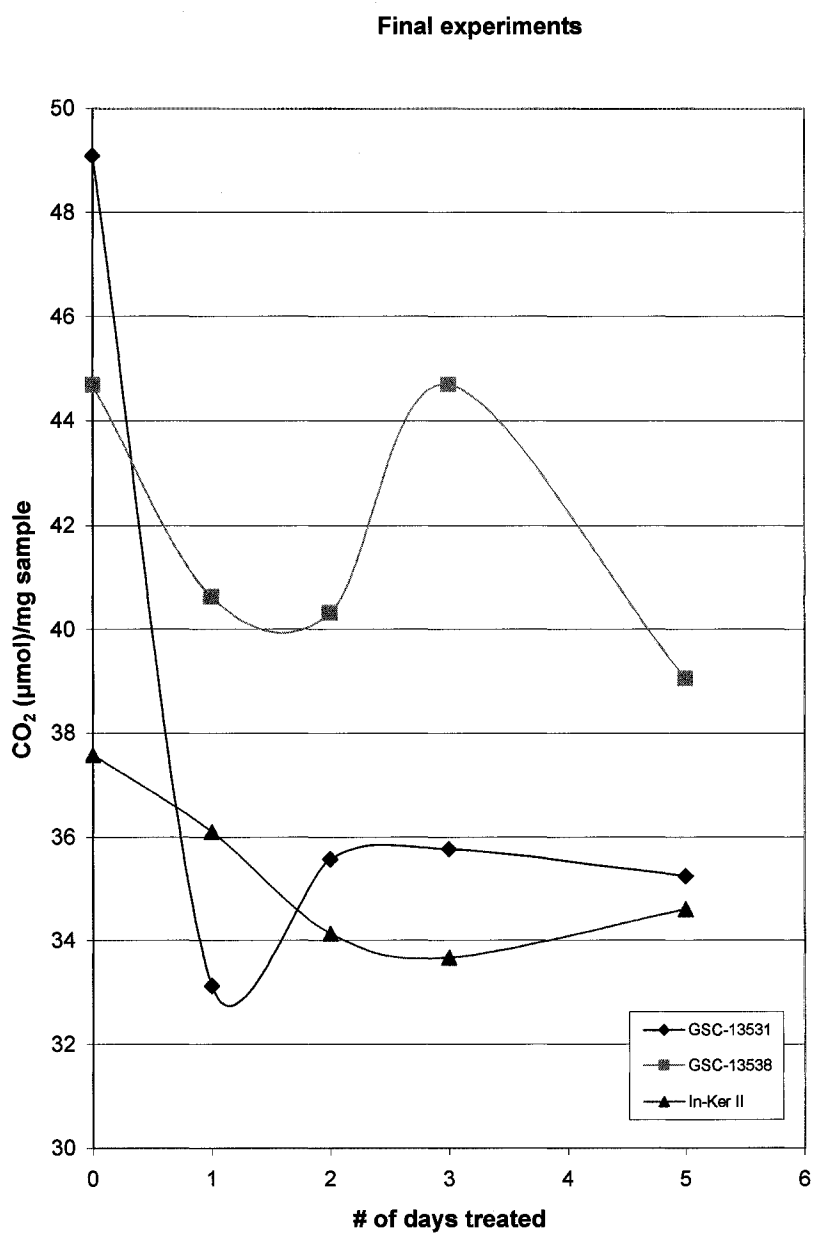
Final experiments

Figure I-15. Yields of CO_2 for final experiments.

with additional days of treatment. Sample GSC-13538 possibly showed this same trend, however GSC-13538-N3 did not fit this trend. The sample nitrated for 3 days had a CO_2 yield nearly identical to the untreated sample. This same sample, GSC-13538-N3, had anomalous results for δD and N_2 yields, which could suggest possible contamination of this sample at some point after the nitration process. The In-Ker II sample also showed a decrease in CO_2 yield, however this decrease was not complete after 1 day of nitration but after 2 days. The δD and N_2 yield for this sample fit with their corresponding trends, so contamination of this sample was not suspected.

The data for hydrogen yields were even less clear (Figure I-16). One sample, GSC-13531, showed the predicted trend of a decrease in the yield of H_2 after 1 day of nitration. This sample, however, was the only sample analyzed in the entire set of experiments that showed the predicted trend. The other two samples in this set of experiments showed the opposite trend of an increase in the yield of H_2 occurring after 1 day of nitration. Data from all three samples indicated that the nitration reaction was complete after 1 day, as there were no major changes in hydrogen yields with an increase in nitration time.
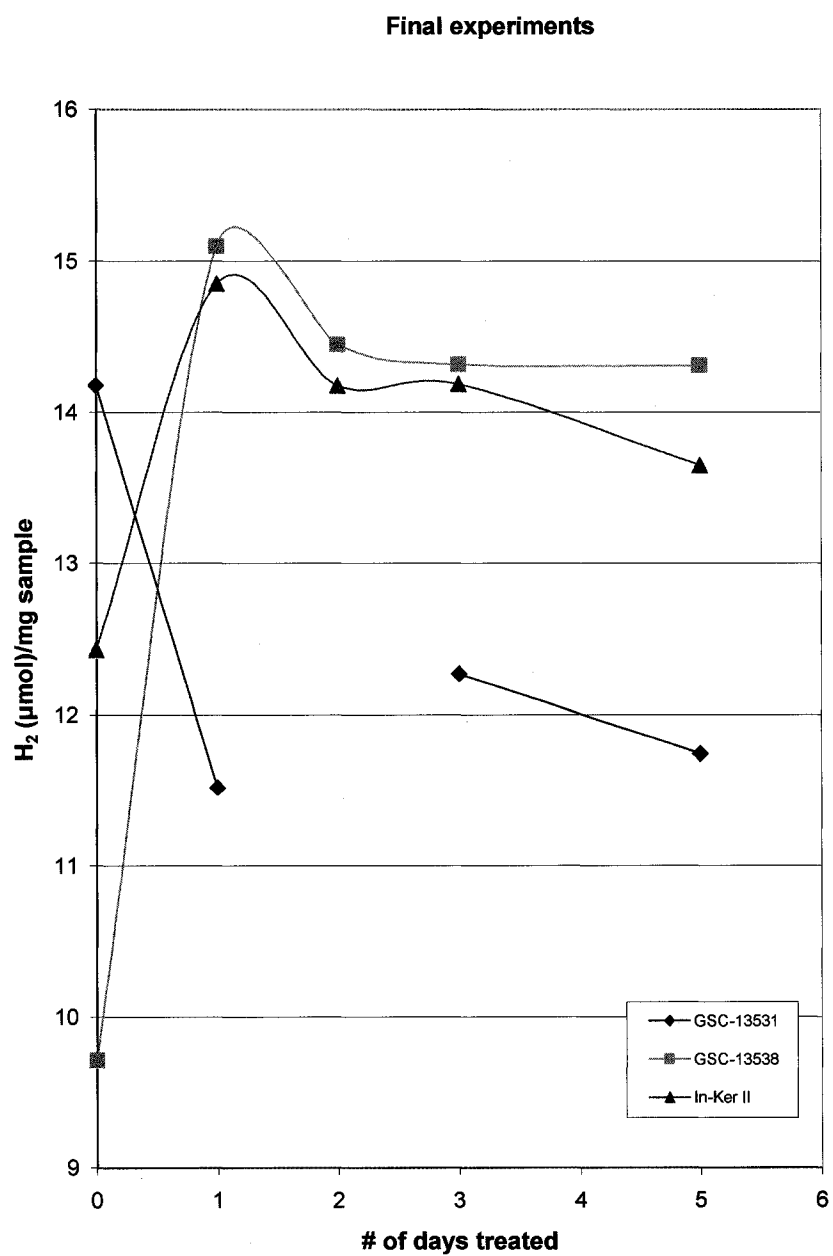
Final experiments

Figure I-16. Yields of H_2 for final experiments.

Conclusions

A series of pilot experiments were conducted to test the hypothesis that nitration of sedimentary organic hydrogen would replace the exchangeable hydrogen with nitrate. The predicted results would be a change in δD values of SOM, an increase in the yield of nitrogen and a decrease in the yield of hydrogen. The results of these pilot experiments indicated strong support that nitration resulted in the replacement of exchangeable hydrogen with nitrate, and that this exchange reaction occurred within 1 day of nitration. This was evident by the change in δD values between untreated samples and samples nitrated for 1 day in most of the samples analyzed. This was also evident in the relatively consistent δD values of samples nitrated for 1 day and longer. Further support for this hypothesis was an increase in the yield of nitrogen after 1 day of nitration in most of the samples analyzed. However, the predicted trend of a decrease in hydrogen yield after nitration was only observed in one sample. In all the various parameters tested, samples obtained from Indiana University gave better results than the Ladd Lake sample and than the charcoal samples. This is most likely due to the more extensive process of isolating SOM in these samples, including the density separation of SOM from HF-resistant heavy minerals by means of $ZnBr_2$. The poor results from the charcoal experiments were likely due to the unknown composition of commercial charcoal. Finally, the Ladd Lake results might have been influenced from hydrogen-bearing acid-resistant inorganic minerals. These results could have been refined through the density separation with $ZnBr_2$.

The ability to extract nonexchangeable hydrogen from SOM has applications as a proxy in paleoclimatology. Hydrogen isotopes obtained from organic material contain hydroxyl-hydrogen, which is a much weaker bond than the C—H bond and thus easily exchanges with water after the biosynthesis of the organic molecules. When the exchangeable hydrogen is replaced with nitrate the original δD value of the water present at the time of biosynthesis can be reconstructed.

Appendix J

Sedimentary organic hydrogen lab data

160

Table 1

sample	weight (mg)	treatment	duration (days)	gas recovered	N2 reading level	N2 yield	CO2 reading	CO2 yield
A(2)redo	17	untreated	0	yes	20.4 mid	13.066	1048.7	691.2433
A-24-n	6.3	nitration	1	yes	37.4 top	4	540.9	356
A2	8.9	nitration	2	yes	42.4 top	5.59	757.2	499.1448
A3	9.7	nitration	3	yes	43.2 top	5.814	675.7	445.4363
A4	8.2	nitration	4	yes	40.1 top	4.946	678	446.952
A5	8.8	nitration	5	yes	42 top	5.478	735	484.515
A6	8.2	nitration	6	yes	40.9 top	5.17	676	445.634
A7	8.8	nitration	7	yes	41 top	5.198	756	498.354
A8	8.6	nitration	8	yes	41.2 top	5.254	674.3	444.5137
A9	10.7	nitration	9	no				
A10	8.9	nitration	10	yes	29.8 top	2.062	257	169.513
A-big-2w-n	17.3	nitration	18	yes	20.1 mid	11.665	1394.6	919.1914
A(1)redo	16.8	untreated	0	yes	29.4 top?	1.76	708.6	467.1174
A(1)-24-n	8.2	nitration	1	yes	42 top	5.288	759.1	500.3969
A(1)-2w-n	7.9	nitration	18	yes	41.5 top	5.148	641.5	422.8985
A-n-2w	6.6	nitration	18	yes	46 top	6.4	560.6	369.5854
A	6	untreated	0	yes	37.8 top	4.1	340.3	224

Table 2

sample	H2 reading level	H2 yield	d13C	d18O	dD	C/N	N2/mg	CO2/mg	H2/mg	notes
A(2)redo	31 mid	62.568	-26.55	-18.12	34.3	26.45199	1.537176	40.66137	7.360941	
A-24-n	22.9 mid	24.7	-27.24	-17.89	33.2	44.5	1.269841	56.50794	7.84127	
A2	26	39.218			-41	44.64623	1.25618	56.08369	8.813034	
A3	27.3	45.289			-37	38.30722	1.198763	45.92127	9.337938	
A4	24.4	31.746			-50.8	45.18318	1.206341	54.50634	7.742927	
A5	26.6	42.02			-16.2	44.22371	1.245	55.05852	9.55	
A6	24.9	34.081				43.09807	1.260976	54.34561	8.312439	
A7	27.4	45.756				47.93709	1.181364	56.63114	10.39909	
A8	28.5	50.893				42.30241	1.22186	51.68764	11.83558	
A9										
A10	27.5	46.223			-12	41.10403	0.463371	19.0464	10.38719	
A-big-2w-n	32.2 mid	68.172	-27.33	-19.54	19.9	39.39955	1.348655	53.13245	7.881156	
A(1)redo	25.2 mid	35.482	-24.92	-16.79	-20.2	132.7038	0.209524	27.80461	4.224048	suspect
A(1)-24-n	29 mid	53.228	-27.94	-18.55		47.31438	1.289756	61.02401	12.98244	
A(1)-2w-n	24.9 mid	34.081	-27.2	-18.4		41.07406	1.303291	53.53146	8.628101	
A-n-2w	24.9 mid	34.081	-27.35	-17.48		28.87386	1.939394	55.99779	10.32758	
A	21.7 mid	19.1	-25.23	-17.39	25.5	27	1.366667	37.33333	6.366667	

days treated	sample	wt (mg)	N2 reading	N2 yield	CO2 reading	CO2 yield	H2 reading	H2 yield	N2/mg	CO2/mg	H2/mg	dD
0	X	9.4	19.9	10.938	700	461.45	20.4	133.2744	1.1636	49.09043	14.178	-120
1	X-N1	4.5	19.6	9.51	226	149.084	28.7	51.827	2.1133	33.12978	11.517	-109
2	X-N2	7.6	21	16.174	410	270.34			2.1282	35.57105		
3	X-N3	5.9	20.3	12.842	320	211.03	33.1	72.375	2.1766	35.7678	12.267	-99
5	X-N5	3.5	19.3	8.082	187	123.383	26.4	41.086	2.3091	35.25229	11.739	-103
0	Y	9.5	19.3	8.082	644	424.546	17.5	92.2191	0.8507	44.68905	9.7073	-128
1	Y-N1	12.2	23.9	29.978	752	495.718	24	184.2396	2.4572	40.63262	15.102	-94
2	Y-N2	10.3	23.2	26.646	630	415.32	21.5	148.8471	2.587	40.32233	14.451	-94
3	Y-N3	10	23.4	27.598	678	446.952	21.1	143.1843	2.7598	44.6952	14.318	-84
5	Y-N5	10.4	22.8	24.742	616	406.094	21.5	148.8471	2.379	39.0475	14.312	-94
0	Z	9.7	41	5.008	553	364.577	19.5	120.5331	0.5163	37.58526	12.426	-91
1	Z-N1	10.5	22.3	22.362	575	379.075	22	155.9256	2.1297	36.10238	14.85	-70
2	Z-N2	9	21.6	19.03	466	307.244	20	127.6116	2.1144	34.13822	14.179	-67
3	Z-N3	6.5	20.5	13.794	332	218.938	17.5	92.2191	2.1222	33.68277	14.188	-70
5	Z-N5	8	21.1	16.65	420	276.93	18.7	109.2075	2.0813	34.61625	13.651	-69
0	376-B	13.1		11.2		389		55.1	0.85	29.69	4.21	-104
1	376-N1A	10.8		17.7		254		64.9	1.64	23.52	6.01	-75.8
3	376-N3	10.4		15.9		239		57.9	1.53	22.98	5.57	-73.4
5	376-N5	9.5		14.9		239		50.9	1.57	25.16	5.36	-77.1
10	376-N10B	10.7		17.7		270		75.6	1.65	25.23	7.07	-75.2
10	376-HW	9.4		4.9		275		17.3	0.52	29.26	1.84	-89.7
0	376	9.6		3.8		244		14.9	0.4	25.42	1.55	-125
1	376-N1B	10.3		16.8		247		62.6	1.63	23.98	6.08	-83.5
0	LLO-A	10.7	20.5	13.533	730	481.22	25.5	205.4751	1.2648	44.97383	2.3832	-118
1	LLO-N1	8.9	21	15.868	453	298.677	46.5	134.953	1.7829	33.55921	5.2247	-101
5	LLO-N5	16.2	22.2	21.472	762	502.308	28.5	247.9461	1.3254	31.00667	1.7593	-107

Appendix K

Permission letters

163

From: David, Natalie (ELS-OXF)
Sent: 13 February 2007 12:49
To: sbeukema@yahoo.com
Subject: RE: Obtain Permission

ELSEVIER

Dear Dr Beukema

We hereby grant you permission to reproduce the material detailed below
in your thesis at no charge subject to the following conditions:

1.   If any part of the material to be used (for example, figures)
has appeared in our publication with credit or acknowledgement to
another source, permission must also be sought from that source. If
such permission is not obtained then that material may not be included
in your publication/copies.

2.   Suitable acknowledgment to the source must be made, either as a
footnote or in a reference list at the end of your publication, as
follows:

            "Reprinted from Publication title, Vol number,
Author(s), Title of article, Pages No., Copyright (Year), with
permission from Elsevier".

3.   Your thesis may be submitted to your institution in
either print or electronic form

4.   Reproduction of this material is confined to the purpose for
which permission is hereby given.

5.   This permission is granted for non-exclusive world English
rights only. For other languages please reapply separately for each one
required. Permission excludes use in an electronic form. Should you
have a specific electronic project in mind please reapply for
permission.

6.   This includes permission for UMI to supply single copies, on
demand, of the complete thesis. Should your thesis be published
commercially, please reapply for permission.

Yours sincerely,

Natalie David
Senior Rights Assistant

Your future requests will be handled more quickly if you complete the
online form at www.elsevier.com/permissions

-----Original Message-----
From: sbeukema@yahoo.com [mailto:sbeukema@yahoo.com]
Sent: 12 February 2007 23:37
To: Rights and Permissions (ELS)
Subject: Obtain Permission

This Email was sent from the Elsevier Corporate Web Site and is related
to Obtain Permission form:

Product: Customer Support
Component: Obtain Permission
Web server: http://www.elsevier.com
IP address: 10.10.24.148
Client: Mozilla/4.0 (compatible; MSIE 7.0; Windows NT 5.1; .NET
CLR 1.1.4322; InfoPath.1)
Invoked from:
http://www.elsevier.com/wps/find/obtainpermissionform.cws_home?isSubmitt
ed=yes&navigateXmlFileName=/store/prod_webcache_act/framework_support/ob
tainpermission.xml

Request From:
 Steven Beukema
Western Michigan University
Geosciences - 1187 Rood Hall
49008
Kalamazoo
United States

Contact Details:
Telephone: 2693240804
Fax:
Email Address: sbeukema@yahoo.com

To use the following material:
ISSN/ISBN:
Title: Earth and Planetary Science Letters
Author(s):   Zhao, J. -X., et al.
Volume: 216
Issue: 1-2
Year: 2003
Pages: 155 - 161
Article title: Speleothem U-series dating of semi-synchron

How much of the requested material is to be used:
Figure 2 on page 158

Are you the author: No
Author at institute: No

How/where will the requested material be used: [how_used]

Details:

In my dissertation, "Late Pleistocene climate variability and chemical
weathering in the Goriganga, Higher Central Himalaya, North India"

Additional Info:

- end -

For further info regarding this automatic email, please contact:
WEB APPLICATIONS TEAM (esweb.admin@elsevier.co.uk)

From: David, Natalie (ELS-OXF)
Sent: 13 February 2007 12:13
To: sbeukema@yahoo.com
Subject: RE: Obtain Permission

ELSEVIER

Dear Dr Beukema

We hereby grant you permission to reproduce the material detailed below
in your thesis at no charge subject to the following conditions:

1.   If any part of the material to be used (for example, figures)
has appeared in our publication with credit or acknowledgement to
another source, permission must also be sought from that source. If
such permission is not obtained then that material may not be included
in your publication/copies.

2.   Suitable acknowledgment to the source must be made, either as a
footnote or in a reference list at the end of your publication, as
follows:

            "Reprinted from Publication title, Vol number,
Author(s), Title of article, Pages No., Copyright (Year), with
permission from Elsevier".

3.   Your thesis may be submitted to your institution in
either print or electronic form

4.   Reproduction of this material is confined to the purpose for
which permission is hereby given.

5.   This permission is granted for non-exclusive world English
rights only. For other languages please reapply separately for each one
required. Permission excludes use in an electronic form. Should you
have a specific electronic project in mind please reapply for
permission.

6.   This includes permission for UMI to supply single copies, on
demand, of the complete thesis. Should your thesis be published
commercially, please reapply for permission.

Yours sincerely,

Natalie David
Senior Rights Assistant

Your future requests will be handled more quickly if you complete the
online form at www.elsevier.com/permissions

-----Original Message-----
From: sbeukema@yahoo.com [mailto:sbeukema@yahoo.com]
Sent: 12 February 2007 23:25
To: Rights and Permissions (ELS)
Subject: Obtain Permission

This Email was sent from the Elsevier Corporate Web Site and is related
to Obtain Permission form:

Product: Customer Support
Component: Obtain Permission
Web server: http://www.elsevier.com
IP address: 10.10.24.148
Client: Mozilla/4.0 (compatible; MSIE 7.0; Windows NT 5.1; .NET
CLR 1.1.4322; InfoPath.1)
Invoked from:
http://www.elsevier.com/wps/find/obtainpermissionform.cws_home?isSubmitt
ed=yes&navigateXmlFileName=/store/prod_webcache_act/framework_support/ob
tainpermission.xml

Request From:
 Steven Beukema
Western Michigan University
Geosciences - 1187 Rood Hall
49008
Kalamazoo
United States

Contact Details:
Telephone: 2693240804
Fax:
Email Address: sbeukema@yahoo.com

To use the following material:
ISSN/ISBN:
Title: Earth and Planetary Sciences Letters
Author(s):   Fang, X. -M., et al.
Volume: 168
Issue: 3-4
Year: 1999
Pages: 219 - 232
Article title: Asian summer monsoon instability

How much of the requested material is to be used:
Figure 4 on page 227

Are you the author: No
Author at institute: No

How/where will the requested material be used: [how_used]

Details:

Figure 4 will be used in my dissertation, "Late Pleistocene climate
variability and chemical weathering in the Goriganga, Higher Central

Himalaya, North India"

Additional Info:

- end -

For further info regarding this automatic email, please contact:
WEB APPLICATIONS TEAM (esweb.admin@elsevier.co.uk)

From: David, Natalie (ELS-OXF)
Sent: 13 February 2007 12:15
To: sbeukema@yahoo.com
Subject: RE: Obtain Permission

ELSEVIER

Dear Dr Beukema

We hereby grant you permission to reproduce the material detailed below
in your thesis at no charge subject to the following conditions:

1.   If any part of the material to be used (for example, figures)
has appeared in our publication with credit or acknowledgement to
another source, permission must also be sought from that source. If
such permission is not obtained then that material may not be included
in your publication/copies.

2.   Suitable acknowledgment to the source must be made, either as a
footnote or in a reference list at the end of your publication, as
follows:

                "Reprinted from Publication title, Vol number,
Author(s), Title of article, Pages No., Copyright (Year), with
permission from Elsevier".

3.   Your thesis may be submitted to your institution in
either print or electronic form

4.   Reproduction of this material is confined to the purpose for
which permission is hereby given.

5.   This permission is granted for non-exclusive world English
rights only. For other languages please reapply separately for each one
required. Permission excludes use in an electronic form. Should you
have a specific electronic project in mind please reapply for
permission.

6.   This includes permission for UMI to supply single copies, on
demand, of the complete thesis. Should your thesis be published
commercially, please reapply for permission.

Yours sincerely,

Natalie David
Senior Rights Assistant

Your future requests will be handled more quickly if you complete the
online form at www.elsevier.com/permissions

-----Original Message-----
From: sbeukema@yahoo.com [mailto:sbeukema@yahoo.com]
Sent: 12 February 2007 23:32
To: Rights and Permissions (ELS)
Subject: Obtain Permission

This Email was sent from the Elsevier Corporate Web Site and is related
to Obtain Permission form:

Product: Customer Support
Component: Obtain Permission
Web server: http://www.elsevier.com
IP address: 10.10.24.149
Client: Mozilla/4.0 (compatible; MSIE 7.0; Windows NT 5.1; .NET
CLR 1.1.4322; InfoPath.1)
Invoked from:
http://www.elsevier.com/wps/find/obtainpermissionform.cws_home?isSubmitt
ed=yes&navigateXmlFileName=/store/prod_webcache_act/framework_support/ob
tainpermission.xml

Request From:
 Steven Beukema
Western Michigan University
Geosciences - 1187 Rood Hall
49008
Kalamazoo
United States

Contact Details:
Telephone: 2693240804
Fax:
Email Address: sbeukema@yahoo.com

To use the following material:
ISSN/ISBN:
Title: Earth and Planetary Science Letters
Author(s):   Huang, C. -Y. et al.
Volume: 146
Issue: 1-2
Year: 1997
Pages: 59 - 72
Article title: Deep sea and lake records of the Southeast Asian

How much of the requested material is to be used:
Figure 4 on page 64 and and Figure 5 (second graph from bottom only -
Castanopsis) on page 66

Are you the author: No
Author at institute: No

How/where will the requested material be used: In a thesis or
dissertation

Details:

In my dissertation, "Late Pleistocene climate variability and chemical
weathering in the Goriganga, Higher Central Himalaya, North India"

Additional Info:

- end -

For further info regarding this automatic email, please contact:
WEB APPLICATIONS TEAM (esweb.admin@elsevier.co.uk)

From: David, Natalie (ELS-OXF)
Sent: 13 February 2007 12:48
To: sbeukema@yahoo.com
Subject: RE: Obtain Permission

ELSEVIER

Dear Dr Beukema

We hereby grant you permission to reproduce the material detailed below in your thesis at no charge subject to the following conditions:

1.   If any part of the material to be used (for example, figures) has appeared in our publication with credit or acknowledgement to another source, permission must also be sought from that source. If such permission is not obtained then that material may not be included in your publication/copies.

2.   Suitable acknowledgment to the source must be made, either as a footnote or in a reference list at the end of your publication, as follows:

            "Reprinted from Publication title, Vol number, Author(s), Title of article, Pages No., Copyright (Year), with permission from Elsevier".

3.   Your thesis may be submitted to your institution in either print or electronic form

4.   Reproduction of this material is confined to the purpose for which permission is hereby given.

5.   This permission is granted for non-exclusive world English rights only. For other languages please reapply separately for each one required. Permission excludes use in an electronic form. Should you have a specific electronic project in mind please reapply for permission.

6.   This includes permission for UMI to supply single copies, on demand, of the complete thesis. Should your thesis be published commercially, please reapply for permission.

Yours sincerely,

Natalie David
Senior Rights Assistant

Your future requests will be handled more quickly if you complete the
online form at www.elsevier.com/permissions

-----Original Message-----
From: sbeukema@yahoo.com [mailto:sbeukema@yahoo.com]
Sent: 12 February 2007 23:42
To: Rights and Permissions (ELS)
Subject: Obtain Permission

This Email was sent from the Elsevier Corporate Web Site and is related
to Obtain Permission form:

Product: Customer Support
Component: Obtain Permission
Web server: http://www.elsevier.com
IP address: 10.10.24.149
Client: Mozilla/4.0 (compatible; MSIE 7.0; Windows NT 5.1; .NET
CLR 1.1.4322; InfoPath.1)
Invoked from:
http://www.elsevier.com/wps/find/obtainpermissionform.cws_home?isSubmitt
ed=yes&navigateXmlFileName=/store/prod_webcache_act/framework_support/ob
tainpermission.xml

Request From:
 Steven Beukema
Western Michigan University
Geosciences - 1187 Rood Hall
49008
Kalamazoo
United States

Contact Details:
Telephone: 2693240804
Fax:
Email Address: sbeukema@yahoo.com

To use the following material:
ISSN/ISBN:
Title: Earth and Planetary Science Letters
Author(s):   Wang, R.L., et al
Volume: 203
Issue: 1
Year: 2002
Pages: 461 - 477
Article title: Later Pleistocene/Holocene climate conditions

How much of the requested material is to be used:
Figure 6 on page 469

Are you the author: No
Author at institute: No

How/where will the requested material be used: In a thesis or
dissertation

Details:

In my dissertation, "Late Pleistocene climate variability and chemical
weathering in the Goriganga, Higher Central Himalaya, North India"

Additional Info:

- end -

For further info regarding this automatic email, please contact:
WEB APPLICATIONS TEAM (esweb.admin@elsevier.co.uk)

BIBLIOGRAPHY

Alley, R.B., Meese, D.A., Shuman, C.A., et al., 1993. Abrupt increase in Greenland snow accumulation at the end of the Younger Dryas event. *Nature* 362: 527 – 529.

Bard, E., Arnold, M., and four others, 1987. Rapid velocity of the North Atlantic polar front retreat during the last deglaciation determined by ^{14}C accelerator mass spectrometry. *Nature* 328: 791 – 794.

Barnard, P.L., Owen, L.A., Finkel, R.C., 2004a. Style and timing of glacial and paraglacial sedimentation in a monsoon-influenced high Himalayan environment, the upper Bhagirathi Valley, Garhwal Himalaya. *Sedimentary Geology* 165/3: 199 – 221.

Barnard, P.L., Owen, L.A., Sharma, M.C., Finkel., R.C., 2004b. Late Quaternary (Holocene) landscape evolution of a monsoon-influenced high Himalayan valley, Gori Ganga, Nanda Devi, NE Garhwal. *Geomorphology* 61: 91 – 110.

Bartarya, S.K., 1993. Hydrochemistry and rock weathering in a subtropical Lesser Himalayan river basin in Kumaun. *Journal of Hydrology* 146: 149 – 174.

Beukema, S.P., 2003. Stratigraphy of Lake Michigan Lobe deposits in Van Buren County, Michigan. Unpublished M.S. Thesis, Western Michigan University, Kalamazoo, Michigan, 140 p.

Björck, S., Walker, M.J.C., Cwynar, L.C., Johnsen, S., Knudsen, K.-L., Lowe, J.J., Wohlfarth, B., Members, I., 1998. An event stratigraphy for the last termination in the North Atlantic region based on the Greenland ice-core record: A proposal by the INTIMATE group. *Journal of Quaternary Science* 13: 283 – 292.

Bond, G., Heinrich, H., Broecker, W., et al., 1992. Evidence for massive discharges of icebergs into the North Atlantic ocean during the last glacial period. *Nature* 360: 245 – 249.

Bowen, G.J., Revenaugh, J., 2003. Interpolating the isotopic composition of modern meteoric precipitation. *Water Resources Research* 39: p.1299.

Broecker, W.S., 1982. Glacial to interglacial changes in ocean chemistry. *Progress in Oceanography* 11: 151 – 197.

176

Broecker, W.S., 1994. Massive iceberg discharge triggers for global climate change. *Nature* 372: 421 – 424.

Broecker, W.S., 1998. Paleocean circulation during the last deglaciation: A bipolar seesaw. *Paleoceanography* 13: 119 – 121.

Broecker, W.S., Bond, G., Klas, M., Clark, E., McManus, J., 1992. Origin of the northern Atlantic's Heinrich events. *Climate Dynamics* 6: 265 – 273.

Cerling, T.E., Harris, J.M., MacFadden, B.J., Leakey, M.G., Quade, J., Eisenmann, V, 1997. Global vegetation change through the Miocene-Pliocene boundary. *Nature* 389: 153 – 158.

Cerling, T., Wang, Y., Quade, J., 1993. Expansion of C_4 ecosystems as an indicator of global ecological change in the late Miocene. *Nature* 361: 344 – 345.

Chamberlin, T.C., 1895. The classification of American glacial deposits. *Journal of Geology* 3: 270 – 277.

Chamberlin, T.C., 1896. Editorial. *Journal of Geology* 4: 872 – 876.

Chandel, H.N., Patel, A.D., Vaghela, H.R., Ubale, G.P., 2006. An effective and reuseable sampling pipe for luminescence dating. *Ancient TL*: 24/1: 21 – 22.

Chappell, J., Omura, A., and five others, 1996. Reconciliation of late Quaternary sea levels derived from coral terraces at Huon Peninsula with deep-sea isotope records. *Earth and Planetary Science Letters* 141: 227 – 236.

Clemens, S., Prell, W., Murray, D., Shimmield, G., Weedon, G., 1991. Forcing mechanisms of the Indian Ocean monsoon. *Nature* 353: 720 – 725.

Cronin, T.M, 1999. Principles of Paleoclimatology. Columbia University Press: New York, 560 p.

Dalai, T.K., Krishnaswami, S., Sarin, M.M., 2002. Major ion chemistry in the headwaters of the Yamuna river system: Chemical weathering, its temperature dependence and CO_2 consumption in the Himalaya. *Geochimica et Cosmochimica Acta* 66/19: 3397 - 3416.

Dansgaard, W., 1964. Stable isotopes in precipitation. *Tellus* 16: 436 – 468.

Dansgaard, W., Clausen, H.B., Gundestrup, N., et al., 1982. A new Greenland deep ice core. *Science* 218: 1273 – 1277.

Dansgaard, W., Johnsen, S.J., Clausen, H.B., et al., 1993. Evidence for general instability of climate from a 250-kyr ice-core record. *Nature* 364: 218 – 220.

Dansgaard, W., Oeschger, H., 1989. Past environmental long-term records from the Arctic. In: *The Environmental Record in Glaciers and Ice Sheets* [H. Oeschger and C.C. Langway, Jr. (eds.)]. John Wiley & Sons, Chichester, United Kingdom, p.287 – 318.

Donner, J., 1995. *The Quaternary history of Scandinavia*. Columbia University Press, Cambridge, UK, 200 p.

Epstein, S., Yapp, C.J., Hall, J.H., 1976. The determination of the D/H ratio of non-exchangeable hydrogen in cellulose extracted from aquatic and land plants. *Earth and Planetary Science Letters* 30: 41 – 251.

Fairbanks, R.G., 1989. A 17,000-year glacio-eustatic sea level record: influence of glacial melting rates on the Younger Dryas event and deep-ocean circulation. *Nature* 342: 637 – 642.

Fang, X.-M., Ono, Y., Fukusawa, H., Bao-Tian, P., Li, J.-J., Dong-Hong, G., Oi, K., Tsukamoto, S., Torii, M., Mishima, T., 1999. Asian summer monsoon Instability during the past 60,000 years: magnetic susceptibility and pedogenic evidence from the western Chinese Loess Plateau. *Earth and Planetary Science Letters* 168: 219 – 232.

Faure, G., 1977. Principles of Isotope Geology. John Wiley & Sons, 464 p.

Feng, X., Krishnamurthy, R.V., Epstein, S., 1993. Determination of D/H ratios of nonexchangeable hydrogen in cellulose: A method based on the cellulose-water exchange reaction. *Geochimica et Cosmochimica Acta* 57: 4249 – 4256.

Flower, B.P., Kennett., J.P., 1990. The Younger Dryas cool episode in the Gulf of Mexico. *Paleoceanography* 5: 949 – 961.

Folland, C.K., Karl, T.R., Christy, J.R., Clarke, R.A., Gruza, G.V., Jouzel, J., Mann, M.E., Oerlemans, J., Salinger, M.J., Wang, S.-W., 2001. Observed climate variability and change. In: *Climate Change 2001: The Scientific Basis. Contribution of Working Group I to the Third Assessment Report of the Intergovernmental Panel on Climate Change* [Houghton, J.T., Ding, Y., Griggs, D.J., Noguer, M., van der Linden, P.J., Dai, X., Maskell, K., Johnson, C.A. (eds.)]. Cambridge University Press, Cambridge, United Kingdom and New York, NY, USA, 881 p.

Frakes, L.A., Francis, J.E., Syktus, J.I., 1992. *Climate Modes of the Phanerozoic.* Cambridge University Press, Cambridge, United Kingdom.

Friedman, I., O'Neil, J.R., 1977. Compilation of stable isotope fractionation factors of geochemical interest. In: *Data of Geochemistry, 6th Edition* [Fleischer, M. (ed.)] ch U.S.G.S. Prof. Paper 440-KK: 1 – 12.

Galy, A., France-Lanord, C., 1999. Weathering processes in the Ganges-Brahmaputra basin and the riverine alkalinity budget. *Chemical Geology* 159: 31 – 60.

Ghosh, P., Bhattacharya, S.K., 2003. Sudden warming epochs during 42 to 28 ky BP in the Himalayan region from stable isotope record of sediment column from a relict lake in Goting, Garhwal, North India. *Current Science* 85/1: 60 – 67.

Gillespie, A., Molnar, P., 1995. Asynchronous maximum advances of mountain and continental glaciers. *Review of Geophysics* 33/3: 311 – 364.

Godwin, H., 1962. Half-life of radiocarbon. *Nature* 195: p.984.

Grove, 1988. *The little ice age.* Methuen, London, 498 p.

Gu, Z.Y., Liu, Q., Xu, B., Han, J.M., Yang, S.L., Ding, Z.L., Liu, T.S., 2003. Climate as the dominant control on C3 and C4 plant abundance in the Loess Plateau: Organic carbon isotope evidence from the last glacial-interglacial loess-soil sequences. *Chinese Science Bulletin* 48/12: 1271 – 1276.

Hajdas, I., Ivy, S., Beer, L., et al., 1993. AMS radiocarbon dating and varve chronology of Lake Soppensee: 6000 – 12,000 14C years BP. *Climate Dynamics* 9: 107 – 116.

Hajdas, I., Zolitschka, B., Ivy-Ochs, S.D., et al., 1995. AMS radiocarbon dating of annually laminated sediments from Lake Holzmaar, Germany. *Quaternary Science Reviews* 14: 137 – 143.

Harris, N., Bickle, M., Chapman, H., Fairchild, I., Bunbury, J., 1998. The significance of Himalayan rivers for silicate weathering rates: Evidence from the Bhote Kosi tributary. *Chemical Geology* 144: 205 – 220.

Heinrich, H., 1988. Origin and consequence of cyclic ice rafting in the northeast Atlantic Ocean during the past 130,000 years. *Quaternary Research* 29: 142 – 152.

Heusser, H., 1944. *Cellulose Chemistry.* J. Wiley & Sons.

Hoffman, P.F., Kaufman, A.J., Halverson, G.P., Schrag, D.P., 1998. A Neoproterozoic Snowball Earth. *Science* 281: 1342 – 1346.

Hong, Y.T. Hong, B., Lin, Q.H., Zhu, Y.X., Shibata, Y., Hirota, M., Uchida, M., Leng, X.T., Jiang, H.B., Xu, H., Wang, H., Yi, L., 2003. Correlation between Indian Ocean summer monsoon and North Atlantic climate during the Holocene. *Earth and Planetary Science Letter* 211: 371 – 380.

http://www.worldclimate.com. Global Historic Climatology Network, Version 1 (GHCN 1), August 1992. Produced jointly by the National Climatic Data Center and Carbon Dioxide Information Analysis Center, Oak Ridge National Laboratory, Oak Ridge, Tennessee, USA.

Huang, C.-Y., Liew, P.-M., Zhao, M., Chang, T.-C., Kuo, C.-M., Chen, M.-T., Wang, C.-H., Zheng, L.-F., 1997. Deep sea and lake records of the Southeast Asian paleomonsoons for the last 25 thousand years. *Earth and Planetary Science Letters* 146: 59 – 72.

Jacobson, A.D., Blum, J.D., Walter, L.M., 2002. Reconciling the elemental and Sr isotope composition of Himalayan weathering fluxes: Insights from the carbonate geochemistry of stream waters. *Geochimica et Cosmochimica Acta* 66/19: 3417 – 3429.

Jin, Z.-D., Wu, Y., Zhang, X., Wang, S., 2005. Role of late glacial to mid-Holocene climate in catchment weathering in the central Tibetan Plateau. *Quaternary Research* 63: 161 – 170.

Johnson, S.J., Clausen, H.B., Dansgaard, W., et al., 1992. Irregular glacial interstadials recorded in a new Greenland ice core. *Nature* 359: 311 – 313.

Jouzel, J., Barkov, N.I., Barnola, J.-M., et al., 1993. Extending the Vostok ice-core record of paleoclimate to the penultimate glacial period. *Nature* 364: 407 – 412.

Jouzel, J., Lorius, C., Petit, J.R., Genthon, C., Barkov, N.I., Kotlyakov, V.M., Petrov, V.M., 1987. Vostok ice core: a continuous isotope temperature record over the last climatic cycle (160,000 years). *Nature* 329: 403 – 408.

Jouzel, J., Waelbroeck, C., Malaize, B., Bender, M., Petit, J.R., Stievenard, M., Barkov, N.I., Barnola, J.M., King, T., Kotlyakov, V.M., Lipenkov, V., Lorius, C., Raynaud, D., Ritz, C., Sowers, T., 1996. Climatic interpretation of the recently extended Vostok ice records. *Climate Dynamics* 12: 513 – 521.

Juyal, N., Pant, R.K., Basavaiah, N., Yadava, M.G., Saini, N.K., Singhvi, A.K., 2004. Climate and seismicity in the higher Central Himalaya during 20 – 10 ka: evidence from the Garbayang basin, Uttaranchal, India. *Palaeogeography, Palaeoclimatology, Palaeoecology* 213: 315 – 330.

Kehew, A.E., Beukema, S.P., Bird, B.C., Kozlowski, A.L., 2005. Fast flow of the Lake Michigan Lobe: evidence from sediment-landform assemblages in southwestern Michigan, USA. *Quaternary Science Reviews* 24: 2335 – 2353.

Kennett, J.P., 1982. *Marine geology*. Prentice-Hall, Inc., Englewood Cliffs, N.J., 813 p.

Krishnamurthy, R.V., Atekwana, E.A., Guha, H., 1997. A simple, inexpensive carbonate-phosphoric acid reaction method for the analysis of carbon and oxygen isotopes of carbonates. *Analytical Chemistry* 69/20: 4256 – 4258.

Krishnamurthy, R.V., Bhattacharya, S.K., Kusumgar, S., 1986. Palaeoclimatic Changes deduced from $^{13}C/^{12}C$ and C/N ratios of Karewa lake sediments, India. *Nature* 323: 150 – 152.

Krishnamurthy, R.V., Syrup, K.A., Baskaran, M., Long, A., 1995. Late glacial climate record of Midwestern United States from the hydrogen isotope ratio of organic matter. *Science* 269: 1565 – 1567.

Kudrass, H.R., Hofmann, A., Doose, H., Emeis, K., and Erlenkeuser, H., 2001. Modulation and amplification of climatic changes in the Northern Hemisphere by the Indian summer monsoon during the past 80 k.y. *Geology* 29: 63 – 66.

LeMasurier, W.E., 1990. Late Cenozoic volcanism on the Antarctic plate: an overview, in LeMasurier, W.E., and Thomson, J.W., eds., *Volcanoes of the Antarctic plate and the southern oceans*: Am. Geophys. Union, Antarctic Research series, 48: 1 – 17.

Leng, M.J., Marshall, J.D., 2004. Palaeoclimate interpretation of stable isotope data from lake sediment archives. *Quaternary Science Reviews* 23: 811 – 831.

Liu, W., Huang, Y., An, Z., Clemens, S., Li, L., Prell, W., Ning, Y., 2005. Summer monsoon intensity controls C_4/C_3 plant abundance during the last 35 ka in the Chinese Loess Plateau: Carbon isotope evidence from bulk organic matter and individual leaf waxes. *Palaeogeography, Palaeoclimatology, Palaeoecology* 220: 243 – 254.

Lovan, N.A., 1998. A paleoclimatic study of the Midwestern United States from the stable isotope records in lake sediments. Ph.D. dissertation, Western Michigan University, 263 p.

Lundqvist, J., 1986. Late Weichselian glaciation and deglaciation in Scandinavia, in Sibrava, V., Bowen, D.Q., and Richmond, G.M., eds., Quaternary glaciations in the Northern Hemisphere. *Quaternary Science Reviews* 5: 269 – 292.

Lutgens, F.K., Tarbuck, E.J., 1998. *The Atmosphere: an introduction to meteorology*. Prentice Hall, Upper Saddle River, NJ, 434 p.

Mangerud, J., 1991. The last interglacial/glacial cycle in northern Europe, in Shane, L.C.K., and Cushing, E.J., eds., *Quaternary landscapes*: Univeristy of Minnesota Press, Minneapolis, MN, p.38-75.

Mangerud, J., Anderson, S.T., Birklund, B.E., Donner, J.J., 1974. Quaternary stratigraphy of Norden, a proposal for terminology and classification. *Boreas* 3: 109 – 128.

Mastalerz, M., Schimmelmann, A., 2002. Isotopically exchangeable organic hydrogen in coal relates to thermal maturity and maceral composition. *Organic Geochemistry* 33: 921 – 931.

Meyers, P.A., Leenheer, M.J., Eadie, B.J., Maule, S.J., 1984. Organic geochemistry of suspended and settling particulate matter in Lake Michigan. *Geochimica et Cosmochimica Acta* 48: 443 – 452.

Morrill, C., Overpeck, J.T., Cole, J.E., Liu, K-b., Shen, C., Tang, L., 2006. Holocene variations in the Asian monsoon inferred from the geochemistry of lake sediments in central Tibet. *Quaternary Research* 65/2: 232 – 243.

Murray, A.S., Roberts, R.G., 1998. Measurement of the equivalent dose in quartz using a regeneration-dose single aliquot protocol. *Radiation Measurements*, 29: 503 – 515.

Murray, A.S., Wintle, A.G., 2000. Luminescence dating of quartz using an improved single aliquot regenerative dose protocol. *Radiation Measurements*, 32: 57 – 73.

Oeschger, H., Stauffer, B., Finkel, R., Langway, C.C., Jr., 1985. Variations of the CO_2 concentration of occluded air and of anions and dust in polar ice cores. In E.T. Sundquist and W.S. Broeker, eds., *The carbon cycle and atmospheric CO_2: Natural variations Archean to present, American Geophysical Union Monograph* 32: 132 – 142.

Owen, L.A., Sharma, M.C., 1998. Rates and magnitudes of paraglacial fan formation in the Garhwal Himalaya: implications for landscape evolution. *Geomorphology* 26: 171 – 184.

Pagani, M., Arthur, M.A., Freeman, K.H., 1999a. Miocene evolution of atmospheric carbon dioxide. *Paleoceanography* 14: 273 – 292.

Pagani, M., Freeman, K., Arthur, M.A., 1999b. Late Miocene atmospheric CO_2 concentrations and the expansion of C4 grasses. *Science* 285: 876 – 879.

Pandey, S.K., Singh, A.K., Hasnain, S.I., 1999. Weathering and geochemical processes controlling solute acquisition in Ganga Headwater-Bhagirathi River, Garhwal Himalaya, India. *Aquatic Geochemistry* 5: 357 – 379.

Pant, G.B., Kumar, K.R., 1997. *Climates of South Asia*. John Wiley & Sons, 320 p.

Pant, R.K., Juyal, N., Basavaiah, N., Singhvi, A.K., 2006. Late Quaternary glaciation and seismicity in the Higher Central Himalaya: evidence from Shalang basin (Goriganga), Uttaranchal. *Current Science* 90/11: 1500 – 1505.

Patterson, C.J., 1997. Southern Laurentide ice lobes were created by ice streams: Des Moines Lobe in Minnesota, USA. *Sedimentary Geology* 111: 249 – 261.

Pearson, P.N., Palmer, M.R., 1999. Middle Eocene seawater pH and atmospheric carbon dioxide concentrations. *Science* 284: 1824 – 1826.

Peason, P.N., Palmer, M.R., 2000. Atmospheric carbon dioxide concentrations over the past 60 million years. *Nature* 406: 695 – 699.

Petit, J.R., Jouzel, J., Raynaud, D., Barkov, N.I., Barnola, J. –M., Basile, I., Bender, M., Chappellaz, J., Davis, M., Delayque, G., Delmotte, M., Kotlyakov, V.M., Legrand, M., Lipenkov, V.Y., Lorius, C., Pepin, L., Ritz, C., Saltzman, E., Steivenard, M., 1999. Climate and atmospheric history of the past 420,000 years from the Vostok ice core, Antarctica. *Nature* 399: 429 – 436.

Prentice, I.C., Farquhar, G.D., Fasham, M.J.R., Goulden, M.L., Heimann, M., Jaramillo, V.J., Kheshgi, H.S., Le Quéré, C., Scholes, R.J., Wallace, D.W.R., 2001. The carbon cycle and atmospheric carbon dioxide. In: *Climate Change 2001: The Scientific Basis. Contribution of Working Group I to the Third Assessment Report of the Intergovernmental Panel on Climate Change* [Houghton, J.T., Ding, Y., Griggs, D.J., Noguer, M., van der Linden, P.J., Dai, X., Maskell, K., Johnson, C.A. (eds.)]. Cambridge University Press, Cambridge, United Kingdom and New York, NY, USA, 881 p.

Raymo, M.E., 1992. Global climate change: A three million year perspective, in Kukla, G.J., and Went, E., eds., *Start of a glacial*. Springer-Verlag, Berlin, Heidelberg, 353 p.

Raymo, M.E., Ruddiman, W.F., 2004. DSDP Site 607 isotope data and age models. IGBP Pages/World Data Center for Paleoclimatology, Data Contribution Series #2004-010. NOAA/NGDC Paleoclimatology Program, Boulder, Colorado, USA.

Raymo, M.E., Ruddiman, W.F., Backman, J., Clement, B.M., Martinson, D.G., 1989. Late Pliocene variation in Northern Hemisphere ice sheets and North Atlantic deep circulation. *Paleoceanography* 4: 413 – 446.

Rhodes, T.E., Gasse, F., Ruifen, L., Fontes, J.-C., Keqin, W., Bertrand, P., Gibert, E., Melieres, F., Tucholka, P., Zhixiang, W., Zhi-Yuan, C., 1996. A Late Pleistocene-Holocene lacustrine record from Lake Manas, Zunggar (northern Xinjiang, western China). *Palaeogeography, Palaeoclimatology, Palaeoecology* 120: 105 – 121.

Robl, T.L., Burtron, H.D., 1993. Comparison of the HF—HCl and HF—BF$_3$ maceration techniques and the chemistry of resultant organic concentrates. *Organic Geochemistry* 20/2: 249 – 255.

Robert, C., Kennett, J.P., 1994. Antarctic subtropical humid episode at the Paleocene-Eocene boundary: Clay mineral evidence. *Geology* 22: 211 – 214.

Robinson, D.A., 1997. Hemispheric snow cover and surface albedo for model validation. *Annals of Glaciology* 25: 241 – 245.

Robinson, D.A., 1999. Northern Hemisphere snow cover during the satellite era. *Proceedings of the 5th Conference on Polar Meteorology and Oceanography*, Dallas, TX, American Meteorological Society, Boston, MA, p. 255 – 260.

Rozanski, K., Araguas-Araguas, L., Gonfiantini, R., 1993. Isotopic patterns in modern global precipitation. In: *Climate Change in Continental Isotope Records* [Swart, P.K., Lohman, K.C., McKenzie, J., Savin, S., (eds.)]. *American Geophysical Union Monograph* 78: 1 – 36.

Ruddiman, W.F., Raymo, M.E., Martinson, D.G., Clement, B.M., Backman, J., 1989. Mid-Pleistocene evolution of Northern Hemisphere climate. *Paleoceanography* 4: 353 – 412.

Sarin, M.M., Krishnaswami, S., Dilli, K., Somayajulu, B.L.K., Moore, W.S., 1989. Major ion chemistry of the Ganga-Brahmaputra River system: Weathering processes and fluxes to the Bay of Bengal. *Geochimica et Cosmochimica Acta* 53: 997 – 1009.

Schimmelmann, A., Lewan, M.D., Wintsch, R.P., 1999. D/H isotope ratios of kerogen, bitumen, oil, and water in hydrous pyrolysis of source rocks containing kerogen types I, II, IIS, and III. *Geochimica et Cosmochimica Acta* 63: 3751 – 3766.

Scotese, C.R., 2001. *Atlas of Earth History, Volume 1, Paleogeography,* PALEOMAP Project, Arlington, Texas, 52 p.

Sharma, M.C., Owen, L.A., 1996. Quaternary glacial history of NW Garhwal, Central Himalayas. *Quaternary Science Reviews* 15: 335 – 365.

Shi, Y., 2002. Characteristics of late Quaternary monsoonal glaciation on the Tibetan Plateau and in East Asia. *Quaternary International* 97 – 98: 79 – 91.

Singh, A.K., Hasnain, S.I., 1998. Major ion chemistry and weathering control in a high altitude basin: Alaknanda River, Garhwal Himalaya, India. *Hydrological Sciences Journal* 43: 825 – 843.

Singh, A.K., Pandey, S.K., Panda, S., 1998. Dissolved and sediment load characteristics of Kafni Glacier meltwater, Pindar Valley, Kumaon Himalaya. *Journal of the Geological Society of India* 52: 305 – 312.

Singhvi, A.K., Bluszcz, A., Bateman, M.D., Rao, S., 2001. Luminescence dating of loess-paleosol sequences coversands: methodological aspects and paleoclimatic implications. *Earth Science Reviews*, 54: 193 – 211.

Sinha, A., Cannariato, K.G., Stott, L.D., Li, H.-C., You, C.-F., Cheng, H., Edwards, R.L., Singh, I.B., 2005. Variability of Southwest Indian summer monsoon precipitation during the Bølling-Allerød. *Geology* 33/10: 813 – 816.

Sirocko, F., Sarnthein, M., Erlenkeuser, H., Lange, H., Arnold, M., Duplessy, J.C., 1993. Century-scale events in monsoonal climate over the past 24,000 years. *Nature* 364: 322 – 324.

Smith, B.N., Epstein, S., 1971. Two categories of $^{13}C/^{12}C$ ratios for higher plants. *Plant Physiology* 47: 380 – 384.

Stuiver, M., Grootes, P.M., 2000. GISP2 oxygen isotope ratios. *Quaternary Research* 53: 277 – 284.

Szabo, B.J., Ludwig, K.R., and two others, 1994. Thorium-230 ages of corals and duration of the last interglacial sealevel high stand on Oahu, Hawaii. *Science* 266: 93 – 96.

Teller, J.T., Kehew, A.E., 1994. Introduction to the last glacial history of large proglacial lakes and meltwater runoff along the Laurentide Ice Sheet. *Quaternary Research* 13: 795 – 799.

Thompson, L.G., Mosley-Thompson, E., Davis, M.E., et al., 1995. Late-glacial stage and Holocene tropical ice core records from Huascarán, Peru. *Science* 269: 46 – 48.

Thompson, L.G., Yao, T., Davis, M.E., Henderson, K.A., Mosley-Thompson, E., Lin, P.-N., Beer, J., Synal, H.-A, Cole-Dai, J., Bolzan, J.F., 1997. Tropical climate instability: the last glacial cycle from a Qinghai-Tibetan ice core. *Science* 276: 1821 -1825.

Tiezen, L.L., Senyimba, M.M., Imbamba, S.K., Tronghton, J.H., 1979. The distribution of C3 and C4 grasses and carbon isotope discrimination along an altitudinal and moisture gradient in Kenya. *Oecologia* 37: 337 – 350.

Valdiya, K.S., 2001. Reactivation of terrane-defining boundary thrusts in central sector of the Himalaya: implications. *Current Science* 81: 1418 – 1430.

Vandenberghe, J., 1992. Geomorphology and climate of the cool oxygen isotope stage 3 in comparison with the cold stages 2 and 4 in the Netherlands. In: *Geomorphology and geoecology: Glacial and polar geomorphology* [Staeblein, G., French, H.M., Marcus, M.G., (eds.)]. *Zeitschrift für Geomophologie*, Supp. 86: 65 – 75.

Wang, R.L., Scarpitta, S.C., Zhang, S.C., Zheng, M.P., 2002. Later Pleistocene/Holocene climate conditions of Qinghai-Xizhang Plateau (Tibet) based on carbon and oxygen stable isotopes of Zabuye Lake sediments. *Earth and Planetary Science Letters* 203: 461 – 477.

Wang, U.J., Cheng, H., Edwards, R.L., An, Z.S., Wu, J.Y., Shen, C.-C., Dorale, J.A., 2001. A high-resolution absolute-dated late Pleistocene monsoon record from Hulu Cave, China. *Science* 294: 2345 – 2348.

Webb, T., III., Bartlein, P.J., Kutzbach, J.E., 1987. Climatic change in eastern North America during the past 18,000 years: Comparisons of pollen data with model results. In: *North America and adjacent oceans during the last deglaciation* [Ruddiman, W.F., Wright, H.E., Jr. (eds.)]. Geological Society of America, *The geology of North America* v.K-3, p.447 – 462.

Yapp, C.J., Epstein, S., 1977. Climatic implications of D/H ratios of meteoric water over North America (9500 – 22,000 B.P.) as inferred from ancient wood cellulose C—H hydrogen. *Earth and Planetary Science Letters* 34: 333 – 350.

Zhao, J.-X., Wang, Y.-J., Collerson, K.D., Gagan, M.K., 2003. Speleothem U-series dating of semi-synchronous climate oscillations during the last deglaciation. *Earth and Planetary Science Letters* 216: 155 – 161.